Development of a tissue engineered, *in vitro* model of smooth muscle contraction

By

Jack Christopher Bridge

A thesis submitted to the University of Nottingham, in partial fulfilment of the requirements for the degree of Doctor of Philosophy

November 2015

Declaration

I declare that this thesis is my own unaided work. It is being submitted for the degree of Doctor of Philosophy at the University of Nottingham.

It has not been submitted before for any degree or examination in any other university.

Name of candidate: Signature:

Date:

Abstract

Smooth muscle (SM) tissue is found in many parts of the body, primarily in sheets or bundles surrounding hollow organs. The main function of the tissue is the regulation of organ tone *via* its contractile state. Dysfunction of SM in diseases such as asthma and atherosclerosis affect millions worldwide.

Current methods for studying SM primarily rely on *ex vivo* animal tissues or 2D *in vitro* models. Animal models do not accurately recreate human disease states and 2D models are cultured on stiff surfaces lacking the elastic properties and 3D morphology found in natural extracellular matrix *in vivo*. Therefore it is desirable to develop both an *in vitro* model of SM that possesses the ability to contract and a method in which this contraction can be measured.

In order to achieve this, primary rat aortic SM cells and primary human airway SM cells were cultured in collagen hydrogels; both free floating in the form of collagen disks and under uniaxial tension in order to generate aligned SM collagen constructs. When stimulated with contractile agonists, these constructs contract in a uniaxial fashion. The design of the constructs allows them to be attached to a force transducer allowing the physical force of contraction to be measured. The force of contraction was dependant on the agonist concentration and could be antagonised by the presence of an L-type calcium channel blocker.

In order to improve the alignment and uniformity of the smooth muscle population a range of aligned electrospun scaffolds were produced from polyethylene terephthalate (PET), cross-linked gelatin and cross-linked gelatin methacrylate (GelMa). The average fibre diameter of the scaffolds ranged from approximately 200 nm to several micrometres. Additionally the Young's moduli of the scaffolds ranged from around $1x10^5$ to $1x10^8$ Pa. In all cases, scaffolds were highly aligned; alignment was achieved by using a rapidly rotating collector mandrel.

Culture of primary SM cells upon these scaffolds showed that the cells readily adhered to and proliferated upon the scaffolds over a 10 day culture period. The

cells formed a highly aligned population following the topographical cues of the aligned fibrous scaffolds. Additionally, the cells stained positive for SM markers in all cases, indicative of a contractile phenotype. When stimulated with 100 μM UTP, the SM cells were able to contract the gelatin and GelMa scaffolds but not the PET scaffolds.

SM seeded GelMa scaffolds were cultured for 10 days prior to attachment to the previously mentioned force transducer apparatus. Upon stimulation the seeded scaffolds contracted generating forces greater than those achieved by the hydrogel model, and was reproducible over several experiments.

Contents

List of tables and figures

List of abbreviations

2D	Two dimensional
3D	Three dimensional
ADP	Adenosine diphosphate
ASM	Airway smooth muscle
ATP	Adenosine triphosphate
BSA	Bovine serum albumin
CFM	Culture force monitor
COPD	Chronic obstructive pulmonary disease
CTAB	Cetrimonium bromide
DAG	Diacyl glycerol
DAPI	4',6-diamidino-2-phenylindole
DCM	Dichloromethane
DM	Differentiation media
DMEM	Dulbecco's modified eagle medium
EAR	Early asthmatic response
ECM	Extracellular matrix
EDC	1-Ethyl-3-(3-dimethylaminopropyl)carbodiimide
EDTA	Ethylenediaminetetraacetic acid
EFS	Electrical field stimulation
FBS	Foetal bovine serum
FITC	Fluorescein isothiocyanate
GelMa	Gelatin methacrylate
GM	Growth medium

GPCR	G protein coupled receptor
HASM	Human airway smooth muscle
HDM	House dust mite
HFIP	Hexafluoroisopropanol
HUVEC	Human umbilical vein endothelial cell
ICC	Immunocytochemistry
IP$_3$	Inositol-1, 4, 5 triphosphate
LAR	Late asthmatic response
MHC	Myosin heavy chain
MLC	Myosin light chain
MLCK	Myosin light chain kinase
NHS	N-Hydroxysuccinimide
NMR	Nuclear magnetic resonance
OVA	Ovalbumin
PBS	Phosphate buffered saline
PDC	Copolyetheresterurethane
PDMS	Polydimethylsiloxane
PEO	Poly(ethylene oxide)
PET	Polyethylene terephthalate
PIP$_2$	Phosphatisylinositol 4, 5-biphosphate
PKC	Protein kinase C
PLC	Phospholipase C
PLGA	Poly(lactic co-glycolic aclid)
PLLA	Poly(L-lactic acid)

PTFE	Polytetrafluoroethylene
PVA	Poly(vinyl alcohol)
RASM	Rat aortic smooth muscle
Rho	Rhodamine
ROCC	Receptor operated calcium channel
SEM	Scanning electron microscope OR standard error of the mean
SM	Smooth muscle
SOCC	Store operated calcium channel
TBS	Tris-buffered saline
TCLS	Thin cut lung slices
TCP	Tissue Culture Plastic
TEAC	Tetraethylammonium chloride
TFA	Trifluoroacetic acid
TRITC	Tetramethylrhodamine isothiocyanate
UP	Unrestrained plethysmography
UTP	Uridine triphosphate
UV	Ultra violet
VDCC	Voltage dependant calcium channel

Acknowledgements

Firstly I would like to thank my supervisors Dr Felicity Rose, Prof. Mark Lewis and Dr Jonathan Aylott for investing their time in me, sharing their guidance and knowledge, and helping me to develop both as a person and as a scientist during the last three years. Thanks to Dr Gavin Morris for his mentorship throughout the project and the lab training that allowed me to carry out my experiments.

I would like to thank the staff and students of the EPSRC Doctoral Training Centre in Regenerative Medicine for giving me the opportunity to undertake this study and providing a unique social and learning experience. Thank you to the EPSRC for funding such a great programme.

Thank you to all members of the Tissue Engineering group at the University of Nottingham for their help and making my time in the labs an enjoyable one. Also, thanks to members of the Aylott group for welcoming me into your lab and putting up with my electrospinning for 3 years. I would also like to thank Teresa Marshall for helping me with any technical requests and Christine Grainger-Boultby for keeping the SEM running smoothly. I am grateful to Dr William Dunn for allowing me to collect rat tissue during my final year and to Esther and Hamidah for their help in organising tissue collections. Similarly, I would like to thank members of the Lewis research group at Loughborough University for allowing me to share their facilities and inviting me to many entertaining round table meetings. A special thanks for Dr Darren Player and Dr Neil Martin for their constant positivity and help with the CFM and the muscle physiology apparatus respectively, it is much appreciated.

Thank you to my parents who have always supported me in whatever I choose to do. Finally to my wife Michaela, who has shared this journey with me, this is for you. Thank you for always being there, through the highs and the lows. I could not have done this without you and I look forward to what the future brings us, I love you.

To my two boys, I'll see you soon!

1. Introduction

The experiments described in this thesis represent an attempt to develop and characterise a tissue engineered smooth muscle model using cultured primary smooth muscle cells seeded upon electrospun scaffolds. The model was designed to be used in studies directly measuring the contractile force generated by smooth muscle cells and has potential for future use in studies concerned with smooth muscle function in disease, specifically diseases affecting airway smooth muscle (such as asthma). Asthma is defined in the Global Initiative for Asthma (GINA) Guidelines as "a chronic inflammatory disorder of the airways in which many cells and cellular elements play a role. The chronic inflammation is associated with airway hyperresponsiveness that leads to recurrent episodes of wheezing, breathlessness, chest tightness and coughing… episodes are usually associated with widespread, but variable, airflow obstruction within the lung that is often reversible…" (GINA 2006). Asthma classification is determined by the frequency severity of exacerbations and can be classified either by clinical features or by the level of asthma control. This classification is described in **tables 1.1** and **1.2** respectively. The major effector cells causing airway obstruction in asthma are the airway smooth muscle cells. Development of a model that can monitor the contractile state of smooth muscle tissue in different environments (e.g. in the presence of immune cells simulating an inflammatory response) in response to various agonists/ antagonists would enable further investigations into the roles of smooth muscle tissue within asthma and would also have the potential to be used as a test bed for new asthma therapies. This introduction will focus on the morphology of smooth muscle *in vivo* and how smooth muscle contraction occurs. Additionally this section will look at current models used to investigate smooth muscle function; both *in vivo* animal models and *ex vivo* tissues, as well as recently developed tissue engineered alternatives to these models.

Intermittent	Mild persistent	Moderate persistent	Severe persistent
Symptoms less than once a week	Symptoms more than once a week but less than once a day	Symptoms daily	Symptoms daily
Brief exacerbations	Exacerbations may affect activity and sleep	Exacerbations may affect activity and sleep	Frequent exacerbations
Nocturnal symptoms not more than twice a month	Nocturnal symptoms more than twice a month	Nocturnal symptoms more than once a week	Frequent nocturnal asthma symptoms
FEV_1 or PEF ≥80% predicted	FEV_1 or PEF ≥ 80% predicted	Daily use of inhaled short-acting β 2-agonist	Limitation of physical activities
PEF or FEV_1 variability < 20%	PEF or FEV_1 variability < 20–30%	FEV_1 or PEF 60–80% predicted	FEV_1 or PEFs 60% ≤ predicted
		PEF or FEV_1 variability > 30%	PEF or FEV_1 variability > 30%

Table1.1: Classification of asthma by clinical features. Adapted from (GINA 2006)

Characteristic	Controlled (all of the following)	Partly controlled (any measure present in any week)	Uncontrolled
Daytime symptoms	None (twice or less/week)	More than twice/week	Three or more features of partly controlled asthma present in any week
Limitations of activities	None	Any	
Nocturnal symptoms/awakening	None	Any	
Need for reliever/rescue treatment	None (twice or less/week)	More than twice/week	
Lung function (PEF or FEV_1)	Normal	< 80% predicted or personal best (if known)	
Exacerbations	None	One or more/year	Once in any week

Table1.2: Classification of asthma by disease control. Adapted from (GINA 2006)

(FEV_1= 1-second forced expiratory volume; PEF= peak flow)

Smooth muscle is an involuntary contractile tissue that can be found in many locations throughout the body, the majority of which is found in the walls of hollow organs such as blood vessels (named vascular smooth muscle (Wynne et al. 2009)) or the airways (airway smooth muscle (ASM) (Ouedraogo & Roux 2014)). In locations such as these it occurs as either broad, thin sheets or arrays of bundles that surround the vessels circumferentially. Their main function is to control the tone of the vessels *via* contraction and relaxation responses, regulating luminal area. Smooth muscle can also be found connecting hair follicles to surrounding tissues (Jahoda et al. 1991) and is even present in the eye, with a small ring found close to the pupillary edge of the iris (Jensen 2005).

The name smooth muscle arose due to the lack of striations when compared to skeletal and cardiac muscles, as their name suggests, their primary function is to contract, and do so in response to chemical (Borkowski et al. 1995; Matsui et al. 2002) and physical signals (Kirber et al. 1988; Davis et al. 1992). Smooth muscle contraction can be classed as either tonic or phasic; tonic smooth muscle contracts slowly over prolonged periods of time and is generally found in the vasculature, airways, the eye, urinary tract and reproductive organs. Phasic smooth muscle contracts quickly and for short periods, the majority of this is visceral smooth muscle (Thornbury 1999). Given the wide range of locations in the body in which smooth muscles are found, it is unsurprising that their contractile behaviour differ greatly to suit their purpose. Their contractile speed, force and duration in addition to their stiffness, shortening ability, energy consumption and importantly, the contraction inducing stimuli, all vary depending on their location *in vivo*. These differences partly stem from the chemical composition of their contractile machinery. For example, different isoforms of both the heavy (Babij & Periasamy 1989; Nagai et al. 1989; Rovner et al. 1986) and light (Nabeshima et al. 1987) chains of myosin are known to contribute to these differences in contractile behaviour.

1.1   Smooth muscle morphology

Smooth muscle cells possess a spindle-like morphology, varying in length dependent on their location *in vivo*. The cells contain a complex network of structural and contractile proteins in the form of filaments (thin, thick and intermediate), dense bodies and dense bands that all play important roles in the contractile function of the tissue. Important structural features such as cell junctions and caveolae are found within the plasma membranes of smooth muscle cells.

Cell junctions can be classified as either intermediate (also called adherens) junctions or gap junctions. The former provide mechanical coupling between cells and represent two paired dense bands from adjacent cells, separated by 10-20 nm whose intercellular space is occupied by rod-shaped molecules bridging the membranes (Hirokawa & Heuser 1981; Miyaguchi 2000). Gap junctions provide ionic/ electrical coupling between adjacent cells with a gap of only 2-4 nm between parallel membranes (Alberts et al. 2002). This small gap allows for the pairing of connexons (a circular array of six connexins) on each cell membrane to form single ionic channels connecting the cytoplasm of the two cells. This aids in the transmission of contractile stimuli between cells. Within smooth muscles a single gap junction is thought to contain as many as 1400 connexons per cell (Gabella 1981).

Caveolae are omega shaped 50-100 nm invaginations of the cell membrane that occur across the cell, dispersed between dense bands (Razani et al. 2002). They are formed from cholesterol and sphingolipid-rich lipid rafts that bind to specific caveolae proteins; caveolins. The plasma membrane regions within caveolae contain multiple membrane receptors (including muscarinic and adrenergic receptors), second messenger generators (such as, phospholipase C), G proteins, kinases, and ion channels in close proximity. This creates a specialised area for the regulation of cellular activity (Ostrom & Insel 2004), including contraction. The presence of calcium pump ATPase within caveolae membranes (Fujimoto 1991) and high calcium concentrations within caveolae (found by electron probe

studies (Popescu & Diculescu 1975)) also suggest that caveolae are involved in the influx of extracellular calcium.

Intermediate filaments are more plentiful in smooth muscle tissues than other tissues, in some cases constituting 5% of the total protein content (Huiatt et al. 1980). They vary in length and are approximately 10 nm in diameter. The protein content of intermediate filaments varies throughout the body; within visceral muscles, the major component is the 53.5 kDa protein (Geisler & Weber 1983) desmin which has been shown to reconstitute intermediate filaments *in vitro* (Ip et al. 1985). Vascular smooth muscle cells on the other hand possess little to no desmin with vimentin being the key constituent of intermediate filaments (Gabbiani et al. 1981). Few smooth muscle cells express both desmin and vimentin (Schmid et al. 1982). Intermediate filaments form a structural network throughout the cell, they associate with dense bodies (Cooke & Chase 1971; Tsukita et al. 1983) within the cell (forming side-to-side links) and membrane bound dense bands, linking the two providing 3-dimensional integrity (Small & Gimona 1998). In addition to providing structural support, the intermediate filaments are also important in mechanotransduction, converting mechanical stimuli into a biological response. This has been shown in several studies; for example, mice genetically modified to be deficient in desmin (Loufrani et al. 2002) and vimentin (Schiffers et al. 2000) both display alterations in vasomotor properties such as agonist sensitivity and impaired flow-dependent dilation. This suggests that the intermediate filament proteins are involved in sensing mechanical cues from outside the cell. A diagram of the distribution of intermediate filaments (in addition to thin and thick filaments) within smooth muscle cells is shown in **Figure 1**.

Dense bodies are distributed throughout the cytoplasm of smooth muscle cells and are rich in α-actinin (Aguilar & Mitchell 2010). In addition to intermediate filaments, they associate with thin (actin) filaments; this association of actin with the α-actinin of dense bodies is very similar to that seen at Z lines within striated muscles (Fay et al. 1983). Their association to thin filaments makes them appear to act as anchors from which the thin filaments can exert forces during cell

contraction. In addition to contractile actins, they also associate with the cytoskeletal β-actin (Aguilar & Mitchell 2010), suggesting that they are arranged within the cell cytoskeleton. Dense bodies are called so due to their electron dense appearance under an electron microscope, they elongate along the cell length and are variable in size. Dense bands (also known as dense plaques) are similar in appearance to dense bodies but appear exclusively bound to the cell membrane. They link contractile actin filaments to the cell membrane and in turn, to the ECM or neighbouring cells. Some dense bands are also linked to dense bodies *via* intermediate filaments. They are found across the whole membrane, covering 30-50% of the cell surface, with a greater density at the tapered ends of the cells. Again, α-actinin is found within dense bands although the focal adhesion protein vinculin is only found in dense bands. In dense bands that bind to the surrounding ECM, talin is also present (Drenckhahn et al. 1988).

Thin/ actin filaments are part of the contractile machinery within smooth muscle cells. They are 7-8 nm in diameter and form branched fibrous networks, terminating within dense bodies or bands. The filaments are formed from polymerisation of globular actin subunits which form chains twisted into a double helix configuration with a rotation of 166.15° around the axis between subunits (Egelman et al. 1982). Associated to the actin filaments are
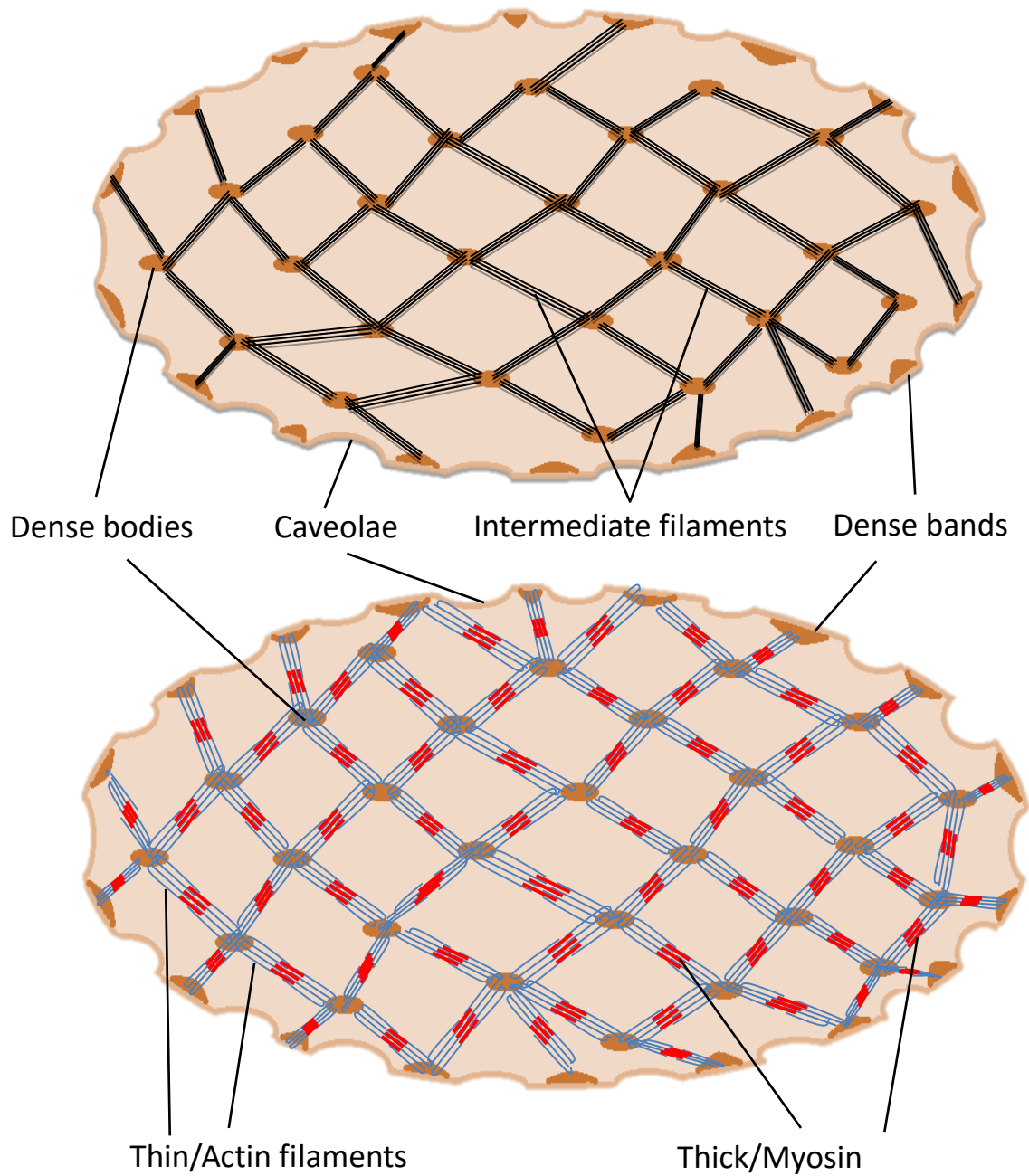
Figure 1.1: Assembly of structural and contractile filamentous proteins within smooth muscle cells.

tropomyosin, calponin and/or caldesmon (**Figure 2A**). Within smooth muscle cells there are two major groups of filamentous actin. The first group is composed of α and γ actin and form the thin filaments described above; these slide along myosin filaments during contraction (Draeger et al. 1990). β-actin on the other hand, is a structural cytoskeletal protein found below the plasma membrane. It is known to polymerise in the presence of contractile agonists, strengthening the plasma membrane. This is thought to play an integral role in developing mechanical tension during contraction (Gunst & Zhang 2008). The ratio of actin to myosin filaments is higher in smooth muscle than in striated muscles (Murphy et al. 1977), suggesting that not all actin filaments interact directly with a myosin filament.

Thick filaments are formed from aggregates of myosin, are around 14-18 nm in diameter and cylindrical in shape. The term myosin encompasses a large superfamily of proteins that share the ability to bind to actin and possess ATPase enzyme activity. Class II myosin is the predominant myosin within the contractile apparatus of human muscles. It is a hexamer formed from two intertwined myosin heavy chain (MHC) molecules and four myosin light chain (MLC) molecules . Each heavy chain (approximately 200kDa each) consists of a head, neck and tail domain; the head domains contain the globular N-terminals that protrude laterally from the myosin filament, they also contain the sites for actin binding and ATP hydrolysis. The neck domains create the angle between the head and tail domains and are the site of binding for the MLC molecules, the tail domains are made up of the C-terminal ends of the MHC molecules, and the two are intertwined in a helical rod that forms the major constituent of thick filaments. Two different MLCs exist, with molecular weights of 20 kDa (MLC_{20}) and 17 kDa (MLC_{17}) known as regulatory light chain and essential light chain respectively. One of each MLC binds to the neck domain of each MHC, forming the myosin II hexamer. A diagram of the myosin II hexamer is shown in **Figure 2B**. MLC_{20} has a pivotal role in regulating vascular smooth muscle contraction.

A
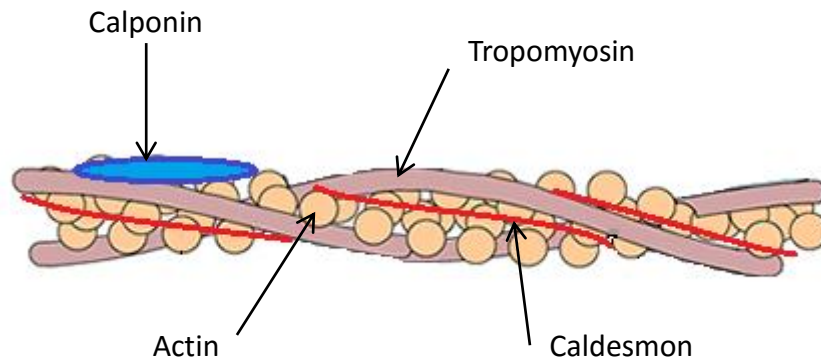
B
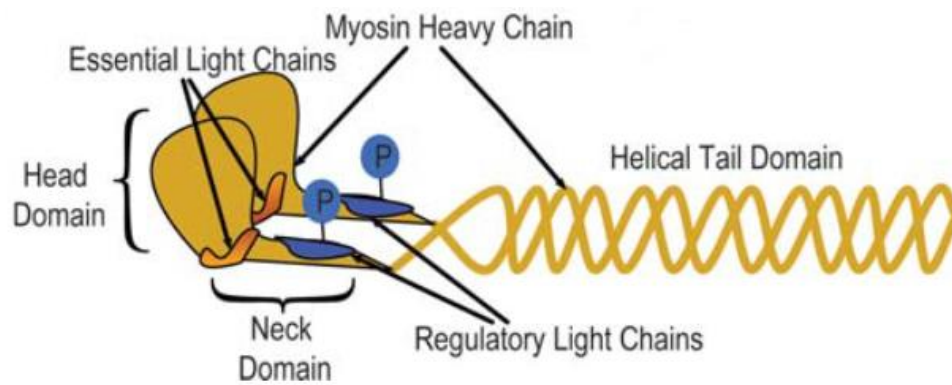
Figure 1.2: Structure of actin and myosin. A diagram of a thin/ actin filament filaments (A; adapted from http://www.ivyroses.com/). A diagram of a myosin II hexamer (B; adapted from (Aguilar & Mitchell 2010))

(Górecka et al. 1976; Arner & Pfitzer 2005), the role of MLC_{17} is unclear but is thought to contribute to the structural stability of the myosin heads

Other proteins of interest associated with thick and thin filaments are tropomyosin, calponin, caldesmon. Tropomyosin binds to actin filaments spanning 7 actin monomers and is laid out end to end over the length of the thin filaments. Within striated muscles, it enhances actin-myosin interactions however its role in smooth muscles is not clear. Calponin is expressed at similar levels to actin and is thought to act as a load bearing protein; it also binds to actin and inhibits myosin ATPase activity, displaying a similar function to troponin in striated muscles (which is not present in smooth muscles), and inhibiting actin sliding. Phosphorylation of calponin with protein kinase C (PKC) alleviates this inhibitory effect, promoting actomyosin activity (Pohl et al. 1997). Caldesmon is thought to be involved in the tethering of actin, myosin and tropomyosin and is also thought to act as a molecular switch, inhibiting myosin ATPase activity depending on its phosphorylation state.

1.2   Smooth muscle contraction

Smooth muscle contraction is principally regulated by chemical or mechanical stimulation of the contractile proteins actin and myosin. In the case of chemical stimuli; binding of an agonist (such as histamine) to a G-protein-coupled-receptor (GPCR) stimulates phospholipase C (PLC) activity (**Figure 3**). In parallel, this stimulates the influx of extracellular calcium into the cell through receptor operated calcium channels (ROCCs) and voltage dependant calcium channels (VDCCs). PLC is an enzyme specific for the membrane bound lipid phosphatisylinositol 4, 5-biphosphate (PIP_2) cleaving it into two potent second messenger molecules; inositol-1, 4, 5 triphosphate (IP_3) and diacyl glycerol (DAG). DAG, along with Ca^{2+} ions, activates PKC which phosphorylates tissue specific target proteins in addition to actin bound calponin, which promotes actin-myosin cross-bridging. IP_3 stimulates the release of intracellular calcium from IP_3 sensitive stores in the sarcoplasmic reticulum. This calcium increase triggers the activation of the calcium dependent cytosolic protein calmodulin,
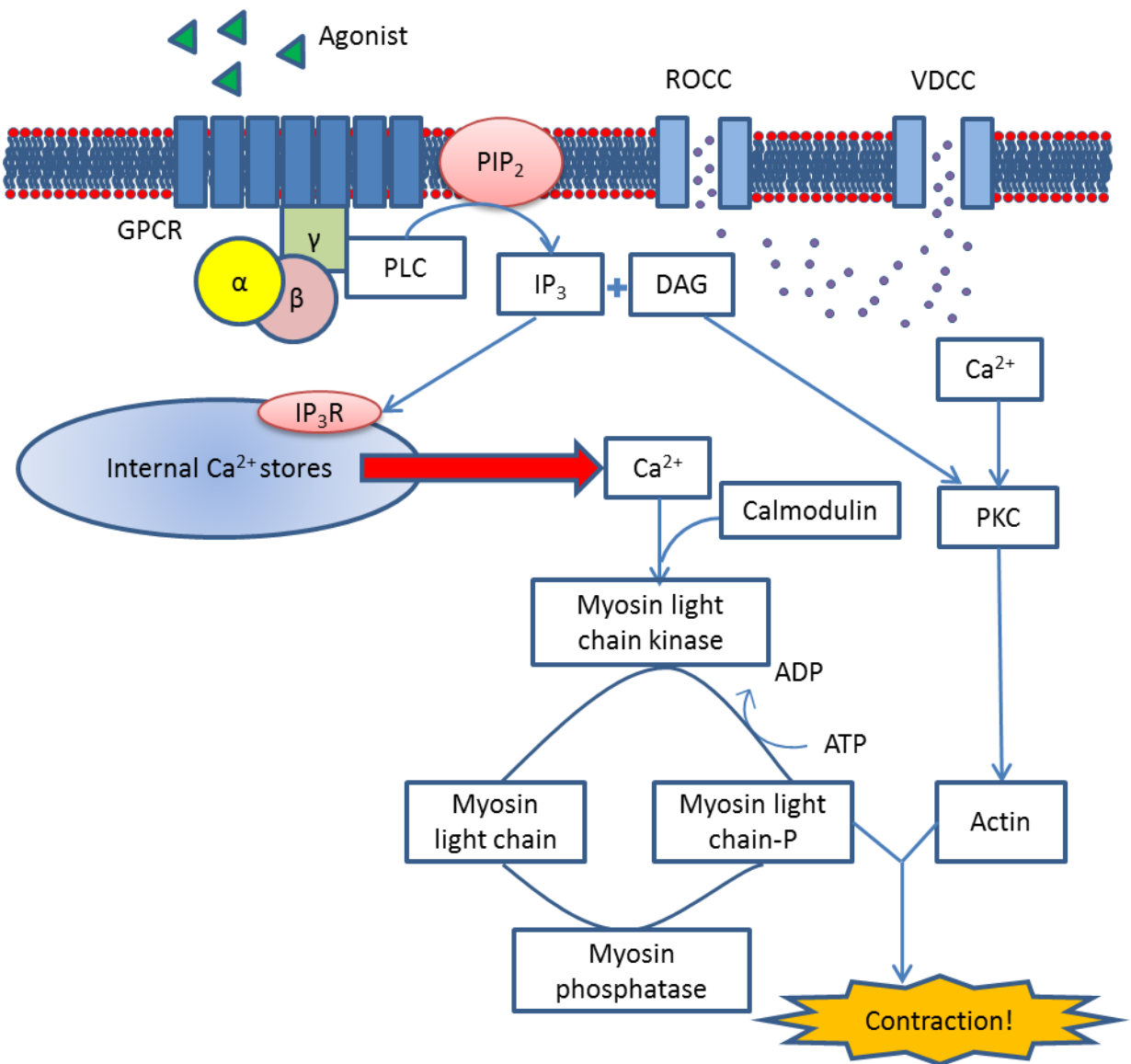
Figure 1.3: Mechanism of initial and sustained ASM contraction. Schematic adapted from (Word & Kamm 1997)

which binds to four Ca^{2+} ions (Johnson et al. 1996). This Ca-calmodulin complex activates the enzyme myosin light chain kinase (MLCK), a key enzyme in the actin-myosin cross-bridging mechanism, which phosphorylates the regulatory light chain (MLC_{20}) using ATP in the process. Phosphorylation of MLC results in cross-bridge attachment, cycling, and force development within the cell (Kamm & Stull 1986; Murphy 1994). Studies have shown that phasic smooth muscles develop force more rapidly than tonic smooth muscles (Horiuti et al. 1989). This difference in cross-bridge cycling rates could be accounted for by a higher ADP affinity of myosin heads in tonic muscles (Khromov et al. 1995). Working against the activity of MLCK is myosin phosphatase which continuously dephosphorylates the activated MLC_{20}. Therefore, In order to maintain contraction, the high level of cytosolic calcium needs to be sustained in order to preserve a high level of activated MLCK (MLCK > myosin phosphatase). As the internal calcium stores are used, it has been proposed that store-operated calcium channels (SOCCs) allow calcium influx (Putney 1993). Additionally, receptor-operated calcium channels (ROCCs), activated by the GPCR, also allow continued influx of calcium ions into the cell (Murray & Kotlikoff 1991). Calcium influx through SOCCs and ROCCs contribute to both the refilling of the internal calcium stores and maintaining smooth muscle contraction *via* a PKC dependent mechanism (Giembycz & Raeburn 1992).

When stimulation is reduced or removed from the cell, the rate of calcium ions entering the cytosol *via* calcium channels will fall. Subsequently, levels of cytosolic calcium fall as ions are sequestered back into depleted internal calcium stores resulting in a decrease of calcium bound to calmodulin. This is turn leads to a reduced MLCK activity and myosin phosphatase activity predominates preventing further actin-myosin cross bridging. As this process continues the force generated by the cell reduces and the cell begins to relax back to a resting state. As mentioned above, relaxation can be caused by a cessation of stimulation but it can also be triggered by the presence of certain chemicals. One example of this would be caffeine. Caffeine has been found to relax noradrenaline-induced contraction of the aorta and the carbachol induced

contraction of the taenia coli (Ahn et al. 1988). This is in part due to caffeine's inhibiting action of cyclic AMP breakdown. Additionally, caffeine may also inhibit Ca^{2+} influx by binding to Ca^{2+} channels (Martin et al. 1989) reducing the concentration of intracellular calcium.

1.3   Animal models of smooth muscle

As the long term aim of this thesis is to develop a tissue engineered model of smooth muscle to investigate airway disease and potentially replace currently used animal models, this section will focus on animal models to study specifically airway smooth muscle.

There has been a wide variety of *in vitro, in vivo* and *ex vivo* studies to investigate the role of smooth muscle in asthma, however each model is not without its limitations. *In vivo* the majority of studies have been undertaken in rodents (Meurs et al. 2006; Lundblad et al. 2007; Kucharewicz et al. 2008), as well as dogs (Stephens et al. 1986), pigs (Turner et al. 2002), horses (Herszberg et al. 2006), sheep (Koumoundouros et al. 2006) and primates. Mice are favoured for *in vivo* studies due to their low cost, short breeding periods and importantly, the well characterised genome of the mouse gives the ability to knock out specific genes to study specific pathways in asthma. They are easily sensitised to a number of antigens including ovalbumin (OVA, the most common method of sensitisation) (Zosky et al. 2004), and other allergens such as house dust mite (HDM) (Fattouh et al. 2005). This induces an asthmatic state in the mice causing airway hyperresponsiveness (Zhang et al. 1997) or airway remodelling (Lloyd 2012) depending on the protocol used to sensitize the mice, key features being the mouse strain used (Shinagawa & Kojima 2003) as well as the route (Shore 2003) and duration (Lloyd 2012) of allergen exposure. Transgenic technology, coupled with the well characterised genome of the mouse makes mice ideal candidates for mechanistic studies where manipulation, antagonism, suppression or upregulation of a particular molecular pathway can be carried out to examine its role and importance in the development of symptoms of asthma (Elias et al. 2003). Transgenic studies in mice have acknowledged the importance of the Th-2

phenotype in the progression of allergic disease and additionally, the importance of the cytokines IL-4 (Pauwels et al. 1997), IL-5 (Foster et al. 1996) and IL-13 (Fish et al. 2005) in allergic inflammation and the development of airway hyperresponsiveness. This has led to the development of several treatments targeting these cytokines. However, even though effective in mouse models, the same results were not seen in humans (Taube et al. 2004).

Rats are commonly used in asthma studies due to their sensitivity to allergens such as OVA (Hylkema et al. 2002) and HDM (Liu et al. 2005) and their ability to replicate features of airway inflammation seen in humans such as early asthmatic responses (EAR) and late asthmatic responses (LAR) following allergen challenge (Eidelman et al. 1988). When exposed to broncho-constricting agents however, they produce relatively weak contractile responses (Kucharewicz et al. 2008); therefore, although useful as a model of inflammation, rats do not replicate the levels of ASM contraction seen in humans.

As with rats, guinea pigs also display EAR and LAR; in addition, their mast cells release histamine and leukotrienes upon allergen challenge. They are often used to screen drugs that act through pathways thought to be relevant to human asthma and have been used in the development of drugs such as β_2 receptor-agonists and corticosteroids (Selig & Chapman 1999). However the low number of inbred strains and lack of guinea-pig-specific reagents available currently limit mechanistic guinea pig studies.

Although animal models can be used effectively to study airway inflammation and remodelling, the lung mechanics of mice are not highly relevant for modelling human lung function due to their difference in resting posture (Bettinelli et al. 2002), airway branching patterns (Schlesinger & McFadden 1981; Plopper et al. 1983) and low amounts of smooth muscle tissue in proportion to humans (Karol 1994). Despite this, mice have still been used for such studies and several methods exist for assessing lung function in mice. Unrestrained plethysmography (UP) is a non-invasive technique that measures the pressure changes in a box containing a free moving animal. The changes in pressure can

be used to directly measure airway resistance but these measurements can also be affected by the absolute lung volume and tidal volume of the animal, which when challenged by bronchoconstrictors are both changed. Therefore UP has very limited accuracy and obviously cannot be used to directly measure ASM contraction but is able to monitor changes in airway resistance without altering the behaviour of the animal (Hamelmann et al. 1997). On the other hand, breathing behaviour can be experimentally controlled by forced oscillation leading to much more accurate measurements of airway resistance. This accuracy comes at a cost however and requires that the animal is anesthetised, paralyzed and has a tracheostomy, completely removing the animal from a relaxed, natural state. Therefore any method of physical measurement of lung function *in vivo* suffers from a trade-off between invasiveness and accuracy (Bates & Irvin 2003).

1.4 *Ex vivo* models

In order to directly assess physical ASM function, using techniques such as myography (Liu et al. 2006), it is much easier to use *ex vivo* models. Several methods of analysing airway tissue *ex vivo* exist, with excised bronchial segments, isolated ASM strips or rings and thin cut lung slices (TCLS) all used to assess ASM contraction. Isolated ASM strips can be used to directly measure the contraction of the muscle through mounting the strips upon a force transducer in an organ bath and directly stimulating by electrical or chemical means. This has clear benefits as the degree of muscle shortening can be directly measured and comparisons between asthmatic and non-asthmatic ASM can be made. The contraction measured may not accurately predict contraction *in vivo* however due to the muscle being removed from the surrounding airway wall and other cell types that would regulate contraction. Whilst this is a useful tool for studying the contractile ability of both healthy and asthmatic ASM a major limitation is the limited availability of human tissue samples. In addition, challenging protocols to extract tissue require a high level of technical expertise.

1.4.1 Bronchial segments

By using bronchial segments and ligating the side branches of the segments to prevent leaking, changes in airway pressure and volume can be directly measured (Gunst & Mitzner 1981). This relates to the contraction of ASM within the bronchial segment. Compared to *in vivo* models, airway segments allow for protocols which would not be possible in a live animal such as electrical stimulation of the tissue or the direct application of a pharmacological agent to the ASM (Mitchell & Sparrow 1994). Bronchial segments from pigs have been used to assess the effects of load (due to surrounding tissues) on airway narrowing in response to electrical field stimulation (EFS) and acetylcholine (Noble et al. 2002). Bronchial narrowing was measured using an endoscope and was found to be greater and faster in segments where the surrounding cartilage had been removed. Additionally, the effects of allergen sensitisation have been studied using bronchial segments from (ovalbumin sensitised and challenged) hyperresponsive pigs. Airway narrowing in these segments was found to be less than control segments, showing reduced contraction to acetylcholine (Turner et al. 2002). Another study using bronchial segments was able to explore the effects of cyclic strain applied to the airway prior to stimulation (Noble et al. 2004). It was found that following 10 minutes intraluminal pressure oscillation, there was a modest increase in the response to EFS compared to static controls. Within the same study, isolated ASM strips had a decreased response to EFS following similar cyclic strain protocols, indicating that the airway wall modifies ASM response to cyclic strain. A later study by the same group carried out similar experiments on bronchial segments from asthmatic and non-asthmatic donors. They recorded that there was no difference in sensitivity between the two donor groups although asthmatic donors had significantly increased levels of ASM tissue; therefore displayed greater maximal airway narrowing than non-asthmatics (Noble et al. 2013).One large drawback of bronchial segments is that they only last for around one day in culture however and therefore are not suitable for long term studies.

1.4.2 Thin cut lung slices

TCLS can last up to seven days in culture allowing for longer *ex vivo* studies when compared to bronchial segments. These are produced by filling *ex vivo* animal lungs with a low gelling temperature agarose gel to preserve alveolar structure and gives better tissue compliance (Siminski et al. 1992). The tissue is then cut into multiple slices (over 150µm in thickness) and incubated. An advantage that these slices have over airway segments when studying ASM contraction is the presence of the surrounding parenchyma which retains the mechanical structure found *in vivo*. As parenchymal load can oppose contraction; by removing this load, the contraction seen would be less representative of an *in vivo* airway. By partially digesting the mechanical environment of TCLS it has been found that the parenchymal load resisting contraction is mainly due to the presence of elastin whereas the level of airway stiffness is attributable to the level of collagen (Khan et al. 2010).

Dandurand *et al*. were the first to visualise contraction in lung slices using video microscopy and digital imaging (Dandurand et al. 1993) making it possible to also quantify airway contraction. This approach was then developed further by Martin *et al.* who assessed the effects of methacholine concentration on contraction (Martin et al. 1996). They found that the level of contraction in the lung slices was concentration dependent and additionally the presence of hydrocortisone increased the EC_{50} of the methacholine by a factor of six. Confocal microscopy allows for calcium imaging of smooth muscle cells within thin cut lung slices. Bergner and Sanderson imaged murine lung slices in the presence of acetylcholine. The magnitude of the airway contraction, the initial Ca^{2+} transient and the frequency of subsequent calcium waves were all found to be dependent on the concentration of acetylcholine (Bergner & Sanderson 2002a). In a similar study, they looked at the effects of ATP analogues on airway contraction and calcium release. ATP (10µM) was found to induce Ca^{2+} oscillations for up to a minute whereas adenosine 5'-O-(3-thiotriphosphate) (0.5

μM) induced oscillations that lasted over 2 minutes (Bergner & Sanderson 2002b).

In addition to chemical agonist stimulation, lung slices have also been stimulated using EFS; airway contraction increased with higher frequencies with larger airways having stronger responses (Schlepütz et al. 2011). Guinea pig lung slices were found to be more appropriate for modelling human airway pharmacology than other rodent models with similar responses between several agonists except for serotonin which is a potent bronco-constrictor in guinea pigs but not in humans (Ressmeyer et al. 2006). Delmotte and Sanderson studied the effects of the two enantiomers of the β_2 adrenergic agonist albuterol (commonly used as a bronchodilator to treat asthma) using murine lung slices, recording airway contraction and Ca^{2+} signalling (Delmotte & Sanderson 2008). They discovered that (R)-albuterol relaxed airways in a dose-dependent manner whereas (S)-albuterol had no effect on the airways. A similar effect was seen in the calcium imaging experiments where (R)-albuterol decreased the frequency of methacholine induced Ca^{2+} oscillations, whereas (S)-albuterol had no effect. Lung slices have been used to test the efficacy of potential drug candidates. One example is a study by Fitzpatrick *et al*. who compared prostaglandin E_2 (PGE_2) with the commonly used β_2-adrenoceptor agonist salbutamol where PGE_2 was found to be more potent than salbutamol in opposing contraction initiated by all stimuli tested (Fitzpatrick et al. 2013). Kudo *et al.* reported using lung slices to study the effects of IL-17A on methacholine stimulated contraction. At multiple concentrations of methacholine studied, IL-17A significantly enhanced the levels of airway contraction recorded; removal of the epithelium enhanced the contractile forces further (Kudo et al. 2012). Other areas where TCLS have been used is in the study of the effects of tobacco smoke (Churg et al. 2009; Streck et al. 2010; Lin et al. 2012) and vehicle emissions (Bion et al. 2002; Fall et al. 2008; Morin et al. 2008) on the airways. One key drawback of TCLS is that as they are essentially a 2D section of the lung where the ASM is exposed and not protected by an epithelial layer as it would be in the 3D airway; this may lead to stronger

ASM contraction as any contractile agonist would hit the ASM directly instead of first passing through the epithelium.

1.5 *In vitro* cell culture

In vitro cell culture is not necessarily limited by sample availability and can be used to assess ASM cells over a longer period of time to look closely at the biological pathways involved in ASM contraction. ASM can be obtained from trachea or bronchi tissue samples *via* enzymatic digestion or explant culture. Due to the stiff surfaces used to culture cells *in vitro*, assessment of ASM contraction is not possible; however Ca^{2+} imaging of cells can be used to monitor the Ca^{2+} signalling pathway involved in contraction. Also, immunostaining of ASM cells as well as 2D protein gel assays can be used to determine the levels of smooth muscle phenotype markers such as contractile proteins, specific receptors, ion channels and cell junctions. Clear disadvantages of *in vitro* culture are the lack of a 3D structure which affects cell morphology and behaviour as well as the progressive loss of the contractile phenotype over time (Hirst 1996; Wright et al. 2013; Roscioni et al. 2011). A current method of measuring the contraction of ASM *in vitro* requires seeding the cells within a collagen hydrogel. Upon addition of a contractile stimulus, the gels contract and the change in gel area can be used to estimate the extent of gel contraction. This method has had some successful results such as showing that asthmatic ASM shows a stronger contraction when exposed to histamine than ASM from non-asthmatics (Matsumoto et al. 2007). This contraction cannot be wholly attributed to the contraction of the ASM however as the ASM will naturally remodel the structure of the collagen gel, decreasing the gel size. Due to this, prolonged culture or repeat tests on these collagen gels are not possible.

1.6 Tissue engineered models of smooth muscle

Tissue engineering is a multidisciplinary field bringing together materials scientists, biologists, chemists, engineers and clinicians (amongst others) aiming to develop strategies for the creation or replacement of living tissues. The

approaches taken to achieve this goal include; using isolated cells (such as stem cells), using biochemical and physicochemical factors (such as growth factors) to encourage specific tissue-growth and combining isolated cells with synthetic materials that attempt to recreate the extracellular matrix found *in vivo* in order to produce a 3D living tissue. Although arguably still in its infancy, this field of study which has grown rapidly over the last 2 decades due to the potential for tissue engineering to deliver innovative products and therapies to meet unmet clinical needs. One of which is the currently limited supply of human donor organs. Success stories such as the production and implantation of a tissue engineered trachea (Macchiarini et al. 2008) have only led to increased interest and investment into the field.

In addition to producing tissues for clinical purposes, tissue engineering holds the potential to further develop our understanding of cellular mechanisms and drug interactions *via* the development of more accurate/ representative pre-clinical models. This can be achieved by culturing primary cells or cell lines on 3D matrices which resemble the natural environment of living tissue. This could be used to potentially merge aspects of all the previously described ASM culture techniques, making a more accurate and flexible tool for investigating ASM *in vitro*. Unsurprisingly, several tissue engineered airway models have been developed in recent years. In most cases the models include ASM cells and other airway cells being seeded onto a 3D scaffold, the main variable between the models being the scaffold used. Scaffolds can range in complexity from simple collagen gels (Choe et al. 2006), similar to those previously discussed, through to de-cellularised airway tissue (Macchiarini et al. 2008). Although de-cellularised tissue completely replicates the natural ECM, the demand for tissue will always exceed availability. Also, due to donor variability it is impossible to fully characterise the composition of each donated tissue. Therefore, matrices made from ECM derived proteins and synthetic polymers offer an alternative.

Collagen gels have been used as a 3D scaffold in several airway models. Gerthoffer *et al.* seeded ASM cells into collagen gels in wells containing a central polydimethylsiloxane (PDMS) post (Gerthoffer et al. 2007). When set and

removed from around the PDMS post, the gel then possessed a ring like structure representative of an airway. The ASM rings were exposed to constricting agents and the response measured using myography (the study of muscle contraction, a myograph measures the contractile properties of muscles through direct mechanical coupling to a force transducer). Collagen hydrogels have also been used in developing more complex airway models. Multi-cell layered collagen tubes composing of epithelial cells, fibroblasts and ASM have been constructed by Miller *et al.* (Miller et al. 2010). These tubes were cultured in a bioreactor for up to 60 days where they were mechanically stimulated in order to simulate breathing. Contraction of the tubes was measured but this was only in respect to remodelling of the gels, not contraction of the ASM in response to a stimulus. Cells seeded in collagen gels set around micro-scale cantilevers known as microfabricated tissue gauges can be used to measure and manipulate ASM contraction (Legant et al. 2009). By knowing the stiffness of the cantilevers, displacement of them can relate to the force generated due to the contraction of the gel. Also, stiffer cantilevers would resist against contraction, creating a more *in vivo* environment for the ASM within the collagen. Using these microfabricated tissue gauges, ASM response to histamine, KCl and acetylcholine have all been recorded (West et al. 2013). Unfortunately, long term studies are not possible with these tissues as they lose structural integrity as the cells remodel the gel (50% of tissues fail after 7 days).

Synthetic materials are an alternative to natural ECM proteins and can be advantageous in that their physical properties and surface chemistry can be modified for biological purposes. Muscular thin film technology (Alford et al. 2010) features an elastic film of PDMS used to culture a sheet of cells. The films possess geometric cues to aid cell organisation and can be used to measure the contractile properties of the tissues on them by measuring the degree of film contraction using imaging techniques. This technique has been demonstrated with vascular smooth muscle cells where endothelin-1 was used to trigger contraction (Alford et al. 2011). This approach has since been adapted for 'muscle on a chip' experiments (Grosberg et al. 2012) and repeated using airway

smooth muscle cells (Nesmith et al. 2014). Film cultures however are essentially 2D cultures and therefore do not replicate the ECM found *in vivo*.

Electrospinning is a method of producing fibres in the nanofibre to microfibre range whereby a plethora of different polymers, both natural and synthetic, can be used (electrospinning theory will be discussed in further detail in chapters 2 and 4). Electrospinning has previously been used to generate a range of scaffolds for the culture of smooth muscle including tubular structures simulating blood vessels for the culture of vascular smooth muscle (Wang et al. 2014; Elsayed et al. 2015)and nanofibre scaffolds for assessing smooth muscle growth and ECM production *in vitro* (Zhong et al. 2015).

1.7 Thesis Aims

The overall aim of this thesis is to develop a tissue engineered model of smooth muscle contraction that can be used to directly measure contractile force in response to different agonists. The model will be created using primary cells (with the future potential to use cell lines or stem cell derived SM cells) cultured upon aligned electrospun fibrous scaffold that will facilitate the proliferation of a uniaxially aligned confluent population of cells. The design of the model will allow it to be attached to force transducers, in a similar manner to *ex vivo* smooth muscle strips, allowing direct force measurement during contraction. The developed model could be used in drug screening test or to investigate mechanisms in smooth muscle contraction and/ or diseases that affect smooth muscle function such as asthma. This will reduce the need for *ex vivo* tissues and provide a reproducible model that can be used in both mechanistic and pharmacologic tests.

In order to reach this aim, the following milestones will have to be met:

- A method of isolating of primary smooth muscle cells should be established.
- A method of measuring smooth muscle contraction directly using force measurement apparatus should be established.

- The key parameters in the electrospinning process should be identified and investigated in order to produce uniform, aligned scaffolds.
- A range of flexible scaffolds that can support SM contraction should be produced.
- Primary SM cells should be cultured upon the scaffolds; cell phenotype and proliferation should be monitored during culture.
- The attachment of cell seeded scaffolds to the force monitoring apparatus in order to directly measure agonist induced SM contraction should be carried out.

2. General Materials and Methods

2.1 Electrospinning

Electrospinning is a process of drawing out polymer fibres from a polymer solution or melt through a capillary/needle using a high voltage. A typical electrospinning setup consists of a syringe containing the polymer solution, a needle, a syringe pump, a high voltage power supply and a collector. The capillary is charged and a grounded collector plate is placed facing opposite the capillary. Once the electrostatic forces overcome the surface tension of the polymer solution, the polymer is ejected from the capillary in a jet and it is collected as fibres on the grounded collector. Aligned fibres can be collected using a rotating mandrel collector. A diagram of the typical electrospinning setup used in this work is displayed in **Figure 2.1**.

Solutions of the desired polymer were stirred using a magnetic stirrer overnight at room temperature. The solutions were added to a 10 ml (PET) or 5 ml (gelatin and GelMa) polypropylene syringe (BD Falcon™, Oxford, UK) and placed in a syringe pump (Harvard Apparatus Ltd., Kent, UK). A needle was then attached to the syringe (18G blunt tip unless otherwise stated) and using crocodile clips, the needle was attached to a high voltage power supply and the collector plate/mandrel was grounded. The syringe pump was allowed to run until the solution first passed through the needle tip before applying an electric potential to the needle. Pump rates, spinning times and voltage applied were dependant on the solution concentration and polymer and are detailed in the relevant results chapters. Fibres were collected on either a stainless steel plate or a rotating mandrel. Mandrel speeds were dependant on desired fibre orientation ranging from 60 to 2000 rpm. A needle to collector distance of 15 cm was used in all electrospinning processes. All electrospinning was carried out at ambient temperature and humidity in a ventilated fume cabinet.
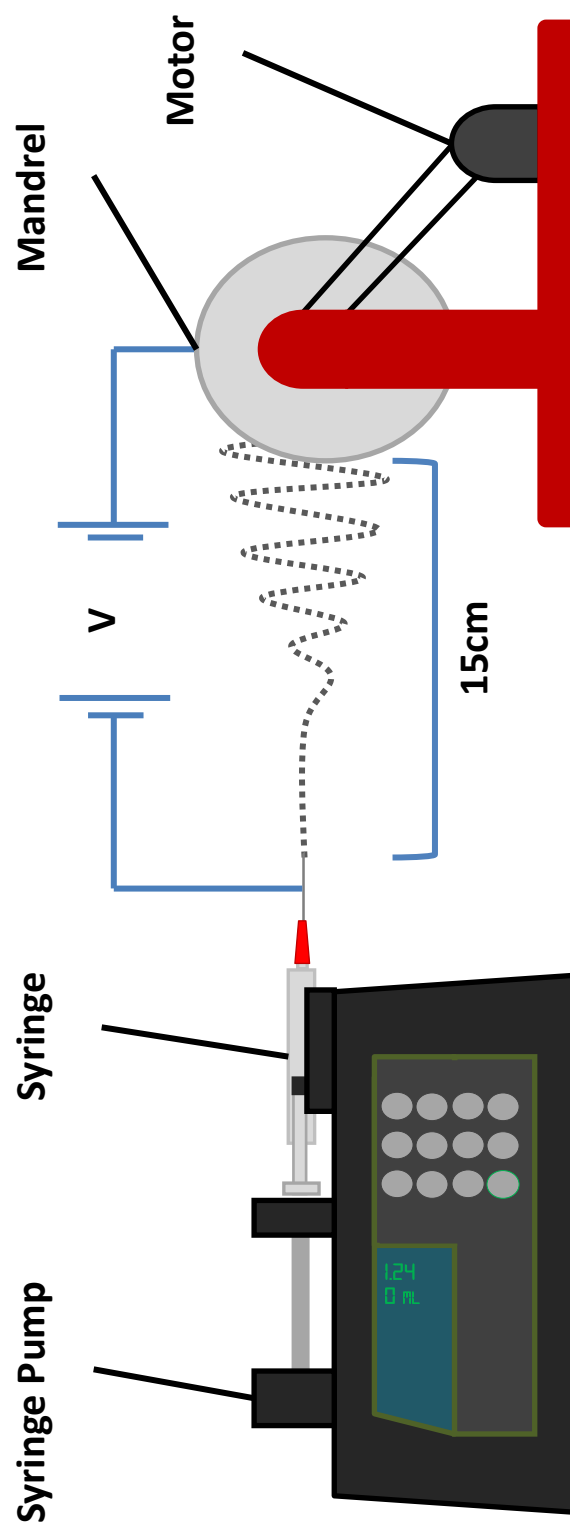
Figure 2.1: Diagram of a typical electrospinning setup with the capability to generate aligned fibrous scaffolds**.** The setup as shown was housed in an externally vented fume hood.

2.2 Scanning Electron Microscopy

Scanning electron microscopy (SEM) is a form of microscopy that involves the use of a focussed beam of electrons ejected from a heated filament (usually tungsten). The electrons act as a source of illumination which gives a much higher resolution than light microscopy (which is limited by the wavelength of visible light). The electron beam scans the surface of the sample and secondary electrons are released by the sample. Secondary electrons are detected and used to generate an image of the sample, giving structural and topographical information about the sample (Reimer 1998).

Samples of electrospun scaffolds were cut out using an 8.0 mm diameter biopsy pen and mounted on SEM holders using graphite adhesive SEM pads (Agar Scientific, Essex, UK). Samples were gold coated for 5 minutes (Balzers Union SCD 030, Balzers Union Ltd., Liechtenstein). Samples were then imaged at 20-30 kV using a scanning electron microscope (JEOL JMS-6060 LV, JEOL Ltd., Welwyn Garden City, Hertfordshire, UK) at different magnifications.

2.3 Uniaxial Tensile Testing

Uniaxial tensile tests were performed on 3 replicate samples of the aligned PET scaffolds and cross-linked gelatin scaffolds (n=3). Samples of PET scaffolds were cut out (30mm in length and 3 mm in width) using a 'dog-bone' shape stencil and blade so that the fibres ran parallel to the direction of the applied load. Samples of cross-linked gelatin scaffolds held in acetate frames (available scaffold size 32 x 12.5 mm; fibres aligned parallel to length) were prepared by cutting the scaffold away from the frame along the length of the sample and cutting the frame on each side. Samples were tested on a 5969 Universal testing system (Instron, High Wycombe, UK) with a 50N load cell operating with an extension rate of 5 mm min^{-1}. A Video Gauge (Imetrum Ltd., Bristol, UK) was used to measure the strain. The Young's moduli of the samples were calculated from the resultant stress/strain curves.

2.4 Mammalian Cell Culture

2.4.1 Primary Human Airway Smooth Muscle (HASM) Cells

Primary HASM cells from non-asthmatic individuals were isolated from bronchial biopsies at the Glenfield General Hospital (Leicester, UK) as described previously (Kaur et al. 2006). The research was approved by the Leicestershire Ethics Committee, and patients gave their written, informed consent. Primary HASM cells (frozen) were received from colleagues at Glenfield General Hospital between passage 2 and 6. Cells were defrosted and cultured (up to passage 8) in DMEM (Gibco, Fisher Scientific, Loughborough, UK) supplemented with 10% (*v/v*) FBS (Sigma Aldrich, Dorset, UK), 1% (*v/v*) antibiotic antimycotic solution (10000 units ml^{-1} penicillin G, 100 mg ml^{-1} streptomycin sulphate and 25 µg ml^{-1} amphotericin B) (Fisher Scientific), and 1x non-essential amino acids (Sigma Aldrich). Cells were cultured in 75 cm^2 tissue culture flasks at 37°C, 5% CO_2 in air.

2.4.2 Isolation of Primary Rat Aortic Smooth Muscle (RASM) Cells

Male Wistar rats (200-225g) were killed by stunning and exsanguination, using an approved Schedule 1 method of euthanasia. All procedures were approved by the animal welfare and ethical review body of the University of Nottingham. Rats were sacrificed for a separate study; the unwanted aorta was harvested for this study. The rat aorta was dissected from the aortic arch to the abdominal aorta and placed in a zero Ca^{2+} dissection buffer solution (5.40 mM KCl, 137.0 mM NaCl, 0.50 mM $NaHPO_4$, 0.44 mM NaH_2PO_4, 10.0 mM glucose, 10.0 mM HEPES, 1.0 mM $MgCl_2$) on ice. The aorta was washed in ice-cold zero Ca^{2+} dissection buffer and excess connective tissue removed using forceps. The aorta was placed in a low Ca^{2+} buffer (5.40 mM KCl, 137.0 mM NaCl, 0.50 mM $NaHPO_4$, 0.44 mM NaH_2PO_4, 10.0 mM glucose, 10.0 mM HEPES, 1.0 mM $MgCl_2$, 0.10 mM $CaCl_2$) and incubated at 37°C for 5 minutes. The aorta was cut into small sections and placed in 2 ml papain solution (≥15 units ml^{-1} papain from papaya latex, 5.83 mM 1,4-dithioerythritol, 0.90 mg ml^{-1} BSA, 5.40 mM KCl, 137.0 mM NaCl, 0.50 mM $NaHPO_4$, 0.44 mM NaH_2PO_4, 10.0 mM glucose, 10.0 mM HEPES, 1.0 mM $MgCl_2$,

0.10 mM $CaCl_2$; Sigma Aldrich) before incubation at 37°C for 45 minutes. Aortic tissue was extracted from the papain solution and washed in BSA (Sigma Aldrich) solution (low Ca^{2+} solution plus 0.90 mg ml^{-1} BSA) 3 times before transferring into 3 ml RASM media (high glucose DMEM supplemented with 10% (*v/v*) FBS and 1% (*v/v*) antibiotic/antimycotic solution (10000 units ml^{-1} penicillin G, 100 mg ml^{-1} streptomycin sulphate and 25 μg ml^{-1} amphotericin B). The tissue was firmly agitated by pipetting for 30 seconds to release cells from the digested tissue before the cell suspension was transferred into two collagen coated T-25 flasks (flasks were incubated in 0.03 mg ml^{-1} type I bovine collagen (PureCol®, Advanced Biomatrix, San Diego, CA) in PBS (Fisher Scientific) solution at 37°C for 60 minutes) containing 5 ml RASM media. Flasks were incubated (at 37°C, 5% CO_2 in air) for 48 hours before the media was changed to remove decellularised tissue and unattached cells.

2.4.3 Culture of RASM cells

RASM cells at P0 obtained from enzymatic digestion of rat aorta (section 2.4.2) were cultured in RASM media at 37°C, 5% CO_2 in air. Cells were cultured for 5 days following isolation before first passage. Subsequent passages were carried out every 7 days; cells were split using a 1 in 6 dilution and cultured up to passage 3 in collagen coated flasks. Cells seeded into collagen gels and onto scaffolds were used at passage 2-3.

2.4.4 Passaging cells

SM cells that had reached approximately 90% confluency were deemed ready for passage; C2C12s (discussed in chapter 3) were passaged between 70 – 80% confluency. Culture media was aspirated from flasks and cells washed thoroughly with PBS solution. Trypsin-EDTA (0.05%) solution (Fisher Scientific) was added in sufficient volume to cover the surface of the culture flask and the flask incubated (at 37°C, 5% CO_2 in air) for 5 minutes to allow for cell detachment. Detachment of cells was assessed visually under a light microscope. RASM cell detachment also required the use of a cell scraper to detach all cells. The trypsin was

deactivated by the addition of serum containing culture medium (volume was equivalent to 2 times the volume of trypsin added) and the cell suspension transferred to a centrifuge tube. Cells were collected by centrifugation (200XG) and supernatant removed. The cell pellet was re-suspended in a known quantity of culture medium and counted. Cells were then re-plated into T-flasks or used for experiments.

2.4.5 Counting Cells

Cells in a suspension of known volume were counted using a Neubauer haemocytometer. Cell suspension (10 µl) was added to 90 µl of trypan blue solution (Sigma Aldrich) and mixed thoroughly by pipetting. The resultant cell suspension (10 µl) was added to each chamber of the haemocytometer. The number of viable cells in each corner 1 mm^2 square (of both chambers) was counted under a light microscope (viable cells do not take on the trypan blue dye due to possessing intact plasma membranes).The total number of viable cells was divided by 8 to calculate the average number of viable cells per corner square; this was then multiplied by 10 to account for the dilution factor in trypan blue. This number was multiplied further by 1x10^4 to calculate the number of cells per ml of the original cell suspension.

2.4.6 Freezing and Resuscitation of Cells

Excess C2C12 cells were frozen down following cell passage and counting. Cells were suspended in C2C12 growth medium (90% *v/v*) and dimethyl sulfoxide (10% *v/v*) at a density of 2x10^6 cells ml^{-1}. Each 1ml of cell suspension was transferred to a 1.8 ml cryovial (Fisher Scientific) and cooled at a rate of approximately -1°C minute^{-1} (using a Mr Frosty (Fisher Scientific)) to -80°C overnight. The cryovials were then transferred to storage under liquid nitrogen. HASM cells were received cryopreserved and were stored under liquid nitrogen until required.

Cells were resuscitated from cryopreservation by rapidly warming to 37°C in a water bath and plated into a T-75 flask containing 10 ml of C2C12 growth media/ HASM culture media.

2.5   Cell Viability Assays

The active chemical of both the alamarBlue® and PrestoBlue® assays is the blue, weakly fluorescent dye resazurin (7-Hydroxy-3H-phenoxazin-3-one 10-oxide). Upon entering metabolically active cells, the dye is reduced in the mitochondria to resorufin which is highly fluorescent. Measuring the fluorescence of a sample of dye solution that has been incubated with cells is therefore a good indicator of metabolic activity and therefore viability (O'Brien et al. 2000). The protocols for each assay are described in detail in the chapters 3 and 5 respectively.

2.6   Immunocytochemistry

Immunocytochemistry (ICC) provides a method of visualising specific proteins within cells by using antibodies that bind specifically to epitopes on the protein of interest (Bancroft & Gamble 2001). In order to carry out ICC, samples firstly need to be fixed and permeablised. Fixation denatures proteins within the cell by either coagulation or by forming crosslinks between proteins in the cells, binding soluble proteins to the cytoskeleton. This prevents the decay of the tissue and preserves the cells within. This is commonly done by incubating the sample in an aldehyde solution (such as formaldehyde or glutaraldehyde). Formaldehyde binds to the residues of basic amino acids such as lysine, glutaraldehyde has a similar method of fixation however as it is a larger molecule, can form cross-links between more distant molecules. Another fixation method is to dehydrate the sample using alcohols such as methanol and ethanol. This causes soluble proteins within the cell to precipitate. One advantage of fixing with alcohols is that they can permeablise the cells during fixation. Prolonged chemical fixation can lead to excessive crosslinking and the masking of target proteins. Where permeablisation is necessary, this can be achieved using detergents such as saponin, Triton X-100 and Tween-20. Following sample fixation and permeablisation, samples require blocking. Blocking involves incubation of the samples in a serum solution (usually the same species as in which the secondary antibody is raised) which binds to non-specific sites within the cells. This

prevents the secondary antibody (bound to the fluorophore) from binding to sites other than the intended antigen; preventing background fluorescence or a false positive. Following blocking, the samples can be incubated with the necessary antibodies. Primary antibodies (usually monoclonal antibodies) are added to bind to the protein of interest. Although some antibodies are also tagged with a fluorophore (direct immunofluorescence), most are not and so a secondary antibody is required; this two antibody approach is known as indirect immunofluorescence and is the method used in this body of work. Secondary antibodies are conjugated to a fluorophore (usually fluorescein isothiocyanate (FITC) or tetramethylrhodamine isothiocyanate (TRITC)) and are targeted towards IgG in the species in which the primary antibody was raised. This results in the secondary antibody binding to the primary antibody, allowing it to be visualised under light of a specific wavelength. Samples stained using ICC are imaged using fluorescence microscopy. The individual steps of indirect immunofluorescence are illustrated in **Figure 2.2**.

All samples were washed with PBS prior to fixation with 3.8% (w/v) paraformaldehyde (10 minutes at room temperature). Samples were permeablised using a 0.5% (*v/v*) Triton X-100 in PBS (5 minutes, 4°C) and then blocked sequentially with a 3% (*v/v*) BSA, 1% glycine (*w/v*) solution (1 hour, room temperature) followed by a 10% (*v/v*) goat serum solution in PBS (1 hour, room temperature). Samples were incubated with primary antibodies (1 in 200 dilution in 10% (*v/v*) goat serum in PBS) at 4°C overnight. Fluorescently tagged secondary antibodies (1 in 800 dilution in PBS) were then used to visualise the desired proteins. All antibodies used in this thesis are listed in **Table** 1; all listed antibodies were used at a dilution of 1:200. Nuclei were stained with Hoechst dye (Fisher) using a 1 in 833 dilution in PBS (10 minutes) or DAPI (Fisher) (1 in 10000 dilution, 10 minutes) and actin was stained (1:100 dilution, 10 minutes) using Alexa Fluor 488 conjugated phalloidin (Life Technologies, Paisley, UK). Samples were imaged using a Leica TCS SP2 laser scanning confocal inverted microscope (Leica Microsystems Ltd, Milton Keynes, UK) or a Leica DM2500 M fluorescent microscope.
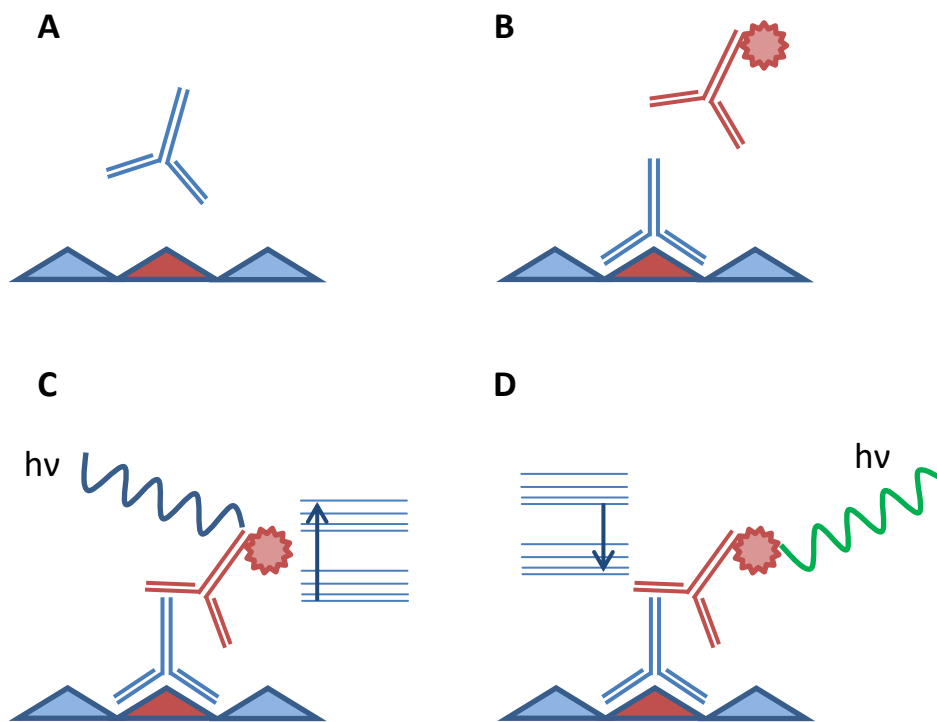
Figure 2.2: Steps involved in indirect immunofluorescence. Primary antibody binds specifically to antigen of interest (**A**). Secondary antibody binds to primary antibody (**B**). Fluorophore is excited by photon of specific wavelength (**C**). Fluorophore emits lower energy photon (**D**).

2.6.1 Analysis of ICC images

Fluorescently stained samples were visualised using Leica Application Suite, images were then analysed using ImageJ. Nuclei alignment was calculated using particle analysis on binary images of Hoechst stained cell nuclei. Surfacecoverage was determined by calculating the fraction of confocal z-stack images that were not stained for SM22α. SM marker positivity was calculated by counting the number of nuclei co-expressing the marker of interest and subtracting from the total nuclei present. Cell density was determined by dividing the number of nuclei visible per micrograph by micrograph area.

2.7 Statistical Analysis

All statistical tests were carried out using the GraphPad prism 6 software package (GraphPad Software Inc. San Diego, CA). Each statistical test carried out is stated in the relevant chapters and figure legends. Statistically significant results are represented with asterisk(s) (*, **, ***, ****) and represent P values ≤0.05, 0.01, 0.001 and 0.0001 respectively

	Antibody	Species	Supplier	Product Code
Primary	Calponin	Rabbit	Abcam	ab46794
	Connexin	Rabbit	Sigma Aldrich	C6219
	Desmin	Mouse	Sigma Aldrich	D1033
	SM22α	Rabbit	Abcam	ab14106
	Vinculin	Mouse	Sigma Aldrich	V4505
Secondary	Alexafluor 488 anti rabbit IgG	Goat	Invitrogen	A-11008
	Rhodamine ant mouse IgG	Goat	Invitrogen	R-6393

Table 2.1: List of antibodies used for immunostaining

3. Developing a hydrogel based model of smooth muscle contraction

3.1 Introduction

Organ bath studies using isolated tissue preparations are well-established procedures within the field of pharmacology and have been carried out for over a century (Waugh Young 1914). Traditionally used to investigate the physiological and pharmacological response of contractile tissues such as smooth and skeletal muscle, organ baths allow the force or displacement generated by *ex vivo* tissue preparations in response to stimulation to be measured. A typical organ bath setup consists of a vessel containing an oxygenated physiological buffer solution maintained at 37 °C with a fixed anchor point at the bottom and a force transducer above. By attaching a tissue preparation to these two points (usually *via* a cotton thread or nylon suture), any contraction of the tissue can be detected by the force transducer. An example of this is the study by Urquilla who investigated the dose dependent effects of the pyrimidine nucleotide uridine 5'-triphosphate (UTP) on the contraction of SM within human and canine cerebral arteries (Urquilla 1978). In the study it was found that UTP stimulated dose-related contractions within the range of 1.7 µM to 170 µM in canine arteries. Later organ bath studies testing UTP on bovine cerebral artery strips found that UTP can also stimulate vascular SM relaxation *via* an endothelium mediated mechanism in addition to contraction (Miyagi et al. 1996).

The main drawback of using organ bath studies to assess the pharmacological effects of new drug candidates in humans is that in order to carry out the studies, freshly isolated human tissue is required. This can require tissue from both healthy and diseased donors which creates problems such as limited tissue availability, donor site morbidity and, (depending on the tissue required) the necessity for skilled individuals to carry out complex biopsies (Clark et al. 1977).

With increasing evidence that animal models do not accurately predict clinical outcomes in humans (Shin et al. 2009) an attractive alternative to using human tissue would be to use tissue engineered constructs; tissues created from isolated human cells seeded within or upon a biomimetic and biocompatible scaffold. This would allow for multiple cell-scaffold constructs to be produced from a single donor; additionally, if human derived stem cells were to be used as the cell source, this would reduce the need for donor tissue altogether. In order to pass as a suitable replacement however, these tissue engineered alternatives need to provide functional outputs that correlate with those obtained from *ex vivo* tissue and ultimately with the tissue *in vivo*. In the case of tissue engineered muscle constructs, both smooth and skeletal, the key functional output is contraction. In order to measure contraction, these cell-scaffolds constructs therefore also need to be mechanically robust to survive contraction assays similar in nature to organ bath experiments.

Hydrogels made from naturally occurring ECM proteins such as collagen (Antoine et al. 2014) have received a lot of attention in the field of engineering muscle tissues *in vitro*, with collagen hydrogels used in cartilage (Bosnakovski et al. 2005), nerve (Martens et al. 2014), skin (Lee et al. 2009), skeletal (Vandenburgh et al. 2008), cardiac (Duan et al. 2011), and smooth muscle (Berglund et al. 2003) engineering. Collagen is the most abundant protein found within the human body with type I collagen being a key component of the ECM in connective tissues (Di Lullo et al. 2002).The structure of collagen comprises of a tight triple helix of two identical chains and a third chain with a differing composition of amino acids. Glycine is the most abundant amino acid within collagen appearing at every third residue in the peptide chain. This allows the tight triple helix to exist as glycine is the smallest amino acid offering the least steric hindrance. Proline and hydroxyproline are the next most common residues in collagen with glycine-proline-hydroxyproline being the most common motif in the amino acid sequence (Ramshaw et al. 1998). Collagen hydrogels are therefore a favourable cell matrix scaffold for use in tissue engineering applications (DeLustro et al. 1986). In addition, the hydrogels can be set within specific shaped moulds (Yost

et al. 2005) or possess micro patterned surfaces (Chiu et al. 2012); and the low stiffness of collagen hydrogels (Achilli & Mantovani 2010) can allow cells to contract and remodel them (Legant et al. 2009).

The disadvantages of collagen gel studies are that bulk gels do not give any topographical or directed mechanical cues to cells seeded within them leading to randomly displaced and oriented cell populations (Ceresa et al. 2009). This does not represent the anisotropic nature of many of the tissues that these gels attempt to recreate. This can be overcome by culturing the gels between two fixed points such as posts (Oishi et al. 2000), cantilevers (Boudou et al. 2012), or mesh frames (Smith et al. 2012). Cellular attachment to the fibrillar matrix leads to the formation of uniaxial tension between the two points; this creates a mechanical cue which cells then align upon. Additionally, due to their low mechanical properties, collagen gels are very fragile meaning that attaching them to force measuring equipment such as organ baths usually results in failure. Allowing the cells to remodel the gels prior to force measurement studies however, does increase the stiffness (Raub et al. 2010) and compliancy to an extent but they remain more fragile than *ex vivo* tissues.

By seeding SM cells within collagen gels in well plates it is possible to visually assess the contraction of the gels due to both remodelling (Kuzuya et al. 2004) and agonist induced contraction (Rosenfeldt et al. 2003) It is also possible to assess the effects of antagonists on SM contraction (Sakota et al. 2014). By using this experimental design, Matsumoto and co-workers were able to assess the contractile properties of airway SM cells from donors both with and without asthma. In the study they found that asthmatic airway SM seeded gels contracted more in response to histamine than those seeded with non-asthmatic airway SM cells (Matsumoto et al. 2007). Contraction was measured in all of these studies by measuring the reduction in collagen gel size, an indirect way of measuring force which will not take into account the increasing stiffness of the gels as they contract. As the gels contract due to cellular attachment without agonist stimulation, the cell density of the gels can be a limiting factor in these experiments. Additionally, due to the circular shape of the gels, contraction is

radial which leads to an uneven distribution of cells within the gel. Although useful at observing the effects of pharmacological agents on SM cells, more accurate data on SM contraction would be obtained if uniaxial contractile force could be directly measured in gels containing an aligned population of cells.

Studies that set out to directly measure the mechanical forces generated by cells within a collagen hydrogel matrix require the experimental apparatus with the capability to do so. However it is only within recent years that commercially available bioreactors have entered the market with the ability to measure force and/ or apply a mechanical load to cultures; examples include the Ebers TC-3F (www.ebersmedical.com) and the TA Electroforce bioreactor (http://www.tainstruments.com). Therefore, many early studies investigating mechanical forces generated in tissue engineered constructs required the in house development of bespoke apparatus. One design that was developed by Eastwood and co-workers (Eastwood et al. 1994; Eastwood et al. 1996) was the culture force monitor (CFM), which contains a force transducer that can measure uniaxial force generated within contracting collagen gels. The first studies using the CFM investigated the attachment forces generated by fibroblasts at different densities and from different tissue types finding different contraction profiles generated by different cell populations. The majority of later studies using the CFM have focussed on analysing contraction produced by tissue engineered skeletal muscle constructs however one study by Cheema *et al* investigated the contraction of separate collagen gels seeded with rabbit bladder SM cells as well as those seeded with human dermal fibroblasts and mouse myofibroblasts (C2C12). In this study, the rabbit SM constructs were found to produce greater contraction than both the fibroblast and C2C12 constructs over a 24 hour period (Cheema et al. 2003). It is worth noting however, that this study was looking at the initial contractile forces associated with cellular attachment to the collagen matrix; the SM cells in this study were not chemically stimulated to contract. Over time, the size of the collagen constructs tested on the CFM has been scaled down. Earlier experiments attached 5 ml constructs to the CFM (Cheema et al. 2003; Brady et al. 2008; Mudera et al. 2010), with 3 ml constructs later used by

Sharples *et al* on an amended CFM (referred to as CFM mk2) (Sharples et al. 2012). Currently, 2 ml collagen constructs are regularly tested using CFM (unpublished data). In addition to the CFM, other bespoke devices such as the Mechanical Cell Stimulator (MCS) have been developed with similar objectives (Powell et al. 2002). Images of both the CFM and MCS are shown in **Figure 3.1 A** and **B** respectively. The MCS is designed to house commercially available 6 well plates containing collagen based skeletal muscle constructs which can be mechanically stimulated using a stepper motor. The MCS, likewise to the CFM, also contains two load cells that can monitor the tension within two of the constructs within the well plate. Both the MCS and CFM have been used to measure the contractile forces of skeletal muscle cells cultured within collagen constructs (Sharples et al. 2012; Powell et al. 2002). It is worth noting however, that in both studies the contraction measured was not active contraction of the muscle cells but the contraction of the engineered constructs caused my cellular remodelling of the collagen hydrogels.

An alternative approach to building force monitoring apparatus is to design the engineered tissue in a way that allows it to be directly attached to a force transducer with very little manual manipulation required. Dennis and Kosnik cultured myooids from rat myogenic precursor cells around synthetic tendons pinned into a sylgard coated petri dish (Dennis & Kosnik 2000). Over time, the cells formed a muscle like structure between the two synthetic tendons. By attaching the minuten pin holding one of the tendons in place to a force transducer and gently removing it from the sylgard base; they managed to directly attach the tissue engineered myooid to the transducer without handling the construct itself. The other tendon remained pinned to the dish to act as an anchor point. This allowed them to electrically stimulate the constructs and directly measure active force generation. This experimental design was used and adapted by Baar and co-workers to measure the contractile force of cultured skeletal muscle constructs from both primary rat cells (Huang et al. 2005) and C2C12s (Khodabukus & Baar 2009) seeded within fibrin based gels. This approach to measuring the contraction of skeletal muscle constructs in fibrin gels has
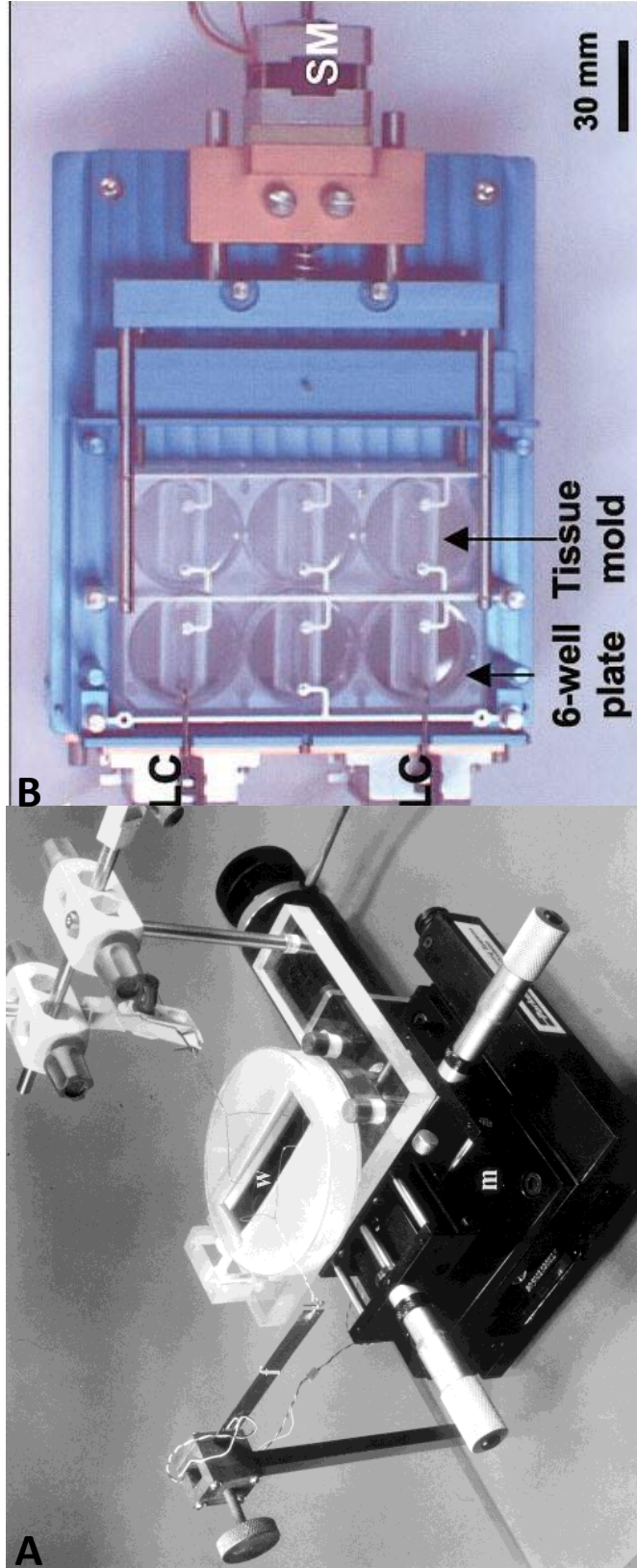
Figure 3.1: Apparatus for measuring forces in 3D constructs. Images of the CFM developed by Robert Brown and co-workers at University College London (**A,**(Eastwood et al. 1998)) and the MCS developed by Herman Vandenburgh and co-wowkers at Brown University, Rhode Island (**B,** (Powell et al. 2002)).

recently been applied to co-cultures of myoblasts and motor neurons (Martin et al. 2015).

This chapter explores the ability of primary SM cells to contract collagen based hydrogels due to both initial cellular attachment and agonist stimulated contraction of the SM cells. It will investigate methods to culture the gels in a way that can induce an aligned cell population within the gel and importantly, to develop methods to measure SM contraction; both indirectly through imaging of the gels, and directly by live measurement of the force generated during agonist induced contraction.

3.2   Chapter Aims

The work carried out within this chapter aims to achieve the following:

Develop a method for measuring the forces generated during the agonist induced contraction of smooth muscle cells seeded within a 3D matrix. This will be achieved by:-

- Using image analysis techniques, measure the level of contraction of SM seeded collagen gels in response to a chemical agonist.

- Replicate an established C2C12 collagen gel based skeletal muscle model and use it to assess the suitability of the CFM for measuring SM contraction.

- Adapt the C2C12 model design for the culture of SM constructs.

- Measure the contractile force of these SM constructs using live force monitoring apparatus such as the CFM.

- Test the sensitivity of the constructs to agonist concentration and investigate how this affects contractile force.

- Assess the effects of antagonists of SM contraction in SM constructs.

3.3 Materials and methods

3.3.1 HASM collagen gel contraction assay

Primary human airway SM cells from 3 separate donors (passage 2-4) were seeded into a collagen solution at a final density of 4×10^5 cells ml^{-1}. Collagen solution (2 mg ml^{-1}) was made up (per ml of collagen solution) by adding 598 µl PureCol® type I bovine collagen solution (conc. 3 mg ml^{-1}) in 0.01 M HCl (Advanced Biomatrix, San Diego, CA) to 74 µl 10X DMEM (Sigma) and mixed thoroughly. The mixture was neutralised with ($\approx$ 40 µl) 4M NaOH (made from NaOH pellets, Sigma) until a colour change (yellow to pink) was seen. SM cell suspension in (288 µl) serum free DMEM (Gibco, Life Technologies) was added. The collagen solution was then pipetted into a 24 well plate (Nunc, Thermo Scientific) (500µl per well) and incubated for 60 minutes (37°C, 5% CO_2 in air) to allow the gels to set. Gels were carefully detached from the sides of wells using a sterile needle before the well plate was imaged using a flatbed scanner (Epson UK, Hertfordshire, UK). Serum free DMEM (1ml) ± agonist (histamine 100µM (Sigma), bradykinin 100nM (Sigma)) was added to each well and the gel constructs incubated. Plates were imaged at selected time points to assess gel contraction. Images were analysed using ImageJ. N=3 gels per condition, 3 separate experiments using cells from 3 different donors.

3.3.2 RASM collagen gel contraction assay

Primary rat aortic SM cells (RASM cells) obtained from 3 separate rats were trypsinised and counted at passage 3. The cells were seeded into a collagen solution at 3 densities; 2×10^5, 5×10^5 and 1×10^6 cells ml^{-1}. Collagen solution (2 mg ml^{-1}) was made up (per ml of collagen solution) by adding 598 µl PureCol® type I bovine collagen solution (conc. 3 mg ml^{-1}) in 0.01 M HCl (Advanced Biomatrix) to 74 µl 10X DMEM (Sigma) and mixed thoroughly. The mixture was neutralised with $\approx$ 40 µl 4M NaOH (made from NaOH pellets, Sigma) until a colour change

(yellow to pink) was seen. The different cell suspensions in (288 µl) serum free DMEM (Gibco, Life Technologies) were then added to the collagen solution and mixed thoroughly. The collagen solutions were pipetted into a 24 well plate (Nunc, Thermo Scientific) (500µl per well) and incubated for 60 minutes (37°C, 5% CO_2 in air) to polymerise. Gels were carefully detached from the sides of wells using a sterile needle before the well plate was imaged using a flatbed scanner (Epson UK,). 1ml RASM culture media was added to each well and the plate incubated (37°C, 5% CO_2 in air) overnight to allow the cells to remodel the gel *via* cellular attachment. The plate was then imaged before the media was aspirated and the gels washed with PBS (Fisher Scientific) 3 times. Serum free DMEM (1ml) ± UTP (Fisher) at multiple concentrations (1 µM, 10 µM, 100 µM and 1mM) was added to each well and the gels incubated. The plate was imaged after 30 min to assess gel contraction. Images were analysed using ImageJ. N=3 gels per condition, 3 separate experiments using cells from 3 different donors.

3.3.3 C2C12 cell culture

C2C12 murine skeletal myoblasts(Yaffe & Saxel 1977) (HPA Culture Collections) were cultured in T75 and T175 flasks in C2C12 growth media (GM) consisting of DMEM (Gibco, Life Technologies) supplemented with 20% (v/v) FBS (Pan Biotech, Aidenbach, Germany) and 1% (v/v) 100X penicillin-streptomycin solution (10,000 U ml^{-1}) (Invitrogen, Paisley, UK). Cells were incubated at 37°C, 5% CO_2 in air until 80-90% confluent before passaging. Cells were used between passages 5 and 10.

3.3.4 Collagen construct apparatus preparation

Three rectangles (15.0 x 6.0 x 1.5 mm) cut from 10 count (10 holes inch^{-1}) polyethylene mesh (Darice Inc., Strongsville, OH, USA) were bound together using 0.3 mm stainless steel orthodontic wire to create 'floatation bars'. Orthodontic wire (0.7 mm) was folded unto a U-shape hook and driven into each floatation bar to create 'A-frames' that are used to attach the floatation bars to glass chambers with specific dimensions (45 x 20 x 7 mm). Once assembled
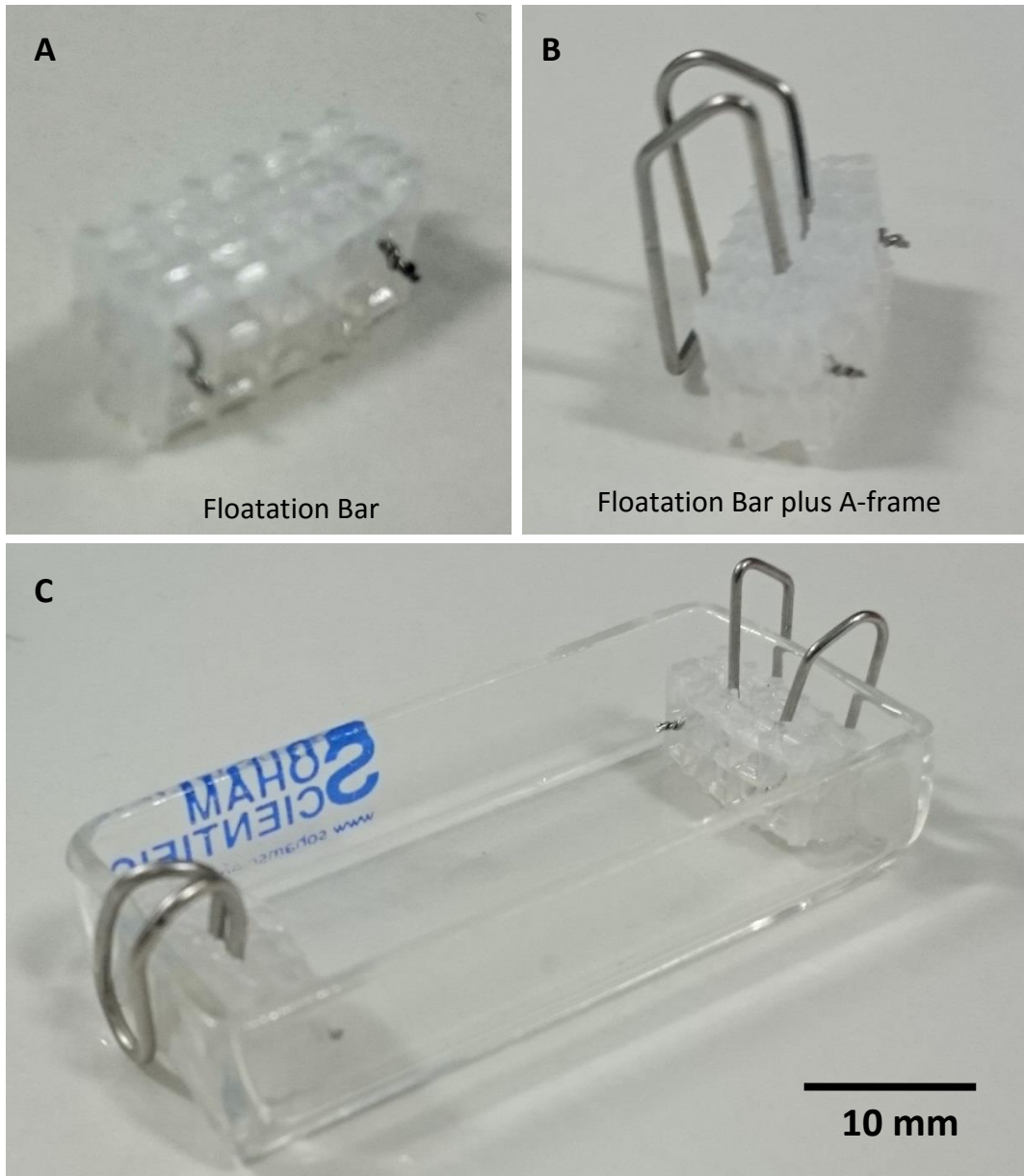
Figure 3.2: Collagen construct setup. Floatation bar manufactured from polyethylene mesh (**A**) and A-frame inserted into the centre of the floatation bar (**B**). Final setup containing two floatation bars in A-frames at each end of a rectangular glass bath(**C**).

(**Figure 3.2**), the chambers with floatation bars and A-frames were sterilised using 70% IMS and UV radiation for 30 minutes before use.

3.3.5 Manufacture of C2C12 Collagen Constructs

The protocol for the manufacture of C2C12 collagen constructs was adapted from those detailed elsewhere (Sharples et al. 2012), (Smith et al. 2012). C2C12 murine skeletal myoblasts at 80-90% confluency between passage 8 and 10 were trypsinised and counted. PureCol® type I bovine collagen solution (1196 µl; conc. 3 mg ml^{-1}) in 0.01 M HCl (Advanced Biomatrix) was added to 148 µl 10X DMEM (Sigma) and mixed thoroughly. The mixture was neutralised with ≈ 80 µl 4M NaOH (made from NaOH pellets, Sigma) until a colour change (yellow to pink) was seen. C2C12 cells ($8x10^6$) suspended in 576 µl of C2C12 GM were added to the collagen mixture and mixed thoroughly. The cell/ collagen solution was then pipetted into a sterile glass chamber fitted with floatation bars and A-frames and incubated (37°C, 5% CO_2 in air) for 60 minutes to allow the gels to set. The gels were detached from the sides of the glass bath using a sterile needle and 4ml C2C12 GM was added to the chamber. Constructs were either immediately attached to the CFM (n= 5 constructs) or cultured to allow formation of myotubes. A flow chart of the individual steps taken to produce the collagen construct is shown in **Figure 3.3**. Constructs used to culture myotubes were incubated at 37°C 5% CO_2 in air for 4 days, during this time the media was refreshed twice every 24 hours. The media was then changed to C2C12 differentiation media (DM) (consisting of DMEM (Gibco, Life Technologies) supplemented with 2% (v/v) horse serum (Pan Biotech, Aidenbach, Germany) and 1% (v/v) 100X penicillin-streptomycin solution (10,000 U ml^{-1}) (Invitrogen) for a further 10 days. The media was changed once every 24 hours during this time. Throughout culture constructs were imaged using a flatbed scanner (Epson); n= 5 constructs.

3.3.6 Manufacture of RASM collagen constructs

The protocol for the manufacture of RASM collagen constructs was adapted from the C2C12 collagen construct protocol. Primary RASM cells at passage 3 were
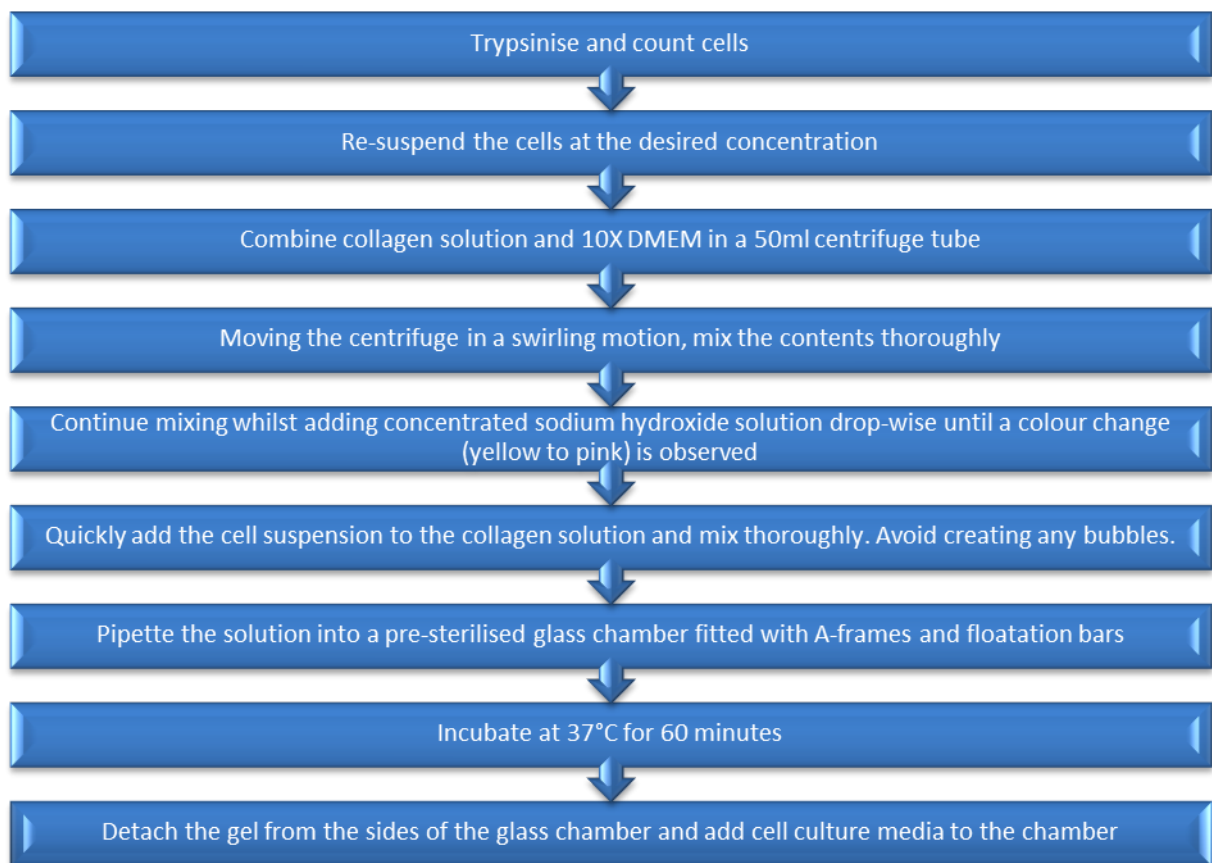
Figure 3.3: Manufacture of collagen constructs. Flow chart dictating the steps required to produce collagen constructs.

trypsinised and counted. PureCol® type I bovine collagen solution (1196 µl; conc. 3 mg ml^{-1}) in 0.01 M HCl (Advanced Biomatrix) was added to 148 µl 10X DMEM (Sigma) and mixed thoroughly. The mixture was neutralised with ≈ 80 µl 4M NaOH (made from NaOH pellets, Sigma) until a colour change (yellow to pink) was seen. RASM cells (1x10^6) suspended in 576 µl of RASM media were added to the collagen mixture and mixed thoroughly. The cell/ collagen solution was then pipetted into a sterile glass chamber fitted with floatation bars and A-frames and incubated (37°C, 5% CO$_2$ in air) for 60 minutes for the gels to set. The gels were detached from the sides of the glass bath using a sterile needle and 3ml RASM media added. Gels were imaged using a flatbed scanner (Epson) and incubated (37°C, 5% CO$_2$ in air) for 3 days. During this period gels were imaged every 24 hours. Media was changed every 24 hours. After 3 days the constructs were used for contractile assays.

3.3.7 Immunostaining of cell seeded collagen constructs

Collagen constructs were detached from the glass chamber *via* removal of the A-frames. Media was removed from the glass chambers and the constructs washed with TBS three times before fixation using an ice cold methanol/acetone solution for 15 minutes. Constructs were then washed with TBS three times before the floatation bars were removed. Samples were then immunostained following the protocol described earlier (**section 2.6**)

3.3.8 Measuring construct contraction using the culture force monitor

Whilst attached to the glass chamber, *via* the A-frames, stainless steel loops made from 0.7 mm orthodontic wire were pressed into each of the floatation bars until secure before removal of the A-frames. All media was aspirated from the glass chamber and the construct was transferred to a PTFE chamber containing 5 ml of serum free DMEM (Gibco) (5 ml of C2C12 GM used for C2C12 constructs). The PTFE chamber was placed in the CFM housing incubator (37°C , 5% CO$_2$ in air) and the stainless steel hoops were placed over the two attachment

hooks of the CFM. This enabled a sensitive force transducer (Measurements Group, Basingstoke, UK) to measure the real-time cell contraction of the collagen gel. The analogue output signal was amplified, digitized and processed through a model P3 strain indicator and recorder (Vishay, Basingstoke, UK). Positionaladjustment of the transducer and fixed hook allows careful positioning of the constructs in the CFM system. Constructs were positioned so that they were straight, free floating and without slack. A diagrammatic explanation of setting up the CFM is given in **Figure 3.4**. The CFM reading was adjusted to zero and recording started. C2C12 constructs were incubated whilst attached to the CFM for 24 hours. RASM constructs were attached to the CFM until a constant force reading was attained. Following this constructs were stimulated with the addition of 1 ml of 600 µM UTP in serum free DMEM to the PTFE chamber. N= 2 RASM constructs tested.

3.3.9 Visual assessment of RASM collagen construct contraction

RASM collagen constructs were removed from incubation 3 days after manufacture. Media was aspirated from the glass chambers and constructs washed twice with serum free DMEM. 2 ml serum free DMEM was then added to each chamber. One A-frame was removed from each construct leaving one floatation bar attached to the glass chamber and the other free floating. Half of the gels tested had the free floatation bar carefully removed from the gel. Glass chambers were placed on a flatbed scanner (Epson) and imaged. UTP (1 ml; 300 µM) was added to each chamber (1 ml serum free DMEM for controls) and chambers imaged every minute for 30 minutes. Images were analysed using ImageJ. N= 5 constructs per condition (attached/ detached).

3.3.10 Measuring RASM collagen construct contraction using muscle physiology apparatus

RASM collagen constructs were removed from incubation 3 days after manufacture. Media was aspirated from the glass chambers and constructs
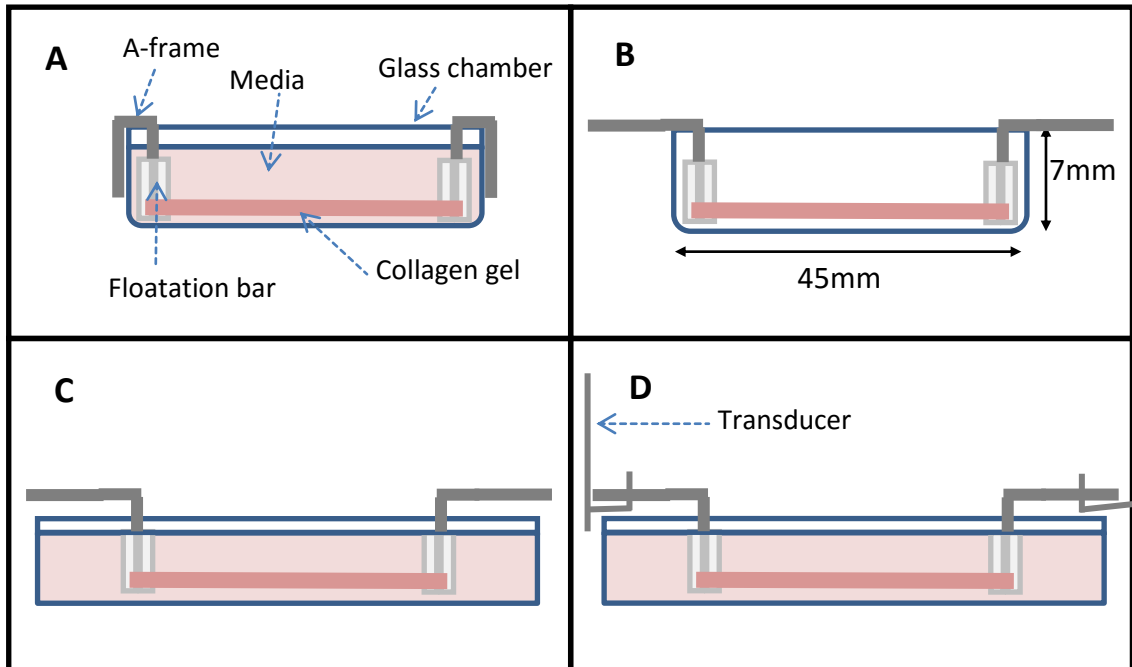
Figure 3.4: Attaching collagen constructs to the CFM. A glass bath containing a set collagen gel construct (**A**) is removed of media and A-frames are replaced with wire hoops (**B**). Construct is placed into a larger PTFE bath (**C**) and hoops are hooked around the force transducer (**D**, left) and fixed anchor (right).

washed twice with serum free DMEM. 2 ml serum free DMEM was then added to each chamber. One A-frame was removed from its floatation bar and a minuten pin adhered to a glass bead was threaded through the underside of the construct in a central position approx. 4 mm away from the floatation bar (**Figure 3.5**). The pin was then attached to a model 403A force transducer (Aurora Scientific,Dublin, Ireland) using canning wax. The force transducer was connected to a Powerlab 4/25T unit with associated software (AD Instruments, Oxford, UK). Force was measured at a frequency of 1 kHz. Once stable, the baseline force of the resting constructs was measured for 3 minutes before the addition of 500 µL of 500 µM UTP in serum free DMEM (500 µL serum free DMEM in control experiments). Contraction was then measured for 60 minutes. N= 4 individual RASM constructs measured following treatment with 100 µM UTP.

3.3.11 Evaluating the effects of agonist concentration on RASM collagen construct contraction

RASM collagen constructs were removed from incubation 3 days after manufacture and attached to a model 403A force transducer (Aurora Scientific) as described in section 3.3.10. Once stable, the baseline force of the resting constructs was measured for 2 minutes before the addition of 500 µl of 50 nM UTP in serum free DMEM once peak force had been attained at this concentration, 500 µl of the media was removed from the glass chamber. After 60 seconds, the UTP concentration was increased by a factor of 10 *via* the addition of 500 µl of a 500 nM solution. The process of increasing the UTP concentration by a factor of 10 for each measurement following the attainment of peak force was repeated until the final concentration added to the bath was 5 mM UTP. N=6 RASM constructs tested.
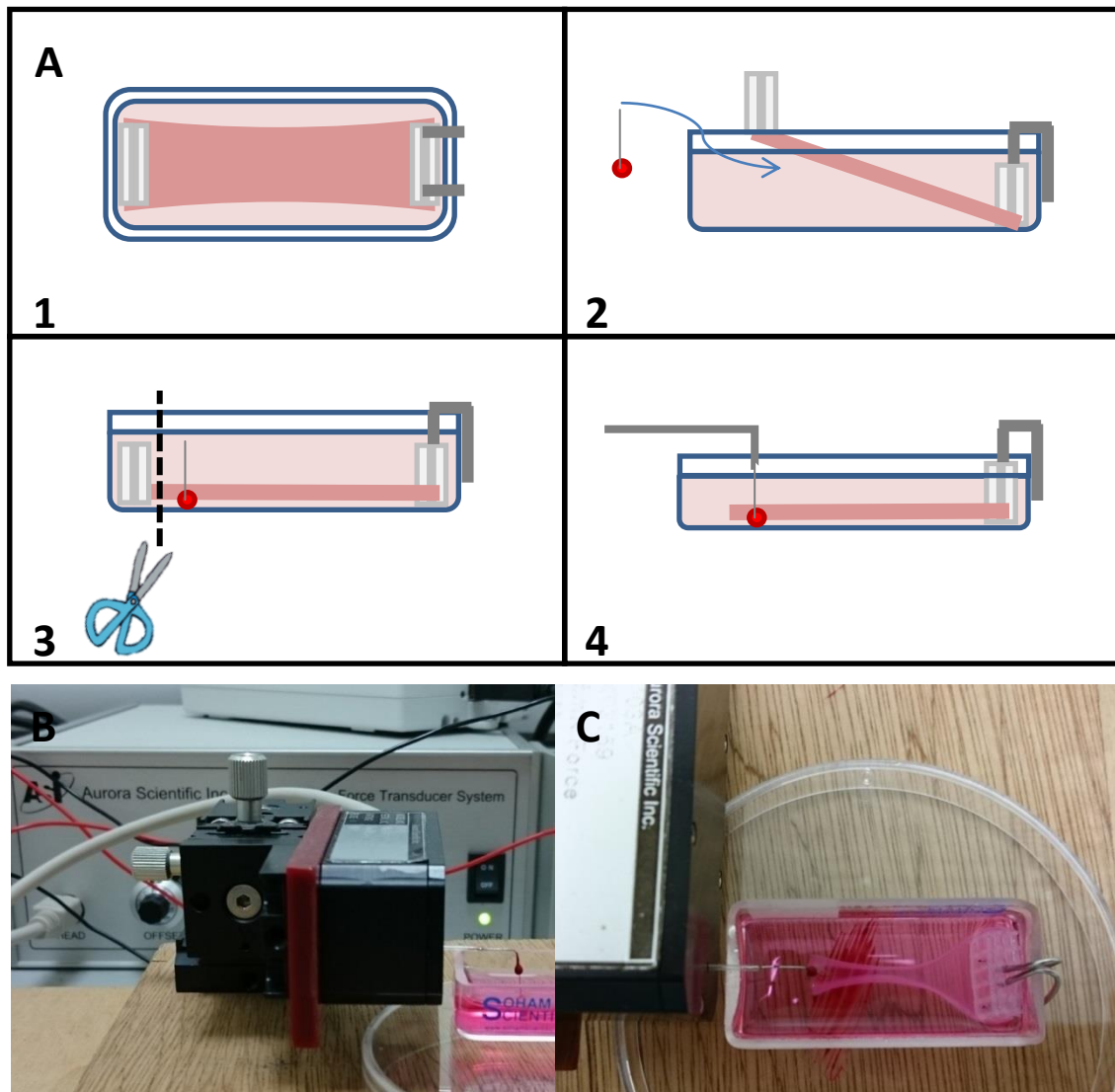
Figure 3.5: Attaching smooth muscle constructs to muscle physiology apparatus. Diagrams describing the protocol steps involved when attaching a RASM collagen construct to the force transducer (**A**). Photographs showing a side on and aerial view of the final setup (**B** and **C** respectively)

3.3.12 Evaluating the effects of antagonists on RASM collagen construct contraction

RASM collagen constructs were removed from incubation 3 days after manufacture and attached to a model 403A force transducer (Aurora Scientific) as described in section 3.3.10. Once stable, the baseline force of the resting constructs was measured for 3 minutes before the addition of 500 µl of 500 µM nifedipine (500 µl serum free DMEM in control experiments). After 5 minutes treatment with nifedipine, 200 µl of 1.25 mM UTP was added to the glass chambers and force recorded for 30 minutes. N= 3 constructs per condition (control/ nifedipine).

3.4   Results

3.4.1 HASM seeded collagen gel contraction in response to chemical stimuli

In *vivo* SM tissue contracts in response to a range of physiochemical stimuli. In order to determine whether collagen based constructs could be used to measure the force of SM contraction in response to such stimuli, an established well plate assay (Matsumoto et al. 2007) was used. HASM cells seeded into 500 µl collagen hydrogels in a 24 well plate were stimulated with histamine, bradykinin or serum free media (control) and imaged over 150 minutes (**Figure 3.6 A**). All gels, including the controls, contracted over the time period for all donors. Final gel size (as a percentage of original size) reached for each condition was 69.21 ± 18.23%, 49.84 ± 12.26% and 41.92 ± 10.52% (mean ± standard deviation) for the control, histamine and bradykinin gels respectively. The bradykinin stimulated gels contracted significantly more than control gels (**Figure 3.6 B**) from t=60 to t=150 minutes (P<0.05 Tukey's Two-Way ANOVA with Multiple Comparisons). There was no significant difference seen between histamine stimulated gels and control gels.

3.4.2 Isolation and characterisation of primary RASM cells

Due to the limited availability of primary human tissue, especially from within the peripheral airways, an alternate source of SM cells was required for optimisation of the contraction model. As an alternative source of SM tissue, aortic tissue was dissected from male Wistar rats and enzymatically digested. The dissociated aortic SM cells were seeded onto collagen coated tissue culture flasks and expanded up to passage 3. Upon digestion of the aortic tissue, an average of $2.74 \times 10^6 \pm 9.78 \times 10^5$ cells (n=6, mean ± standard deviation) were isolated, 66.34% of which were viable (determined using trypan blue dye
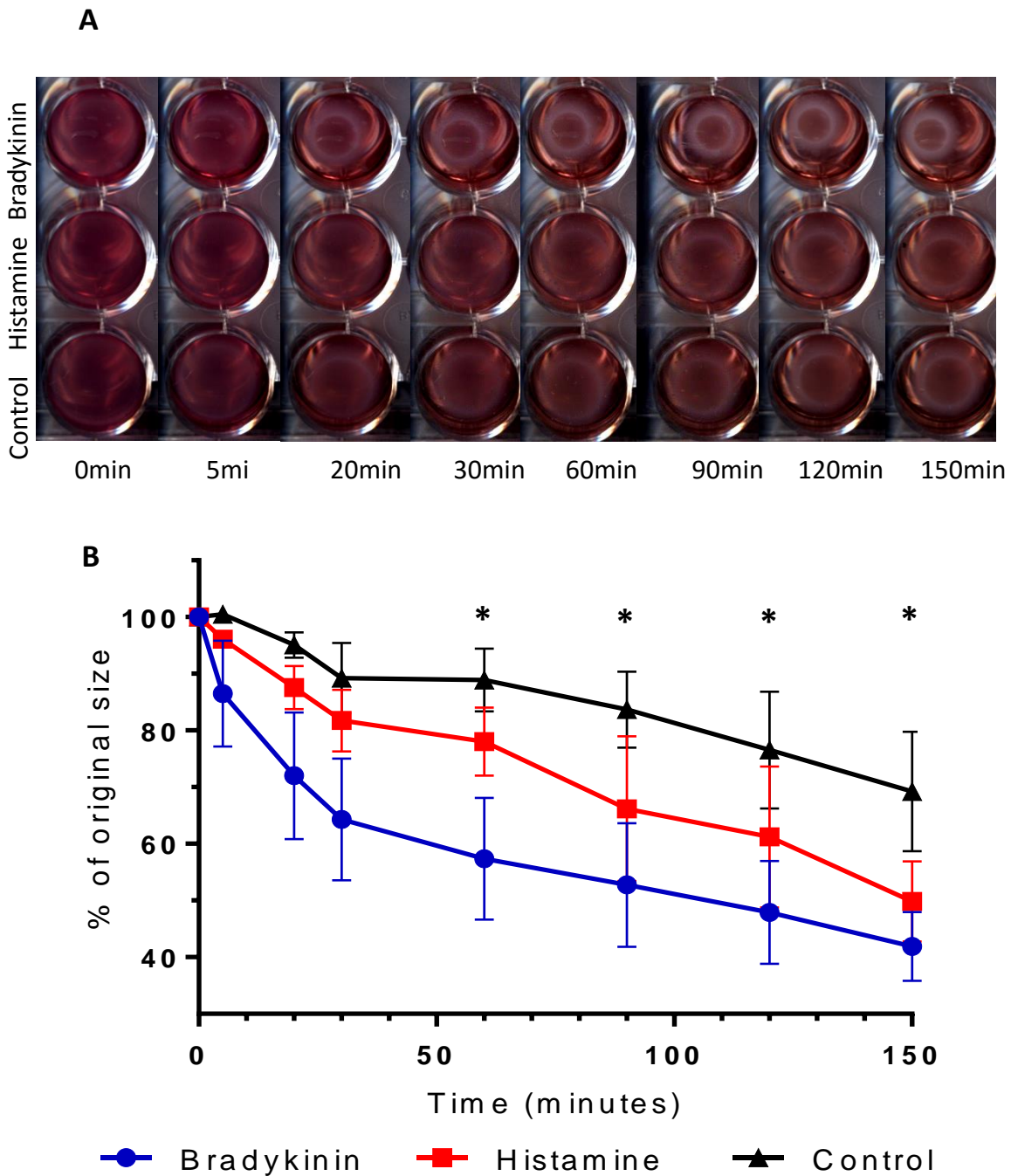
Figure 3.6: Contraction of ASM cells in collagen gels. Primary human ASM cells from 3 separate donors were seeded into 500μl collagen gels in a 24 well plate. Gels were treated with a solution of bradykinin, histamine or serum-free DMEM for 150 minutes . The gels were imaged at designated time intervals (**A**) and gel size measured, graph shows mean contraction (n=3), error bars display standard error of the mean (**B**). Gels stimulated with bradykinin contracted significantly more than control gels from T=60 minutes onward (*P<0.05. Tukey's Two-Way ANOVA with Multiple Comparisons). Indicating that the addition of bradykinin increased the level of contraction when compared to the unstimulated control.

exclusion). At passage 1 an average of $3.43 \times 10^6 \pm 1.88 \times 10^6$ cells (n=6, mean ± standard deviation) were isolated, 78.36% of which were viable.Isolated RASM cells seeded onto glass coverslips were fixed and immunostained for smooth muscle markers (n= 5 donors, 3 images per donor **Figure 3.7**). The RASM cells stained for smooth muscle specific markers SM22α and calponin (**Figure 3.7A, B** respectively) with high expression of both markers seen (94.60 ± 2.75% and 82.52 ± 5.32% respectively; mean ± standard deviation, n=5 donors, 3 images per donor). Staining was also seen for the focal adhesion protein vinculin (**Figure 3.7D**) with clear focal adhesion points visualised at the cell extremities. High expression of the gap junction protein connexin was seen in the samples with a granular appearance concentrated around the nucleus (**Figure 3.7C**). The majority of RASM cells within the samples stained negative for the intermediate filament protein desmin (**Figure 3.7C**).

3.4.3 Contraction of RASM seeded collagen gels

As seen with primary HASM cells, SM cells seeded within collagen hydrogels were able to contract the gel without the addition of an agonist due to the attachment of the cells to the collagen fibrils within the gel structure. With the addition of an agonist to the culture media, the level of contraction seen is significantly greater. In order to determine the difference between cell attachment mediated gel contraction and agonist induced cell/ gel contraction, RASM cells were seeded into collagen gels at three different densities and stimulated with a range of agonist (UTP) concentrations (n=3). After cell seeding, gels were incubated overnight (17 hours) for the gel to set and gel remodelling to occur (**Figure 3.8 A**). Gels seeded at a density of 2×10^5 cells ml^{-1} contracted due to remodelling significantly less (62.48% original size) than gels seeded at a density of 5×10^5 and 1×10^6 cells ml^{-1} (32.91% and 23.19% of original size respectively (P<0.01 and P<0.001 respectively. Tukey's two-way ANOVA with multiple comparisons) **Figure 3.8 D**). Remodelled gels were stimulated by addition   of   a   UTP   solution   for   30   minutes
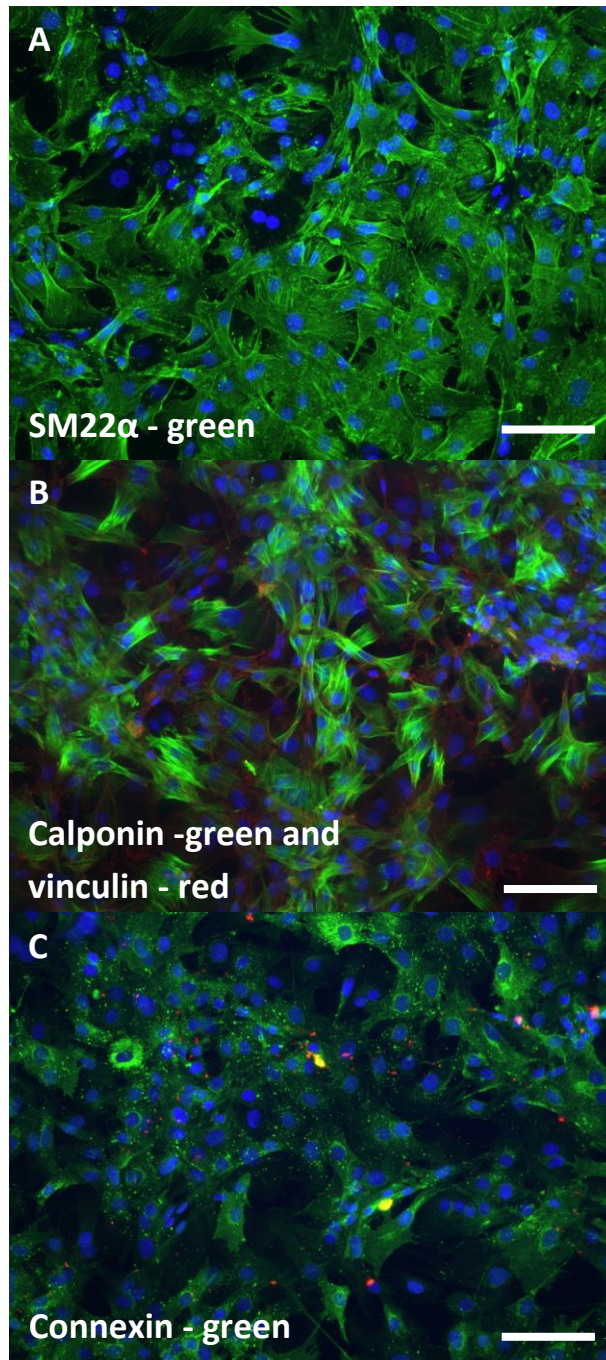
Figure 3.7: Characterisation of primary rat aortic smooth muscle cells. Primary rat SM cells from 4 separate donors were seeded onto glass coverslips and cultured for 10 days. Cells were fixed and immunostained for smooth muscle markers SM22α (green, **A**) and calponin (green, **B**), intermediate filament protein desmin (red, **C**) as well as gap junction protein connexin (green) (**C**) and focal adhesion protein vinculin (red, **B** and **D**). Scale bars = 100μm. All samples were additionally stained with the nuclear stain Hoechst 33342 (blue). All donors displayed high positivity for all markers.
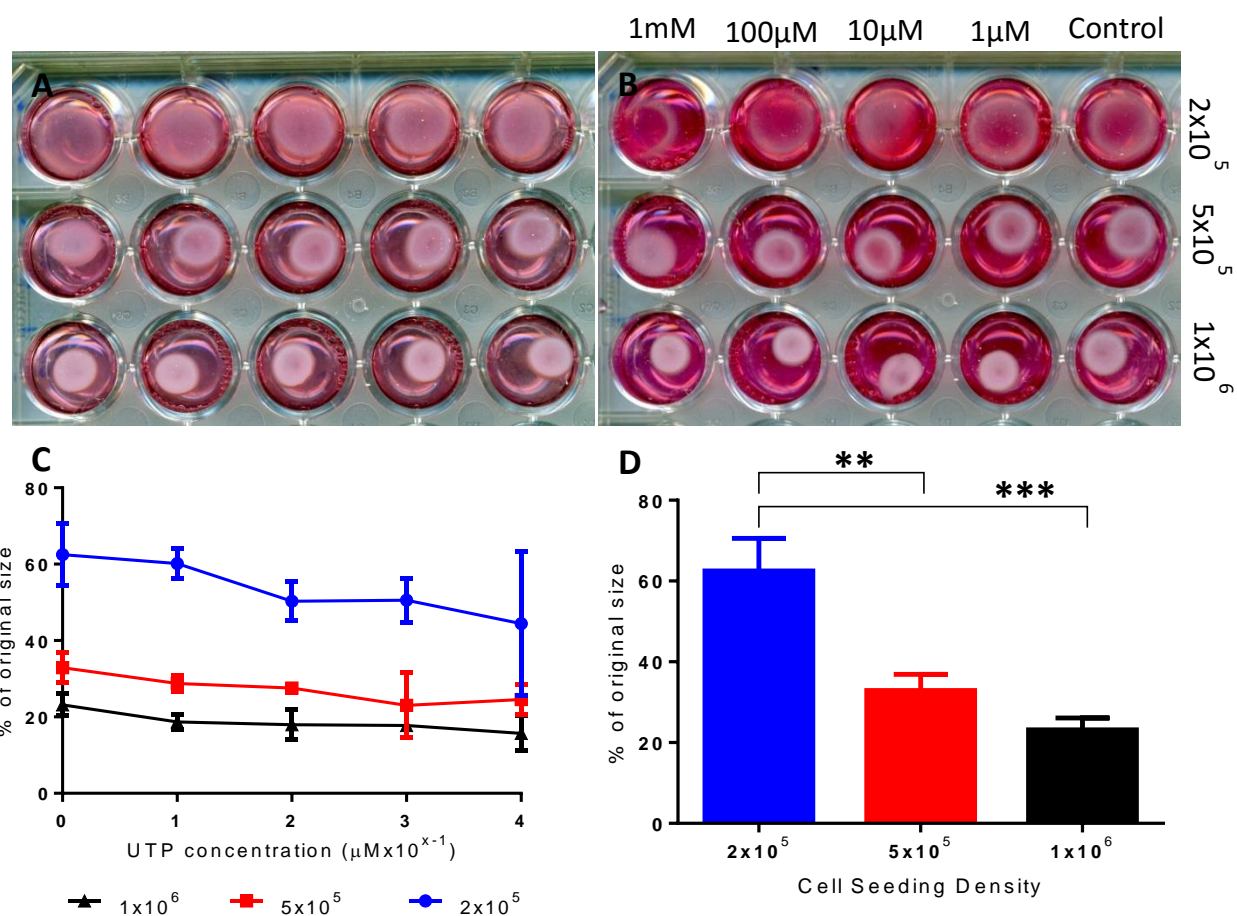
Figure 3.8: Effects of UTP concentration and cell density on gel contraction. Scanned images of RASM collagen gels at T=0 minutes (**A**) and T=30 minutes (**B**) after stimulation. Graph of percent gel contraction against UTP concentration at various cell densities, error bars represent standard deviation (**C,** n=3). Graph of initial remodelling of the gels after 17 hours in culture, error bars represent standard deviation (**D**, n=3). Gels seeded with $2x10^5$ cells ml^{-1} contracted significantly less than those seeded with $5x10^5$ and $1x10^6$ cells (P<0.01 and P<0.001 respectively. Tukey's One-Way ANOVA with Multiple Comparisons.)**.** Cell densities are expressed in cells ml^{-1}

(**Figure 3.8 B**). The greatest observable change in gel size when compared to controls was seen in 2 x 10^5 cells ml^{-1} gels treated with 1 mM UTP (44.43 ± 18.8% vs 62.48 ± 8.12% , mean ± standard deviation) however as seen in Figure 3.6 C, the variability in results at this density was higher than in other gels. At a density of 5 x 10^5 cells ml^{-1} the greatest gel contraction was seen when stimulated with 100 μM UTP (23.06 ± 8.53% of original size) when compared to the control (32.91 ± 3.96%). Although UTP stimulated contraction was measured in 1 x 10^6 cells ml^{-1} gels, it was not possible to observe a difference between UTP concentrations. This is possibly because the gels cannot contract further beyond a maximum cell density where there is less collagen matrix to contract. The optimal conditions for measuring maximum agonist stimulated contraction in collagen gels therefore was observed when using gels seeded at a density of 5 x 10^5 cells ml^{-1} stimulated by 100 μM UTP.

3.4.4 Measurement of force generated during contraction of an established C2C12 model using the culture force monitor

The forces generated by initial cell attachment by various cell types including SM cells (rabbit bladder) and C2C12s (Cheema et al. 2003) within collagen gels have been measured using a CFM, a bespoke piece of equipment consisting of a force transducer parallel to a fixed anchor point, designed for measuring uniaxial contraction in hydrogel cultures (Brady et al. 2008)(Eastwood et al. 1994). In order to replicate similar experiments and validate the CFM for use in measuring SM contraction, C2C12 collagen constructs were manufactured. Constructs were rectangular in shape and were made from 2 ml of C2C12 cells (4 x 10^6 cells ml^{-1} a density published previously (Sharples et al. 2012)) suspended in a collagen solution (**Figure 3.9A**). When maintained in culture, cellular attachment caused remodelling of the constructs leading to a reduction in gel width (**Figure 3.9B**). The majority of gel contraction was seen in the first 36 hours of culture where the average gel width reduced down to 50.55 ± 5.50% (mean ± standard
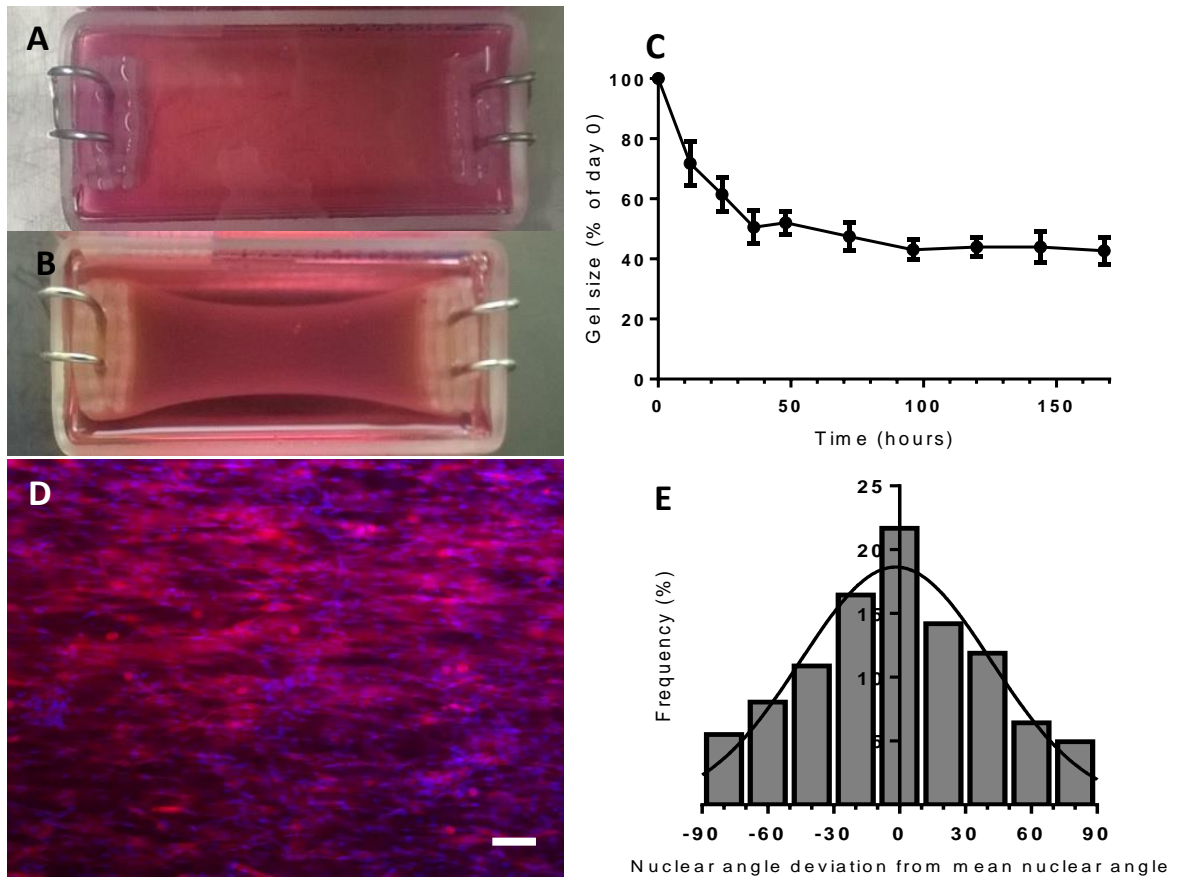
Figure 3.9: Remodelling effects of C2C12's within a collagen gel under uniaxial tension. Photographs of a C2C12 seeded 2ml collagen gel at day 0 (**A**) and day 4 (**B**). A graph showing the reduction of gel width over time (**C**), error bars show standard deviation (n=4). Image of C2C12 seeded gel immunostained for desmin (red) and the nuclear stain DAPI (blue) after 14 days in culture, scale bar = 100µm(**D**). Distribution curve showing nuclear alignment within the collagen gels after 14 days (n=5, 3 images per n taken) (**E**).

deviation, n=4) of the width at day 0. After 4 days of culture, no more remodelling was seen with the gel width reaching 43.07 ± 3.22% of the original width (**Figure 3.9C**). When allowed to differentiate over 14 days, the C2C12s fused into myotubes (**Figure 3.9D**) which align along the lines of tension that form within the gel, perpendicular to the two floatation bars. The alignment of cells within the constructs was determined by measuring the angles of individual nuclei. 21.67% of nuclei (nuclei analysed from 3 constructs, 5 images analysed per construct) were within 10° of the mean nuclear angle.

Initial remodelling forces were measured by attaching newly formed constructs (allowed to gel for 60 minutes) to the CFM and measuring the force for at a frequency of 0.167 Hz (1 reading per minute) for a 24 hour period (**Figure 3.10A**). The majority of the recorded gel contraction occurred within the first 80 minutes after attachment to the CFM (**Figure 3.10B**). After this time, the force reading plateaued. The average peak force reading for C2C12 constructs was 502 ± 129 µN (mean ± standard deviation, n=5). The highest rate of contraction (10.2 ± 4.3 µN min^{-1}, mean ± standard deviation, n=5) was seen in the first 10 minutes with the rate of contraction gradually declining to 0.8 ± 1.1 µN min^{-1} after 60 minutes (**Figure 3.10C**).

C2C12 constructs that were attached to the CFM for 24 hours were fixed and immunostained for desmin and counterstained with DAPI (**Figure 3.11A**) The C2C12 cells within the constructs were highly aligned with 31.78% of cell nuclei within ± 10° of the mean nuclear angle (**Figure 3.11B**). This indicates that uniaxial tension is formed within the constructs whilst attached to the CFM system.

3.4.5 Measurement of RASM contraction using the CFM system

As seen with the remodelling of C2C12 constructs, the CFM can be used to measure collagen construct contraction in a uniaxial manner. Therefore, RASM constructs were manufactured following the same design of the 2 ml C2C12 constructs in order to measure the force generated during agonist induced
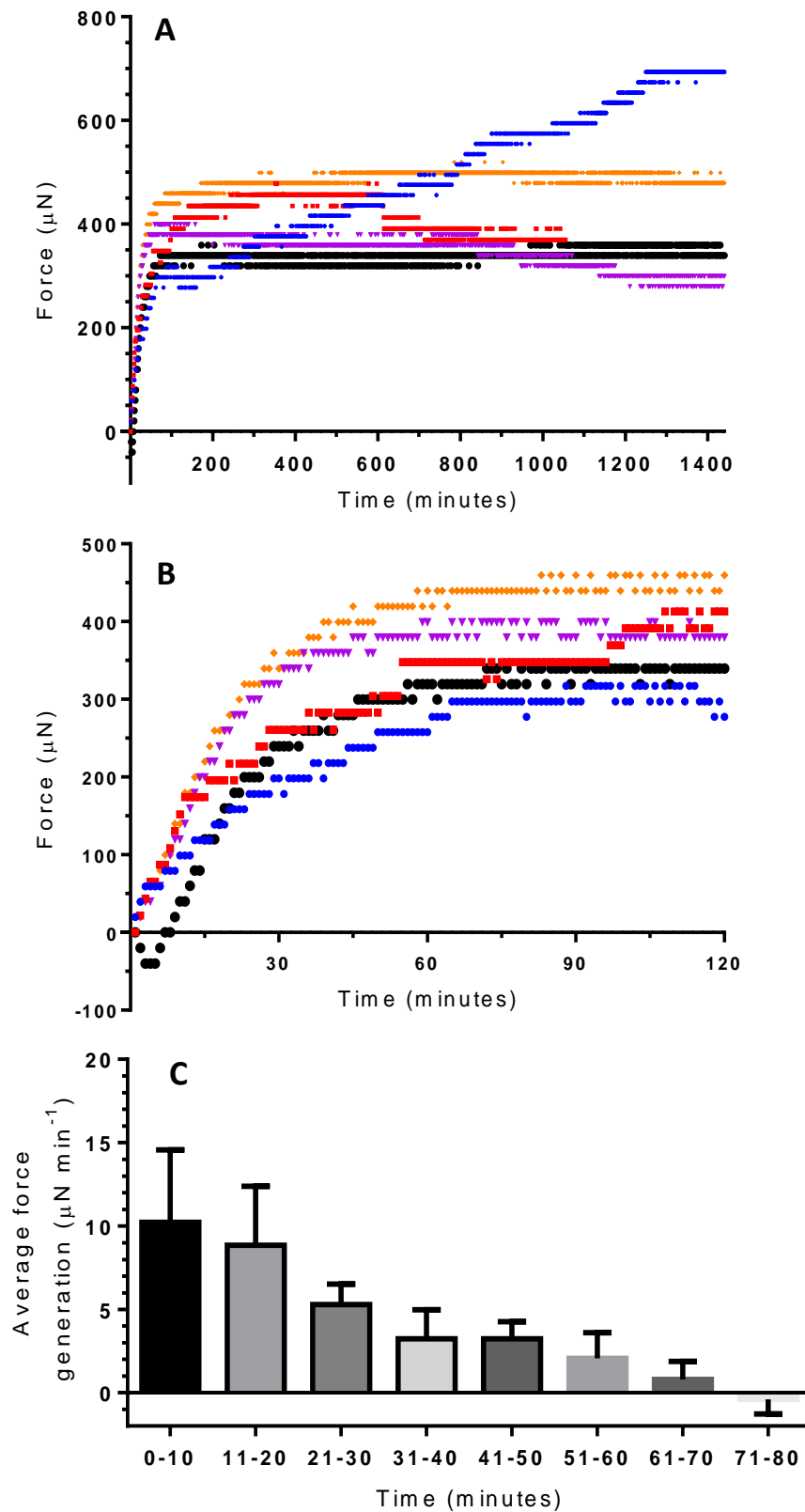
Figure 3.10: C2C12 gels initial cell attachment forces. CFM traces of 5 separate C2C12 gels over a 24 hour period (**A**), the majority of the force measured was generated within the first two hours after placing on the CFM (**B**). Average rates of contraction over the first 80 minutes after attachment to CFM (**C**). Error bars represent standard deviation.
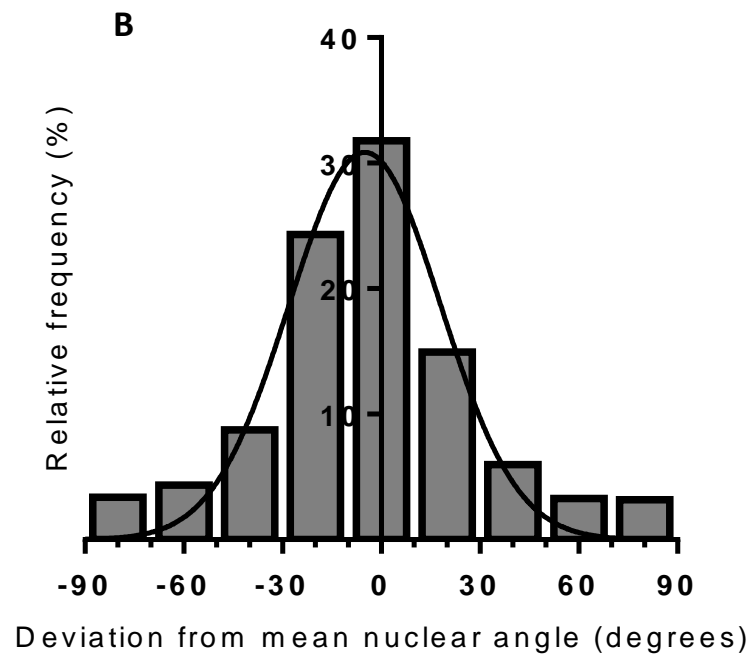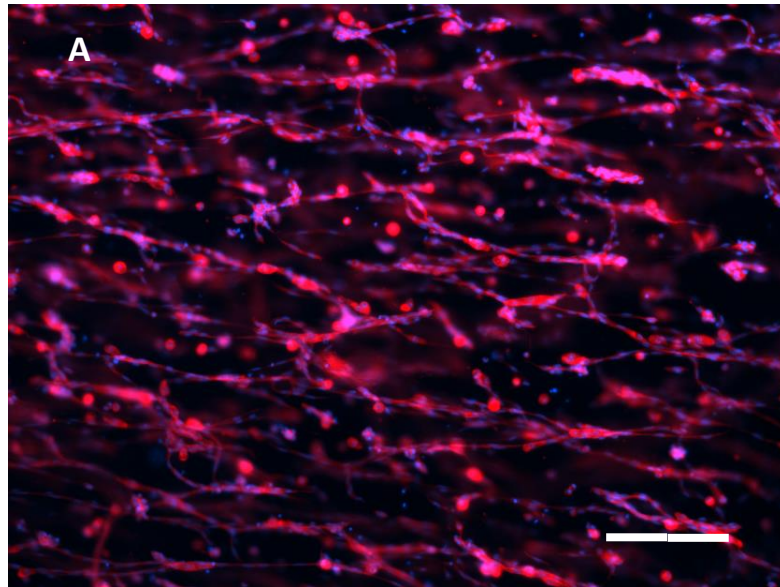
Figure 3.11: Cell alignment on the CFM. Image of C2C12 seeded gel immunostained for desmin (red) and the nuclear stain DAPI (blue) after 24 hours on CFM, scale bar = 100µm (**A**). Distribution curve shows nuclear alignment within the collagen gels after 24 hours on the CFM (**B**)

contraction of RASM cells. Using the results obtained whilst studying RASM collagen gel contraction in 500 µl round gels, the cell density used for the RASM collagen constructs was 5 x 10^5 cells ml^{-1}. The constructs were cultured for 3 daysto allow the initial cell attachment and gel remodelling to take place. Additionally, this allows the cells to form an aligned population as they align parallel to the tension that is generated within the gels. This will ultimately result in a more accurate force measurement during contraction. When cultured over 3 days, the RASM collagen constructs remodelled due to cellular attachment (**Figure 3.12A-E**). At 72 hours after construct formation, the mean gel width had reduced to 33.8 ± 6.6% of the original gel size (mean ± standard deviation, n=3 donors, 6 gels per donor). Cellular morphology was observed over the first 3 days following polymerisation. Immediately after polymerisation the majority of cells had a round morphology with no visible protrusions (**Figure 3.12F**); at 24 hours after manufacture, cell morphology was much more spindle like with some alignment seen (**Figure 3.12G**). Following 72 hours after manufacture, cells remained spindle shaped and elongated; additionally, the cell density appeared greater due to gel contraction and the cell population appeared to be highly aligned (**Figure 3.12H**).

Immunostaining of RASM constructs allowed for more accurate measurements of cellular alignment and density within the constructs. Cell alignment and density was not homogenous throughout the construct and varied between different areas. Cells were much more aligned (38.18% of nuclei within 10° of the line parallel to the length of the gel) along the edges of the constructs than in the centre of the gels (14.57%) or close to the floatation bars (7.35%, **Figure 3.13B**; n= 3 gels, 6 images per region per gel). The majority of cells within the floatation bar regions of the constructs are almost perpendicular to the orientation of cells along the edges with 7.56% and 8.77% of cells in this area orientated in the -75° to -85° and 75° to 85° ranges. The edges of the constructs were also the most densely populated areas (281.7 cells mm^{-2}) with the floatation bars (175.3 cells mm^{-2}) and the centre (61.78 cells mm^{-2}) being
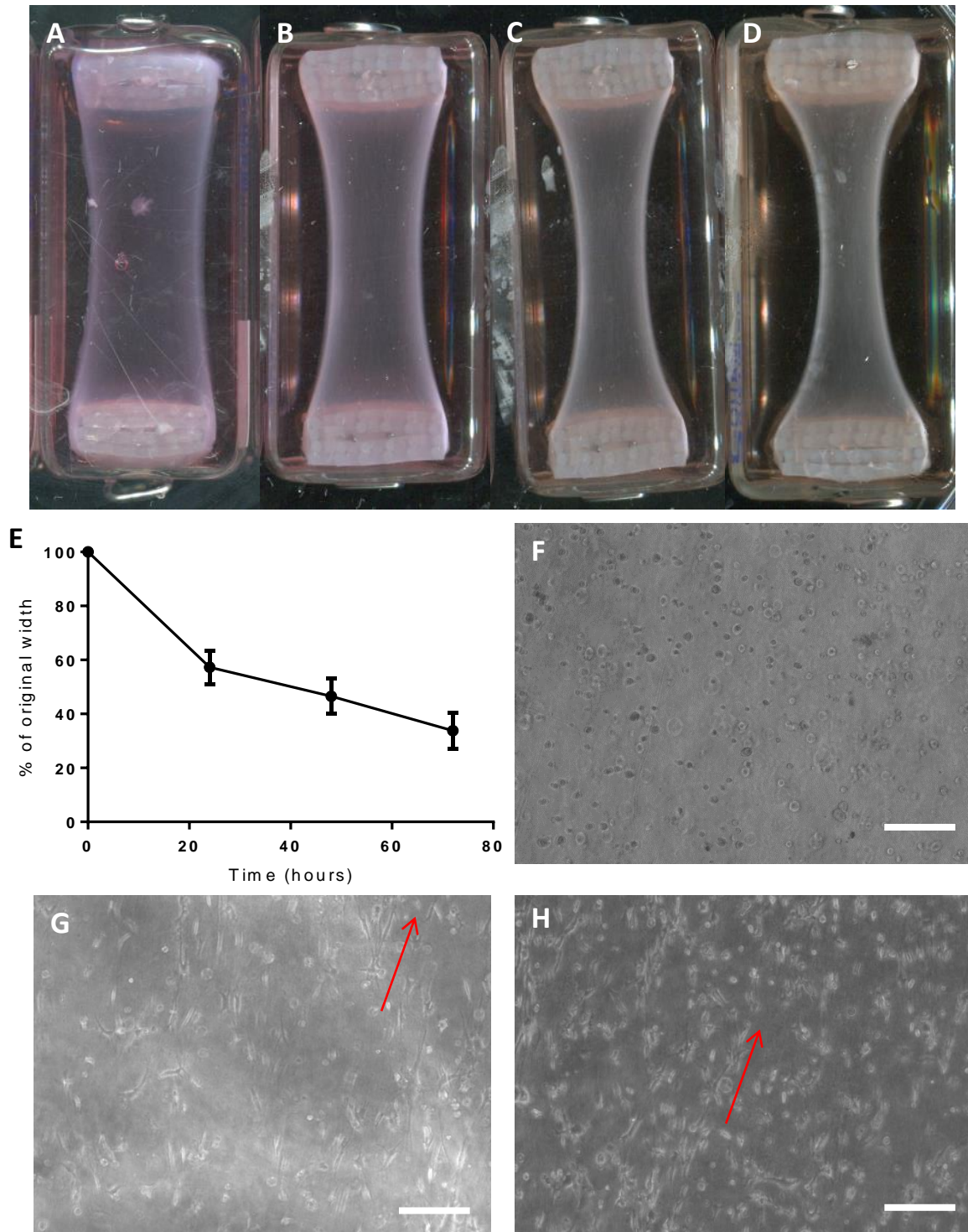
Figure 3.12: Remodelling effects of RASM cells on collagen gels. Images of 2 ml collagen constructs at T= 12hours (**A**), 24 hours (**B**), 48 hours (**C**) and 72 hours (**D**) after initial seeding. Average reduction in gel width was measured over time (**E**, n= 3 donors, 6 gels per donor. Error bars show standard deviation). Micrographs of constructs taken on a light microscope at T= 1 hour (**F**), 24 hours (**G**) and 72 hours (**H**) after initial seeding. Scale bar = 100 µm, red arrows indicate the orientation of the gels, perpendicular to the floatation bars.
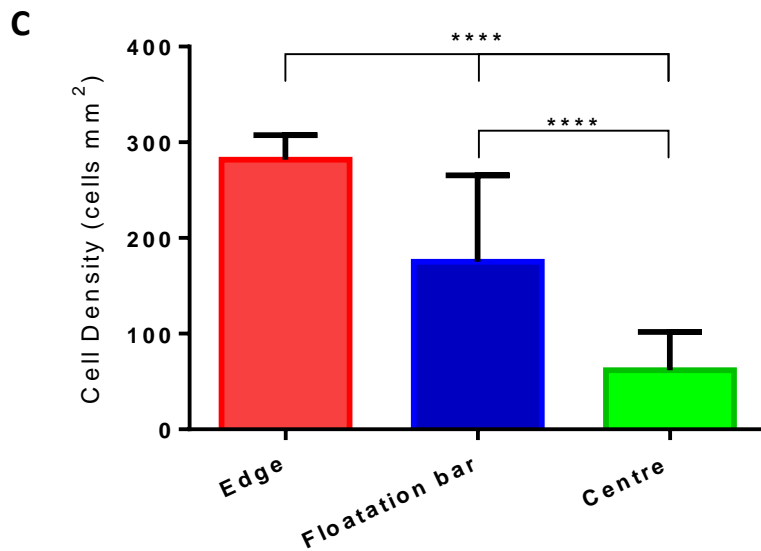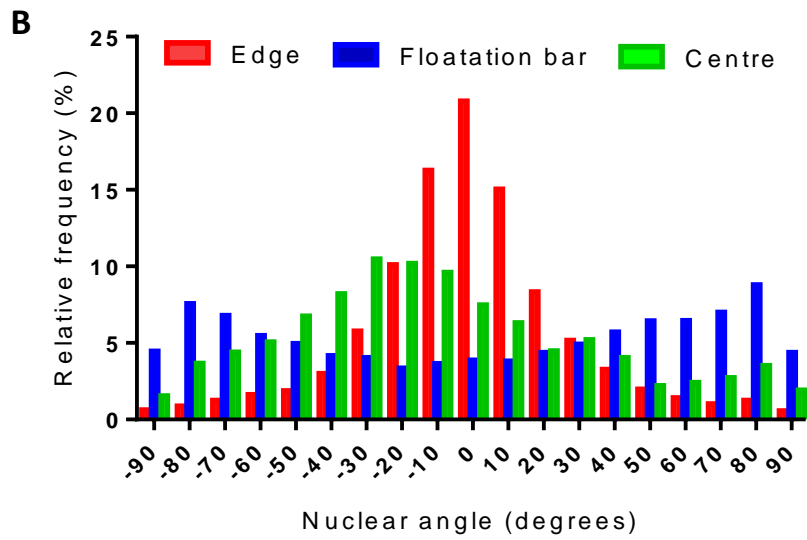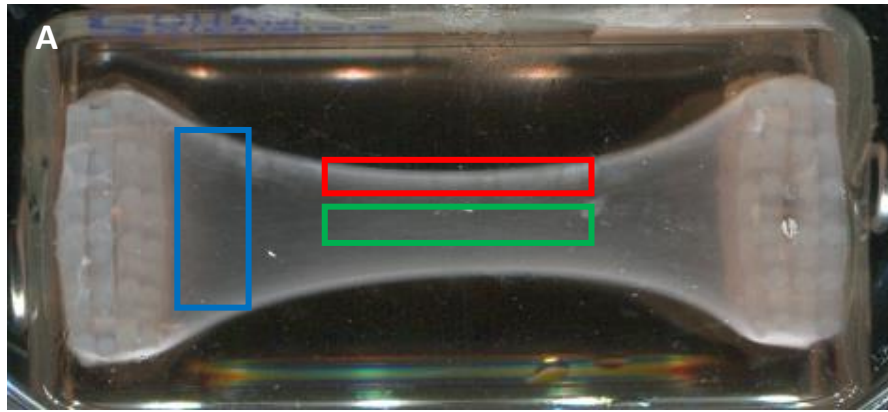
Figure 3.13: Cellular alignment and distribution of cells within RASM constructs. Photograph of a RASM collagen construct with the analysed regions highlighted (**A**). Graphs of nuclear angle distribution (**B**) and cell density (**C**) within specific areas of the constructs

significantly less densely populated (**Figure 3.13C**; n= 3 gels, 6 images per region per gel). RASM cells within the constructs stained positive for smooth muscle markers SM22α and calponin as well as focal adhesion protein vinculin and gap junction protein connexion. Constructs did not stain for intermediate filament protein desmin. No difference in expression could be seen for any marker in different areas of the gel (**Figure 3.14**). By culturing RASM constructs for 3 days prior to attachment to the CFM, cells were given sufficient time to attach to collagen fibrils within the gels. This remodels the gels causing uniaxial tension to form along which the RASM cells align themselves. It is important that this occurs before measuring agonist stimulated contraction for two main reasons: firstly, gel contraction due to cellular attachment would mask agonist stimulated contraction if both were to be measured simultaneously; secondly, an aligned population of cells will contract in the same direction, which better represents *in vivo* smooth muscle and also will generate a larger force in the direction of the force transducer. When attached to the CFM, RASM constructs were left to equilibrate within the system for at least 30 minutes or until the force reading was stable for 1 minute. The constructs were then stimulated to contract using 100 μM UTP solution in serum free DMEM. No contractile force was measured when gels were stimulated once (**Figure 3.15A**) or twice (**Figure 3.15B**) with UTP. An increase in force was seen immediately after addition of the UTP solution however this was due to the change in volume within the chamber, an effect seen in control experiments.

In order to investigate why no RASM contraction could be detected on the CFM, the contractile ability of free floating constructs were tested. In the experiment, one set of constructs had one A-frame removed whereas the other set had were completely detached from A-frame and floatation bar at one end (**Figure 3.16A** and **B** respectively). Both were stimulated with 100 μM UTP and serum free DMEM was used as a control. The gels were imaged at set time intervals and change in gel length was measured (**Figure 3.16E**), n=5 for attached stimulated constructs. Error bars display standard error of the mean). Constructs that were
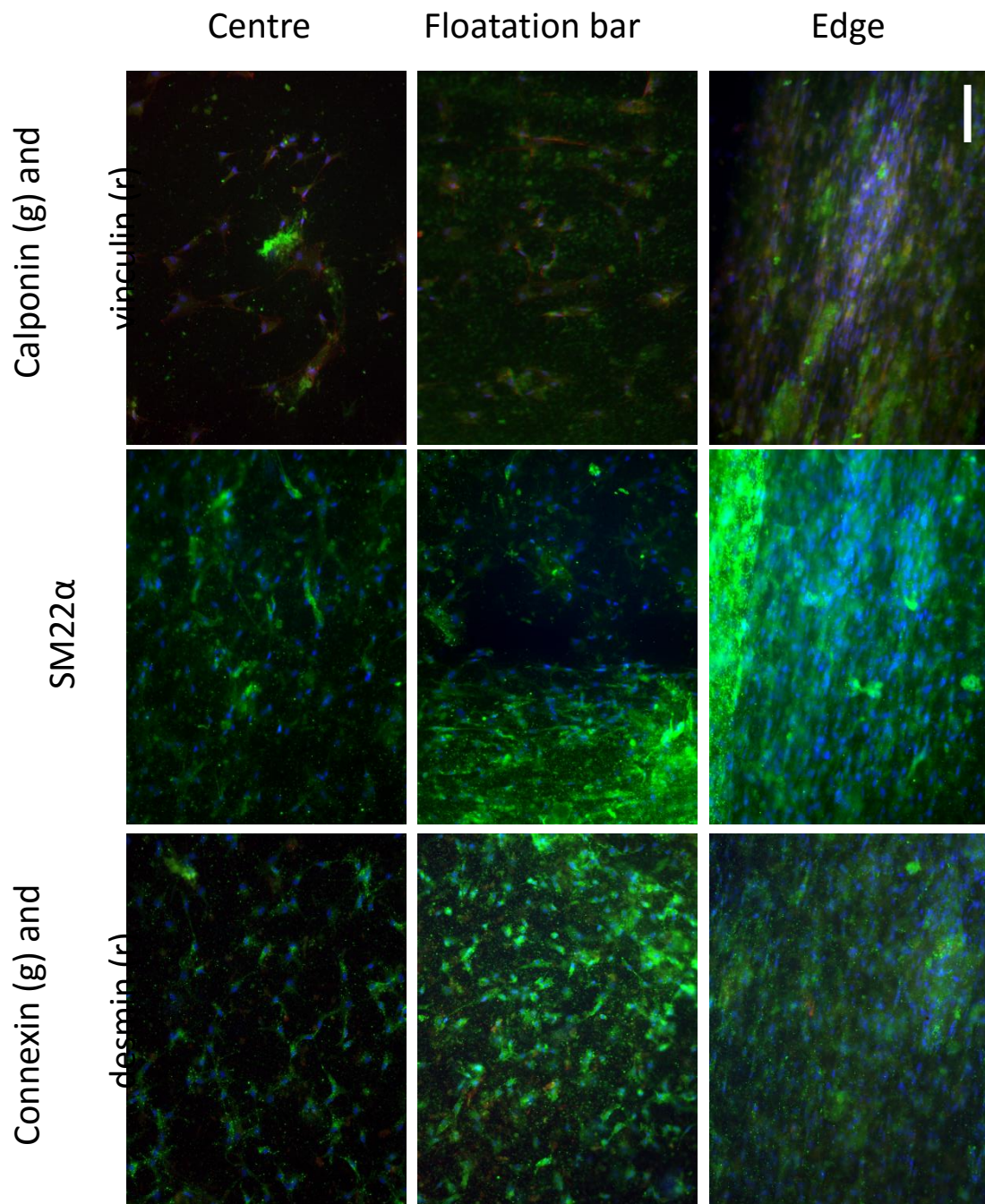
Figure 3.14: Characterisation of RASM cells within collagen constructs. Fluorescence microscope images of RASM cells stained for smooth muscle markers SM22α and calponin as well as connexin (all green) and vinculin (red). All samples were counterstained with nuclear stain DAPI (blue). Images were taken from 3 different regions within the construct. Scale bar = 100 µm.
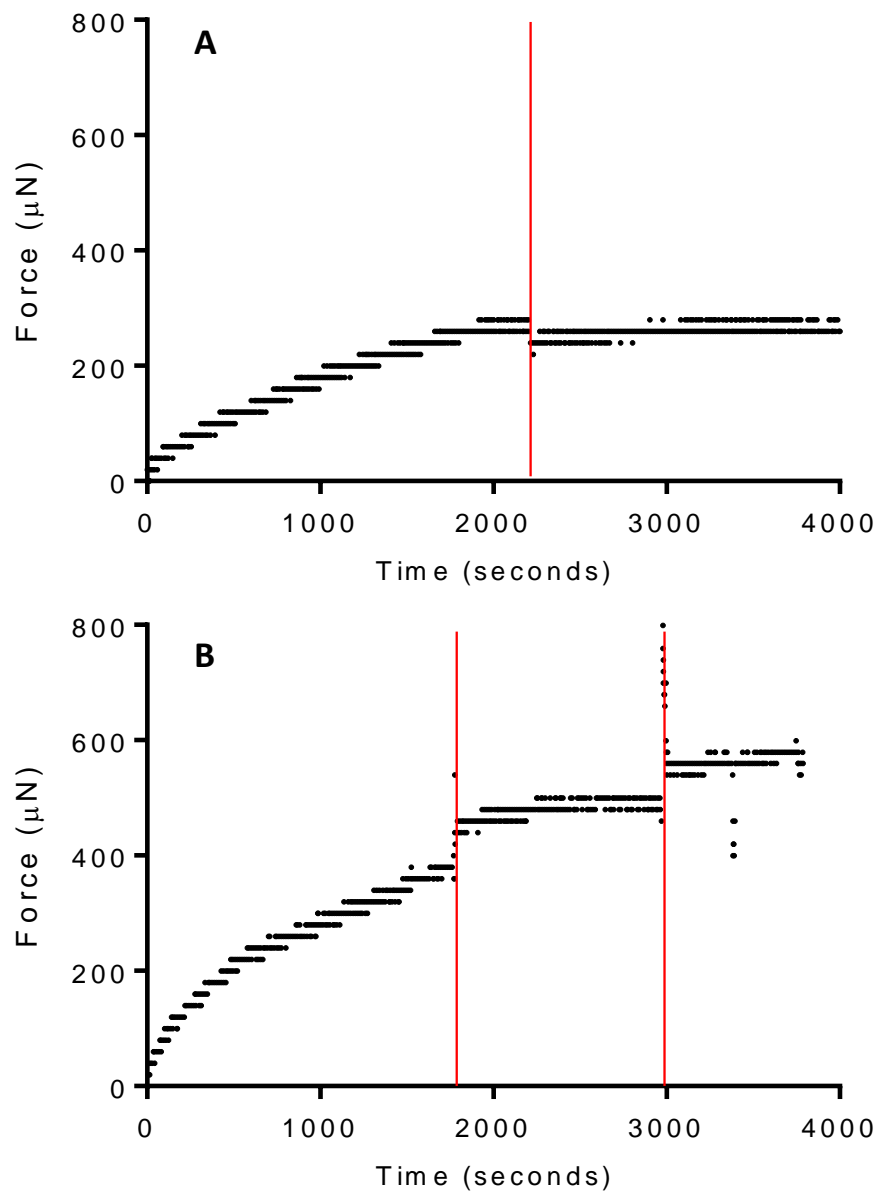
Figure 3.15: Measurement of RASM contraction in response to UTP using the CFM. Force trace generated by RASM constructs stimulated once (**A**) and twice (**B**) by 100 µM UTP solution measured using the CFM. Red lines indicate the addition of UTP solution
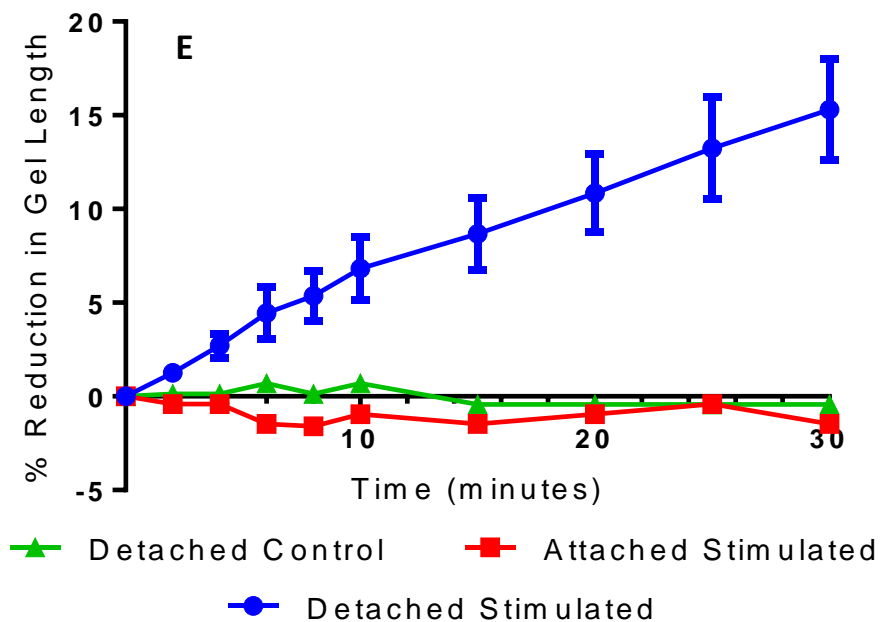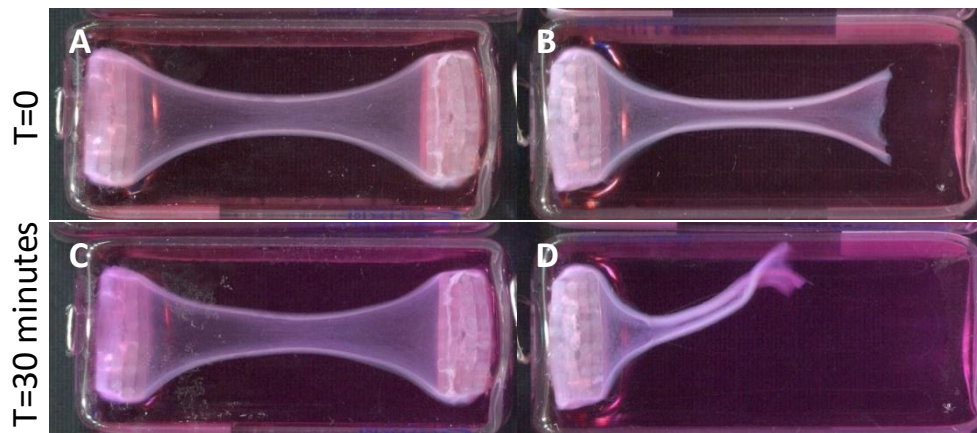
Figure 3.16: Effect of floatation bars on RASM construct contraction. Images of RASM constructs with one A-frame removed (**A**), and completely detached from one floatation bar (**B**). Images of the same gels 30 minutes after stimulation with 100 μM UTP (**C,D**). Graph showing reduction in length over time of stimulated and unstimulated constructs (**E**).

completely detached reduced in size (**Figure 3.16D**) by 15.31 ± 5.97% (mean ± standard deviation). Constructs that were still attached to floatation bars showed no visible reduction in gel size (**Figure 3.16 C**). Unstimulated constructs showed nosigns of contraction. Therefore, the load applied by the mass of the floatation bars was too great for the constructs to pull. The rate of contraction within the free floating stimulated gels was greatest within the first 10 minutes with the greatest percent decrease seen between 8 and 10 minutes (0.73% min-1) after stimulation. Between 10 and 30 minutes post stimulation, the rate of contraction was stable at 0.42% min^{-1}. A time lapse video of RASM construct contraction is shown in **supplementary video 1**. Constructs were able to contract with the floatation bars attached when seeded with 4 x 10^6 RASM cells (2 x 10^6 cells ml^{-1}) although the reduction in construct size was still much less than detached gels seeded at 5 x 10^5 RASM cells ml^{-1}. A video of this can be seen in **supplementary video 2**. It was necessary therefore, to develop a novel method of measuring the contractile forces generated by collagen constructs without the use of the floatation bars.

3.4.6 Development of a novel method to measure contractile force in free floating collagen constructs.

RASM collagen constructs contract in response to stimulation by an agonist (in this case, UTP). However, whilst the constructs are attached to the floatation bars used to manufacture the gels, this contraction is greatly restricted. When measuring contraction on the CFM, the floatation bars are used to attach the fragile collagen constructs to the force transducer. In order to accurately measure the contractile force therefore, a new method for measuring uniaxial contractile force in collagen hydrogels would have to be developed. In typical *ex vivo* organ bath studies the methodology used involves directly attaching the tissue to a force transducer using cotton thread or a pin. This experimental design was used as a template to overcome the problems encountered previously, removing the necessity of the floatation bars. By attaching the

constructs to a more sensitive force transducer (used to measure isometric contraction) using the method outlined in **section 3.3.10**, this was achieved. The additional load applied to the gel previously when using the floatation bars (2.59 ± 0.19mN plus 3.30 ± 0.69mN applied by mass of floatation bar plus hoops; mean ± standard deviation, n=6 for floatation bars, n=4 for hoops) was massively reduced by using a minuten pin adhered to a fine glass bead (0.070 ± 0.006 mN, n=6) to attach the construct to the transducer. RASM constructs were cultured for 3 days prior to attachment to the transducer. Once attached, the force was allowed to stabilise before recording started. The stable force reading was measured for 3 minutes before the constructs were stimulated with 100 μM UTP in serum free DMEM, controls were stimulated with serum free DMEM. An increase in force was detected within seconds of adding the agonist solution and continued to rise for up to 30 minutes before beginning to plateau (**Figure 3.17A**). The maximal force and therefore rate of force generation varied greatly between individual constructs (**Figure 3.17B**). The maximal force generated by the RASM constructs ranged from 196.33 μN to 542.36 μN with the average max force being 394.30 ± 147.76 μN (mean ± standard deviation). If the data is expressed as the percentage of the maximal contractile force measured however, the contraction profiles of the different gels appear to be highly similar (**Figure 3.17C**) and are logarithmic in shape. The majority of contraction occurs within the first 5 minutes following stimulation with 46.00 ± 7.77% of the maximal force measured occurring within this time; 76.20 ± 6.41% measured 10 minutes following stimulation and 94.66 ± 3.44% after 20 minutes stimulation.

The constructs all responded to the addition of 100 μM UTP; in order to investigate the sensitivity of the constructs and the contraction assay, a dose response experiment was carried out whereby the dose of UTP was increased by an order of magnitude once the force had plateaued at the current concentration. The lowest concentration tested was 10 nM increasing up to 1 mM (**Figure 3.18A**). At doses of 10 nM UTP, there was no significant difference detected in the force readings when compared to the resting construct. A small change in force was detected at 100 nM although this was not large enough to
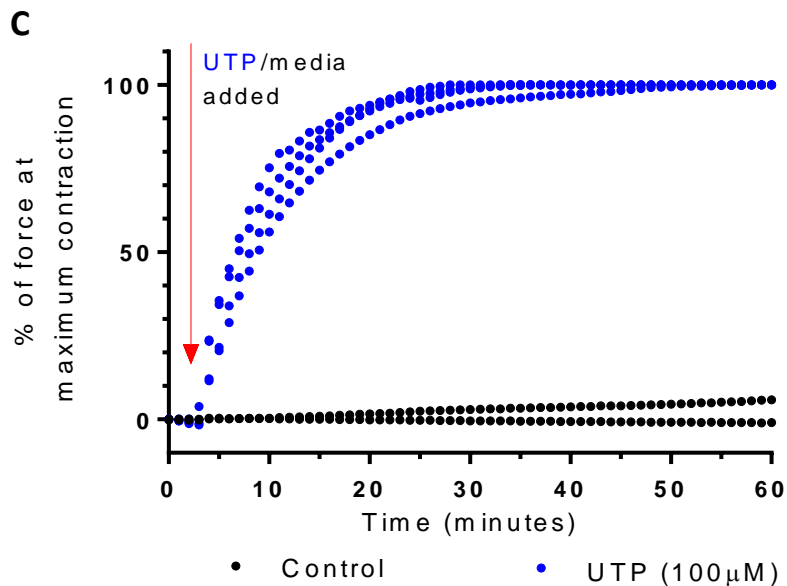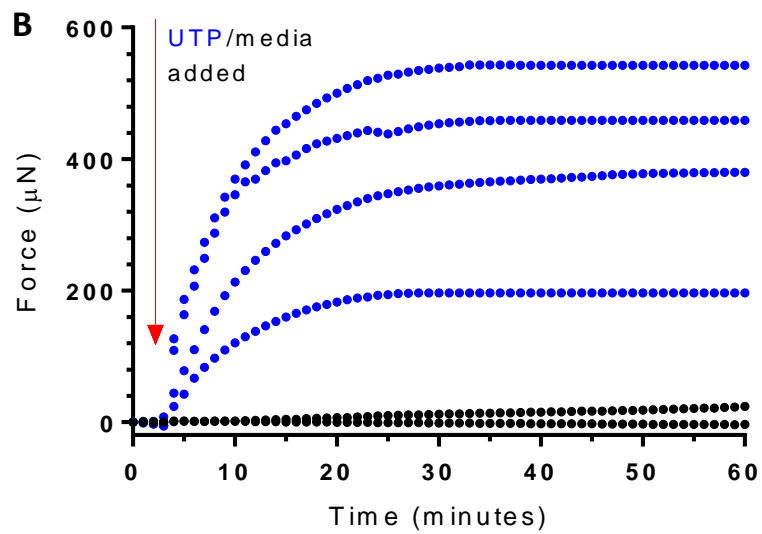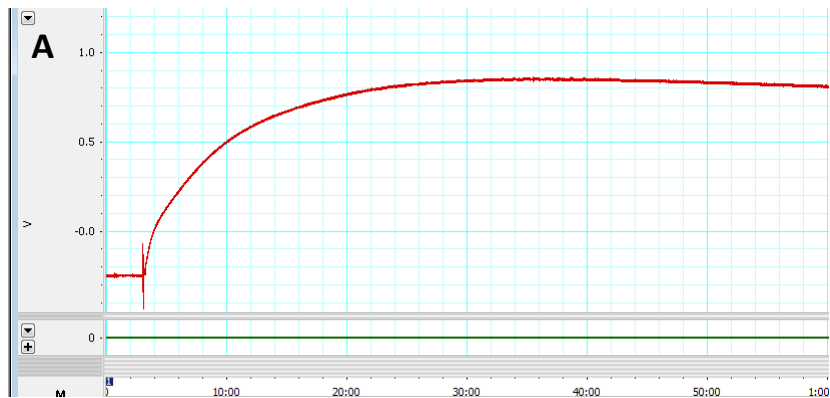
Figure 3.17: Measuring contractile force of RASM constructs attached to an isometric force transducer. Representative force trace of a RASM construct stimulated with 100 µM UTP over 60 minutes (**A**). Graph of force over time for four different RASM constructs (**B**). The same constructs are shown on a graph of % maximum force over time (**C**).
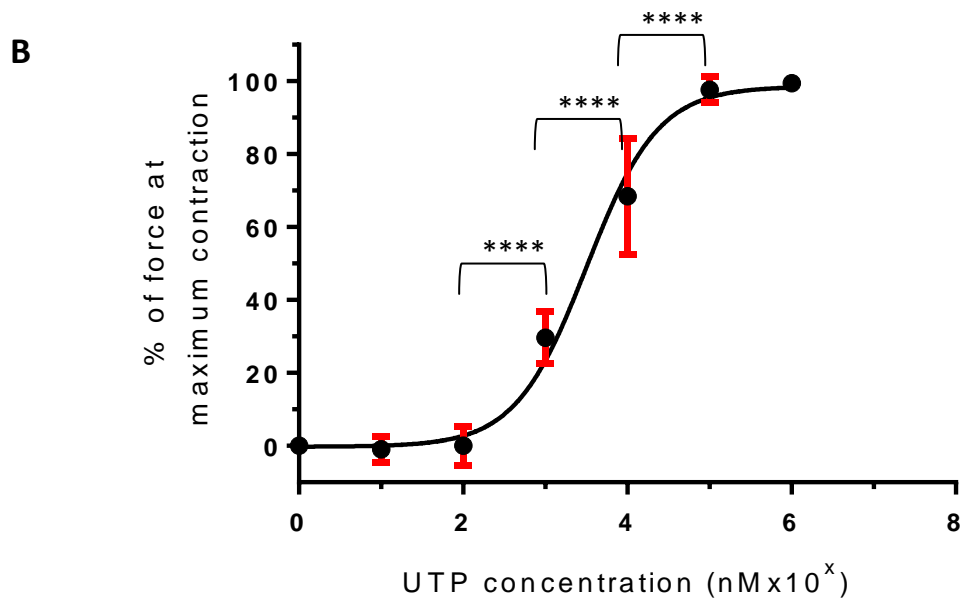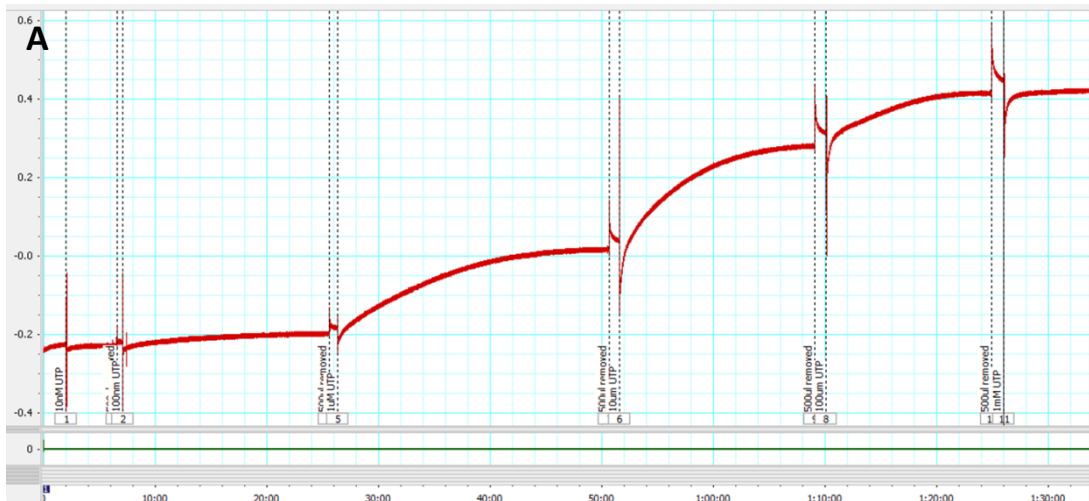
Figure 3.18: Effects of UTP concentration on the magnitude of force generated. A representative force trace of a RASM construct stimulated consecutively with increasing doses (**A**). A graph of % maximum contraction against UTP concentration (**B**), error bars represent standard deviation (n= 6; p<0.0001, One Way ANOVA with Tukey's multiple comparisons test)

be statistically significant. When stimulated with 1 µM UTP, a large significant increase in force (p < 0.0001) was measured with 29.66 ± 7.1% (mean ± standard deviation, n=3 donors, 2 constructs per donor) of the maximal force observed at this concentration (**Figure 3.18B**). The force increased to 68.44 ± 15.94% of maximum force at 10 µM UTP and 97.68 ± 3.56% at 100 µM, both of these concentrations produced a significantly greater (p<0.0001) contraction than the previous. There was no statistically significant difference between the contractile forces recorded when constructs were stimulated with 100 µM and 1mM UTP indicating that the maximal dose is in the region of 100 µM. Using statistical analysis software (GraphPad Prism), the EC_{50} of UTP in stimulating the RASM constructs was calculated to be 3.19 µM.

Due to the methods employed in the dose-response experiments it was not possible to tell whether the increases observed in force between UTP concentrations were due to the concentration rise or the addition of more UTP to the glass chamber. Therefore a repeat dose experiment was carried out to determine if the contractile force changed when constructs were stimulated repeatedly with the same dose. Constructs were stimulated with 10 µM UTP and the force allowed to plateau, the constructs were then stimulated with the same dose and allowed to plateau 3 more times. Finally, the constructs were stimulated with 100 µM UTP and left for the force to plateau a final time (**Figure 3.19**). Following the initial stimulation with 10 µM UTP, the construct contracted as seen previously resulting in an increase in force. Once the force had plateaued, the repeat stimulations did not cause any increase in contraction and after two doses of 10 µM UTP, the force actually started to decline. When stimulated with the final 100 µM dose, the force measured rose to a level much higher than any previously registered force.

The previous experiments show that the RASM collagen constructs can be used to assess SM contraction in response to chemical agonists at different concentrations. The final experiment of this chapter sought to investigate whether the RASM constructs could be effective in testing the effects on
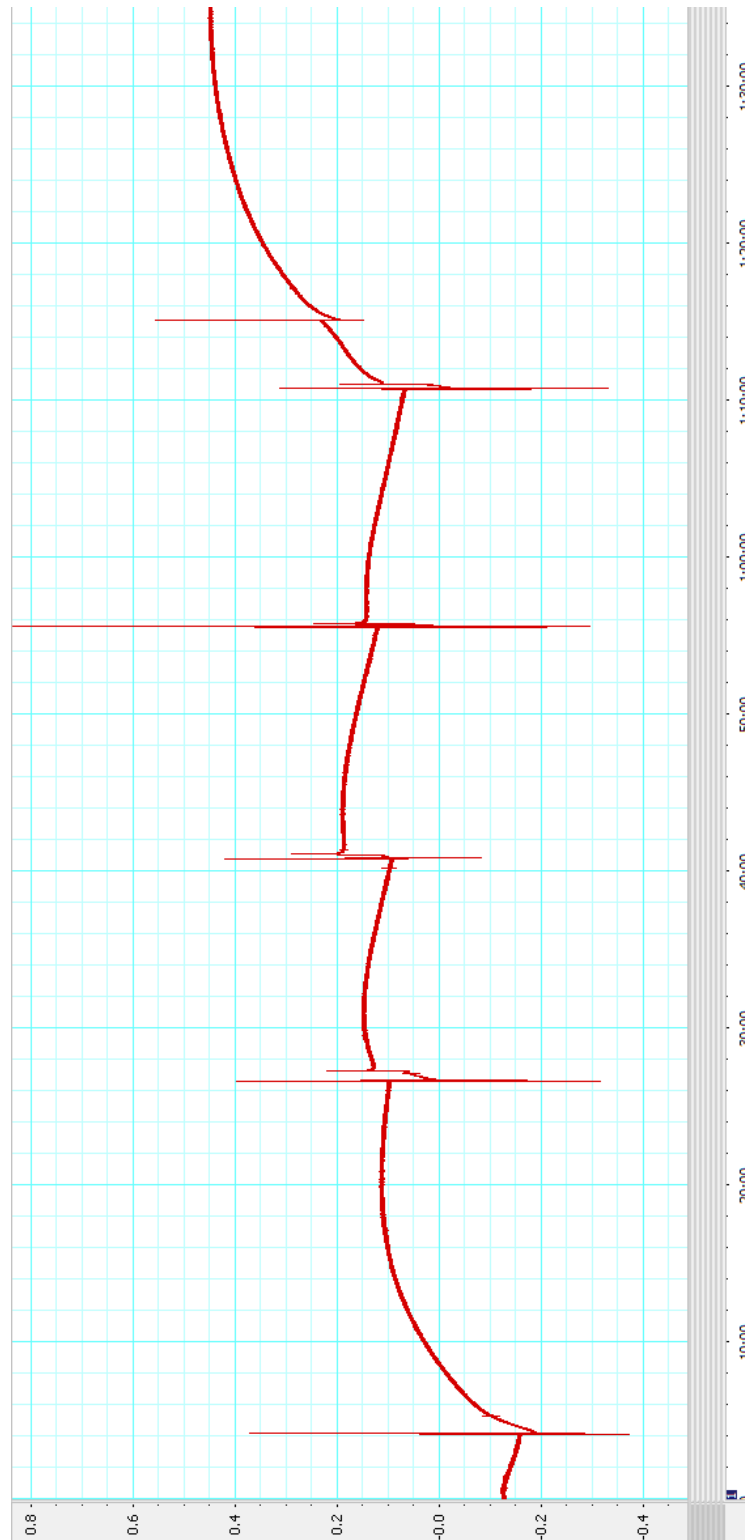
Figure 3.19: Effects of repeat dosing on RASM constructs. A representative force transducer trace of a RASM construct stimulated repeatedly with a 10 µM dose of UTP before a final 100 µM dose.
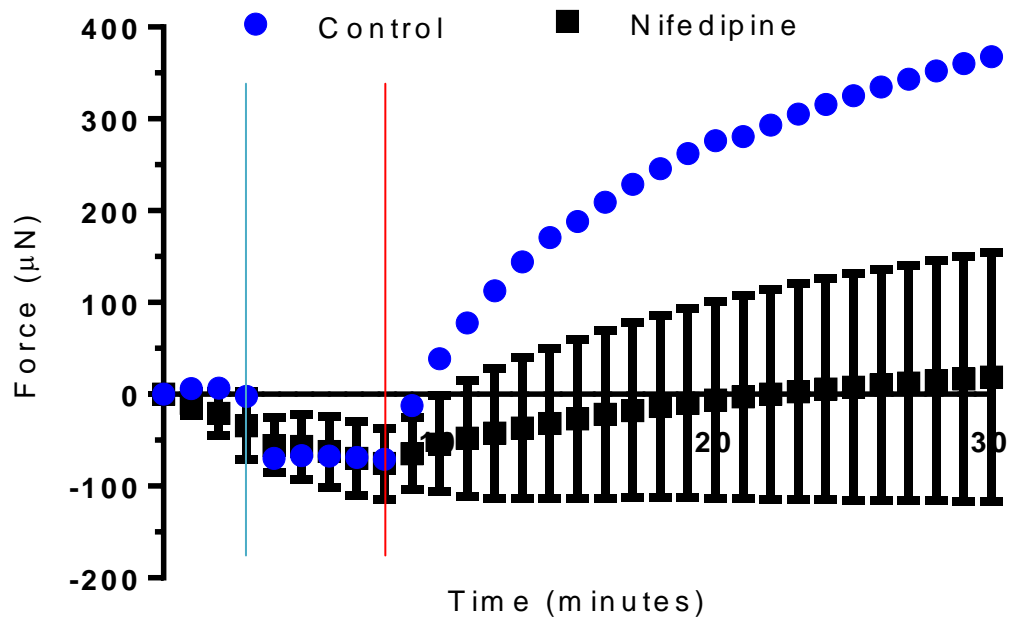
Figure 3.20: Effects of the calcium channel inhibitor nifedipine on the contractile response of RASM constructs. A graph of force over time for RASM constructs stimulated with UTP following pre-incubation with nifedipine or serum free DMEM (control). Blue line indicates addition of 100 μM nifedipine solution. Red line indicates stimulation with 100 μM UTP. Error bars represent standard deviation.

chemicals that act as contractile antagonists. RASM constructs were attached to the force transducer and pre-incubated with nifedipine, a calcium channel inhibitor, for 5 minutes before being stimulated with 100 µM UTP (**Figure 3.20**). Although contractile force was measured upon UTP stimulation in all constructs, those that were pre-incubated with nifedipine prior to UTP stimulation produced significantly less contractile force than those that were pre-incubated in serum free DMEM (n=3; p< 0.0001, paired t-test).

3.5 Discussion

SM contraction *in vivo* contributes to shortening of the muscle tissue and narrowing of hollow organs such as blood vessels and airways. In diseases such as asthma (Heard & Hossain 1973; Hossain 1973) and atherosclerosis (Pasterkamp et al. 1996; Pasterkamp et al. 1997), where remodelling of the tissue is a key feature, narrowing of the organs due to SM contraction can be excessive leading to temporary obstruction of the vessel/ airway. In order to fully investigate the biological processes that influence SM contraction and to develop therapeutic agents that can regulate it in diseases such as those mentioned above, effective models of SM contraction need to be developed. As discussed earlier, *ex vivo* tissue preparations from both humans (Lee et al. 1999) and animals (Prendergast et al. 2006) can be stimulated using organ baths. However human tissue is limited in availability and due to fundamental differences between humans and animals (Ginis et al. 2004; Castellano et al. 2015), animal tissue may not fully recreate human responses. Although tissue engineering strategies to recreate smooth muscle contraction have been developed (Matsumoto et al. 2007; Sakota et al. 2014; Ilagan et al. 2010; Margulis et al. 2009), very few have been designed to be used in force measurement studies (Gilmont et al. 2013; Oishi et al. 2000; Oishi et al. 2002). Here, new methods were developed to measure the contractile force of aligned SM cells seeded within collagen gels in real time. Agonist induced contraction was concentration dependant and could be negated by the presence of antagonists.

3.5.1 Measuring SM contraction *via* image analysis of collagen gels

Visual assessment of both primary human airway and primary rat aortic SM contraction within collagen gels in response to chemical agonists was carried out. Initial experiments using primary human cells found that gels exposed to bradykinin and histamine both reduced in size at a faster rate than unstimulated gels. These results are similar to those obtained by Matsumoto *et al.* who stimulated gels seeded with airway SM cells from donors both with and without

asthma with 100 µM histamine (Matsumoto et al. 2007). Both sets of gels were found to contract much more than the unstimulated controls with asthmatic SM gels contracting significantly more. Sakota and co-workers also stimulated human airway SM seeded gels with 100 µM histamine, finding that the gels contracted to around 50% of their original size 60 minutes after stimulation (Sakota et al. 2014). In our study, the gels continued to contract over the full course of the experiment (150 min), much longer than the time to reach maximum gel contraction found by both Matsumoto (15.7 min) and Sakota (approx. 50 mins). This is most probably due to differences in the methodology of each study. In this case, the gels were stimulated 1 hour after plating which did not allow time for the gels to attach or remodel the collagen prior to stimulation. Sakota incubated the gels for 3 days prior to stimulation but allowed the gels to remain attached to the well plate until stimulation whereas Matsumoto incubated detached gels for 24 hours prior to stimulation. Due to this, in our experiments it is highly probable that the contraction measured within these gels is due to a mixture of cellular attachment to the matrix, unloading of the gels from the well plates and agonist induced contraction.

In order to remove the noise created by initial cell attachment mediated contraction from the experiment; the subsequent contraction assay (using RASM cells, discussed in **section 3.5.2**) allowed the detached gels to incubate overnight for 17 hours before stimulation. In this case, although using a different SM source and agonist, the time to maximum contraction was much closer to that observed in other studies (25 min). Therefore, in order to accurately depict SM contraction in response to an agonist, it is important to allow the gels to contract prior to stimulation. Cell density had a direct effect on the level of the initial gel contraction, an observation found in collagen constructs containing fibroblasts (Redden & Doolin 2003) and mesenchymal stem cells (Nirmalanandhan et al. 2006). At a density of 1×10^6 cells ml^{-1} the initial gel contraction was too great to observe any further contraction when stimulated. Therefore, 5×10^5 cells ml^{-1} was chosen for further experiments. During this assay it was found that stimulation with 100 µM UTP resulted in the maximal gel contraction at a density of 5×10^5

cells ml^{-1}, a similar finding to that found by Urquilla, who recorded maximum contraction of canine cerebral artery segments at a concentration of 170 µM UTP (Urquilla 1978).

3.5.2 Isolation of vascular smooth muscle cells from rat aorta

Primary human airway SM cells were initially used in the collagen contraction experiments described within this chapter. Due to the limited availability of primary human tissue it was decided that another cell source should be used in the initial optimisation and development of the contraction assays. Within the Queen's Medical Centre, University of Nottingham, male Wistar rats are sacrificed for various studies on a regular basis. As these animals are readily available and that using tissues from them would be in line with 3Rs principles (replacement, reduction and refinement), primary RASM cells were used as a readily available alternative to human cells. Isolated RASM cells were immunostained for smooth muscle markers SM22α and calponin at passage 3.

Smooth muscle phenotype was confirmed *via* a high level of expression of both SM22α and calponin. SM22α is a Ca^{2+} sensitive 22kDa protein which binds to F-actin (Kobayashi et al. 1994) originally isolated from chicken gizzard (J. P. Lees-Miller et al. 1987). It is thought to be specific to SM cells (Solway et al. 1995; J P Lees-Miller et al. 1987) although its exact role within SM remains unknown. Recent studies propose that SM22α has an important role in the regulation of basal tone within SM cells as upregulation of SM22α within tonic SM resulted in relaxation of the cells. Conversely, temporary silencing of SM22 caused contraction within both phasic and tonic SMs (Rattan & Ali 2015). Calponin is a 34 kDa protein that binds to F-actin, tropomyosin and calmodulin (Takahashi et al. 1986) that is found within smooth muscle cells (North et al. 1994). It is thought to regulate SM contraction by inhibiting actin-activated myosin MgATPase activity (Winder & Walsh 1990) which is reversed *via* calponin phosphorylation (Pohl et al. 1997); therefore contributing to cross-bridge cycling in SM contraction. The high expression levels of these two markers therefore indicate that the majority of the isolated cells are smooth muscle cells. The low

standard deviation in the expression of these markers indicates that smooth muscle content showed little variation between isolations, regardless of the large differences in initial cell number. Although the intermediate filament protein desmin is frequently observed within SM cells (in addition to cardiac and skeletal cells), it was not expressed in the isolated RASM cultures. This result correlates with results obtained by Gabbiani *et al*. who found that whereas smooth muscle from other areas of the body contain large amounts of desmin; intermediate filaments in vascular smooth muscle contain very little (if any) desmin with vimentin being the key protein expressed (Gabbiani et al. 1981).

3.5.3 C2C12 collagen constructs as a model system to test the force measuring ability of the CFM

C2C12 collagen constructs were successfully manufactured following protocols similar to those previously published (Smith et al. 2012; Sharples et al. 2012). Constructs narrowed over time due to cellular attachment to the collagen matrix. This was to a similar degree as seen in those manufactured by Sharples *et al*. and within the constructs cells aligned along the lines of tension previously predicted by finite element analysis experiments (Eastwood et al. 1998). When placed on the CFM the force generated by this initial cellular attachment and subsequent gel remodelling could be measured. Force traces were similar in shape, peak force and time to reach peak force to those produced by C2C12 collagen constructs manufactured by Sharples *et al.* This is in contrast to the traces generated by C2C12 collagen constructs published by Cheema *et al*. where an 8 hour lag phase was recorded prior to any major contraction (Cheema et al. 2003). This is most probably due to differences in the manufacture of the constructs; primarily, those produced by Cheema and co-workers were 5 ml in volume and seeded with 5×10^6 cells. The resultant cell density used by Cheema (1×10^6 cells ml^{-1}) is much lower than those used here and by Sharples (4×10^6) and cell density has been shown to have a clear effect on both the rate and amount of gel contraction (Awad et al. 2000).

The majority of the force generated by the constructs occurred within the first two hours before shortly plateauing; however when assessing the constructs visually, they continue to remodel for several days. Upon immunostaining the constructs following 24 hours on the CFM, it is clear that the cells are aligning as they would in static isometric culture. This indicates that there is uniaxial tension forming within the constructs. Therefore, it is plausible to suggest that as the constructs contract and displace the force transducer beam; the counter force produced by the beam reaches a point where it is in equilibrium with the force of contraction. It is this that leads to the plateau seen after approximately 2 hours; this theory could be tested by using beams with varying spring constant. According to Hooke's law, those with lower spring constants would produce less force at the same level of displacement.

As the CFM was able to reliably measure the remodelling force of C2C12 constructs up to an average peak force of ≈500 µN, it was decided that the CFM would be suitable apparatus to initially measure the agonist induced contraction of RASM collagen gels.

3.5.4 Manufacture of RASM collagen constructs and contractile force measurement

RASM collagen constructs were manufactured to the same specifications as the C2C12 constructs, differing only in cell density and culture time. RASM constructs remodelled and narrowed over time, due to cellular attachment and alignment, in a similar fashion to their C2C12 counterparts. Alignment however was not found to be uniform throughout the construct, nor was the density of the cells. Cells appeared highly aligned and densely packed at the edges of the constructs but cells located near the floatation bars aligned perpendicular to those on the edge. This is due to uneven distribution of the tension through the gels, an observation found by Eastwood *et al*. when studying fibroblast seeded collagen constructs (Eastwood et al. 1998). They found that the in area directly around the floatation bars (referred to as the 'delta zone'), the gel was supported by the stiffness of the bars resulting in a lack of tension and consequently, a lack of

alignment. In contrast to the RASM constructs however these gels were stimulated with cyclic uniaxial loading for 16 hours, which resulted in more alignment within the centre of the gels than seen in this study. Expression of SM markers did not appear to show any change in phenotype than when cultured upon glass however cell morphology was more spindle-like in nature and expressed less obvious stress fibres due to the 3D collagen matrix (Hakkinen et al. 2011).

When stimulated to contract upon the CFM, RASM constructs registered no increase in force. SM constructs have been found previously to generate measurable force on the CFM; this was however caused by remodelling of the gel and not by agonist stimulation (Cheema et al. 2003). This was found to be because the load applied by the mass of the floatation bars and connecting hoops was too great (2.59 ± 0.19mN plus 3.30 ± 0.69mN applied by mass of floatation bar plus hoops; mean ± standard deviation, n=6 for floatation bars, n=4 for hoops) for the contractile force generated by the cellular contraction to overcome. This was exemplified by the difference noted in contraction between free floating RASM constructs and those still attached to the floatation bars. Additionally, the load applied by the floatation bars is greater than forces recorded in earlier studies of SM gel contraction (Oishi et al. 2000; Gilmont et al. 2013).

In order to measure contractile forces generated by RASM constructs, a simpler experimental setup was used. This setup was similar in concept to both the CFM and traditional organ baths in that it possessed both a fixed point and a force transducer. In this case however, the gels were attached to the transducer *via* a minuten pin (unlike CFM) and no perfusion system was connected to the chamber (unlike organ bath). The pins used to attach constructs to the force transducer applied a much lower initial load (0.070 ± 0.006 mN, n=6) than floatation bars. RASM constructs stimulated with UTP contracted whilst attached to the force transducer setup and force was successfully measured. Although the shape of the force over time curve was very similar between individual constructs, the maximal force generated by constructs varied greatly. This is

most likely due to the experimental setup as the pin has to be passed through the construct manually. As the constructs contract and reduce in size, any item held within the construct (such as a pin) would be displaced in the direction of contraction. Therefore if the pin is placed closer to the end of the construct, it will be displaced more than a pin positioned a few mm further towards the centre of the construct. This is obviously a major limitation of the experimental setup which would require modifying in order to increase the accuracy of the assay. The mean maximal force generated by the constructs was similar to that obtained from tissue engineered internal anal sphincter constructs stimulated with KCl (Gilmont et al. 2013). It was approximately half the level of force achieved by guinea pig stomach smooth muscle cells seeded within collagen gel fibres stimulated with phenylephrine (approx. 1mN), although it is worth noting that the initial seeding density was 3 times higher than in the RASM constructs investigated here (Oishi et al. 2000).

RASM constructs contracted in a dose responsive manner in the range of 0.1 µM to 1mM, a range previously recorded by Miyagi *et al*. who measured the contractile force of bovine middle cerebral artery strips in response to UTP. The dose response curve produced by RASM construct contraction is very similar to curves of inositol (poly)phosphate accumulation in response to UTP stimulation of rat aortic SM cells (Harper et al. 1998; Kumari et al. 2003). RASM constructs were found to not increase in force when repeatedly stimulated with the same dose, indicating that contraction was concentration dependant.

Nifedipine is an L-type Ca^{2+} channel blocker that prevents the influx of extracellular calcium into the cell (Hayashi et al. 2010) that is used in the long term treatment of hypertension (Snider et al. 2008). 100 µM nifedipine has been found to inhibit Ca2+-sensitive K+ channels (Thomas-Young et al. 1993) and 10 µM nifedipine reduced calcium ion influx in vascular smooth muscle cells by 44% (Cirillo et al. 1993). Pre-treatment of RASM constructs with 100 µM nifedipine caused a significant reduction in the contractile force produced by the constructs in response to UTP stimulation but did not fully inhibit contraction. This was expected as the initial stage of SM contraction is not dependant on extracellular

calcium and is caused by release of Ca^{2+} ions from the sarcoplasmic reticulum. The influx of extracellular calcium is important for sustained contraction. Although much lower in force, sustained contraction was seen in nifedipine treated RASM constructs and was most probably due to the activity of T-type Ca^{2+} channels which are also present in SM cells (Hayashi et al. 2003; Hayashi et al. 2010) and are much more resistant to dihydopyridine calcium channel blockers (such as nifedipine) than L-type Ca^{2+} channels (Perez-reyes et al. 2009). These results strongly suggest the presence of L-type Ca^{2+} channels, a marker of differentiated vascular SM cells (Gollasch et al. 1998) and also display the ability of the RASM constructs and contraction assay to assess the effects of antagonists (as well as agonists) on SM contraction.

3.5.5 Chapter Summary

Within this chapter of work, RASM cells were successfully isolated and characterised *in vitro*. When seeded into collagen hydrogels they were found to contract them in response to chemical stimuli in a similar manner to primary human airway SM cells. RASM cells expressed high levels of SM markers SM22α and calponin and stained negative for desmin, all of which are expected from contractile vascular SM cells. Using the design of an established C2C12 model, RASM/ collagen gel constructs were established and stimulated to contract whilst free floating and attached to force measurement apparatus. Furthermore, RASM construct contraction was successfully measured using a force transducer. However this was not possible using the CFM due to the added mass of the floatation bars. This was overcome by directly attaching the constructs to a sensitive force transducer *via* a minuten pin. In the contraction studies, RASM construct contraction was found to be agonist concentration dependant and additionally, contraction could be inhibited by L-type Ca^{2+} channel inhibition.

Limitations of the RASM constructs developed and used within the chapter include the heterogeneity of cell alignment and density between different regions of the construct. This may affect the accuracy of uniaxial SM contraction measurement as a minority of the population (predominantly located close to

the floatation bars will contract perpendicular to the direction of force measurement. Finally, the attachment of the constructs to the force transducer currently introduces too much variability into the force measurement results; illustrated by the range of maximum force generated by individual constructs.

Following these studies, the next step was to develop a novel scaffold that could support the growth of a population of smooth muscle cells and improve the levels of alignment seen when compared to the collagen hydrogels which lacked uniformity. Therefore, scaffolds with topographical features that could guide this alignment would be highly beneficial. Electrospinning provides a method to generate fibrous scaffold mats, including those with aligned fibres. By manipulating the electrospinning parameters, it may be possible to produce scaffolds that can support the growth of aligned smooth muscle cells

4. Electrospinning aligned PET scaffolds for the *in vitro* 3D culture of Smooth Muscle cells

4.1 Introduction

As discovered in the previous chapter, collagen hydrogels can be used as a matrix to culture smooth muscle (SM) cells that can contract the gels in response to a stimulus. Additionally, when the gels are cultured under tension, the cells embedded within them align in response to the mechanical cues. However, this alignment is not uniform throughout the gel and additionally, the mechanical properties of the collagen gels (for example, elasticity) are much weaker than the ECM found *in vivo*. Therefore, an alternative scaffold matrix was sought that could not only provide topographical cues to the SM population resulting in a highly aligned population of cells but also possess mechanical properties that more closely represent *in vivo* environments. The field of tissue engineering has investigated and developed multiple ways of producing scaffolds or surfaces that can provide cells with topographical cues. In addition, a number of biocompatible polymers can be used to produce synthetic scaffolds, each with differing mechanical properties. Examples of methods that can be used to design scaffolds with topographic features include 3D printing(Serra et al. 2013), photolithography(Vasiev et al. 2013) and stereolithography (Gauvin et al. 2012). The focus of this chapter of work however will be upon the process of electrospinning, a technique used to draw fibres (usually in the micro or nano scale) from a polymer solution or melt using a high voltage electrical supply. These fibres can be collected as non-woven mats for various applications such as filtration membranes (Guo et al. 2011), textiles (Deitzel et al. 2001), drug delivery vessels (Zeng et al. 2003), wound dressings (Jia et al. 2007) and scaffolds for tissue engineering (Pham et al. 2006).

Electrospinning was first reported in 1934 by Formhals who submitted the patent titled 'Process and apparatus for preparing artificial threads' (Formhals 1934) Although the process of drawing fibres from a solution using an electrical charge had been known for many years before, prior to Formhals' work it was not possible to successfully collect the spun fibres. This was corrected by spinning acetate fibres onto a moving collector device. Formhals went on to refine his electrospinning method in subsequent patents (Formhals 1939) but it was to be another two decades before any further developments in electrospinning would be made. Whilst carrying out studies on the formation of electrically driven jets, Taylor examined the shape of the droplet at the tip of a needle when exposed to an electric field (Taylor 1969). He found that in this state the droplet forms a cone from which jets are ejected from the vertex. This droplet shape subsequently became known as the 'Taylor cone'. Later studies on the electrospinning of fibres began to focus on the morphology of the fibres themselves (Baumgarten 1971) and how the process parameters affected the resultant fibres (Larrondo & Manley 1981a; Hayati et al. 1987). Studies by Reneker and Chun investigating electrospun polyethylene terephthalate (PET) fibres expanded on the previous work by Taylor, describing the electrospinning jet as 4 regions: the base, the jet, the splay and the collection (Reneker & Chun 1996). The base is the droplet at the needle tip and its shape is dependent on both the voltage of the electric field and the surface tension of the solution. If the electrical field is strong enough to overcome the surface tension a jet is ejected from the tip of the cone. Electrostatic forces accelerate the jet as it travels towards the collector causing it to stretch; this coupled with the evaporation of volatile solvents causes the jet to narrow and decrease in velocity. Reneker and Chun hypothesised that charge repulsion within the jet caused it to split (or splay) into multiple equal fibres before being deposited on the collector. This was however later disproved by Shin *et al.* who studied the jet using high speed photography finding that the 'splaying' fibres was actually a single rapidly whipping jet (Shin et al. 2001). An illustrated diagram of the electrospinning process is shown in **Figure 4.1**.
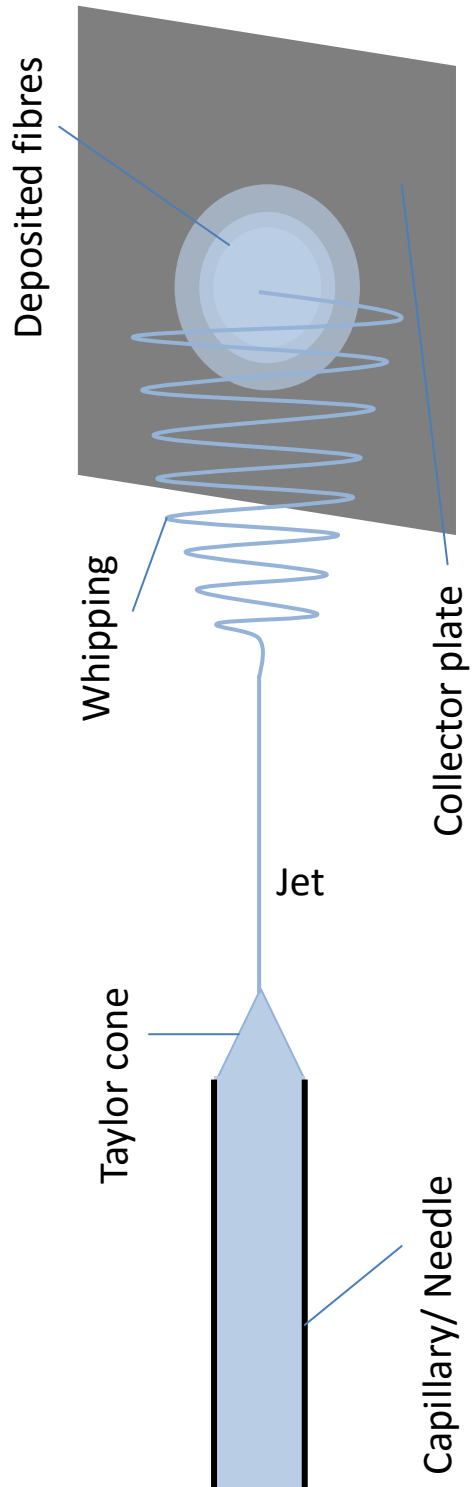
Figure 4.1: Diagram displaying the key aspects of the electrospinning process.

Many factors have been found to affect the morphology of the resultant fibres produced by electrospinning. Properties of the polymer solution, variation in the electrospinning apparatus and external parameters have all been found to play a role in the fate of electrospun fibres. It is worth noting that some parameters have a greater effect on fibre morphology than others and also that some parameters (such as solution viscosity and polymer concentration) are intrinsically linked. Polymer concentration and solution viscosity have been found to have a direct effect on fibre diameter when electrospinning a wide range of polymers such as poly(lactic co-glycolic aclid) (PLGA) (H. S. Kim et al. 2005), PET (Kim et al. 2004), poly(vinyl alcohol) (PVA) (Koski et al. 2004; Zhang et al. 2005), poly(L-lactic acid) (PLLA) (Jun et al. 2003), polystyrene (Jarusuwannapoom et al. 2005) and poly(ethylene oxide) (PEO) (Son et al. 2004). When low polymer concentration solutions are electrospun, the resultant fibres contain non-uniform spherical defects (an effect referred to as beading) caused by the jet breaking down into droplets (Kumbar et al. 2007); a similar result is seen when electrospraying (Bock et al. 2011). At low concentrations the collected fibres may still be wet with solvent resulting in merging of fibres forming 'junctions'(Deitzel et al. 2001). As the concentration and viscosity increase however, the level of beading and junctions observed reduces and the diameter of the fibres increases (Ki et al. 2005; McKee et al. 2004). However, if the solution is too concentrated, the droplet can dry out at the needle, blocking the flow of solution on preventing any further electrospinning (Zong et al. 2002; Duan et al. 2004). The solution conductivity and surface tension have also been found to affect the electrospinning process; for example, beading can be reduced in electrospun fibres by adding salts to increase solution conductivity (Mit-uppatham et al. 2004; Kim et al. 2005) and surfactants to decrease the surface tension (Yao et al. 2003; Lin et al. 2004). Cationic surfactants such as cetyltrimethylammonium bromide (CTAB) (Yang et al. 2009) or tetraethylammonium chloride (TEAC) (Chaurey et al. 2012) can be added to solutions to alter both the conductivity and surface tension of solutions. It is

worth noting that it is also possible to electrospin a polymer from a melt (Larrondo & Manley 1981a; Larrondo & Manley 1981b; Larrondo & Manley 1981c), removing the effects of solvent properties from the electrospinning process. One advantage that melt electrospinning possesses over solution electrospinning is that much greater control over fibre deposition can be achieved (Dalton et al. 2008) allowing for the production of intricate lattices (Hutmacher & Dalton 2011) or even precise writing (Brown et al. 2011).

In addition to the solution concentration, the parameters that are easiest to control are those that are part of the electrospinning setup. These include the flow rate, needle size (and design), applied voltage and the distance between the needle and collector. The rate at which the polymer solution is ejected from the needle has been found to affect the diameter of electrospun fibres. Lowering the flow rate can produce fibres with smaller diameters (Zong et al. 2002). Conversely, increasing the flow rate can lead to wet fibres being deposited on the collector (Yuan et al. 2004). The needle diameter effects the velocity of the solution at a set flow rate, additionally, the shape size and stability of the Taylor cone is linked to needle diameter (Scheideler & Chen 2014). In addition to this, by changing the design of the needle to a co-axial two-capillary design, it is possible to produce hollow fibres (Li & Xia 2004; Yu et al. 2014) or two separate polymers together in a core-shell fibre design (Zhuo et al. 2011; Kriel et al. 2012). This approach can also be used to encapsulate active molecules within the fibres (Yu et al. 2011). The electric potential applied across the electrospinning setup needs to be strong enough to overcome the surface tension of the solution and form a Taylor cone. Several studies have investigated the effects of voltage on the electrospinning process however there does not appear to be a clear correlation between voltage and fibre diameter. Studies electrospinning PDLA (Zong et al. 2002)and PVA (Zhang et al. 2005) reported an increase in fibre diameter with increasing voltage whereas those electrospinning polysulfone (Yuan et al. 2004) and protein polymers (Buchko et al. 1999) have reported the opposite. One effect of applied voltage that is widely reported however, is that too high a voltage will result in beading (Zong et al. 2002; Zhang et al. 2005; Yuan

et al. 2004) due to the Taylor cone receding into the needle tip (Deitzel et al. 2001). The final controlled parameter is the distance placed between the needle tip and the collector. Fibres that are spun too close to the collector will still be wet upon collection resulting in non-uniform fibres or junctions between fibres. Studies by Baker and co-workers suggest that there is a linear trend between the distance and the fibre diameter with diameter reducing as distance increases (Baker et al. 2006). At increased distances beading has been observed (Lee et al. 2004), most probably due to increased jet instability and whipping. Environmental parameters such as temperature and humidity are also known to have effects on the electrospinning process. An increase in temperature can lead to decreased fibre diameter due to reduced solution viscosity (Mit-uppatham et al. 2004) and increased humidity can lead to the development of pores on the surface of fibres (Casper et al. 2004) and a reduction in fibre uniformity (Pelipenko et al. 2013).

In order to produce aligned fibrous scaffolds through electrospinning, the design of the collector needs to be taken into consideration. Electrospinning onto a flat collector plate (in the majority of cases) will result in a randomly oriented scaffold. Therefore, other collector designs have been used in the pursuit of aligned fibres. By electrospinning directly onto a rotating drum or mandrel, it is possible to generate aligned fibre scaffolds; however, the degree of alignment achieved is dependent on the velocity of the drum itself (Bashur et al. 2006; Hadjizadeh et al. 2011a). An alternative method to generate aligned fibres is to use two parallel electrodes to collect fibres. This can be achieved either by using dielectric materials (Yan et al. 2009) or separating two conductive strips by an insulative material such as glass (Li et al. 2003). Chaurey *et al* compared these two methods of aligning electrospun fibres using solutions of PLGA. They found that greater alignment was achieved when using parallel electrodes and that in both methods, fibre alignment increased with fibre diameter (Chaurey et al. 2012).

Both fibre diameter and alignment, in addition to the mechanical properties of the scaffold, have been found to affect the behaviour of cells cultured upon

them. Therefore, when designing electrospun scaffolds for tissue engineering applications, it important to attempt to recreate the extracellular environment found *in vivo.* For example, chondrocytes cultured upon electrospun PLLA were found to have higher rates of proliferation and increased glycosaminoglycan production on nanofibres than on microfibres (Li et al. 2006). This effect was also seen in fibroblasts cultured upon Bombix mori silk fibroin scaffolds with fibres ranging from 250 to 1200 nm. Fibres 250 to 300nm in diameter supported cell proliferation significantly more than those in the 1 µm range (Hodgkinson et al. 2014). In addition, the number of cell-fibre interactions reduced as fibre diameter increased. On the other hand, NIH 3T3 fibroblast proliferation was not significantly altered by the diameter of PLGA scaffolds (Bashur et al. 2006). Schwann cells also have been found to proliferate and adhere faster upon nanofibres than microfibres although cell migration and motility was greater on microfibres (Gnavi et al. 2014). A study by Rueder *et al* cultured human umbilical vein endothelial cells (HUVECs) and SM cells on electrospun copolyetheresterurethane (PDC) fibres ranging from 2 µm to 500 nm in diameter. HUVEC viability and proliferation was higher on microfibre scaffolds whereas nanofibre scaffolds supported SMC viability (Rueder et al. 2013), indicating that cell response to fibre diameter is dependent on the cell type.

Fibre alignment has been reported to have a clear effect on cell morphology and behaviour. For example, human ACL fibroblasts appear spindle-shaped and orientate in the fibre direction of aligned polyurethane fibres. They were also found to synthesize significantly more collagen when cultured upon aligned than randomly orientated fibres (Lee et al. 2005). Aligned PLGA fibres have been reported to enhance the proliferation of rat periodontal ligament cells when compared to randomly aligned and 2D PLGA controls (Shang et al. 2010). Furthermore, aligned fibrous scaffolds have also been found to promote Schwann cell maturation (Chew et al. 2008) and modulate axon organisation (Gnavi et al. 2015). Similar to the study by Rueder *et al* who found differential behaviours between cell types on different diameter fibres, a corneal engineering study by Yan *et al* found that aligned fibres were favoured by

keratocytes whereas corneal epithelial cells interacted better with random fibres (Yan et al. 2012).

SMCs have been cultured on electrospun scaffolds made from several materials including PCL (Zhu et al. 2010), PLLA (Ahvaz et al. 2012), P(LLA-CL) (Xu et al. 2004) and a PCL-gelatin copolymer (Kuppan et al. 2015). SMCs cultured upon aligned fibres are reported to possess a spindle like morphology and higher expression of cytoskeletal markers indicative of a contractile phenotype (Zhu et al. 2010; Xu et al. 2004). In this chapter of work, solutions of PET were electrospun to generate various aligned scaffolds designed for the culture of primary HASM cells with the aim of producing a confluent, aligned population of contractile smooth muscle cells. PET was chosen as the initial polymer to study due to its biocompatibility and chemical stability during electrospinning; it is non-biodegradable (with potential for long culture periods) and also cost effective. The mechanical properties of PET also allow for the manual handling of fibrous scaffolds in cell culture. PET is a member of the polyester family and has the repeating polymer unit displayed in **Figure 4.2**. Some investigations into the effects of electrospinning parameters on PET fibres have already been undertaken (Hadjizadeh et al. 2011a; Veleirinho et al. 2007; Kim et al. 2004) however due to the complex nature of electrospinning, many of the parameters differ between studies.
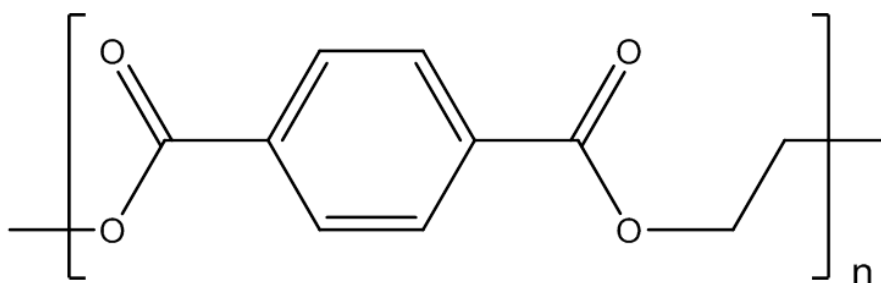
Figure 4.2: Repeating monomer unit of polyethylene terephthalate (PET).

4.2   Chapter Aims

The work carried out within this chapter aims to achieve the following:

Develop a range of electrospun scaffolds that can facilitate the culture of a population of aligned and randomly oriented smooth muscle cells. This will be achieved by:-

- Investigate the effects of electrospinning parameters on the morphology of electrospun PET fibres

- Develop sets of electrospinning parameters that can produce fibres ranging from 100s of nanometres to several micrometres in diameter from solutions of PET.

- To align the electrospun fibres by using a rapidly rotating mandrel to collect the fibres.

- To characterise the physical and mechanical properties of both the random and aligned electrospun scaffolds.

- Assess the effects of fibre diameter and fibre orientation on the resultant morphology and phenotype of cultured HASM cells

- To attempt to stimulate contraction of SM cells cultured upon the PET scaffolds

4.3 Materials and Methods

4.3.1 Production of electrospun PET scaffolds

Solutions of polyethylene terephthalate (PET) at various concentrations were made from PET pellets (Sigma Aldrich, Dorset, UK) or bottles (Lucozade, GSK, UK) by dissolving the PET in a solvent mixture of dichloromethane (DCM, Fisher Scientific, Loughborough,UK) and trifluoroacetic acid (TFA, Fisher Scientific) at a ratio of 1:1. In some cases, solutions were also made with 1% *w/v* cetyltrimethylammonium bromide (CTAB, Sigma Aldrich) or 1% *w/v* Triton X-100 (Sigma Aldrich) in order to increase solution conductivity and reduce surface tension. Solutions were stirred using a magnetic stirrer overnight at room temperature. The PET solutions were added to a 10ml syringe (BD Falcon™, Oxford, UK) and electrospun following the protocols described in **Section 2.1.** Flow rates ranged from 0.5 to 4.0 ml h^{-1}, needle diameters used were either 18 or 23 G and PET concentration ranged from 7 to 50% *w/v*. Voltage (14 kV), volume of solution spun (2.0 ml) and needle-collector distance (15 cm) all remained constant throughout this chapter. The collector mandrel speed ranged from static to 2000 rpm to produce scaffolds that were randomly oriented or aligned. Upon completion of electrospinning, scaffolds were cut from the mandrel using a scalpel blade and stored in aluminium foil.

4.3.2 Analysis of electrospun PET scaffolds

Scaffold fibre diameter and fibre alignment were determined by analysis of SEM micrographs using the image analysis software packages MeasureIT (Olympus Soft Imaging solutions GmbH, Münster, Germany) and ImageJ respectively. Alignment was calculated by expressing individual fibre angles as deviations from the sample mean fibre angle. SEM sample preparation and SEM protocols were as described in **section 2.2**. Scaffold pore size was also measured from SEM

images using the MeasureIT software (Olympus Soft Imaging Solutions, Münster, Germany).

Scaffold porosity was calculated was estimated using the following formula (Hadač et al. 2007):

$$\text{Porosity (\%)} = 1-(ad/bd) \times 100$$

Where ad is the apparent density of the scaffold and bd is the density of pure amorphous PET (1.335 g/cm^3). Samples of scaffold were cut out using an 8.0mm diameter biopsy pen, the mass of these samples measured using a top-pan balance (accurate to 0.1 mg) (Mettler Toledo, Leicester, UK) and the thickness measured using a digital thickness gauge (accurate to 10 μm) (Mitutoyo, Coventry, UK). These measurements were used to calculate the apparent density of the scaffold.

The tensile properties of the scaffolds were determined through uniaxial tensile tests using a Universal testing system (Instron, High Wycombe, UK) and a Video Gauge (Imetrum Limited, Bristol, UK) as described in **section 2.3**. N=3 individual scaffolds per scaffold type, 3 measurements per scaffold

4.3.3   Production of a biphasic electrospun PET scaffold

Biphasic scaffolds were produced by firstly electrospinning a microfibre PET scaffold onto a rotating mandrel (60 rpm/ .022 ms^{-1}). Microfibre scaffolds were produced by spinning 2 ml of a 30% *w/v* PET solution at 2 ml h^{-1} through an 18 G needle. The voltage and needle-collector distance were as previously stated. Once complete, a nanofibre scaffold was electrospun directly onto the existing microfibre scaffold. Nanofibre scaffolds were produced by spinning 1.5 ml of 8% *w/v* PET solution at 0.5 ml h^{-1} through a 23 G needle. Again the voltage and needle-collector distance remained unchanged. The biphasic scaffold was then cut from the mandrel using a scalpel and stored in aluminium foil.

4.3.4 Decellularisation of bronchial tissue

Bronchial tissue segments from 3 individual donors were isolated from bronchial biopsies carried out at the Glenfield Hospital (Leicester, UK) as described previously (Kaur et al. 2006). The procedure was approved by the Leicestershire Ethics Committees and all donors gave their written informed consent. The tissue was frozen at -80 °C and sliced into thin sections using a scalpel blade. The decellularization procedure was modified from a previously published protocol (Schaner et al. 2004). Sections were washed with PBS before being incubated overnight in 0.5% *w/v* SDS solution in PBS at 37 °C overnight on a tube roller. Sections were washed 5 times in PBS (10 minutes per wash) before being fixed in 3% *v/v* glutaraldehyde solution overnight at 4 °C. Sections were washed with PBS 3 times (10 minutes per wash) before being dehydrated through a series of ethanol concentrations: 25%, 50%, 70%, 90%, 95% *v/v* EtOH in H_2O (10 minutes each) before 3 100% EtOH solutions (5 minutes each). Sections were then dried at 37 °C overnight before being prepared for SEM imaging as described in **section 2.3.**

4.3.5 Human Airway Smooth Muscle culture on electrospun PET scaffolds

Primary HASM cells from 3 individual donors (defrosted at passage 6 and cultured until passage 8) were cultured in HASM media as described in **section 2.4.1**. Cells (1×10^5) were seeded onto individual aligned 10%, 20% and 35% PET scaffold samples and cultured in 2 ml HASM media over a 14 day period (at 37 °C, 5% CO_2 in air) to assess cell proliferation and viability. Where necessary, scaffolds (20% and 35%) were adhered to the bottom of well plates using aquarium sealant (Sinclair animal and household care Ltd., Gainsborough, UK) whereas 10% scaffolds were held in place with stainless steel rings. All scaffolds were sterilised by UV treatment for 20 minutes on either face and soaked in a 5% (*v/v*) antibiotic/antimycotic solution (10,000 units ml^{-1} penicillin G, 10 mg ml^{-1} streptomycin sulfate and 25 µg ml^{-1} amphotericin B) overnight at 4°C. Scaffolds were then washed with PBS prior to cell seeding. HASM cells were also cultured

on tissue culture plastic and glass coverslips for immunocytochemistry (**section 2.6**).

4.3.6 AlamarBlue® cell viability assay

HASM viability was measured post seeding on aligned scaffolds using the alamarBlue® assay at various time points across a 14 day period. Samples were washed with PBS prior to were incubation with 1ml alamarBlue® solution (10% (*v/v*) alamarBlue® in HASM culture media) for 90 minutes at 37 °C. The alamarBlue was then collected (100 µL aliquots) and replaced with ASM media. The fluorescence emissions of the collected samples were measured on a plate reader (excitation 560 nm/ emission 590 nm) (Tecan Infinite M200, Reading, UK).

4.3.7 Scaffold contraction assays

Samples of 10% *w/v* PET scaffolds were prepared as described above (**section 4.3.1**) and cut into discs. Scaffolds were placed in 6 well culture plates and sterilised by UV exposure (20 minutes each side) followed by incubation in cell culture media (60 minutes, 37°C) prior to seeding of cells. Primary HASM cells (2 x 10^5) were seeded onto individual PET disks, samples were then incubated for 10 days (37°C, 5% CO_2 in air) to allow cell proliferation.

Following incubation, culture media was aspirated and 1 ml serum free DMEM added to each sample, plates were then imaged using a flatbed scanner. 1 ml serum free DMEM ± 200 µM histamine was then added to each sample. Well plates were then imaged at specific time intervals for 60 minutes. Scanned images were analysed using ImageJ; changes in scaffold surface area were used to determine the level of scaffold contraction.

4.4   Results

In order to develop a model of SM tissue that is more representative than a hydrogel based SM model, a suitable scaffold that could: (1) support the attachment and proliferation of ASM cells, (2) direct the alignment of these cells, and (3) possess the correct mechanical properties to facilitate SM contraction; needed to be developed. The morphologies of electrospun fibres are affected by virtually all electrospinning process parameters (flow rate, needle-collector distance, temperature, humidity etc.). However, not all parameters affect the properties of the final scaffold to the same degree. Due to this, various combinations of differing parameters exist within the literature. The initial parameters chosen to electrospin PET were derived from previous work done within the Tissue Engineering research group at Nottingham and are presented in **Table 1**. The initial source of PET used was from PET pellets (supplied by Sigma). The resultant fibres obtained when using these parameters were analysed using SEM images. The fibres appeared fine and uniform in diameter however they contained many imperfections in the form of beads (**Figure 4.3A**). In order to remove this beading and create a range of scaffolds differing in fibre diameter as well as fibre orientation, several process parameters would have to be changed and this was investigated within this thesis.

PET concentration	Flow Rate	Voltage	Needle-collector distance	Needle	Solvent
8%	0.5 ml h^{-1}	14 kV	15 cm	18 G	1:1 DCM:TFA

Table 4.1: Initial nanofibre electrospinning parameters

4.4.1 Effects of flow rate and PET solution concentration on fibre diameter and morphology

Initial studies into the electrospinning parameters focussed on the PET concentration and the rate at which the solution was expelled from the syringe. A range of concentrations and flow rates were tested and the resultant fibres were imaged using SEM, these are summarised in **Figure 4.3**. When attempting to spin nanofibres, solutions of 7%, 8% and 10% *w/v* PET at a flow rate of 0.5 ml h^{-1} all produced highly beaded scaffolds (**Figure 4.3** images **A** and **C**) although the amount of beading did appear to reduce slightly with increasing concentration. A 12.5% (*w/*v) solution still resulted in beaded scaffolds whilst the fibres were becoming visibly thicker than those produced from lower concentrations of PET. When spinning microfibre scaffolds at concentrations ranging from 25% to 50% *w/v* PET, no beaded fibres were observed. An increase in flow rate when electrospinning 50% *w/v* PET solutions was necessary to produce fibres without blockage of the needle occurring. When increased further, flow rate had a marked effect on the morphology of the fibres produced. When spinning at low rates of 0.5 ml h^{-1}, the electrospinning process failed due to the needle blocking. Doubling the flow rate to 1 ml h^{-1} prevented the solution from drying and blocking the needle but produced flat ribbon-like fibres that lacked uniformity in shape and diameter (**Figure 4.3G**). Electrospinning the same solution at 2ml h^{-1} removed this issue and produced uniform microfibres. Further increasing the flow rate to 4ml h^{-1} did not make any visible difference to the individual fibres produced but the thickness of the scaffolds produced were uneven due to fibres depositing in localised areas on the collector plate rather than being evenly distributed as seen when electrospinning at the slower flow rates.

4.4.2 Effects of the addition of cationic surfactants to PET solution to fibre morphology

Addition of 1% *w/v* of the cationic surfactant cetyltrimethylammonium bromide (CTAB) to the nanofibre PET solutions (8% and 10% *w/v*) caused a visible reduction in the amount of beading in the resultant fibres. **Figure 4.4** displays

	Scaffold	PET concentration (w/v, %)	Flow rate (ml/h)	Needle-collector distance (cm)	Voltage (kV)	Beading observed	Other observations
Nanofibres	A	8.0	0.5	15	14	✓	Very fine fibres with large beads
	B	7.0	0.5	15	14	✓	Very fine fibres with large beads
Microfibres	C	10.0	0.5	15	14	✓	Fibres unevenly distributed. Visible bundles of fibres
	D	12.5	0.5	15	14	✓	Slightly thicker fibres but still many beads
	E	25.0	0.5	15	14		Mainly uniform microfibres with occasional thicker fibres
	F	50.0	0.5	15	14		Failed: Blocked needle
	G	50.0	1.0	15	14		Fibres possess a ribbon like morphology with non-uniform fibre diameters
	H	50.0	2.0	15	14		Uniform microfibres
	I	50.0	4.0	15	14		Uniform microfibres
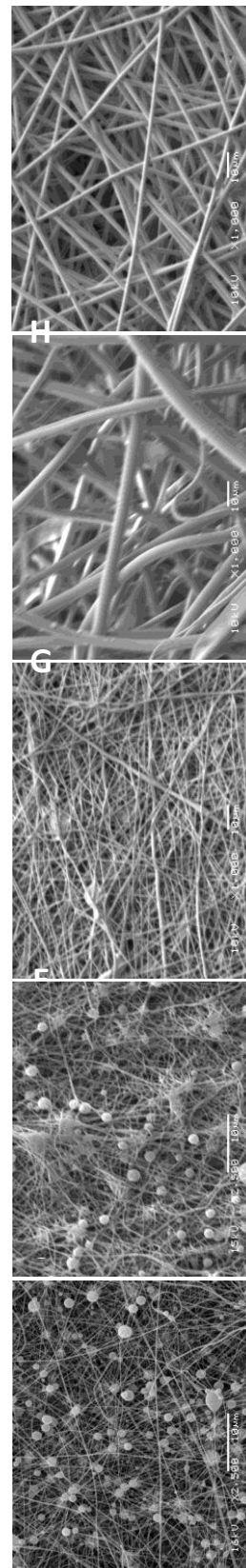
Figure 4.3: Effects of flow rate and PET concentration on fibre morphology and diameter. Matrix describing the initial investigations into the effects of PET concentration and flow rate. In addition, SEM images showing representative images of some scaffolds are shown. Labelling refers to scaffold letters in the matrix.
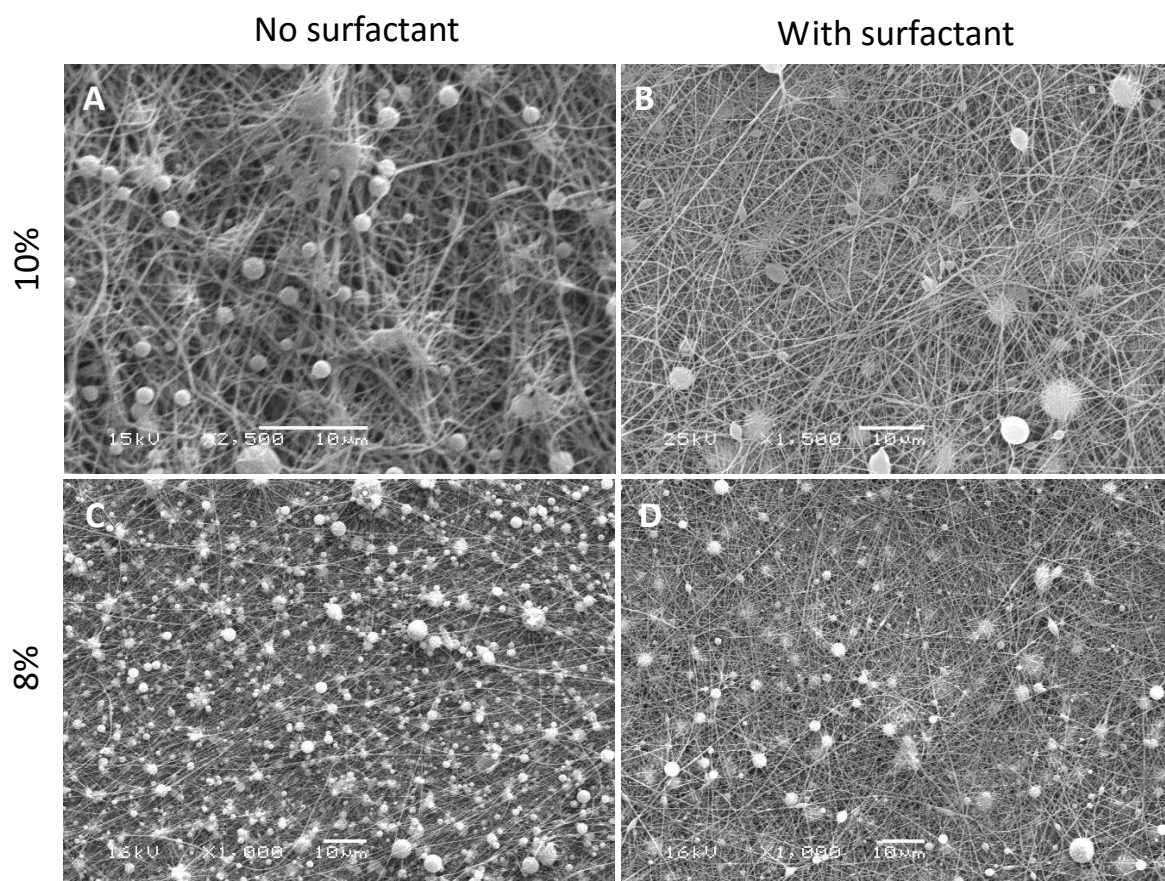
Figure 4.4: Changing scaffold morphology by addition of surfactants. SEM images of nanofibre scaffolds spun from 10% (**A,B**), and 8% (**C,D**) *w/v* PET pellet solutions. Scaffolds **B** and **C** were spun with the addition of 1% CTAB to the PET solution mixture.

SEM images of nanofibre scaffolds electrospun with and without the addition of surfactant in the PET solution. Another cationic surfactant, tetraethylammonium chloride (TEAC) was also added to PET solutions to reduce beading however the resultant electrospun fibres were repelled from the collector plate making itimpossible to collect a scaffold. The non-ionic surfactant Triton X-100 produced similar results to CTAB in terms of fibre morphology but the scaffolds themselves were very thin and fragile, making them impractical for use in cell culture.

4.4.3 Assessing the source of PET used for electrospinning

Solutions of PET made from PET pellets consistently produced cloudy solutions which contained an insoluble precipitate. This made it difficult to ascertain the actual concentration of the PET solutions as the precipitate was not electrospun. In contrast, solutions made from PET originating from plastic bottles produced clear solutions with no precipitate. To investigate this, the ^{1}HNMR spectra of both PET sources were obtained (**Figure 4.5**). The spectra of the PET from both sources were very similar however the spectra obtained from PET pellets contained several small peaks indicative of impurities that were not present in the spectra of PET from bottles.

The difference between using PET pellets and bottles for producing fibrous scaffolds was investigated by electrospinning scaffolds from equivalent concentrations of PET from both sources. The two groups of scaffolds greatly differed in fibre size and morphology (**Figure 4.6**). A 10% *w/v* solution of PET from bottles produced bead free nanofibres (**Figure 4.6A**) whereas the same concentration of PET pellets resulted in beaded nanofibres, even with the addition of cationic surfactants (1% *w/v* CTAB) (**Figure 4.6C**). A 35% *w/v* solution of PET from bottles produced thick uniform microfibres (**Figure 4.6B**) whereas the same concentration solution from PET pellets produced much thinner and less uniform fibres. Due to the improved morphology of both the nanofibre and microfibre scaffolds when using PET sourced from PET bottles, pellets were no longer used as the source of PET for any further experiments.
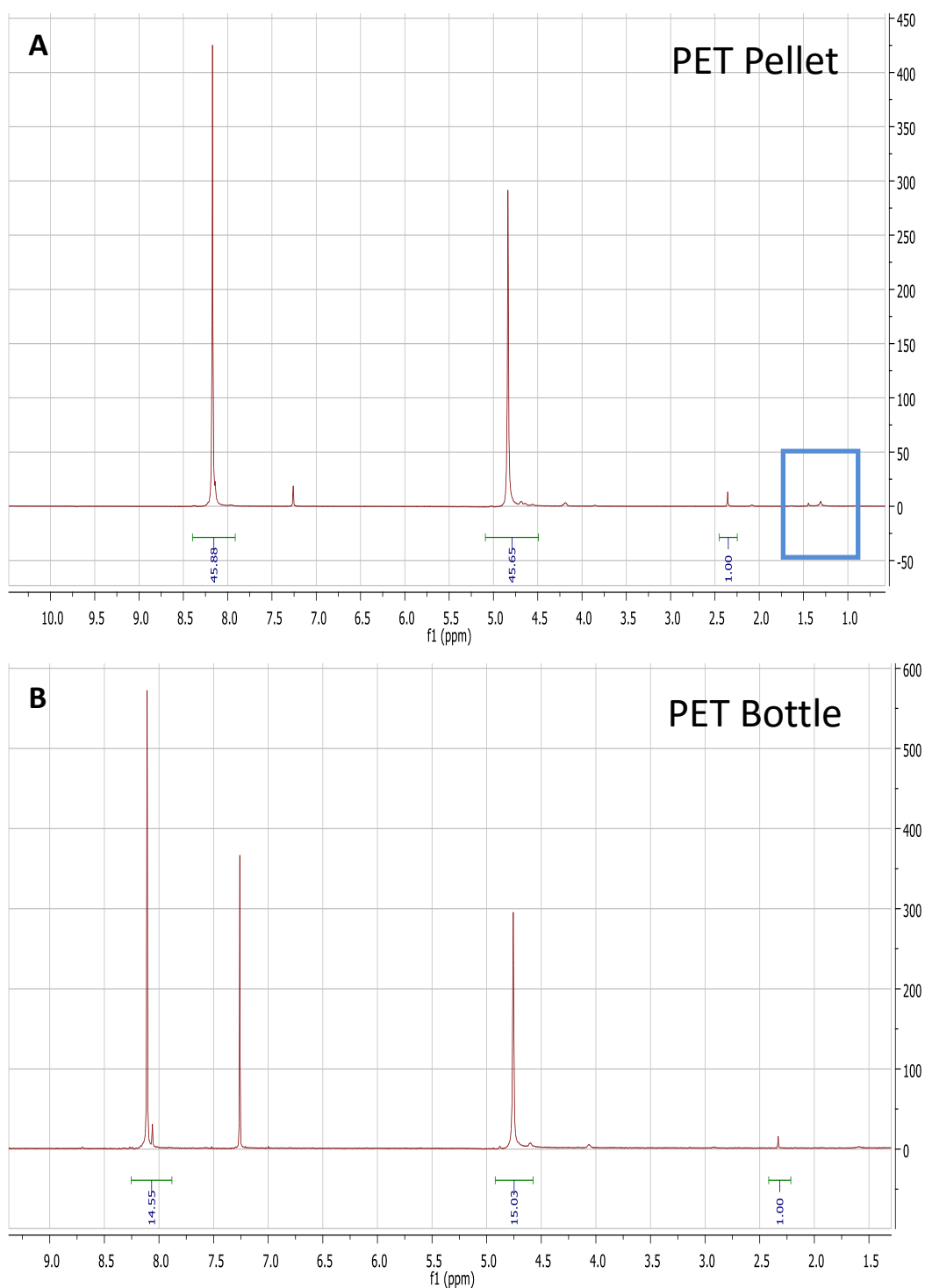
Figure 4.5: ^{1}HNMR spectra of PET pellets (**A**) and bottles (**B**). Possible impurities within the PET pellet spectrum are highlighted with a blue rectangle.

PET pellets

PET bottles

35% PET

10% PET
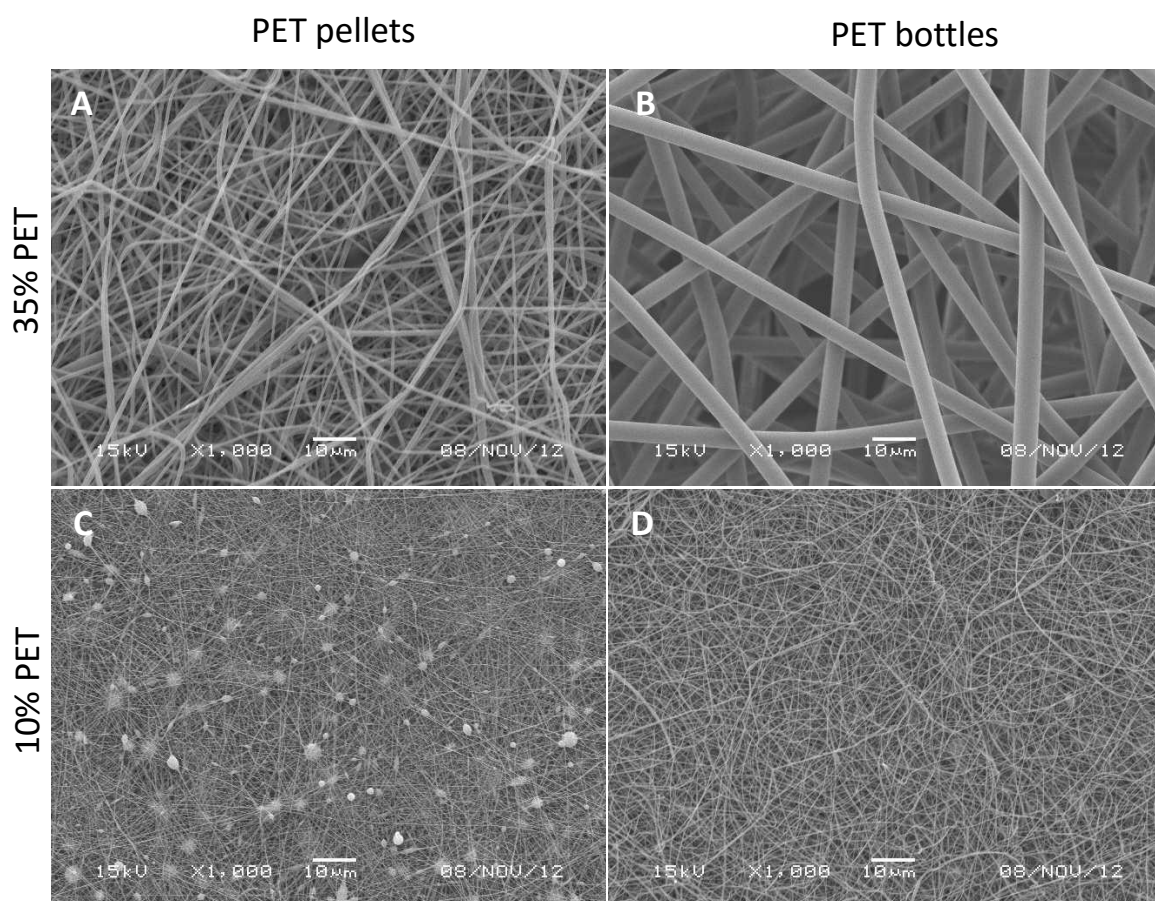
Figure 4.6: PET pellets vs. PET bottles. Representative SEM images of scaffolds spun from PET pellets (**A**,**C**) and PET bottles (**B**,**D**). Microfibre scaffolds (**A**,**B**) spun from 35% *wt/vol* PET solutions and nanofibre scaffolds (**C**,**D**) spun from 10% *wt/vol* PET solutions . 1% *wt/vol* CTAB was also added to the PET solution for scaffold **C**.

4.4.4 The effect of needle size on the production of nanofibres

In order to determine the thinnest obtainable PET nanofibres, the concentration of PET used was reduced from 10% to 8% *w/*v. Nanofibres electrospun from 8% *w/v* PET solutions at a flow rate of 0.5 ml h^{-1} contained a small amount of beads when spun using a blunt tip 18 G needle. When using a narrower 23 G needle instead, the beading was removed, generating uniform bead free nanofibres. **Figure 4.7** shows the effect of the needle used on the morphology of the resultant fibres.

4.4.5 Properties and parameters of optimised PET nanofibre and microfibre scaffolds

The final electrospinning parameters chosen to manufacture uniform, bead free nanofibre and microfibre scaffolds are listed in **Table 2**. Parameters were reached following the investigative steps previously discussed (**sections 4.4.1 – 4.4.4**). In both cases the voltage, solvent ratio and needle tip – collector distance were the same (14 kV, 1:1 DCM:TFA and 15 cm respectively). Microfibres were electrospun using 2 ml of a 30% *w/v* solution of PET sourced from plastic bottles at a flow rate of 2 ml h^{-1} with a blunt tip 18G needle. Nanofibres were electrospun using 1.5 ml of an 8% *w/v* solution of PET from plastic bottles at a flow rate of 0.5 ml h^{-1} with a 23 G needle.

By changing these parameters the scaffolds differed greatly in fibre diameter and thickness. The average fibre diameter in the microfibre scaffolds was 2.50 ± 0.02 µm (mean ± SEM) whereas the average fibre diameter in the nanofibre scaffolds was 255 ± 3.00 nm (mean ± SEM), approximately an order of magnitude smaller than the microfibre scaffolds (average fibre diameter was calculated by measuring the diameter of 20 fibres on 8 SEM images from 3 separate scaffolds (480 total measurements per scaffold type)). The distribution of fibre diameter in the two scaffold types ranged from 160 to 490 nm and 1.22 to 3.88 µm for the nanofibre and microfibre scaffolds respectively (**Figure 4.8**). The fibre diameters
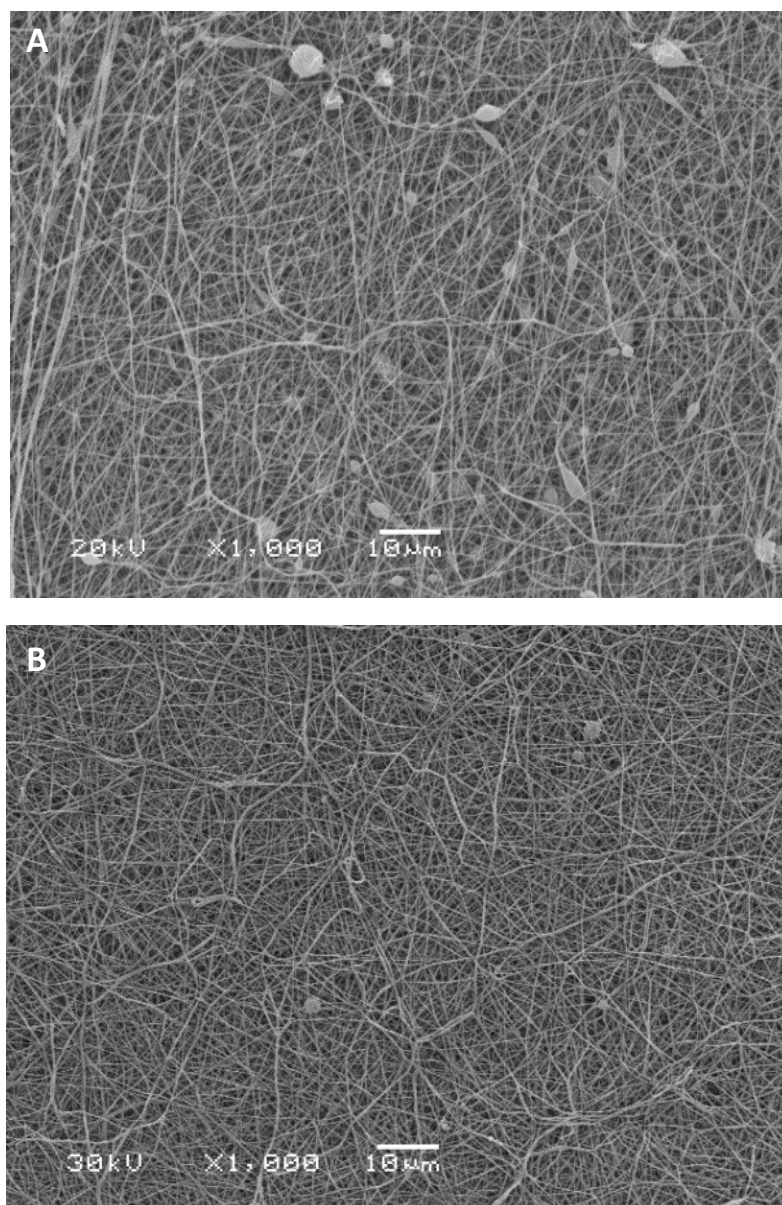
Figure 4.7: Effect of needle size on nanofibre scaffold morphology. Representative SEM images of scaffolds spun through different sized needles. Scaffold **A** was spun using an 18 G needle. Scaffold **B** was spun using a 23 G needle. Reduced beading was seen with the 23 G needle. Both scaffolds were spun from an 8% PET (bottle) solution at a flow rate of 0.5 ml h^{-1}

	Conc. of PET (w/v, %)	Solvent (DCM:TFA)	Voltage (kV)	N-C distance (cm)	Needle Gauge (G)	Flow Rate (ml/h)	Volume (ml)	Fibre Diameter (µm ± SEM)	Thickness (um)	Porosity (%)
Nano	8	01:01	14	15	23	0.5	1.5 ml	0.255 ± 0.003	24	84.26
Micro	30	01:01	14	15	18	2.0	2.0 ml	2.501 ± 0.021	120	89.01
Table 2: Final Electrospinning parameters for production of nanofibre and microfibre PET scaffolds										

Table 4.2: Final Electrospinning parameters for production of nanofibre and microfibre PET scaffolds
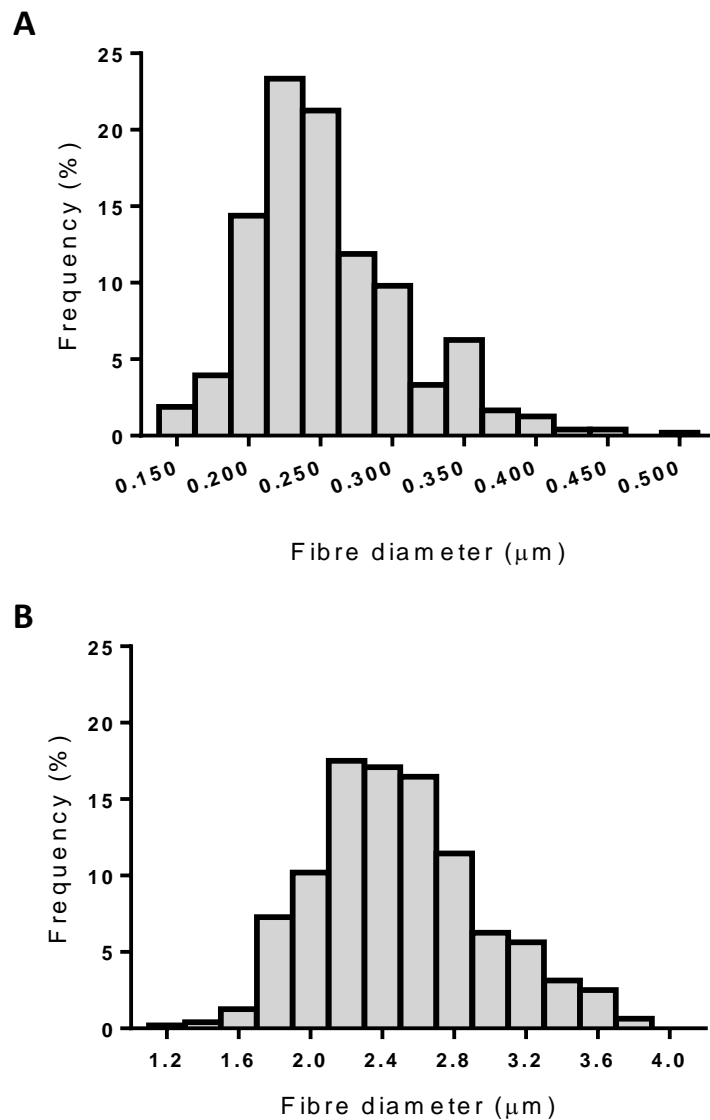
Figure 4.8: Comparison of fibre diameters between nanofibre and microfibre scaffolds. Histograms displaying the distribution of fibre diameters in the nanofibre (**A**) and microfibre (**B**) scaffolds. Fibre diameters were analysed by measuring the diameter of 20 fibres on 8 SEM images from 3 separate scaffolds (480 total measurements per scaffold type)
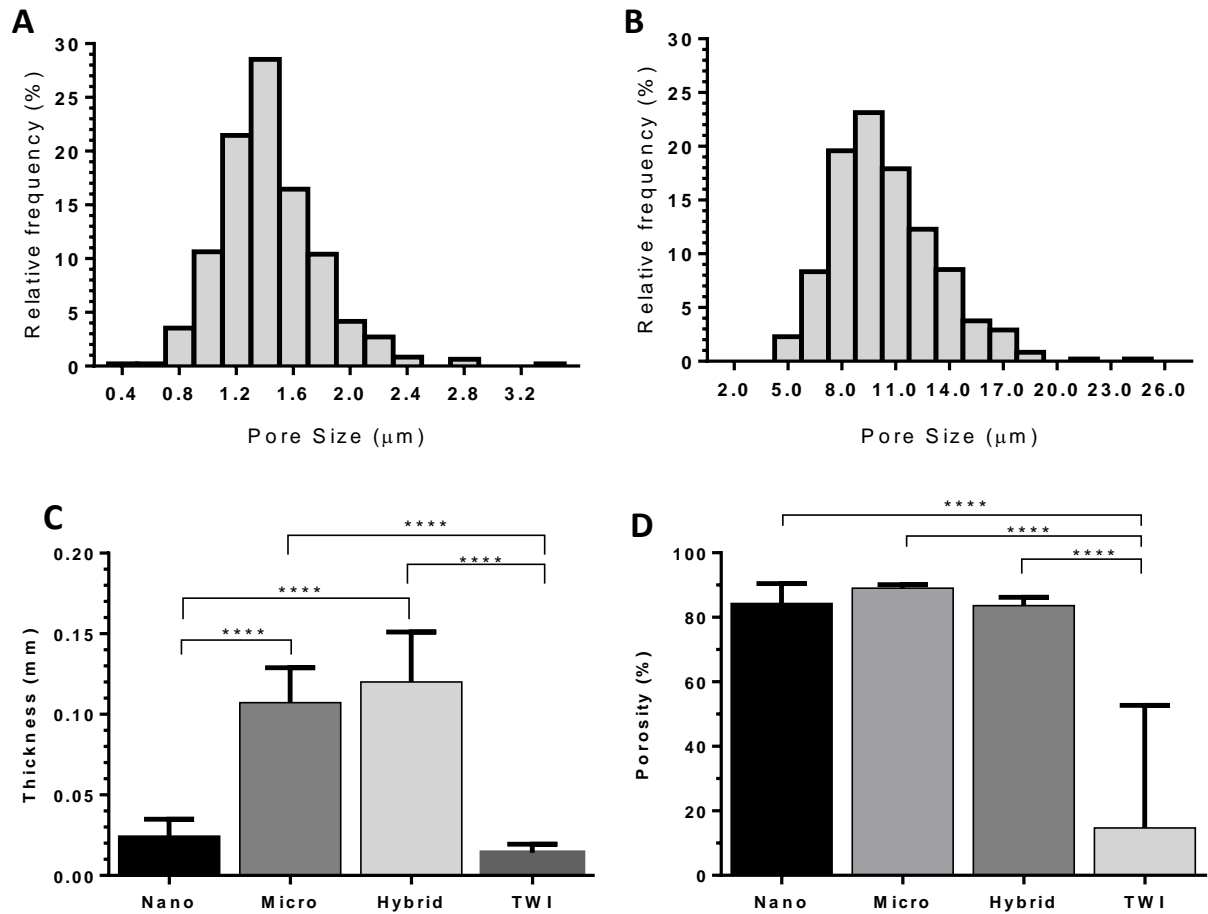
Figure 4.9: Properties of nanofibre and microfibre scaffolds. Pore size distribution of nanofibre (mean fibre diameter = 225 nm) (**A**) and microfibre (mean fibre diameter = 2.50 μm) (**B**) scaffolds, average scaffold thickness (**C**) and average porosity (**D**) of all scaffolds in addition to commercially available trans-well inserts. Error bars display the standard deviation. One way ANOVA with Tukey's multiple comparisons test was carried out between all scaffolds thickness and porosity. All scaffolds were significantly more porous than the trans-well inserts (****$P<0.0001$). N= 3 scaffolds, 3 measurements per scaffold.

of both scaffolds follow a normal distribution, as do the pore sizes in each scaffold (**Figure 4.9 A** and **B**). Scaffold thickness ranged from 10 to 50 µm in the nanofibre scaffolds and 50 to 150 µm in the microfibre scaffolds; average thickness of the nanofibre and microfibre scaffolds were 24 ± 2.5 µm and 107 ± 5.1 µm (mean ± SEM; n=6 scaffolds, 3 measurements per scaffold) respectively. There was a clear statistical difference seen between the two scaffolds ($P < 0.0001$, one way ANOVA with Tukey's multiple comparisons test). The, calculated porosities of the two scaffolds were quite similar with the nanofibre scaffold porosity measuring 84.33 ± 6.21% and the microfibre scaffold 89.06 ± 1.12% (mean ± standard deviation; n=3 scaffolds 3 measurements per scaffold). Although the two scaffolds had a very similar porosity, the average pore size in each scaffold was very different. The microfibre scaffolds had an average pore size of 10.45 ± 0.13 µm (mean ± SEM) whereas the nanofibre scaffolds had an average pore size of 1.43 ± 0.02 µm (mean ± SEM) (average pore size was calculated by measuring the width of 20 pores on 8 SEM images from 3 separate scaffolds (480 total measurements per scaffold type)).

4.4.6 Creating a biphasic scaffold from nanofibre and microfibre scaffolds

By electrospinning nanofibres directly onto pre-spun microfibres it was possible to create a scaffold consisting of two distinct, separate phases; a 'biphasic' or hybrid scaffold. The biphasic scaffold possessed a microfibre layer and a nanofibre layer with little or no merging between the layers. This was created with the intention of providing an environment where two different cell populations could be cultured separately, but within close proximity, on the same scaffold. SEM images of the biphasic scaffold are displayed in **Figure 4.10** where the clear distinction between the nanofibre and microfibre layers can be made. The average fibre diameters of each 'phase' of the scaffold were 280 ± 20 nm and 2.30 ± 0.06 µm for the nanofibre and microfibre layers respectively which are very similar to those seen from the individually spun scaffolds.
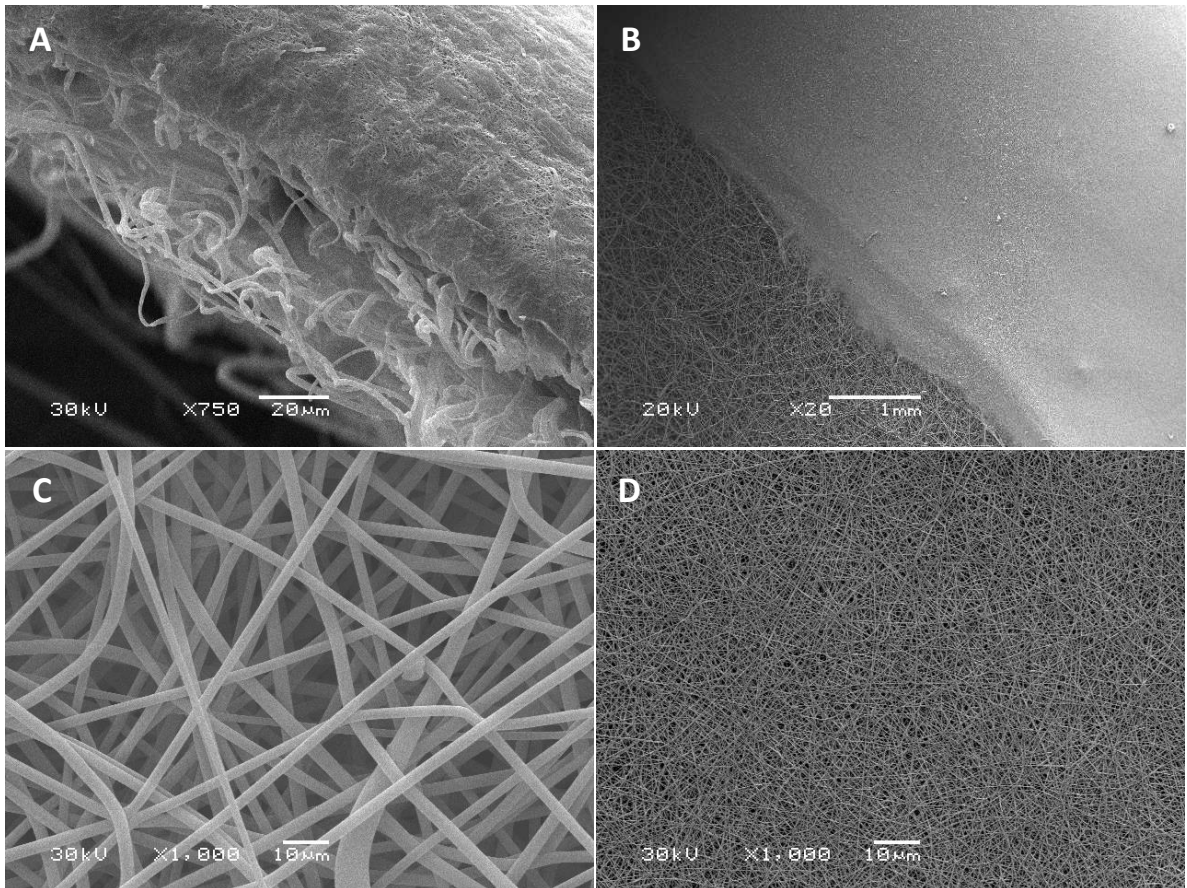
Figure 4.10: Biphasic electrospun scaffolds. A cross sectional view of a biphasic scaffold with the nanofibre scaffold on top of the microfibres (**A**). The two scaffold layers simultaneously from above (**B**) and the individual micro and nanofibre layers (**C** and **D** respectively).

The average thickness of the biphasic scaffold was 120 μm, slightly thinner than the sum of the individual microfibre and nanofibre scaffolds (**Figure 4.9 C**). All electrospun scaffolds were thicker than a commercial trans-well insert (10 μm) with a clear statistical difference (P<0.0001, one way ANOVA with Tukey's multiple comparisons test) seen between the trans-well inserts and both the microfibre and hybrid scaffolds. In addition, the average calculated porosity of the trans-well inserts (14.74%; **Figure 4.9 D**) was statistically much lower than all the electrospun scaffolds (P<0.0001, one way ANOVA with Tukey's multiple comparisons test).

When compared to decellularised bronchiole tissue from human donors (**Figure 4.11B** and **D**), the average fibre diameter of the nanofibre phase (350 ± 218 nm; mean ± SD; n= 3 scaffolds, 20 measurements per scaffold) was thicker than the average fibre diameter measured from the acellular reticular basement membrane which was 153 ± 30.6 nm (mean ± SD, n= 50 measurements) . Similarities in morphology can be seen between the cross sections of biphasic scaffolds and the decellularised tissue (**Figure 4.11C** and **D**), both possess a thin nanofibrous membrane with a thicker and much more porous layer of fibres or matrix proteins underneath.

4.4.7 Developing a rotating mandrel for the electrospinning of aligned fibres

To produce aligned fibres, a rotating mandrel approach was chosen as this method has the potential to produce much larger scaffolds (depending on the drum size) when compared to other methods such as parallel electrodes (Yan et al. 2009). This was necessary for cutting scaffolds for future cell culture and scaffold contraction studies. A mandrel was therefore designed and manufactured in-house by members of the medical engineering unit at the University of Nottingham; this allowed the mandrel to fit all required design specifications. Photographs of the mandrel are shown in **Figure 4.12** as well as a diagram of the mandrel within an electrospinning setup. The developed mandrel

	Scaffold	Decellularised Tissue
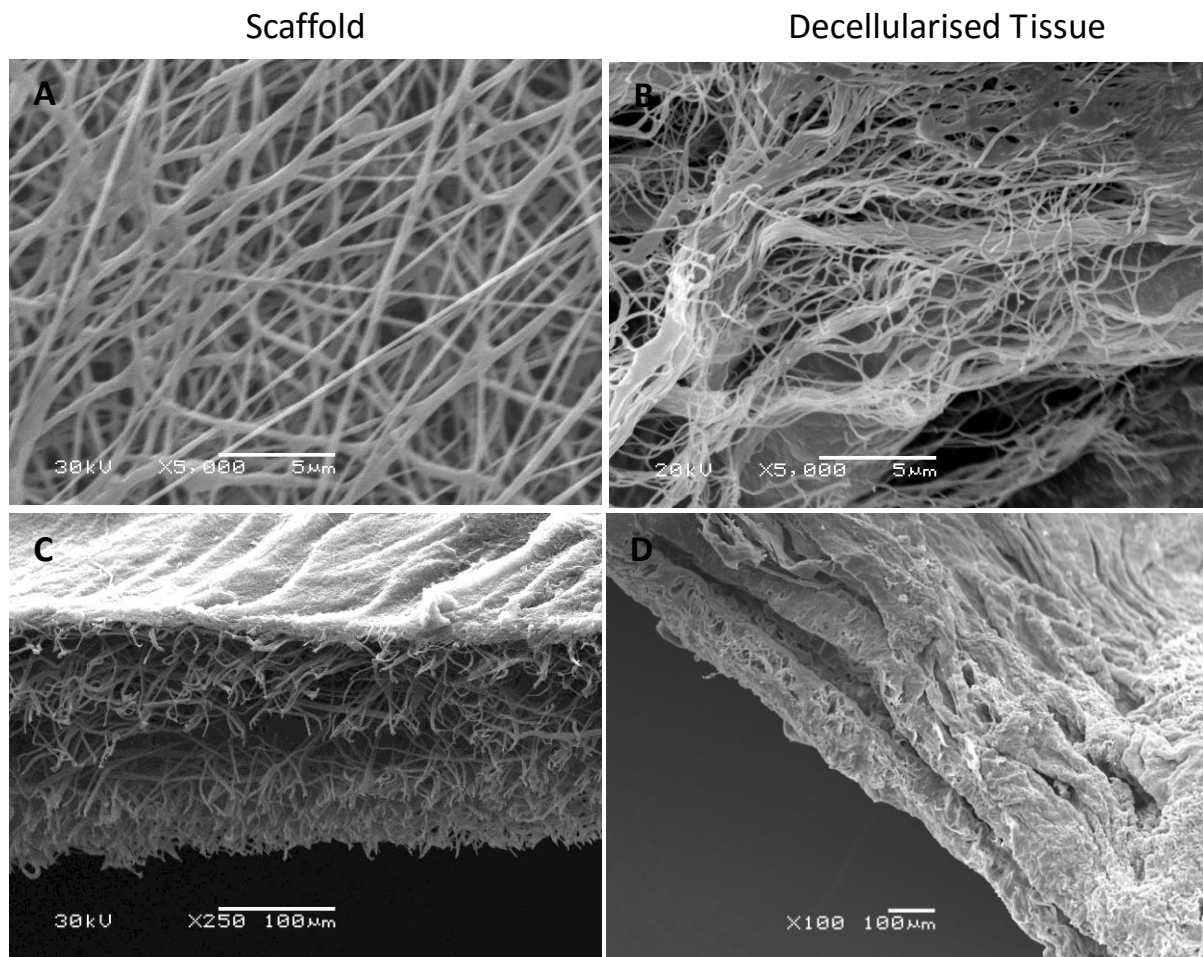
Figure 4.11: Biphasic scaffold vs decellularised tissue. SEM images of nanofibre (**A**) and biphasic (**C**) PET scaffolds. These are compared with decellularised basement membrane (**B**), and a bronchiole cross section (**D**).
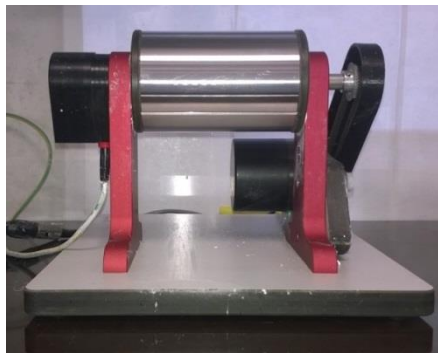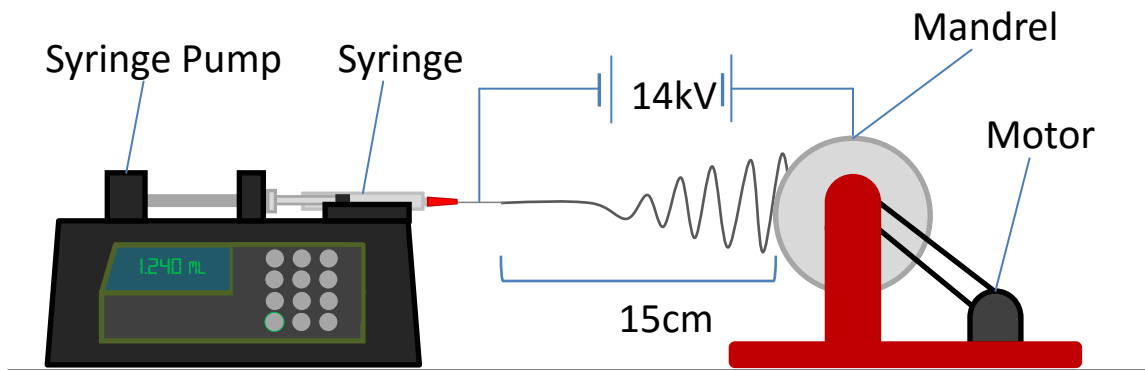
Figure 4.12: A diagram of the electrospinning equipment. A syringe containing the polymer solution (with needle attached) is placed on a syringe pump facing the mandrel. An electric potential is established between the needle and mandrel causing fibres to be ejected from the needle tip and deposited on the rotating mandrel. Additionally, photographs of the mandrel from the front and side.

possesses a stainless steel drum with a width of 10.7cm and a circumference of 22.2 cm meaning that scaffolds produced were rectangular sheets (with diameters length; 22.2cm, width; 10.7cm) where fibres aligned parallel to the length. An additional feature built into the mandrel design included ridges at the sides of the drum and a single ridge running the width of the drum which allow for scaffolds to be cleanly cut away from the mandrel with a scalpel blade. Importantly, the mandrel was able to rotate smoothly at very high speeds (over 2500 rpm) and also features an electrical banana socket allowing for the drum to be earthed attracting the negatively charged electrospun fibres to the drum surface.

4.4.8 Effects of mandrel speed on fibre alignment

In order to achieve aligned fibres, the collector drum has to be rotating at a sufficient speed. In order to find what mandrel speeds were necessary to align PET fibres, scaffolds were electrospun onto the mandrel rotating at various speeds. **Figure 4.13** shows SEM images of PET scaffolds collected whilst the mandrel was rotating at 50, 300 and 2000 rpm respectively. Given the diameter of the mandrel was 22.2cm, this correlates to speeds of 0.19, 1.11 and 7.40 m/s respectively. No fibre alignment was seen at 50 rpm with the scaffold resembling those that were electrospun onto a static collector plate. At 300 rpm the fibres displayed some degree of alignment but several fibres appear to be straying from the direction of the majority. When spun onto the mandrel spinning at 2000 rpm, the scaffold was more highly aligned with very few stray fibres.

4.4.9 Changing aligned fibre size with concentration

A collection of aligned fibre scaffolds varying in fibre diameter was desired in order to assess how the fibre size and resultant scaffold topography affects the growth of smooth muscle cells cultured upon them. To produce aligned nanofibre PET scaffolds, 7.5%, 8%, and 10% *w/v* PET solutions were electrospun onto the mandrel rotating at a rate of 2000 rpm. The resulting scaffolds varied in
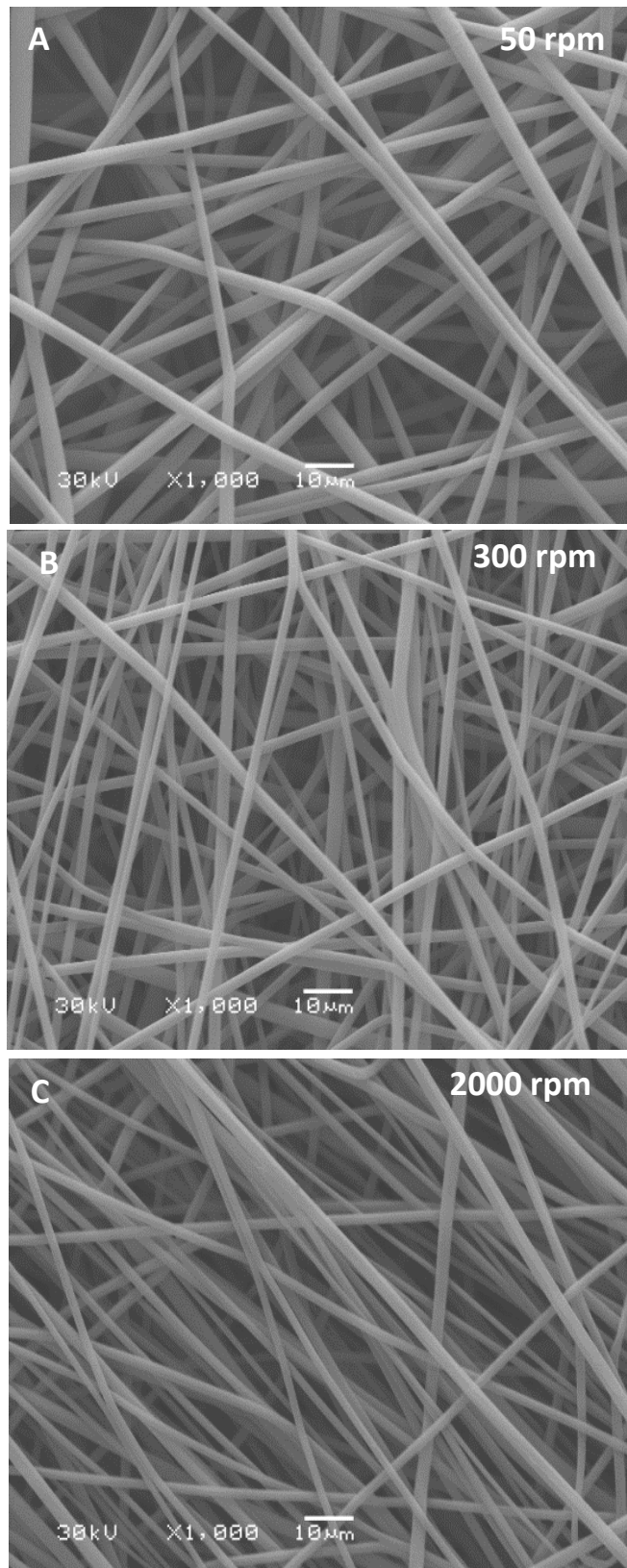
Figure 4.13: Effects of mandrel speed on fibre alignment. Representative SEM images of scaffolds spun on a mandrel rotating at 50rpm (**A**), 300rpm (**B**), and 2000rpm (**C**)

Nanofibre   Microfibre
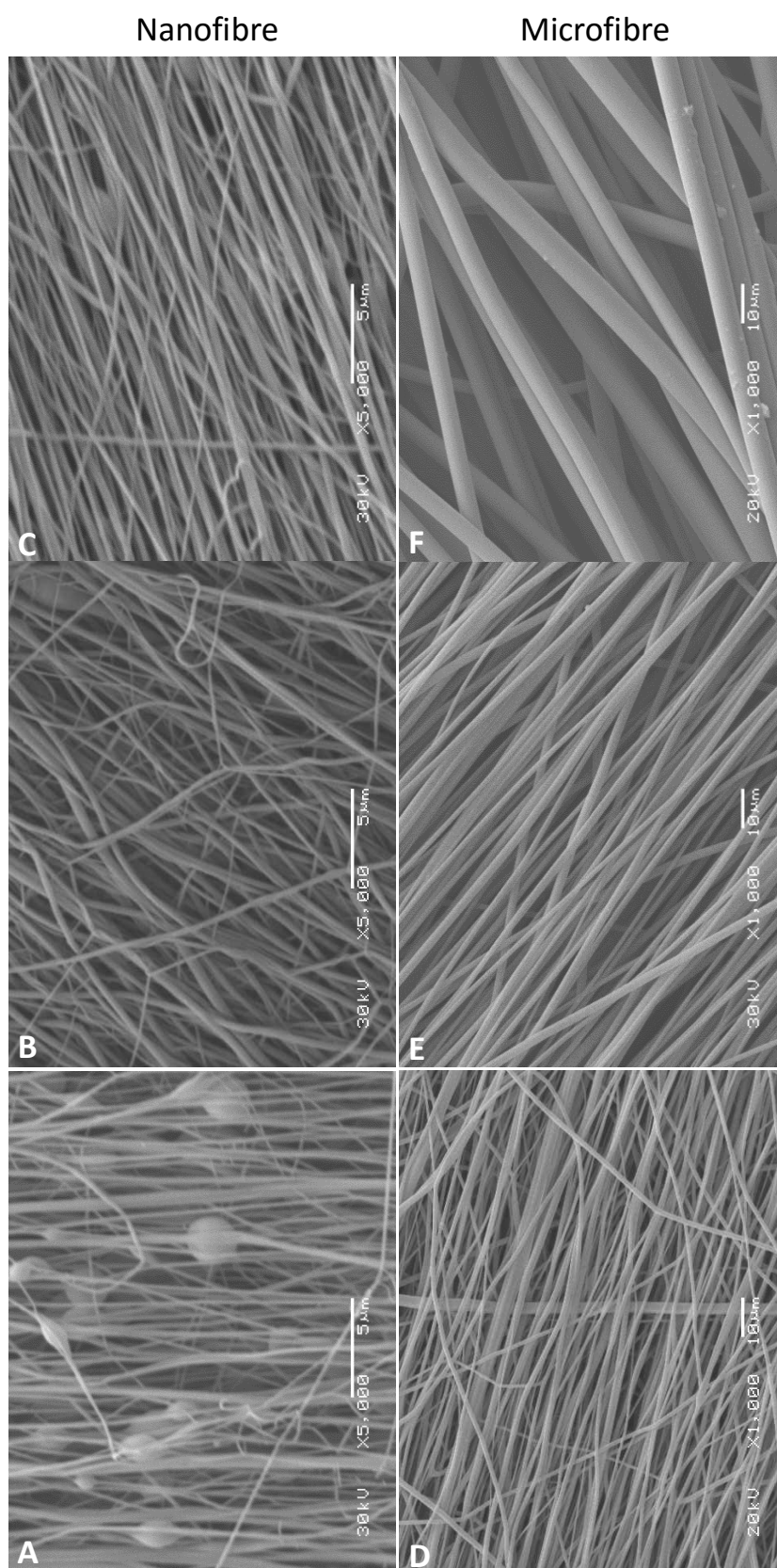
Figure 4.14: Developing a range of aligned electrospun scaffolds. Top (**A** to **C**) 7.5, 8 and 10% *w/v* PET respectively. Bottom (**D-F**) 20, 30 and 35% *w/v* PET respectively. All scaffolds were spun on to a mandrel rotating at 2000rpm.

fibre alignment and morphology. Fibres spun from 7.5% *w/v* PET had highly aligned fibres but also possessed several beads throughout. Fibres spun from 8% *w/v* PET were highly aligned and bead-free. However, the majority of the fibres themselves were not straight and had a wave-like morphology. Highly aligned, straight, bead-free nanofibres were successfully electrospun when using a 10% *w/v* solution of PET. Representative SEM images of scaffolds produced from 7.5%, 8% and 10% *w/v* PET are shown in **Figure 4.14 A-C** respectively. When producing aligned microfibre scaffolds, a range of PET concentrations were tested. These were 20%, 25%, 30% and 35% *w/v* PET. The resultant fibres were all highly aligned and had mean fibre diameters of 1.12, 1.45, 2.20 and 3.53 µm respectively (n=480 for 20% and 35% scaffolds, n=80 for 25% and 30% scaffolds). The 20% and 35% *w/v* PET scaffolds were chosen to be taken forward for cell culture as these gave the greatest range in fibre diameter. Representative images of the 20%, 30% and 35% *w/v* PET scaffolds are shown in **Figure 4.14 D-E** respectively.

4.4.10 Analysis of optimised aligned PET scaffolds

The chosen parameters for electrospinning aligned nanofibre (10% *w/v*) and microfibre (20% and 35% *w/v*) scaffolds are shown in **Table 4.3**. The table also displays the average fibre diameter and fibre alignment data for the scaffolds.

The distribution of fibre diameter in all the scaffolds follows a Gaussian distribution as shown in **Figure 4.15 A-C**. Fibre diameter does not appear to affect the degree of alignment seen in the scaffolds as seen in **Figure 4.15 D** where all 3 scaffold types display a very similar distribution of fibre angles. In all scaffolds, over 50% of fibres are within a ±5° deviation from the mean fibre angle (over 78% within ±10°). When compared to the level of alignment seen in random nanofibre scaffolds (4.79% within ±5°) to the level of alignment in aligned nanofibre (10%) scaffolds (55.21% within ±5°) a clear difference can be seen (**Figure 4.15 E**). These measurements were taken from scaffolds electrospun on 3 different occasions (3 scaffolds per PET concentration). As the

Concentration of PET (w/v, %)	Solvent (DCM:TFA)	Voltage (kV)	N-C distance (cm)	Needle Gauge (G)	Flow Rate (ml/h)	Volume (ml)	Fibre Diameter (µm±SD)	% of fibres within 5° of mean angle
10	01:01	14	15	18	0.5	1.5	0.216±0.095	55.21
20	01:01	14	15	18	1.5	2.0	1.126±0.278	51.67
35	01:01	14	15	18	1.5	2.0	3.527±0.948	57.92

Table 3: Chosen electrospinning parameters for production of a range of aligned PET scaffolds

Table 4.3: Chosen Electrospinning parameters for production of a range of aligned PET scaffolds.
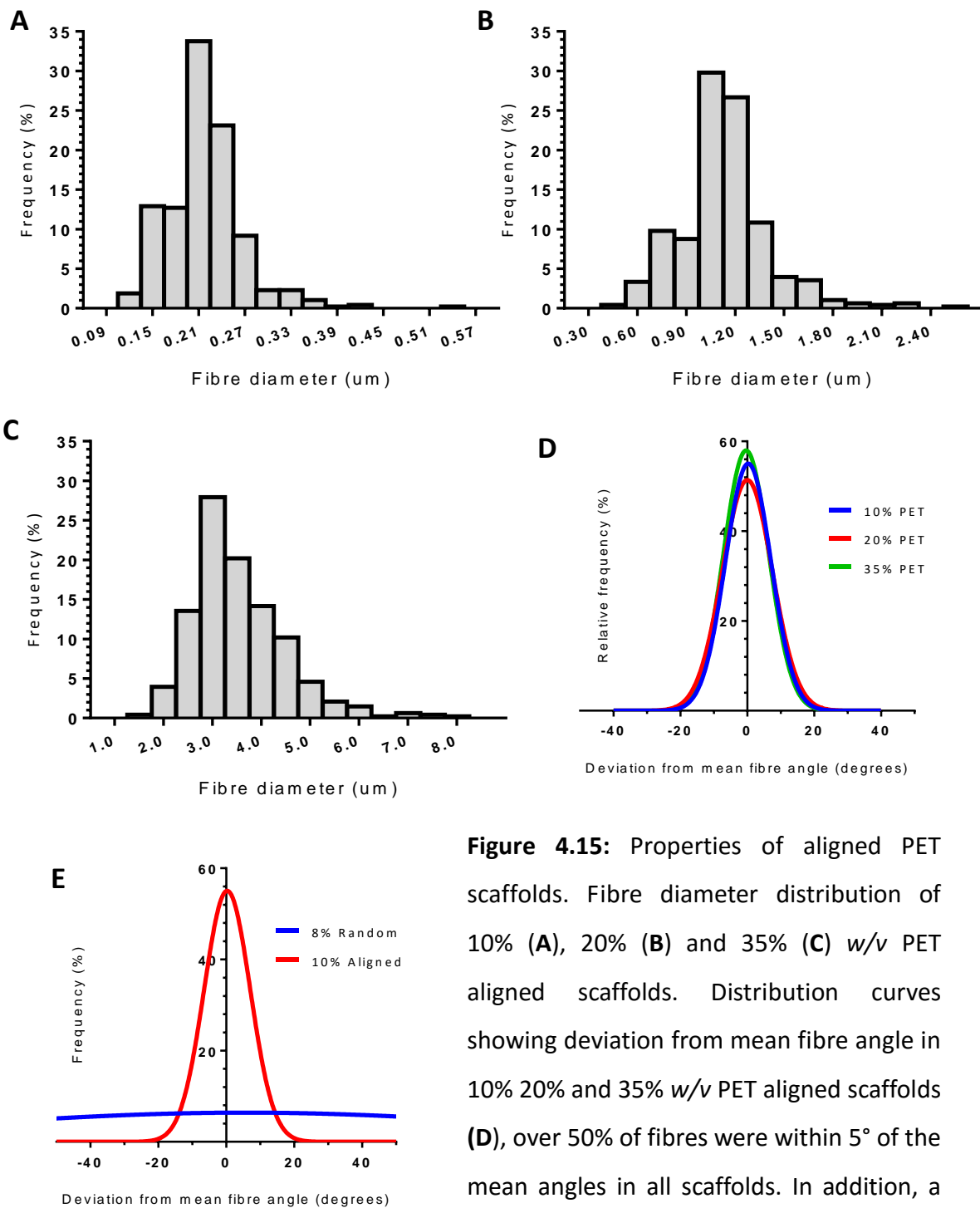
Figure 4.15: Properties of aligned PET scaffolds. Fibre diameter distribution of 10% (**A**), 20% (**B**) and 35% (**C**) *w/v* PET aligned scaffolds. Distribution curves showing deviation from mean fibre angle in 10% 20% and 35% *w/v* PET aligned scaffolds (**D**), over 50% of fibres were within 5° of the mean angles in all scaffolds. In addition, a comparison of the alignment between a random and aligned nanofibre scaffold (**E**) is shown.

electrospinning process can be influenced by external factors such as temperature and humidity, it is important to note any variability seen between scaffold batches. For scaffolds spun from 10% *w/v* PET the mean fibre diameter ranged from 198.7nm to 231.2nm between batches, a difference of 32.4nm (14.75% of the overall mean). For 20% PET scaffolds the mean fibre diameter ranged from 1.087μm to 1.159μm between batches, a difference of 71.3nm (6.38% of the overall mean). The 35% PET scaffolds had the largest batch to batch variance with the batch mean fibre diameters ranging from 2.974μm to 3.872μm, a difference of 897.8nm (25.46% of the overall mean) between them. The ideal scaffold for producing a functional model of SM will be robust enough to allow manual handling during preparation and cell culture but also possess elastic properties that will allow the attached SM cells to contract it in response to a stimulus. In order to obtain the mechanical properties of the aligned scaffolds, uniaxial tensile tests were performed on samples of the 10%, 20% and 35% PET aligned scaffolds. Representative stress/strain curves for each scaffold are shown in **Figure 4.16 A**. The stress strain curves increase in gradient as the thickness of the scaffold fibres increase; this is represented in **Figure 4.16 B** where the Young's moduli for all 3 scaffolds are shown. Young's modulus ranged from 211.2 ± 18.63 MPa for 10% PET scaffolds to 340 ± 18.36 MPa for 35% PET scaffolds (mean ± SEM, n=3 individual scaffolds per scaffold type, 3 measurements per scaffold).

4.4.11 Culture of primary HASM cells on aligned electrospun PET scaffolds

In order to determine whether scaffold fibre diameter had an effect on the ability of SM cells to proliferate and align along them, primary HASM cells were cultured on 10%, 20% and 35% *w/v* electrospun PET scaffolds for up to 14 days. During this time, cell viability/ cell number was monitored using the AlamarBlue® assay and samples were fixed for immunostaining.

Scaffolds seeded with HASM cells were fixed at days 3, 7 and 14 and stained for the SM marker SM22α (**Figure 4.17**). HASM cells were also cultured on glass

A

B
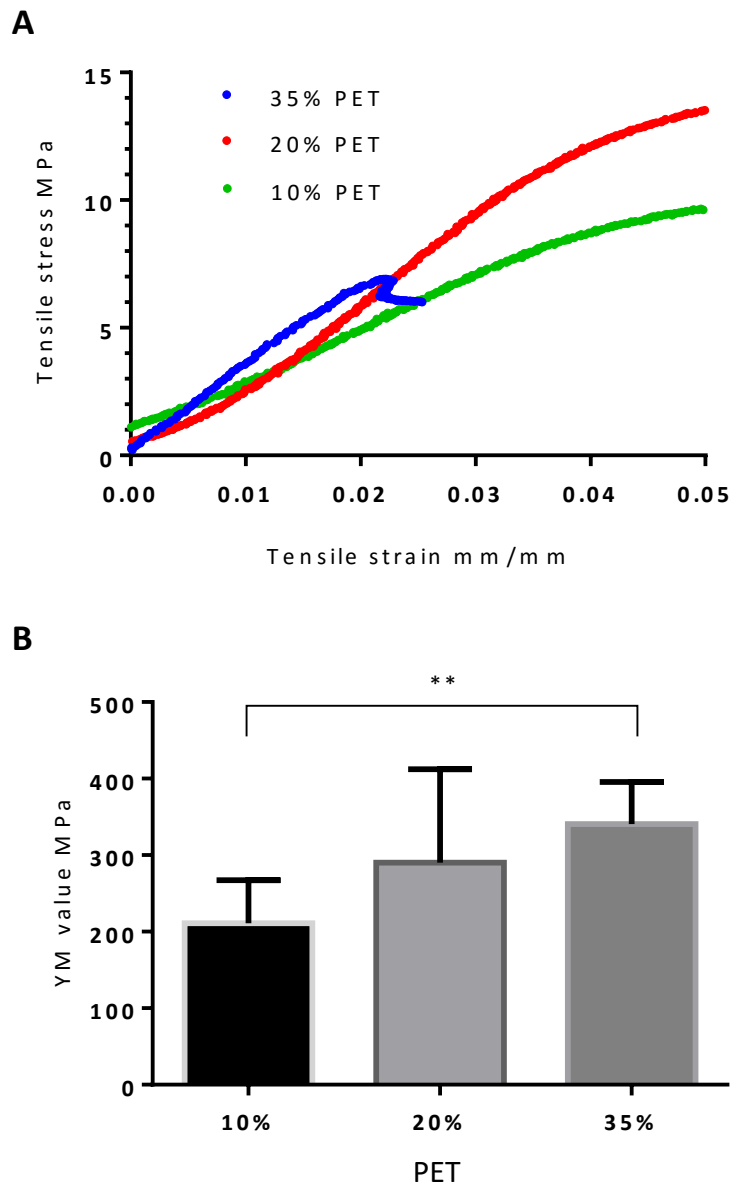
Figure 4.16: Tensile properties of aligned PET scaffolds. Representative stress/ strain curves for the 10%, 20% and 35% *w/v* aligned PET scaffolds (**A**). The Young's modulus of each scaffold is displayed also (**B**). Error bars display standard deviation. One way ANOVA with Tukey's multiple comparisons test was carried out between the Young's modulus of the different scaffolds. There was a significant difference between 10% and 35% PET (**P < 0.01)
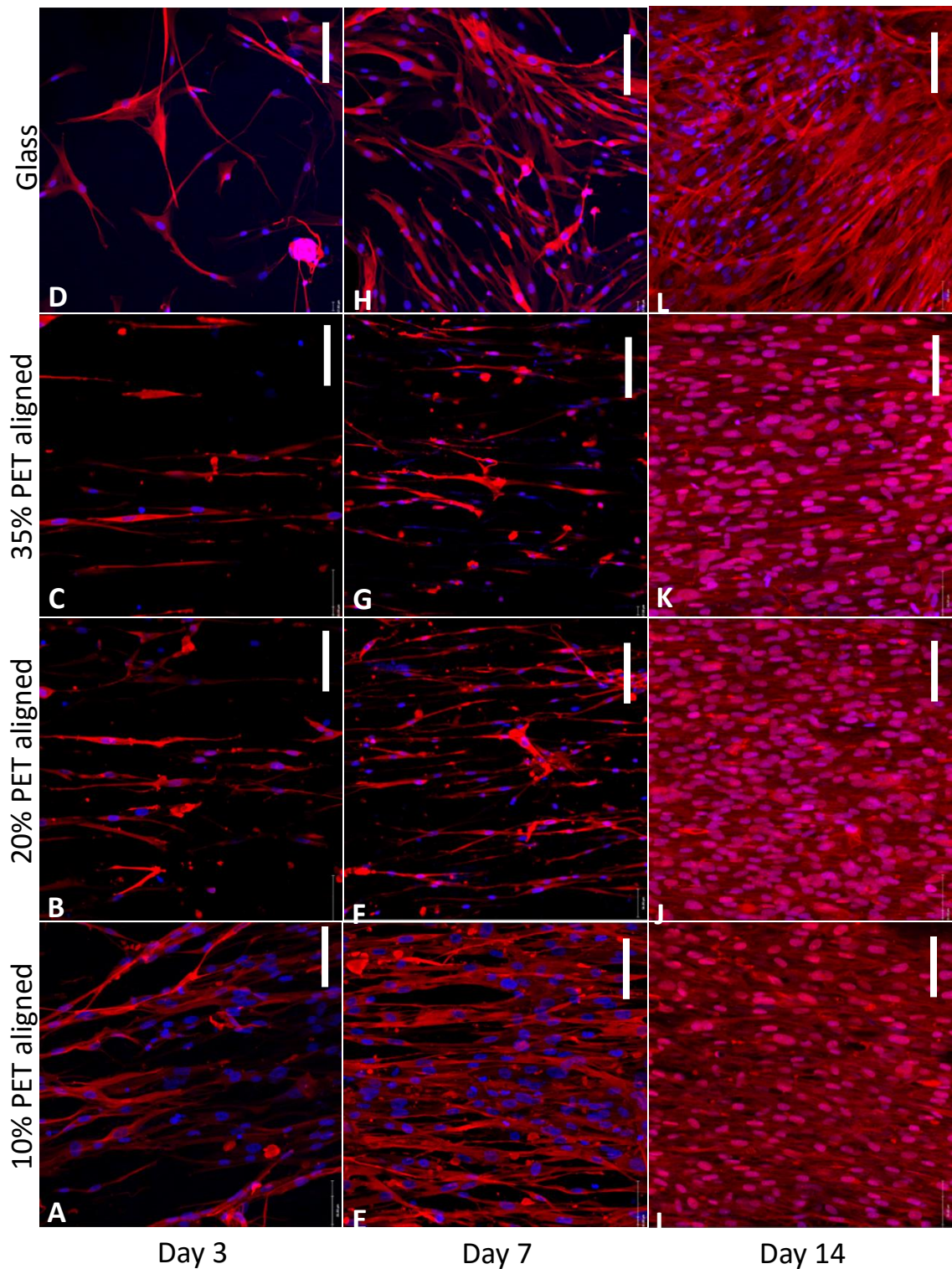
Figure 4.17: Airway SM cells cultured on aligned PET scaffolds. Immunofluorescence images of airway SM cells seeded onto 10% (**A,E,I**), 20% (**B,F,J**) and 35% (w/v) PET scaffolds in addition to glass coverslips (**D,H,L**). Samples were fixed and stained for SM22α and nuclear stain Hoechst at days 3, 7 and 14. Scale bar = 50 µm

coverslips as a 2D control. Several morphological differences can be seen between HASM cultured on glass and PET scaffolds. Firstly, the nuclei of cells cultured on glass appear to be more rounded than those cultured on the scaffolds. Also, although all cells appear spindle like, those cultured on electrospun fibres appear to travel along the direction of individual fibres, especially on the 20% and 35% PET scaffolds where fibre diameter is in the micron range. This has a great impact in the overall alignment of the cell population. Cell alignment on each PET scaffold and glass coverslips at days 3, 7 and 14 is displayed in **Figure 4.18 A-C**. The greatest degree of alignment was seen on 35% PET scaffolds at day 3 with 60.41% of nuclei within 10° of the mean nuclear angle. This reduced to 52.67% at day 7 and 46.93% by day 14. The 10% and 20% PET scaffolds both displayed the greatest alignment of cells at day 7 with 48.78% and 44.57% of nuclei within 10° of the mean nuclear angle respectively. The alignment of cells on glass coverslips was lower than each of the scaffolds on each day (13.95%, 31.70% and 22.49% at days 3, 7 and 10% respectively). Alignment of cells located within HASM bundles (as determined from histology sections donated by colleagues at Glenfield Hospital, Leicester) was found to be slightly higher than that achieved on the scaffolds with 64.89% of nuclei within 10° of the mean nuclear angle.

The metabolic activity of the HASM cells cultured on PET scaffolds (and tissue culture plastic controls) was monitored using the alamarBlue® assay (**Figure 4.19 B**). This was used to estimate the number of cells, and hence the level of cell proliferation, on the scaffolds over the culture period. All scaffolds and controls showed a steady increase in fluorescence over the first 10 days of culture with a sharp increase between days 10 and 14. No observable difference was seen between HASM cells seeded on tissue culture plastic and PET scaffolds. HASMcells cultured upon 10% PET scaffolds produced a fluorescence reading that was consistently lower than other samples. The surface coverage (by cells) of each scaffold at days 3, 7 and 14 is shown in **Figure 4.19A**. The amount of scaffold covered by HASM cells increases over time in correlating with the trend seen in the alamarBlue® results. There appears to be a drop in coverage between
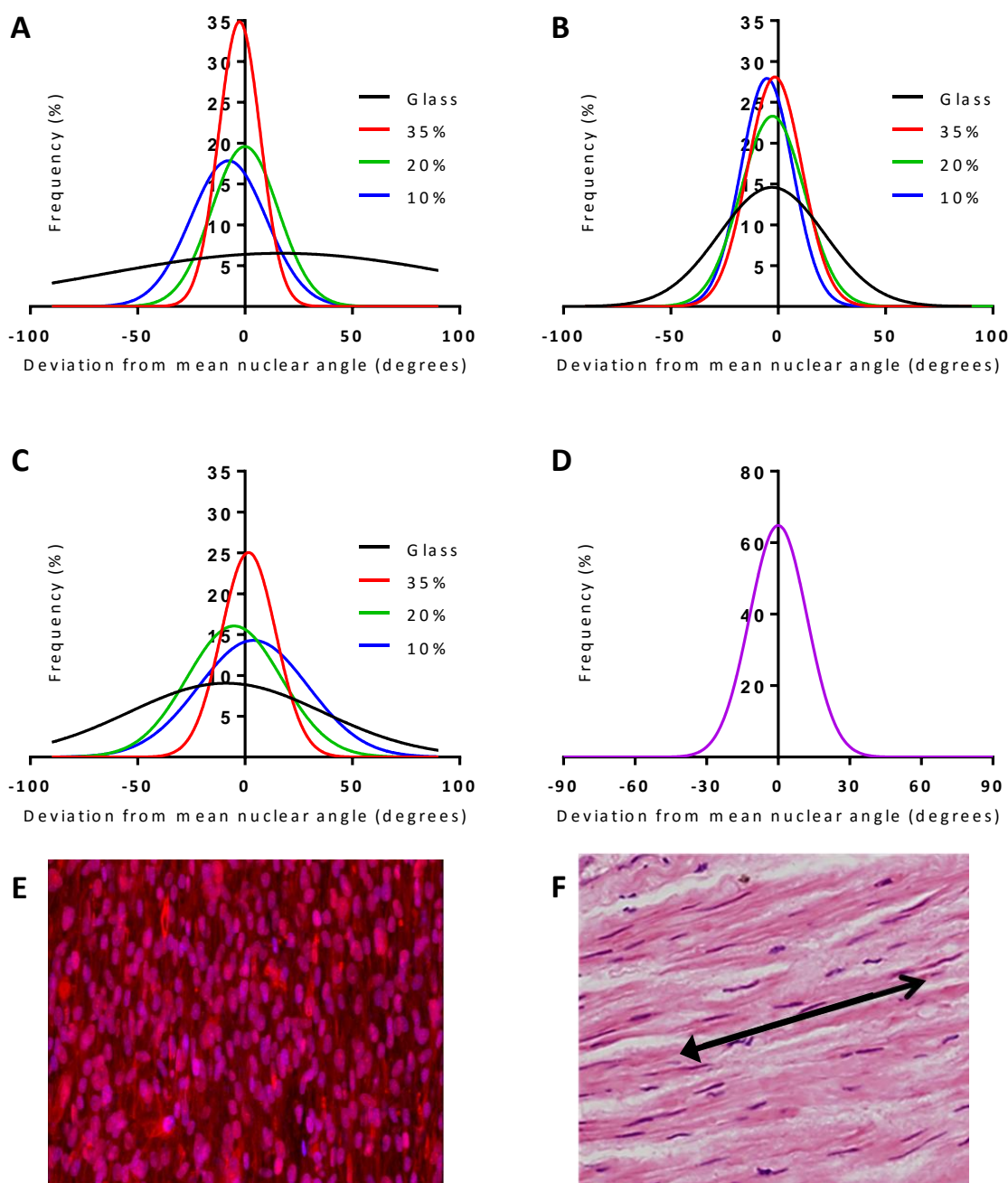
Figure 4.18: Alignment of airway SM cells on aligned PET scaffolds. Distribution curves of nuclei alignment of HASM cells cultured on electrospun PET scaffolds (image **E**) and glass cover slips at day 3 (**A**), 7 (**B**) and 14 (**C**). Distribution curve of nuclear alignment in histological sections of HASM tissue (**D**) (image **F**).

day 3 and 7 on 35% PET scaffolds but by 14 days in culture, virtually the entire scaffold is covered. As are the 10% and 20% scaffolds, indicating a confluent layer of cells after 14 days in culture.

4.4.12 Contraction of HASM cells on electrospun PET scaffolds

Samples of 10% *w/v* aligned PET scaffold seeded with primary HASM cells were cultured for 10 days prior to attempting agonist stimulated contraction. The scaffolds were then stimulated with bradykinin and histamine and the scaffolds imaged over time (**Figure 4.20**). Upon initial stimulation, the image analysis suggested that the scaffolds reduced in size over the first 5 minutes. However, this was due to scaffolds floating after the initial addition of agonist (fluid movement). Over time the scaffolds settled back to the bottom of the well plates, and the scaffold size returns to its original size as seen in **Figure 4.20 B**. No difference in scaffold size was observed between stimulated samples and controls indicating that the HASM cells were unable to contract the PET scaffolds. Therefore a more elastic scaffold had to be developed.
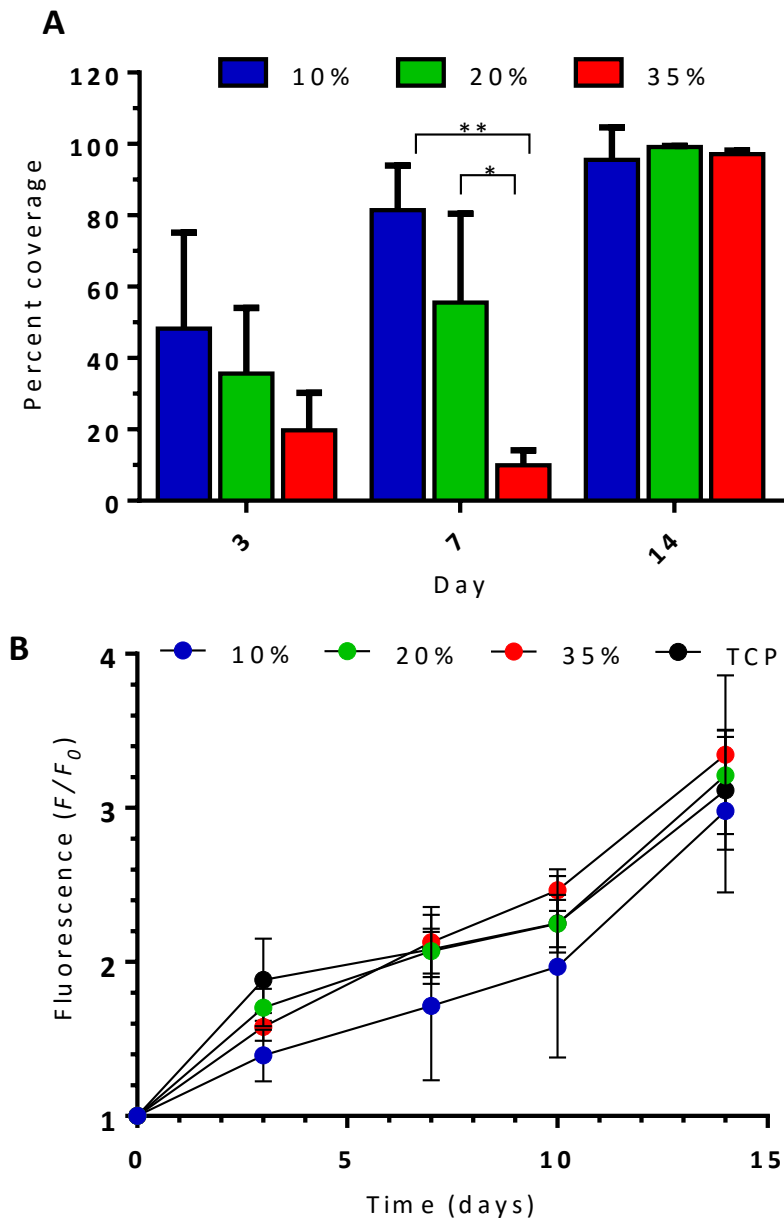
Figure 4.19: Proliferation of airway SM cells on aligned PET scaffolds. Graph displaying percent surface coverage of airway SM seeded scaffolds over time (**A**). Error bars represent standard deviation; one way ANOVA with Tukey's multiple comparisons test was carried out between scaffolds at each time point (*** $P<0.001$, * $P<0.05$), n=5. Graph displaying alamarBlue® data of airway SM cells cultured on all scaffolds over a 14 day period (**B**), n=3. Graph of fluorescence readings taken from alamarBlue® cell viability assay over 14 days for all scaffolds and tissue culture plastic (TCP) controls, error bars represent SEM, n=3.
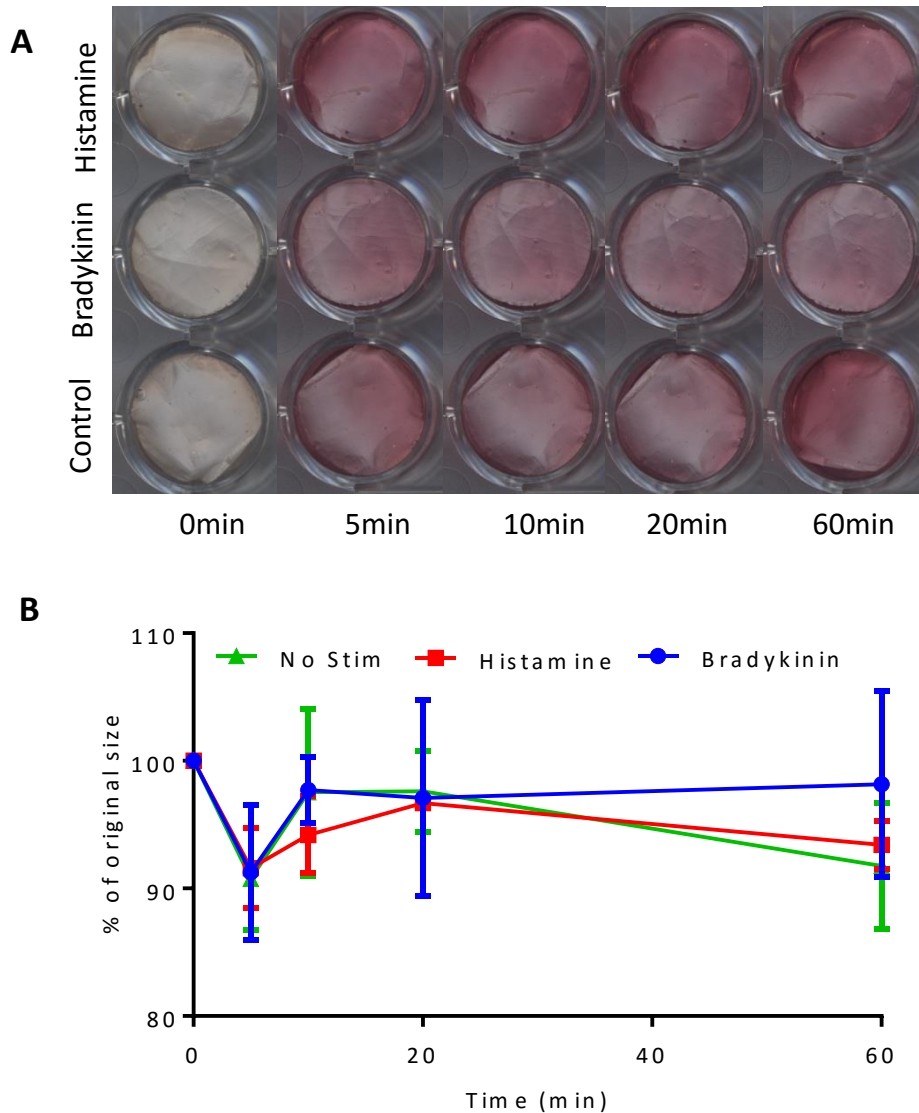
Figure 4.20: Attempted contraction of HASM cells on electrospun 10% (w/v) PET scaffolds. Scanned images of cell seeded scaffolds at various times after stimulation with bradykinin, histamine or serum free media (control) (**A**). A graph of visible scaffold contraction over time was plotted from image analysis of the scanned images (**B**); error bars represent standard deviation (n=2).

4.5 Discussion

Electrospinning provides a method that allows researchers to produce fibrous mats with potential to be used as scaffolds for the culture of cells. By altering the process parameters of the electrospinning process it is possible to fine tune the properties of the resultant scaffold (fibre diameter and orientation, mechanical properties). As cells are known to respond to the surface topography of materials, in addition to the mechanical properties, the customisable nature of electrospinning is of great use when designing scaffolds to suit a specific cell type. *In vivo* SM cells form an aligned population that surrounds hollow vessels such as blood vessels and airways with individual cells having an elongated, spindle-like morphology. This morphology can be recreated *in vitro* by culturing SM cells upon anisotropic scaffolds such as aligned fibrous electrospun mats. Here, the effects of electrospinning parameters of on PET fibre morphology were investigated and a range of aligned fibrous scaffolds (differing in fibre diameter) were electrospun for the culture of HASM cells. Cell morphology and proliferation rate was assessed on the scaffolds and compared to 2D controls.

4.5.1 Investigating the effects of electrospinning process parameters on PET fibre morphology

Initial investigations into electrospinning parameters focussed on the PET solution concentration and the rate at which the solution was extruded from the needle. Concentrations of 12.5% *w/v* and lower all produced fibres with sub-micron diameters however all of these scaffolds contained unwanted beads. Beading is well known to occur when spinning low concentration (or viscosity) polymer solutions (Ki et al. 2005; Hongliang Jiang et al. 2004; Huang et al. 2001). This was overcome by increasing the PET concentration which also led to increased fibre diameter; another widely recorded observation (Ki et al. 2005; Huang et al. 2001; Deitzel et al. 2001; Jarusuwannapoom et al. 2005). When concentration was increased to 50% *w/v* PET, the solution was not able to be electrospun due to the needle blocking, most likely due to the increased solution

viscosity, an observation also made by Garg *et al.* whilst electrospinning high concentration solutions of PEO (Garg & Bowlin 2011). By increasing the flow rate to 1ml h^{-1} this problem was overcome but the resultant fibres possessed a very thick, flat ribbon-like morphology. A possible reason for this could be that the ejected polymer dried before the whipping phase of the electrospinning process. Therefore the fibres were not stretched out as they would do to form rounded fibres. When the flow rate was increased to 2 and 4 ml h^{-1} the fibre morphology was that of uniform microfibres.   When compared to other studies electrospinning PET, different results have been seen at this range of concentrations. Ma *et al* produced fibres ranging from 200-600 nm when electrospinning 20% *w/v* PET (Ma et al. 2005). Veleirinho *et al.* produced fibres within a similar diameter range electrospinning solutions ranging from 10 to 30% PET (Veleirinho et al. 2007). These fibres are thinner than obtained here although the flow rate used by Veleirinho was much higher at 12 ml h^{-1}. In this study beading was also observed when 10 and 20% PET solutions were spun. In contrast, a study by Hadjizadeh *et al* recorded successfully spinning a 7.7% *w/v* solution resulting in average fibres 400 nm in diameter (Hadjizadeh et al. 2011a) . Also worth noting in the study by Hadjizadeh is that solutions greater than 14% PET could not be electrospun, most probably due to needle blockage. These differences in fibre morphology when using similar parameters could be due to the molecular weight of the PET used as all studies use PET from different sources. Polymer molecular weight can have a significant effect on the viscosity and surface tension (and therefore fibre diameter) as shown previously by Kim *et al* (Kim et al. 2004).

When attempting to spin PET fibres in the nanofibre range by lowering the PET concentration, high levels of beading were observed. In an attempt to reduce this beading, the cationic surfactant CTAB was added to the PET solutions to reduce the solution surface tension and increase solution conductivity. Addition of CTAB led to a visible reduction in the level of beading when spinning nanofibres, similar to results seen by Yang *et al* when spinning solutions of polycarbonate with CTAB (Yang et al. 2009). Different results were seen when

the source of PET was changed from PET pellets to PET bottles. Fibres spun from bottles were much thicker at equivalent concentrations and were able to be spun at concentrations as low as 8% *w/v* without any beading occurring. This difference between the two sources is theorised to be due to differences in the average molecular weight of the PET polymer chains in each source, as witnessed by Kim *et al.* (Kim et al. 2004), although this was not proven in the present study. Also worth noting is that PET pellets were not fully soluble in the solvent system, leaving behind a solid residue and a cloudy; due to the inclusion of glass as a stabiliser in the PET pellets. This was not seen with PET obtained from bottles where clear solutions were produced.

Average diameter of PET fibres ranged from 250 nm to 2.5 μm by altering the solution concentration and flow rate. This range is greater than those achieved in previously published research (Ma et al. 2005; Kim et al. 2004; Veleirinho et al. 2007; Hadjizadeh et al. 2011a). Average pore size increased with average pore size although the porosity of scaffolds was unaffected by fibre diameter; two observations also recorded by Hadjizadeh and co-workers.

By electrospinning nanofibres onto microfibres it was possible to create a scaffold with two distinct phases on either side. The reasons were doing this were two-fold. Firstly, nanofibre scaffolds are much thinner than microfibre scaffolds and as a result, much more fragile. Also all, electrospun PET scaffolds proved to be initially highly electrostatic. These two properties of nanofibre scaffolds make them very difficult to handle, especially when attempting to prepare them for cell culture. By spinning them onto a supporting structure of microfibres, the nanofibre scaffolds became much easier to handle with no effect to their fibre morphology. Secondly, by spinning two distinct scaffolds together in close proximity, this would be a good platform for the co-culture of two separate cell types that perform differently on different size/ oriented fibres. This approach would be useful if the SM model in development here was to be expanded to a blood vessel or bronchiole model by co-culture with endothelial or epithelial cells respectively. A similar approach has been made previously to produce bilayer and trilayer scaffolds for tissue culture (Bye et al. 2013) although

different polymers were used for each layer of the scaffold. Biphasic scaffolds were slightly thinner than the sum of individual microfibre and nanofibre scaffolds. As the microfibre scaffolds are spun first, these probably act as an insulative layer upon the collector which reduces the electrostatic attraction to the nanofibres. This results in a slightly thinner deposition of nanofibres than when the microfibre scaffold is not present.

4.5.2 Producing aligned fibrous PET scaffolds

In order to produce aligned fibre scaffolds, it was necessary to use a collector that facilitated this alignment. The design of a rotating mandrel was chosen not only due to its ability to align fibres when rotating at a sufficient speed; but also as the cylindrical shape of the drum can produce large, neat rectangular scaffold sheets that can easily be manipulated for cell culture post-spinning. As the speed of the drum increased so did the degree of fibre alignment seen in the scaffolds, a similar observation that has been made in previous studies (Hadjizadeh et al. 2011a; Bashur et al. 2006). The fibres all seemed to align to a similar degree, regardless of the diameter of the fibres that were spun although 10% PET aligned fibres possessed a slightly thinner diameter than 8% randomly aligned fibres; indicating that the alignment process may cause further elongation of the fibres.

The tensile properties of the aligned scaffolds were measured in order to assess the effect of fibre diameter on scaffold mechanical properties. The Young's modulus of the scaffolds increased with fibre diameter indicating that thicker fibres were stiffer than their thinner counterparts. The Young's modulus of the scaffolds ranged from approximately 210 to 340 MPa, a range that is significantly higher than those previously recorded (Veleirinho et al. 2007; Kim et al. 2004; Hadjizadeh et al. 2011a). It is unclear as to why the scaffolds electrospun here were significantly stiffer than those in other studies, differences in the modes of measuring the scaffold properties may play a part. Additionally, due to the nature of electrospinning (many electrospinning set-ups and protocols developed in-house), it is difficult to directly compare studies as multiple

parameters differ between them, making it difficult to explain differences in the scaffolds produced.

4.5.3 Culture of HASM cells on aligned PET scaffolds

HASM cells cultured upon the electrospun PET scaffolds adopted a spindle-like morphology and aligned along the direction of the fibres; a feature commonly seen in studies where SM cells are cultured upon aligned fibres (Zhu et al. 2010; Xu et al. 2004). Cells stained positive for the SM marker SM22α with no visible difference in expression seen between controls and scaffolds. Cells cultured on scaffolds attached along individual fibres when fibre diameter was in the micron range (20% and 30% PET scaffolds) but appeared to attach to many fibres when cultured on nanofibres. The cells achieved greatest alignment upon the largest fibre diameter scaffolds but seemed to have enhanced surface coverage on the smallest fibres. These results are similar to those found when macrophages were cultured upon quartz etched with grooves of varying diameters (photolithography); cells elongated faster on deep wide grooves but spread more quickly over shallow grooves (Wójciak-Stothard et al. 1995). Cell alignment was higher than seen in controls on all days. Cell alignment seemed to reduce as the cells reached confluency upon the scaffold; this is in part down to the cells attaching to each other in addition to/ instead of the underlying fibres. Cell viability increased over 14 days for all scaffold cultures and controls. Cultures on 10% PET scaffolds appeared to be slightly less viable than the rest; this was probably due to the aluminium rings used to hold the nanofibre scaffolds in place (sealant could not be used like on the thicker scaffolds as it was found to seep through the nanofibrous structure, destroying the topography). The aluminium rings reduced the available surface area of the scaffold providing less room for cell proliferation on the scaffold.

As the HASM cells expressed markers of a contractile SM phenotype, the next set of experiments set out to assess the extent of HASM contraction achievable on the PET scaffolds. When stimulated with bradykinin or histamine no visible contraction was measured. Scaffolds did not change in size or shape indicating

that either the cells were not contracting or that the scaffold fibres were too stiff for the SM cells to displace. Due to the presence of the same markers seen in the collagen gel model (which did contract), it was hypothesised that the scaffolds were restricting SM contraction. Given that the Young's modulus of *in vivo* SM is much lower than the Young's moduli of the PET scaffolds (200-300 MPa). For example, the Young's moduli of human arteries and porcine bronchi range from 0.1 to 1.0 MPa and 0.35 to 1.35 MPa respectively (Riley et al. 1992; Wang et al. 2011). These values are 100 to 1000 times smaller than the values obtained for the PET scaffolds. As a result, a much more elastic material was required to provide suitable mechanical properties that would facilitate SM contraction.

4.5.4 Chapter Summary

Within this chapter of work, PET fibres were electrospun whilst varying the electrospinning parameters in order to produce an array of highly aligned and random, uniform fibrous scaffolds varying in fibre diameter. Solution concentration had a considerable effect on the resultant fibres. As the concentration increased, the flow rate used had to be increased also to accommodate the subsequent change in solution viscosity. Reducing the surface tension and increasing the conductivity of the PET solutions was achieved *via* the addition of a small amount (1% *w/v*) of anionic surfactant. This reduced the amount of beading observed when spinning low concentrations of PET to produce uniform nanofibres. Another method used to reduce beading was to use a narrower needle which increased solution velocity at the same flow rates. By changing the source of PET used, the fibre diameters that were spun were dramatically changed; this was highly likely due to differences in polymer chain length in each source. The porosity of electrospun scaffolds did not vary with increased diameter and all were much more porous than conventional trans-well membranes. Pore size increased with increasing fibre diameter. By electrospinning nanofibres directly onto microfibre scaffolds it was possible to create a two phase scaffold offering different matrices for the co-culture of different cell types. Aligned PET scaffolds were produced successfully with the aid of a rotating mandrel and were used for the culture of HASM cells. Cells

aligned along the direction of the fibres with greater alignment seen when cells were cultured on thicker fibres. Cells proliferated on the surface of the scaffolds and formed a highly aligned, confluent layer of HASM after 14 days in culture.

The aligned PET scaffolds that have been electrospun in this chapter have been found to produce a highly aligned confluent population of SM cells. However, the high Young's moduli of these scaffolds proved to be too stiff for the cells to contract. The following chapter therefore will explore the electrospinning of more elastic natural polymers.

5. Electrospun gelatin based scaffolds as a platform for the culture of contractile smooth muscle cells

5.1 Introduction

The mechanical properties of *in vivo* tissues are determined primarily through the composition of the extracellular matrix (ECM); with proteins such as collagen, elastin fibrinogen and laminin being key components. Natural polymers/ proteins such as these are much more elastic in nature than synthetic polymers (such as PET) and play a key role in the structure and mechanical properties of all tissues (Hinds et al. 2011). They would therefore be ideal candidates to produce electrospun scaffolds with the mechanical properties to facilitate SM contraction.

With collagen being the primary ECM component in tissues, it is unsurprising that the majority of studies electrospinning natural polymers have focussed on electrospinning collagen (Huang et al. 2001; Matthews et al. 2002; Matthews et al. 2003; Sell et al. 2009). Several other natural polymers such as elastin (Li et al. 2005) and fibrinogen (Wnek et al. 2003; M. C. McManus et al. 2007; M. McManus et al. 2007) have also been electrospun previously. Although these natural materials possess desirable mechanical properties and high biocompatibility when compared to synthetic polymers, they do have some disadvantages. For example, many natural polymers are highly soluble in water and therefore require chemical crosslinking prior to use as a scaffold for cell culture. They are also biodegradable which could be of concern in long term *in vitro* studies or if designing a commercial product where shelf life would have to be taken into consideration. Collagen has also been shown to trigger antigenic and immunogenic responses when used *in vivo* (Lynn et al. 2004).

Elastin plays a key role in elastic tissues including arteries, skin, tendon and ligaments (Sandberg et al. 1981) due to its high elasticity (Young's modulus of elastic fibres typically range from 300 to 600 kPa but can be as low as 100 kPa for arterial elastin (Mithieux et al. 2005; Zou & Zhang 2009)) and as such would make an ideal candidate for SM scaffold production. In studies by Nivison-Smith and Weiss, electrospun elastin scaffolds were produced by electrospinning recombinant human tropoelastin prior to chemical cross-linking (Nivison-Smith & Weiss 2012). These scaffolds, when aligned, had an average Young's modulus (111 kPa) within the range of natural aorta elastin (Zou & Zhang 2009) with fibres similar in diameter to elastin fibres found *in vivo* (Parker & Winlove 1988). Additionally, the scaffolds were able to support the growth of primary human vascular SM cells for up to 7 days. No studies investigating SM contraction were reported however. Commercially available tropoelastin is very expensive in the quantities necessary to produce electrospun scaffolds. By genetic modification of bacteria such as *Escherichia coli* however, it is possible to create a reliable source of human recombinant tropoelastin (Vrhovski et al. 1997; Muiznieks et al. 2003); this however, was not in the scope of this thesis.

As seen in chapter 3, collagen hydrogels provided a matrix that SM cells could readily contract both due to remodelling and agonist stimulation. In chapter 4, electrospun scaffolds provided a much more uniform and aligned population than seen in the collagen hydrogels although the scaffolds proved too stiff to contract. It would be intuitive therefore to investigate the possibility of using electrospun collagen scaffolds for a contractile SM model. However, previous studies have found that when electrospinning collagen, the fluorinated alcohols used as electrospinning solvents such as 1, 1, 1, 3, 3, 3 hexafluoroisopropanol (HFIP) and 2, 2, 2 trifluoroethanol (TFE) cause denaturation of the collagen (Yang et al. 2008; Liu et al. 2010), altering the tertiary protein structure. As a result of this there is very little difference between the resultant electrospun collagen fibres and electrospun gelatin fibres (Tsai et al. 2012). Gelatin is a product of collagen hydrolysis and therefore chemically very similar possessing the same amino acid sequences (Lou & Chirila 1999); as collagen is denatured during the

electrospinning process, one study suggested that the electrospinning of pure collagen is an expensive way to make gelatin (Zeugolis et al. 2008). A study comparing electrospun collagen and gelatin scaffolds found that at the same polymer concentration there was no significant difference in fibre diameter between the scaffolds however, when crosslinked using the same method, collagen scaffolds were found to be significantly stiffer than their cross-linked gelatin counterparts (average Young's modulus of 94.29 and 71.88 MPa respectively) (Tsai et al. 2012). This was found to induce differential behaviour of MG-63 osteoblast-like cells cultured upon the different scaffolds.

Due to the fact that electrospun collagen and gelatin are both structurally and chemically almost identical, it is clear that electrospinning gelatin would be a more cost effective way of electrospinning scaffolds that are chemically similar to the collagen gel matrices used in chapter 3. In addition, the apparent reduced stiffness (compared to PET scaffolds) of gelatin scaffolds will prove advantageous when producing a contractile model. As mentioned earlier collagen can have antigenic effects *in vivo*, this has not been observed with gelatin scaffolds (Zhang et al. 2006; Bigi et al. 2002). Like many other biological materials, gelatin is water soluble and therefore requires cross-linking prior to cell culture; cross-linking gelatin can provide stability against enzymatic degradation (Gorgieva & Kokol 2011), lower water solubility and an increase mechanical properties (Zhang et al. 2008). It is of increased importance in electrospun scaffolds where retention of the fibrous structure is necessary for topographical cell guidance. An alternative to cross-linking gelatin scaffolds is to co-electrospin gelatin with a synthetic polymer such as poly(lactic-co-glycolic acid) (PLGA), this also increases the mechanical properties of the scaffolds (Meng et al. 2010).

Methods of cross-linking gelatin in the literature include physical, enzymatic (Yamamoto et al. 2013) and chemical crosslinking. Physical crosslinking methods include using UV radiation (Brinkman et al. 2003; Bhat & Karim 2009), plasma (Prasertsung et al. 2013) or dehydrothermal treatment (Ratanavaraporn et al. 2010). These methods are advantageous in that they do not require any potentially cytotoxic chemicals; however the reaction kinetics are difficult to

control resulting in lower degrees of cross-linking and mechanically weaker constructs compared to chemically cross-linked scaffolds (Khor 1997).

Chemical cross-linking methods can be described as either 'zero-length' or 'non-zero-length' cross-linking. Non-zero-length cross-linking agents act as chemical bridges between amino acid residues in the gelatin structure. They covalently link free amine residues (lysine) in the gelatin structure to each other or to free carboxylic acid residues (aspartic and glutamic acid) also present. This can significantly alter both the biological and mechanical properties of gelatin constructs (Bigi et al. 2002). Typical non-zero-length cross-linking agents include aldehydes such as glutaraldehyde (Matsuda et al. 1999; Talebian et al. 2007), formaldehyde (Usta et al. 2003), and glyceraldehyde (Sisson et al. 2009). Glutaraldehyde is the most commonly used due to its high solubility and fast rate of reactions and increased cross-link stability compared with other aldehydes. The level of cross-linking and therefore the resultant mechanical properties of glutaraldehyde cross-linked scaffolds can also be altered by changing the concentration of glutaraldehyde used (Skotak et al. 2010). One concern when using aldehyde cross-linkers is that upon degradation, the toxic aldehydes are released from the scaffold and taken up by nearby cells. Glutaraldehyde crosslinked constructs have been found to cause inflammation and calcification *in vivo* in rabbits (Vyavahare et al. 1997; Speer et al. 1980). As a result, less toxic non-zero-length cross-linking agents such as genipin (Tsai et al. 2000) have also being used to produce less toxic gelatin based scaffolds (Panzavolta et al. 2011).

Zero-length cross-linking agents are advantageous as they do not add any toxic reagents to the scaffold. They activate the carboxylic groups on aspartic and glutamic acid residues and facilitate their reaction with free amine groups (primarily on lysine residues). This forms an amide bond between the two amino acid residues with no bridging molecule required. Commonly used methods on zero-length crosslinking use a carbodiimide (Kuijpers et al. 2000) or an acyl azide (Jorge-Herrero et al. 1999). A commonly used carbodiimide used in cross-linking is 1-ethyl-3-(dimethyl aminopropyl) carbodiimide (EDC). EDC is usually used in combination with N-hydroxysuccinimide (NHS) to increase the efficiency of the

reaction and reduce the level of side reactions caused by hydrolysis of the EDC-activated carboxylic acid groups (Kuijpers et al. 2000). These two chemicals in combination have been successfully used previously to cross-link electrospun scaffolds of pure gelatin (Tonsomboon & Oyen 2013; Zhang et al. 2008) and poly(glycerol sebacate): gelatin blends (Kharaziha et al. 2013).

Another method of cross-linking gelatin based scaffolds is to chemically modify the gelatin to add a functional group that can be crosslinked under UV light in the presence of a photoinitiator. The most common way of achieving this to use gelatin methacrylate (GelMa), this is synthesised *via* a reaction between gelatin and methacrylic anhydride where free amines on lysine residues reacts with the methacrylic anhydride resulting in multiple methacrylamide groups bound to the gelatin structure (Van Den Bulcke et al. 2000). These can then form chemical cross-links between gelatin molecules in the presence of free radicals from a photoinitiator. This is advantageous as it gives the ability to fine tune the mechanical properties of the materials by altering the degree of methacrylation that occurs and the concentration of GelMa used. Additionally, the level of cross-linking can also be controlled *via* the concentration of photo-initiator used and the amount of UV exposure (Van Den Bulcke et al. 2000). Due to this high flexibility in the cross-linking of GelMa, coupled with the fact that once synthesised no chemicals are required to cross-link the GelMa other than the photoinitiator, GelMa has been seen to hold great potential in the field of tissue engineering. As a result, over the last few years its use has been published in hydrogel cultures (Nichol et al. 2010; Zhao et al. 2015), micropatterning (Ramón-Azcón et al. 2012; Nikkhah et al. 2012), and 3D-printing (Ovsianikov et al. 2011; Bertassoni et al. 2014). It has also been used as a scaffold to support the culture of contractile skeletal muscle tissue (Hosseini et al. 2012), making it a potentially viable material for the production of a contractile SM model. However, in the current literature, there is no evidence of the application of electrospun GelMa; quite possibly due to difficulties in the cross-linking process which will require the scaffolds to be submerged in an aqueous solution. Due to the high solubility of the material in water, this is clearly problematic.

Due to the extremely high Young's moduli of the PET scaffolds discussed in the previous chapter, it is highly unlikely that any SM cells cultured upon the scaffolds would be able to generate sufficient contractile forces to deform the scaffolds to any extent that could be measureable. As a result, new scaffold materials, with mechanical properties that better mimic those found *in vivo*, must be explored. This chapter explores alternative electrospun gelatin scaffolds which possess more elastic properties than PET scaffolds. The possibilities of producing and cross-linking electrospun GelMa scaffolds are explored and their mechanical properties compared to gelatin and PET scaffolds. Finally SM cells are cultured upon both gelatin based scaffolds and the contraction of the cell/ scaffold constructs measured.

5.2 Chapter Aims

The work carried out within this chapter aims to achieve the following:

Develop an aligned electrospun scaffold using gelatin based materials that can facilitate the contraction of smooth muscle cells cultured upon it, ultimately leading to the development of a model that can actively measure smooth muscle contraction. This will be achieved by:-

- Create a range of cross-linked electrospun aligned gelatin scaffolds with similar fibre dimensions and orientation to the PET scaffolds previously produced and characterise their physical and mechanical properties.

- Synthesise and electrospin GelMa to produce aligned scaffolds.

- Develop a method to cross-link the electrospun GelMa scaffolds and characterise their physical and mechanical properties.

- Characterise and assess alignment and proliferation of RASM cells cultured upon both gelatin and GelMa scaffolds

- Test the ability of RASM cells to contract both gelatin and GelMa scaffolds.

- Physically measure the contraction of SM cells cultured on electrospun scaffolds using the equipment and procedures developed in chapter 3.

5.3   Materials and methods

5.3.1 Production of electrospun gelatin scaffolds

Solutions of gelatin at various concentrations (6, 8 and 10% *w/v*) were made by dissolving gelatin powder (type A 300 bloom) (Sigma Aldrich, Dorset, UK) in 100% hexafluoroisopropanol (HFIP) (Sigma Aldrich). Solutions were stirred using a magnetic stirrer overnight at 37°C. The gelatin solutions were added to a 5ml syringe (BD Falcon™, Oxford, UK) and electrospun following the protocols described in **Section 2.1**. For each scaffold 4 ml of solution was electrospun at a flow rate of 1.2 ml h^{-1}. The needle collector distance was 15 cm and the voltage across the apparatus was 15 kV. The collector mandrel was set to spin at a speed of 2000 rpm. Upon completion of electrospinning, scaffolds were cut from the mandrel using a scalpel blade and stored in aluminium foil.

5.3.2 Crosslinking of electrospun gelatin scaffolds

Prior to crosslinking the scaffolds, they were first secured in an acetate frame (5star™, Cambridge, UK) using aquarium sealant (Sinclair animal and household care Ltd., Gainsborough, UK) on either side of the scaffold. Acetate frame size was either 23 x 42 mm with an internal window of 13 x 32 mm or 25 x 25 mm with an internal window of 15 x 15 mm. Once the acetate frames were adhered, the individual scaffolds were cut out and left overnight to dry. **Figure 5.1** illustrates the preparation of the scaffolds within the acetate frames. In order to crosslink the scaffolds, a solution of 250 mM 1-Ethyl-3-(3-dimethylaminopropyl) carbodiimide (EDC) (Applichem, Darmstadt, Germany) and 100 mM N-Hydroxysuccinimide (NHS) (TCI Europe, Zwijndrecht, Belgium) was prepared in distilled water. Ethanol (Sigma Aldrich) was added to the solution until the total volume was 10 times the original volume; the resultant solution was then refrigerated to 4°C. The scaffolds were placed in the EDC, NHS solution for 24 hours at 4°C. The scaffolds were removed from the crosslinking solution and washed in distilled water (x3) before being lyophilised overnight to leave the

Figure 5.1: Preparation of gelatin/ GelMa scaffolds prior to crosslinking. Electrospun scaffold sheet was pinned in place (**A**) before acetate frames were glued (**B**) and placed onto one side of the electrospun scaffold (**C**). Excess scaffold was cut away from the edges of the frames and frames were glued to the other side of the scaffold (**D**). Individual scaffolds were then cut out (**E**), pinned and left to dry (**F**).

dry, cross linked scaffolds. The mechanism of gelatin crosslinking using EDC and NHS is shown in **Figure 5.2**.

5.3.3 Synthesis of gelatin methacrylate

GelMa was synthesised following a previously published method (Nichol et al. 2010). Gelatin powder (10 g; type A 300 bloom) was dissolved in 95 ml PBS at 50°C and stirred for 1 hour. Methacrylic anhydride (8.0 ml) was added to the gelatin solution and stirred for a further 3 hours at 50°C. PBS (400 ml) was added to the mixture and stirred for a further 30 minutes. The solution was then transferred into three dialysis membranes (12-14 kDa cut-off). The membranes were placed in 3.0 L of distilled water and stirred at 50°C. The water was changed twice daily for 7 days before the membranes were removed and the solution inside transferred to plastic beakers and frozen overnight at -80°C. The frozen gelatin methacrylate (GelMa) solution was lyophilised and the GelMa stored at room temperature until ready for use. The mechanism of gelatin methacrylate synthesis is shown in **Figure 5.3**.

5.3.4 Production of GelMa scaffolds

Solutions of GelMa at 10% *w/v* mere made by dissolving freeze-dried GelMa in hexafluoroisopropanol (HFIP) (Sigma Aldrich). Solutions were stirred using a magnetic stirrer overnight at 37°C. The GelMa solutions were added to a 5ml syringe (BD Falcon™) and electrospun following the protocols described in **Section 2.1**. For each scaffold 4 ml of solution was electrospun at a flow rate of 1.2 ml h^{-1}. The needle collector distance was 15 cm and the voltage across the apparatus was 15 kV. The collector mandrel was set to spin at a speed of 2000 rpm. Upon completion of electrospinning, scaffolds were cut from the mandrel using a scalpel blade and stored in aluminium foil at room temperature.
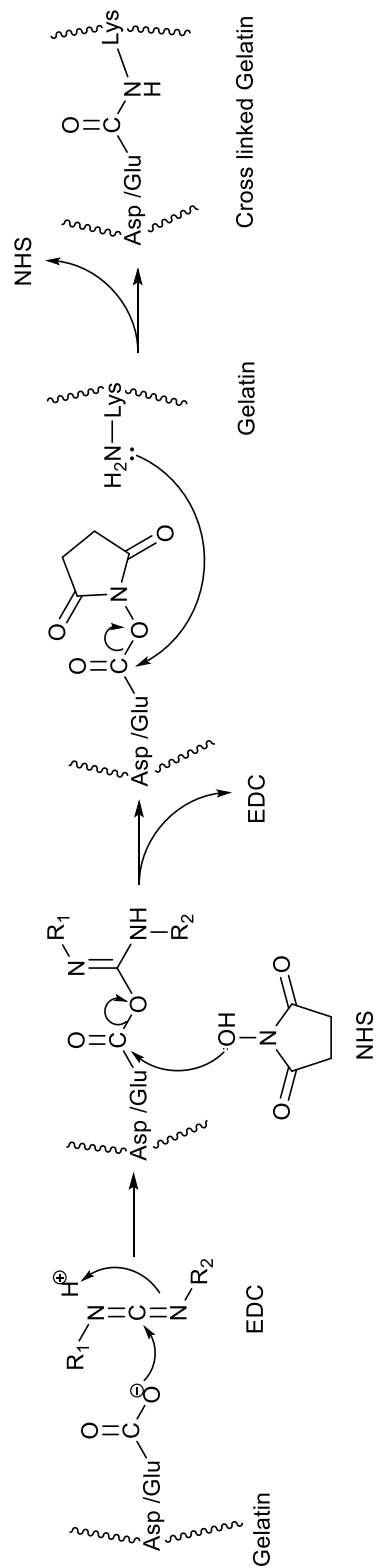
Figure 5.2: Mechanism of gelatin crosslinking with EDC and NHS. Mechanism adapted from (Kuijpers et al. 2000)
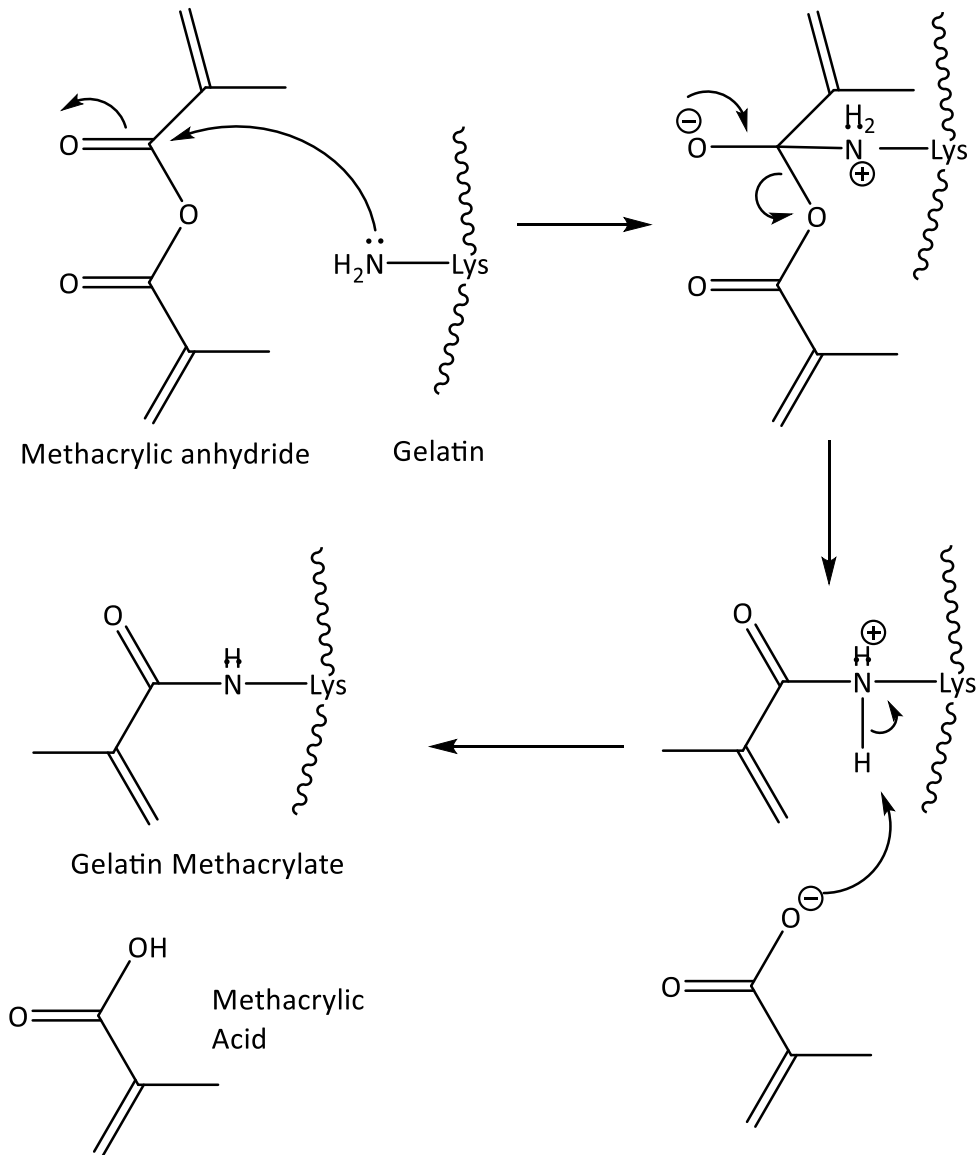
Figure 5.3: Mechanism of reaction between gelatin and methacrylic anhydride.

5.3.5 Crosslinking of GelMa scaffolds

Prior to crosslinking the scaffolds, they were first secured to an acetate frame as described previously. The scaffolds were then submerged in a 1% *w/v* solution of 2-Hydroxy-4'-(2-hydroxyethoxy)-2-methylpropiophenone (photoinitiator) in a solvent mix of ethanol and water. Solvent ratios used ranged from 1:0 to 9:1 ethanol: water. Scaffolds were then exposed to UV radiation (0.5 Wm^2) for 10 minutes. Scaffolds were washed in PBS three times. The proposed mechanism of the crosslinking process is displayed in **Figure 5.**4. Samples used for SEM imaging were washed in dH_2O and freeze-dried prior to analysis. Samples used for cell culture were incubated in antibiotic/antimycotic solution (50000 units ml-1 penicillin G, 500 mg ml-1 streptomycin sulphate and 125 μg ml-1 amphotericin B) (Fisher Scientific) in PBS at 4°C prior to use.

5.3.6 NMR analysis

Samples of gelatin and GelMa were dissolved in D_2O in glass NMR tubes and the NMR spectrum of each sample was determined using a Bruker Avance 600MHz spectrometer (Bruker, Coventry, UK). Spectra were analysed using the MestReNova LITE software package (Mestrelab research, Hereford, UK).

5.3.7 Tensile measurements of GelMa scaffolds

Samples of electrospun GelMa scaffolds were crosslinked in acetate frames (25 x 25 mm with an internal window of 15 x 15 mm) as described above. Crosslinked scaffolds were cut away from the edges of the scaffold along the two sides parallel to the fibre direction using a scalpel. Scaffolds were then placed in a TA.HDPlus Texture Analyser (Stable Micro Systems Ltd, Surrey, UK) with a 5 kg load cell. Samples were held in place using the tensile grips attachment with the fibre direction parallel to the testing direction. Once secure, the acetate frames were cut on the two sides parallel to the fibre direction removing the mechanical support offered by the acetate. Samples were tested at an extension rate of 6
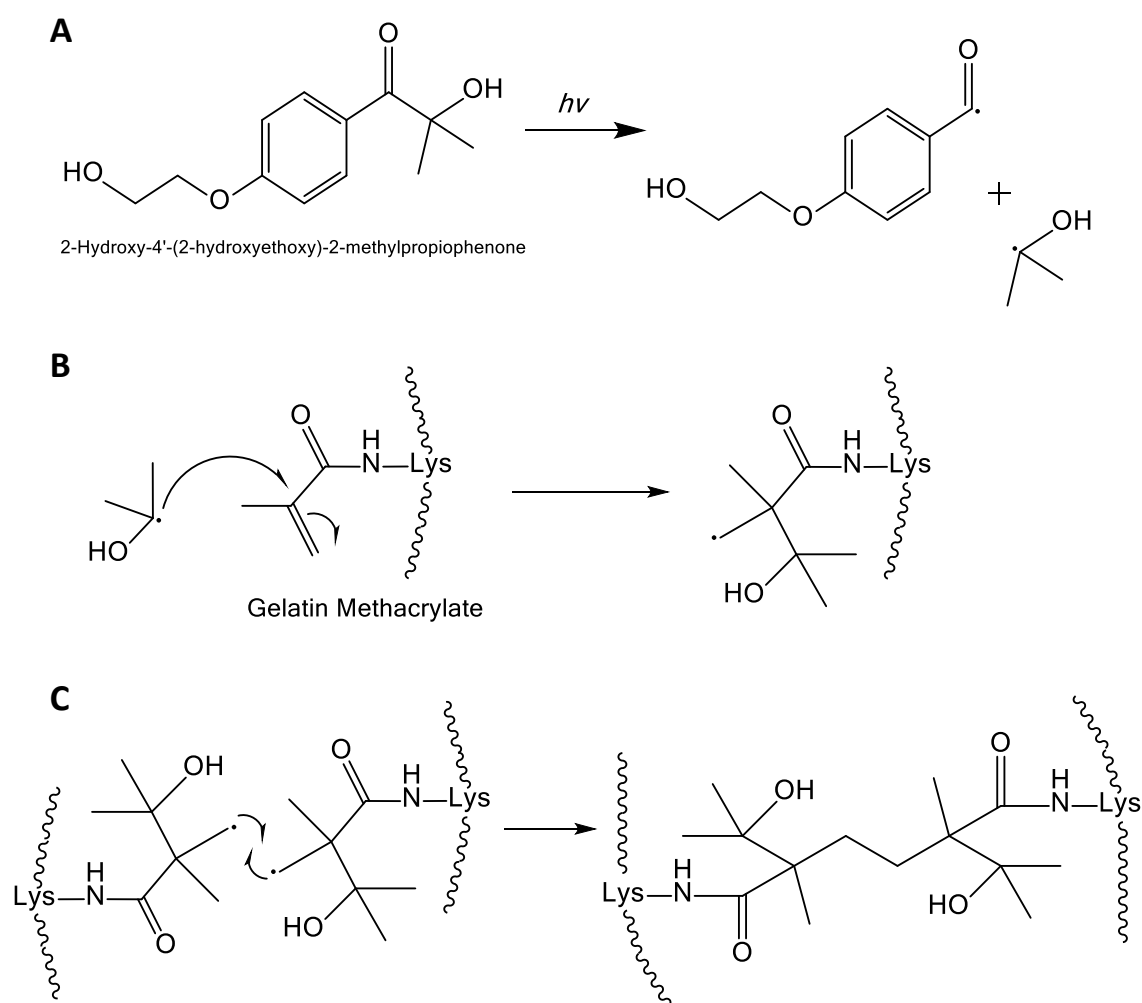
Figure 5.4: Mechanism of photo-initiated crosslinking of GelMa. Decomposition of the photoinitiator (**A**) is followed by reaction of the ketyl radical with the β-carbon atom of the methacrylate enone. (**B**). Two GelMa radicals react to form crosslinked

mm min $^{-1}$. The Young's moduli of the samples were calculated from the resultant stress/strain curves generated from the tests.

5.3.8 PrestoBlue® cell viability assay

RASM cell viability was measured post seeding on aligned scaffolds using the PrestoBlue® assay at various time points across a 10 day period. Samples were washed with PBS prior to incubation with 1ml PrestoBlue® solution (10% (*v/v*) PrestoBlue® in HASM culture media) for 10 minutes at 37 °C. The PrestoBlue was then collected (100 µL aliquots) and replaced with RASM media. The fluorescence emissions of the collected samples were measured in duplicate on a plate reader (excitation 560 nm/ emission 590 nm) (Tecan Infinite M200, Reading, UK) A blank sample reading was subtracted from the fluorescence readings for each sample and duplicate readings were averaged. The resultant readings were then expressed as a fraction of the fluorescence reading at day 0.

5.3.9 Scaffold contraction assays

Samples of crosslinked 10% *w/v* gelatin or GelMa scaffolds were prepared as described above. All scaffolds were placed in 6 well culture plates and sterilised by UV exposure (20 minutes) followed by incubation in cell culture media (60 minutes, 37°C) prior to seeding of cells. Gelatin/ GelMa scaffolds were seeded with RASM cells at a density of 2x 10^5 cells cm^{-2}. All samples were then incubated for 10 days (37°C, 5% CO_2 in air) to allow cell proliferation.

Following incubation, culture media was aspirated and 1 ml serum free DMEM added to each sample, gelatin/ GelMa scaffolds were cut out from their acetate frames and well plates were imaged using a flatbed scanner. Serum free DMEM (1 ml) ± agonist (200 µM UTP) was then added to each sample. Well plates were then imaged at specific time intervals for up to 30 minutes. Scanned images were analysed using ImageJ; changes in scaffold surface area were used to determine the level of scaffold contraction.

5.3.10 Direct force measurement of RASM seeded GelMa scaffold contraction

Rectangular crosslinked GelMa scaffolds (13 x 32 mm) were prepared and sterilised as described above. Scaffolds were seeded with RASM cells at a density of 2×10^5 cells cm^{-2}. Scaffolds were then incubated (37°C, 5% CO_2) for 10 days. Scaffolds were removed from culture media and washed twice with serum free DMEM. Scaffolds were individually placed in an 85 mm petri dish containing a strip of canning wax adhered to the dish surface. Scaffolds were cut away from the acetate frames along the long axis of the scaffold (parallel to fibre direction) using a scalpel and one end of the scaffold was pinned in place by passing a minuten pin through the acetate frame into the canning wax. Serum free DMEM (5 ml) was added to the dish and the acetate frame was cut away along the long axis to leave the scaffold free floating at one end. A minuten pin adhered to a glass bead was threaded through the underside of the scaffold at the free floating end which was then attached to a model 403A force transducer (Aurora Scientific, Dublin, Ireland) using canning wax. The force transducer was connected to a Powerlab 4/25T unit with associated software (AD Instruments, Oxford, UK). Force was measured at a frequency of 1 kHz. Once stable, the baseline force of the resting scaffolds was measured for 3 minutes before the addition of 500 µL of 1 mM UTP in serum free DMEM (500 µL serum free DMEM in control experiments) using a pipette. Contraction was then measured continuously for 60 minutes.

5.4   Results

The overall aim of this chapter was to develop an *in vitro* model of contractile smooth muscle tissue. Smooth muscle cells were successfully cultured upon the electrospun PET scaffolds developed in the previous chapter. However, one noticeable feature of these scaffolds was that they were very stiff with Young's moduli much higher than seen *in vivo* muscle tissue. Therefore, although HASM cells were seen to adhere to and proliferate upon the PET scaffolds, the scaffold fibres proved to be too stiff for cultured smooth muscle cells to contract. Consequently, the next stage of the investigation involves attempting to produce new scaffold material to achieve a contractile SM cell/ scaffold construct. This was achieved by electrospinning and cross-linking gelatin scaffolds.

5.4.1 Electrospinning aligned gelatin scaffolds

Gelatin was chosen to be electrospun as an alternative material to PET due to its more elastic properties and the fact that it is chemically similar to collagen, which was shown in chapter 3 to support the growth of contractile SM cells. Gelatin was electrospun from solutions ranging 6% to 10% (*w/v*) (**Figure 5.5A**, **C** and **E**). As gelatin is water soluble, scaffolds required crosslinking prior to use in cell culture. Scaffolds were successfully crosslinked using EDC and NHS in an ethanol and water mixture. Crosslinking was also attempted by incubating the scaffolds in glutaraldehyde vapour: the resultant scaffolds were still partially soluble in water (insoluble at room temperature but dissolved at higher temperatures necessary for cell culture) and were also very brittle. Consequently, glutaraldehyde crosslinked scaffolds were not further investigated. In both crosslinking methods, the gelatin scaffolds reduced to approximately 25-30% of their original size. This was prevented by holding the scaffolds in place either by using acetate frames or placing the scaffolds in trans-well inserts or CellCrown™ inserts (Sigma). However, due to the eventual need to prepare rectangular constructs for force measurement studies, acetate frames
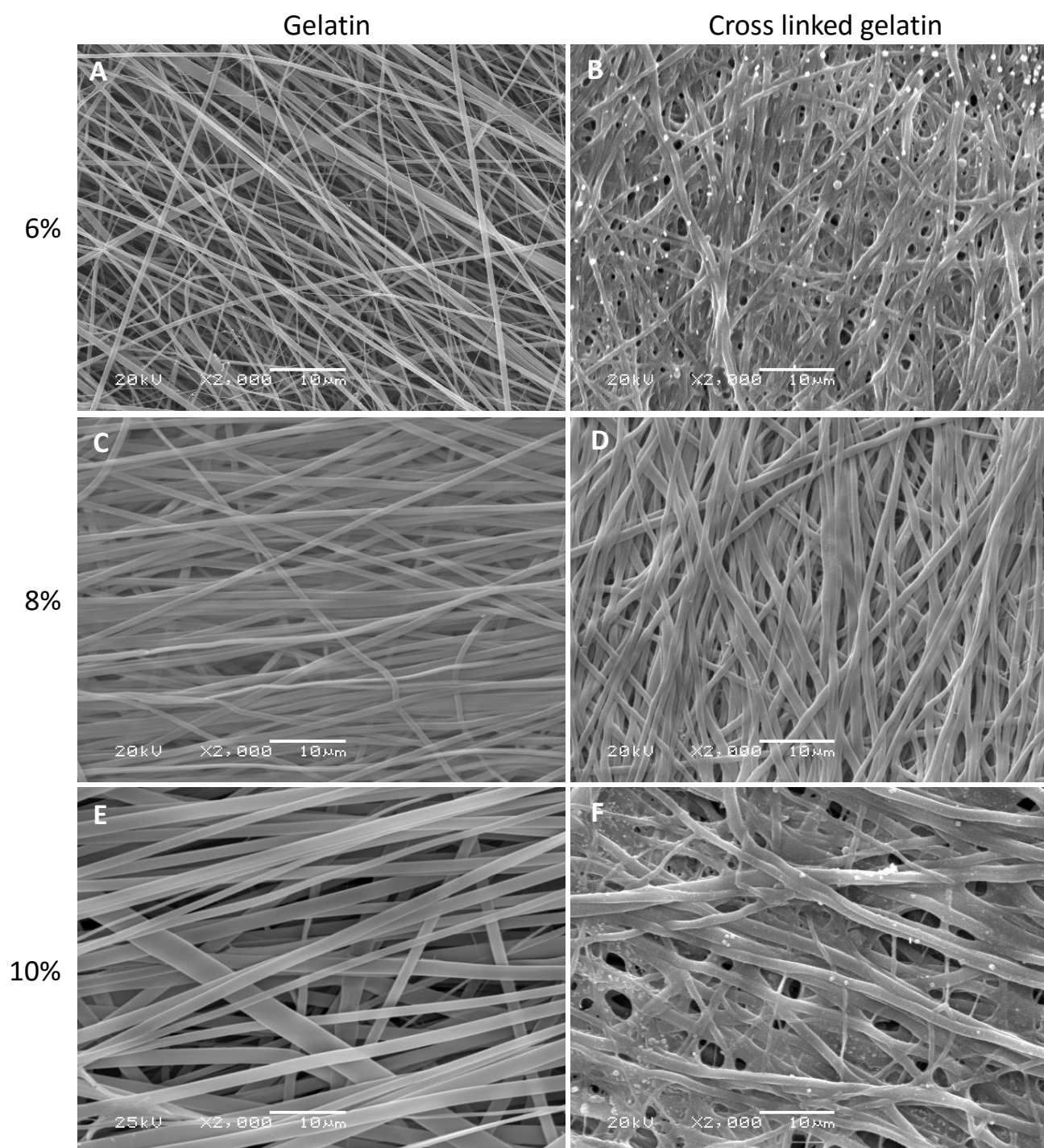
Figure 5.5: Electrospun gelatin scaffolds pre and post crosslinking. Representative SEM images of gelatin scaffolds electrospun from 6%, 8% and 10% *w/v* gelatin solutions (**A,C,E** respectively). The scaffolds were then imaged after crosslinking with EDC and NHS (**B,D,F**)

were chosen as the method to secure the scaffolds during crosslinking. SEM images of the crosslinked gelatin scaffolds are shown in **Figure 5.5** (**B**, **D** and **F**).

In order to compare the stiffness of these gelatin scaffolds to the previously used PET scaffolds, tensile testing was performed on samples of the crosslinked 6%, 8% and 10% (*w/v*) aligned gelatin scaffolds. Representative stress/ strain curves for each scaffold are displayed in **Figure 5.6A**. The gradients of these curves were used to calculate the Young's modulus of each scaffold. The stiffest gelatin scaffold was the 10% gelatin scaffold with a mean Young's modulus value of 3.80 ± 1.69 MPa (almost 100 times lower than the stiffest PET scaffold at 340 MPa). The mean Young's modulus of the 8% and 6% gelatin scaffolds were 2.58 ± 0.72 and 1.54 ± 0.79 MPa respectively (mean ± standard deviation). There was a statistical difference between the stiffness of the 10% and 6% gelatin scaffolds as shown in **Figure 5.6B**(P<0.05).

In addition to the tensile properties of the gelatin scaffolds, the average fibre diameter and degree of fibre alignment were also analysed for each scaffold. Measurements were taken both before and after the scaffolds were crosslinked in order to assess the effect of crosslinking on the morphology of the gelatin scaffolds. As seen when electrospinning PET scaffolds, the fibre diameter of gelatin scaffolds increased with the concentration of the gelatin solution; 10% gelatin solutions produced fibres with an average diameter of 1.24 μm whereas 8% and 6% produced scaffolds with average fibre diameters of 788 and 286 nm respectively. Crosslinking of these scaffolds significantly affected the average fibre diameter (P<0.0001), increasing the diameter in all cases. 10%, 8% and 6% gelatin scaffolds average fibre diameter increased to 1.49 μm, 978 nm and 746 nm, an increase of 20.13%, 24.11% and 160.62% respectively (**Figure 5.7A**).

All gelatin scaffolds were highly aligned with 57.71%, 65.21% and 42.50% of fibres within 10° of the mean fibre angle in 10%, 8% and 6% scaffolds respectively. In all cases fibre alignment significantly dropped (50.6%, 48.3% and 23.0% respectively) after the crosslinking process although clear fibre alignment still remains (**Figure 5.7B**).
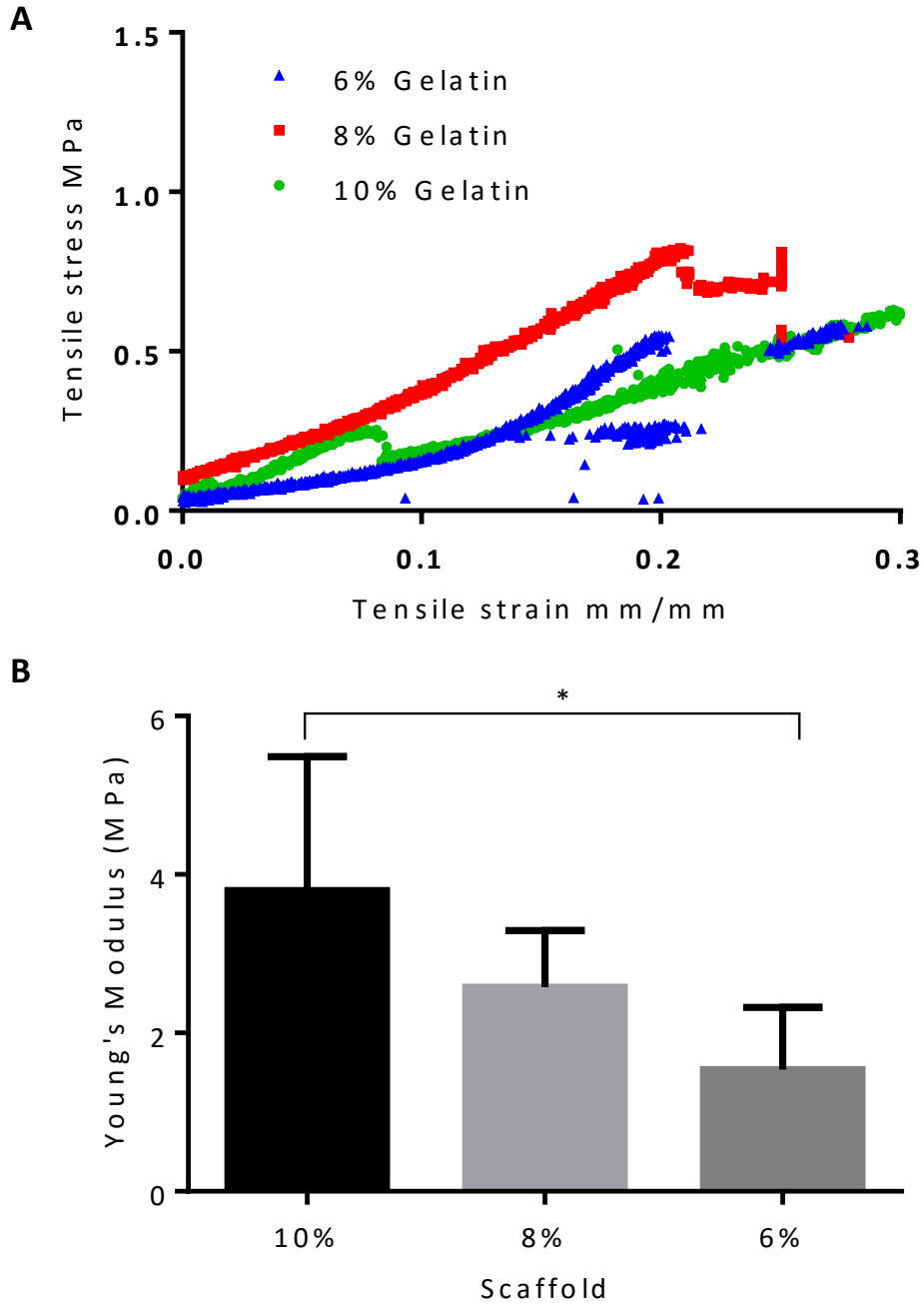
Figure 5.6: Mechanical properties of crosslinked electrospun gelatin scaffolds. Representative stress/ strain curves for three different gelatin scaffolds (**A**). This data was then used to calculate the average Young's modulus for each scaffold (**B**) (error bars represent standard deviation; n= 6). One way ANOVA with Tukey's multiple comparisons test was carried out between the Young's modulus of all scaffolds (P<0.05)
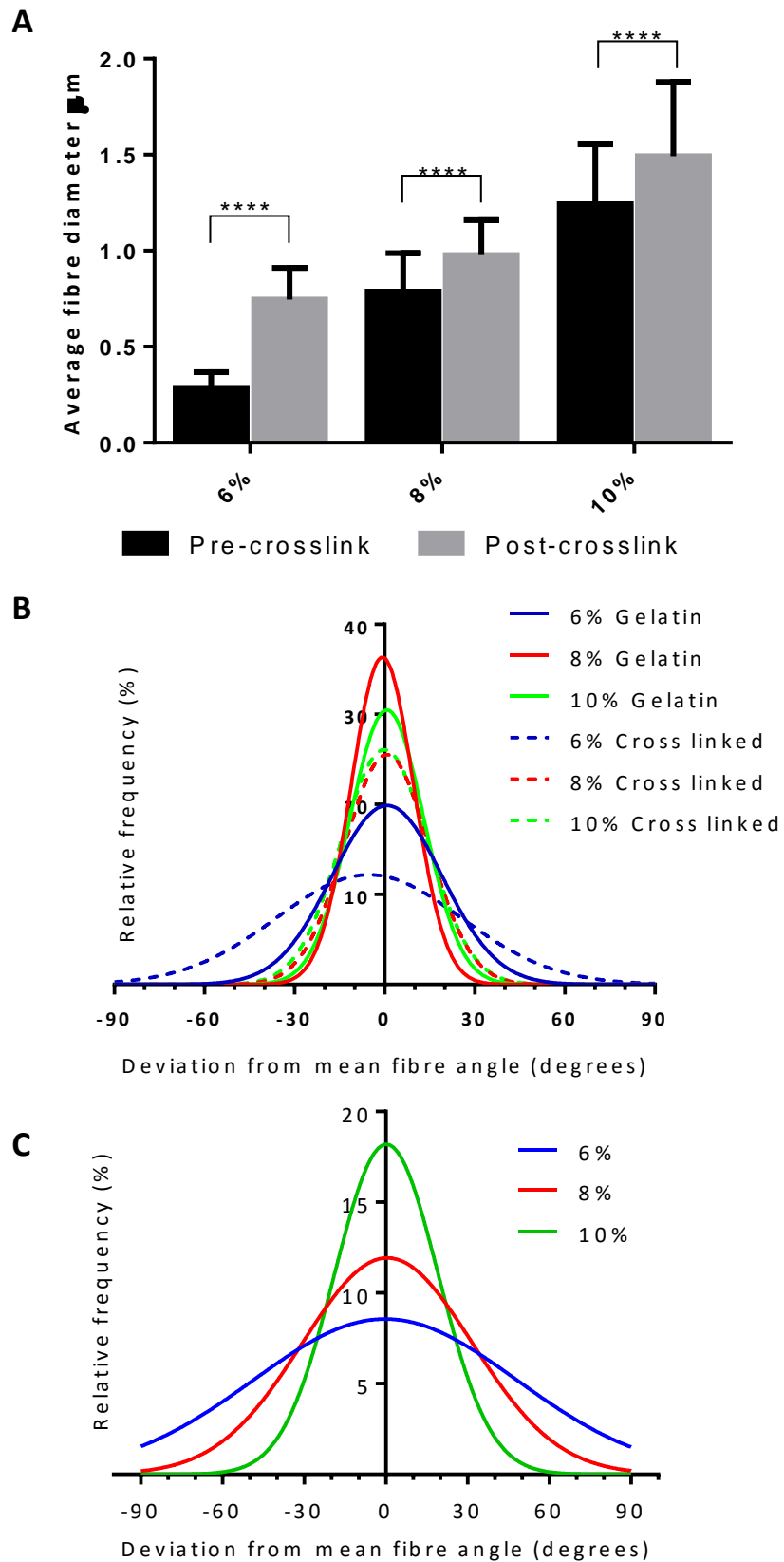
Figure 5.7: Properties of aligned gelatin scaffolds. Average fibre diameters for each gelatin scaffold both before and after crosslinking (**A**), error bars represent standard deviation. Unpaired t-tests were carried out between the fibre diameters of each scaffold before and after crosslinking. Distribution curves illustrating the degree of alignment in each scaffold before and after crosslinking (**B**) and the alignment of RASM cells cultured on the crosslinked scaffolds (**C**).

5.4.2 Culture of RASM cells on gelatin scaffolds

The differences seen in crosslinked gelatin scaffold alignment (10%> 8%> 6%) is reflected in the nuclear alignment of cells cultured upon the scaffolds; RASM cells were more aligned on 10% crosslinked gelatin scaffolds (37.9% within 10° of mean) than on 8% (27.3%) and 6% (20.5%) scaffolds (**Figure 5.7C**). Due to the increased alignment of cells on 10% gelatin scaffolds and only slight increase in stiffness compared to the other gelatin scaffolds, the 10% gelatin scaffolds were chosen to be used for further cell culture studies. These scaffolds were seeded at a range of cell densities and fixed at various time points in order to determine the optimal seeding density and culture period required to produce an aligned confluent sheet of SM cells on the gelatin scaffolds (**Figure 5.8A-I**). Additionally, cell proliferation was monitored using the PrestoBlue assay (**Figure 5.8J**). Cell number appeared to increase steadily over the first 6 days of culture before a large increase between days 6 and 8. No decrease in cell activity was seen over the 10 day study. Confluency was achieved after 9 days when scaffolds were seeded at a density of 2×10^5 cells cm^{-2} (**Figure 5.8I**). When immunostained in order to confirm SM phenotype, SM cells cultured on gelatin scaffolds stained positive for SM markers SM22α (**Figure 5.9A**) and calponin (**Figure 5.9C**). Cells also stained positive for the gap junction protein connexin and negatively for the intermediate filament protein desmin (**Figure 5.9B**). Individual focal adhesions were observed in cells stained for vinculin (**Figure 5.9D**); cells possessed a spindle-like morphology with the majority of focal adhesions occurring at the spindle poles.

5.4.3 Contraction of RASM seeded gelatin scaffolds

Crosslinked 10% gelatin electrospun scaffolds were seeded with RASM cells at a density of 2×10^5 cells cm^{-2} and incubated for 10 days before scaffolds were cut away from the supporting acetate frames. Scaffolds were stimulated with 100 μM UTP and imaged to assess the degree of scaffold contraction. **Figure 5.10A**
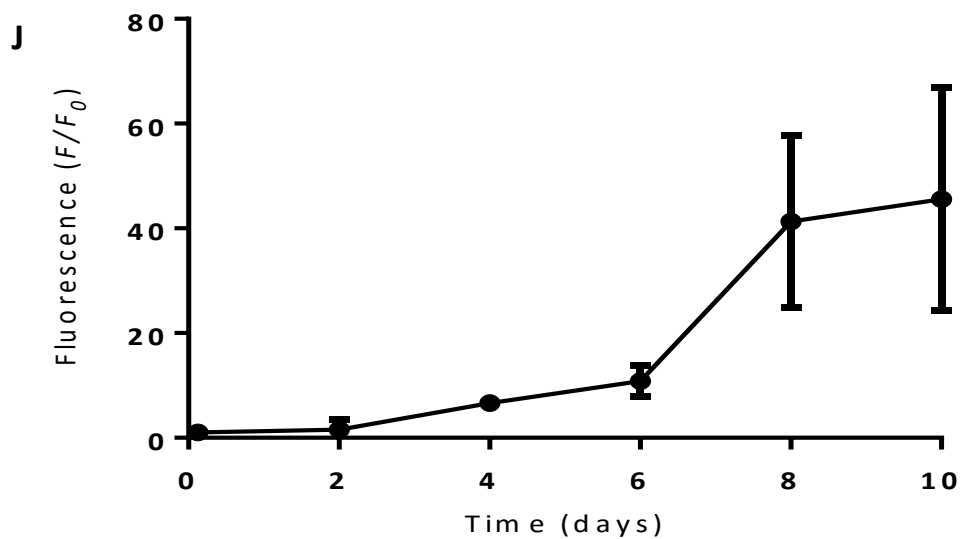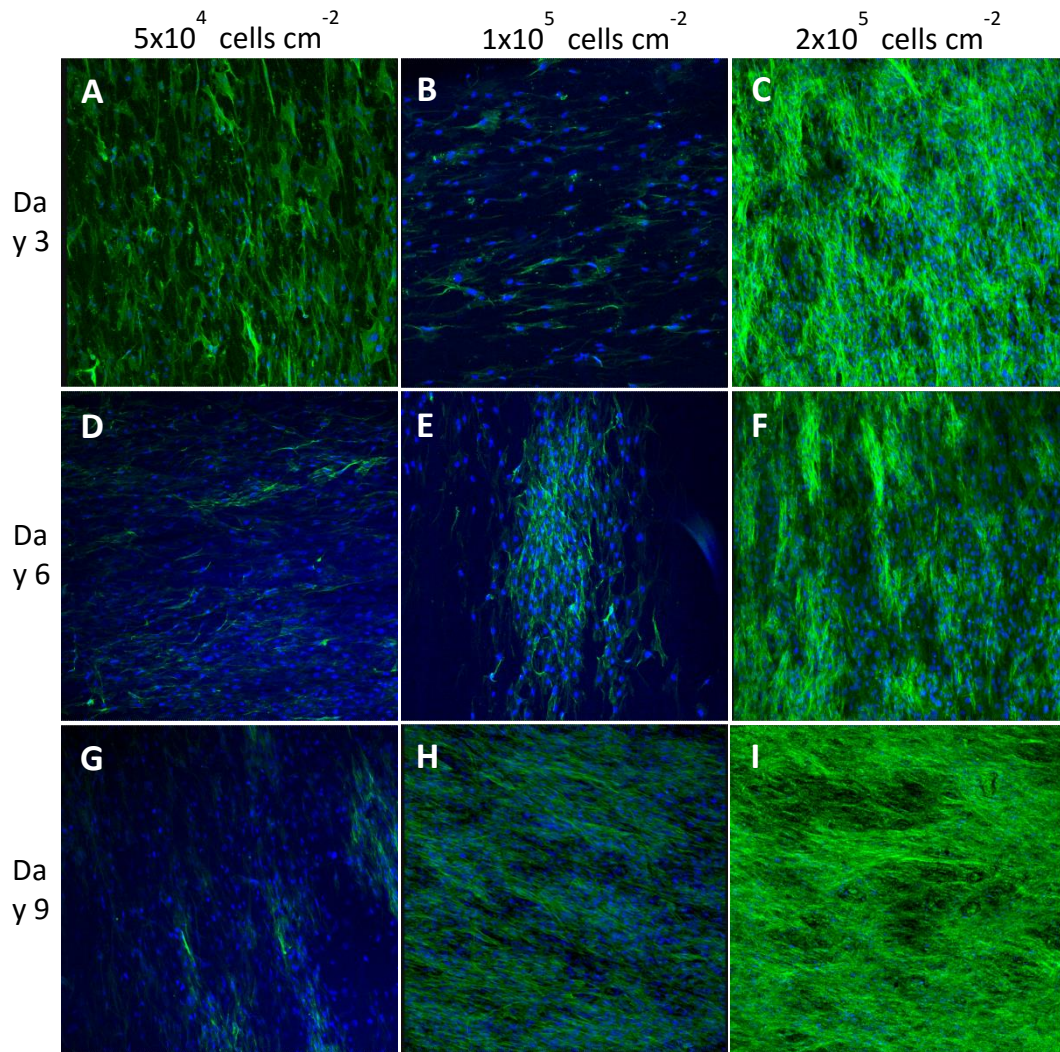
Figure 5.8: Culture of RASM cells on crosslinked gelatin scaffolds. ICC images of RASM cells seeded at various densities on crosslinked 10% gelatin scaffolds at day 3 **(A,B,C)**, 6 **(D,E,F)** and 9 **(G,H,I)**. Cells were stained with fluorescently tagged phalloidin (green) and the nuclear stain Hoechst (blue). Cell metabolism was monitored using the PrestoBlue® assay for 10 days (**J**). Error bars represent SEM; n= 6.
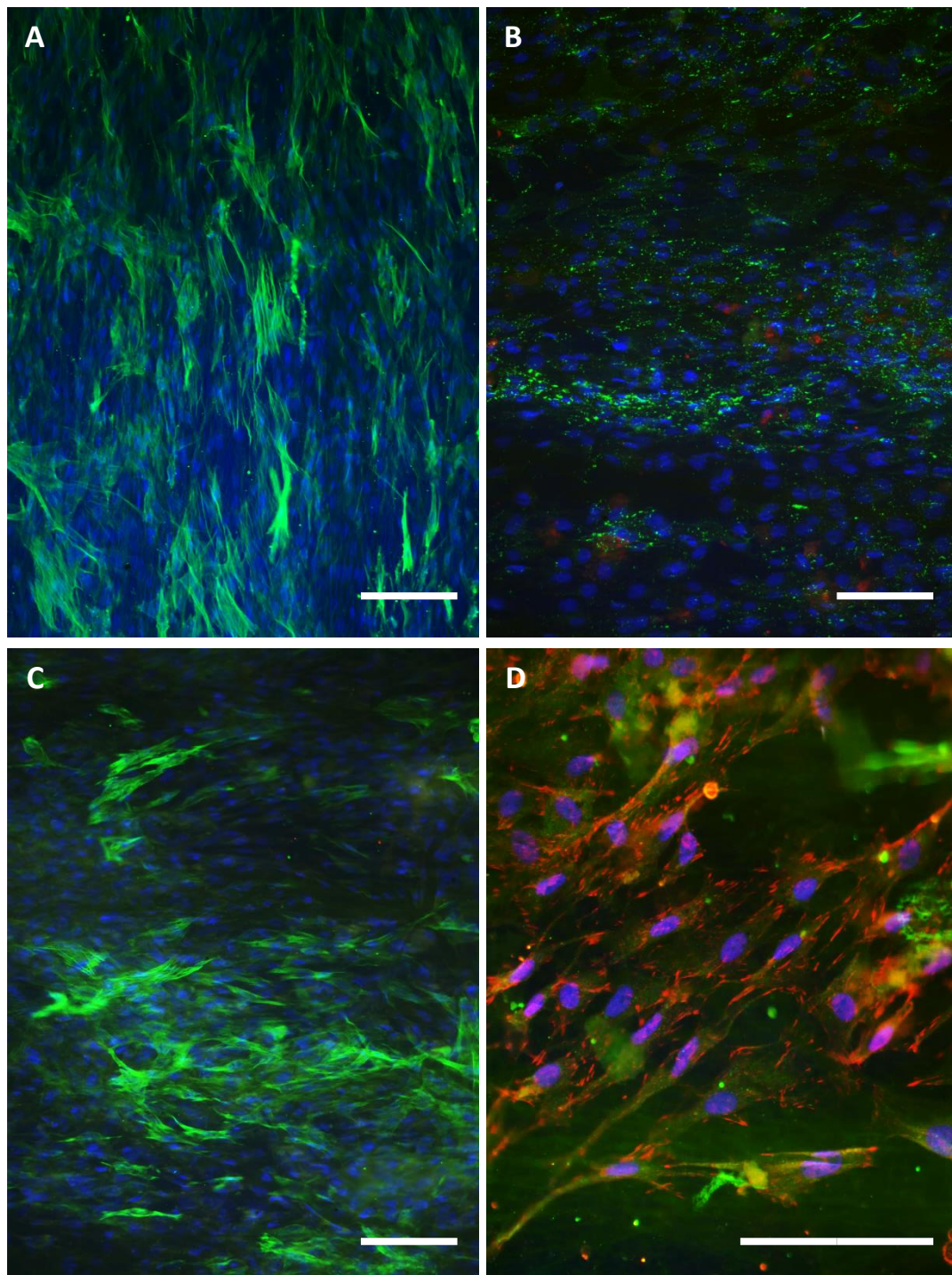
Figure 5.9: Immunostaining of RASM cells on electrospun gelatin scaffolds. RASM cells were fixed and stained with SM22α (**A**), connexin (**B**), and calponin (**C,D**) (all green). Cells were also stained for desmin (**B**) and vinculin (**C,D**) (all red). All samples were additionally stained with the nuclear stain Hoechst 33342 (blue). Scale bars = 100μm.
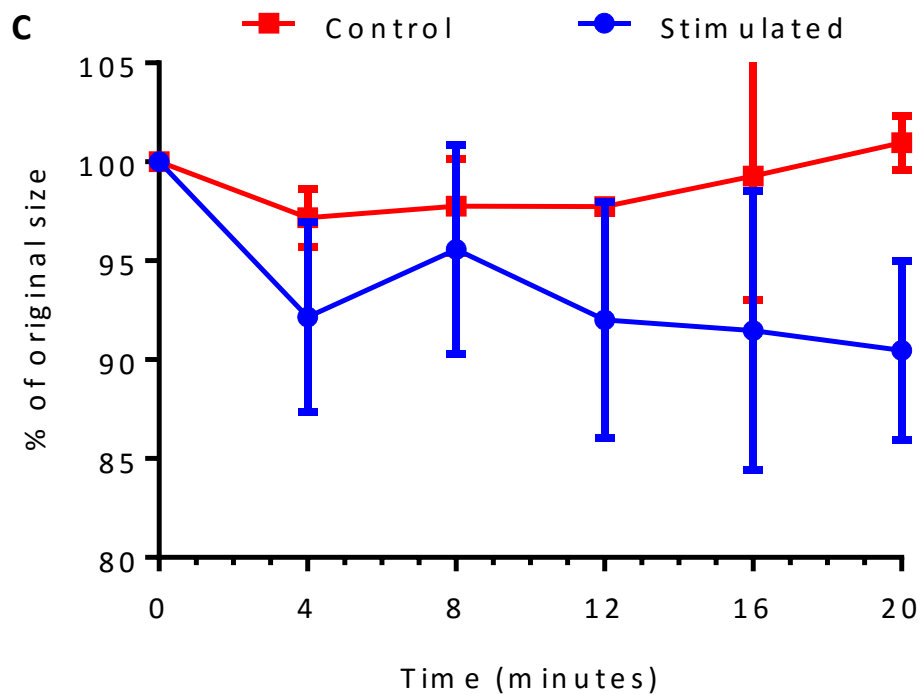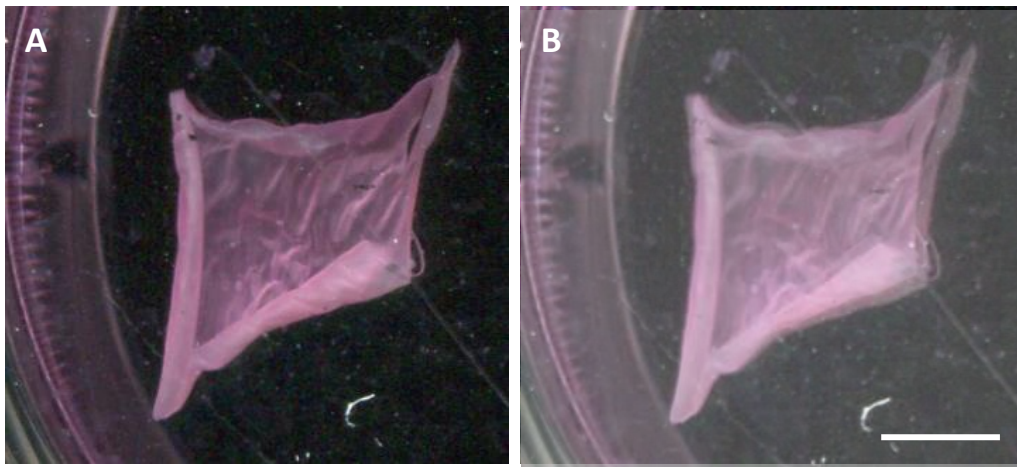
Figure 5.10: Contraction of RASM seeded gelatin scaffolds. Scanned images of a RASM seeded gelatin scaffold at T=0 (**A**) and T=20 minutes (**B**) following stimulation with UTP. Scale bar = 35 nm. To compare the scaffold at the two time points, **A** has been overlaid onto image **B**. Image analysis of the scaffolds at multiple time points was used to assess the level of scaffold contraction (**C**), error bars represent standard deviation (n=4).

and **B** displays images of a RASM seeded gelatin scaffold at times t=0 and t=20 minutes respectively. By comparing the surface area of the scaffold across this time period, RASM contraction can be measured (**Figure 5.10C**). Over the 20 minute period, scaffolds reduced to 90.5 ± 4.5% (mean ± standard deviation) of their original size, after 20 minutes no further contraction was seen. Unstimulated controls remained close to 100% their original size throughout the study. Although some scaffold contraction could be seen in this study, the amount of contraction (reduction in size) is still much lower than witnessed in the collagen hydrogels. By choosing an alternative, more controllable method of crosslinking the gelatin based scaffolds; it may be possible to alter the stiffness of the scaffolds to allow further cell mediated contraction. For this reason, the electrospinning of chemically modified (methacrylated) gelatin was investigated.

5.4.4 Production of electrospun GelMa scaffolds

Gelatin can be methacrylated *via* a nucleophilic substitution reaction with methacrylic anhydride. During this process, free amines found within lysine residues in the gelatin structure become methacrylated. The degree of methacrylation can be controlled by the ratio of gelatin: methacrylic anhydride in the initial reaction mixture. Once methacrylated, the gelatin methacrylate (GelMa) can be crosslinked under UV light in the presence of a photoinitiator. Therefore, the level of GelMa crosslinking can be controlled by the initial level of methacrylation, the amount of photoinitiator used, the amount of UV exposure and the solvents used in the crosslinking process. The methacrylation of gelatin was confirmed and degree of methacrylation calculated analysed using proton NMR spectroscopy (**Figure 5.11**). Comparing the ^{1}HNMR spectrum of synthesised GelMa to that of gelatin, there are two clear additional peaks in the GelMa spectrum at approximately 5.3 and 5.6 ppm. These peaks are due to the two protons found on the methacrylate vinyl group. The degree of methacrylation was calculated using a previously published method (Ovsianikov et al. 2011). The peak at 0.84 ppm can be used as a reference peak ascribed to the hydrophobic side chains of valine, leucine and isoleucine; the integration of this peak ($I_{0.84}$)
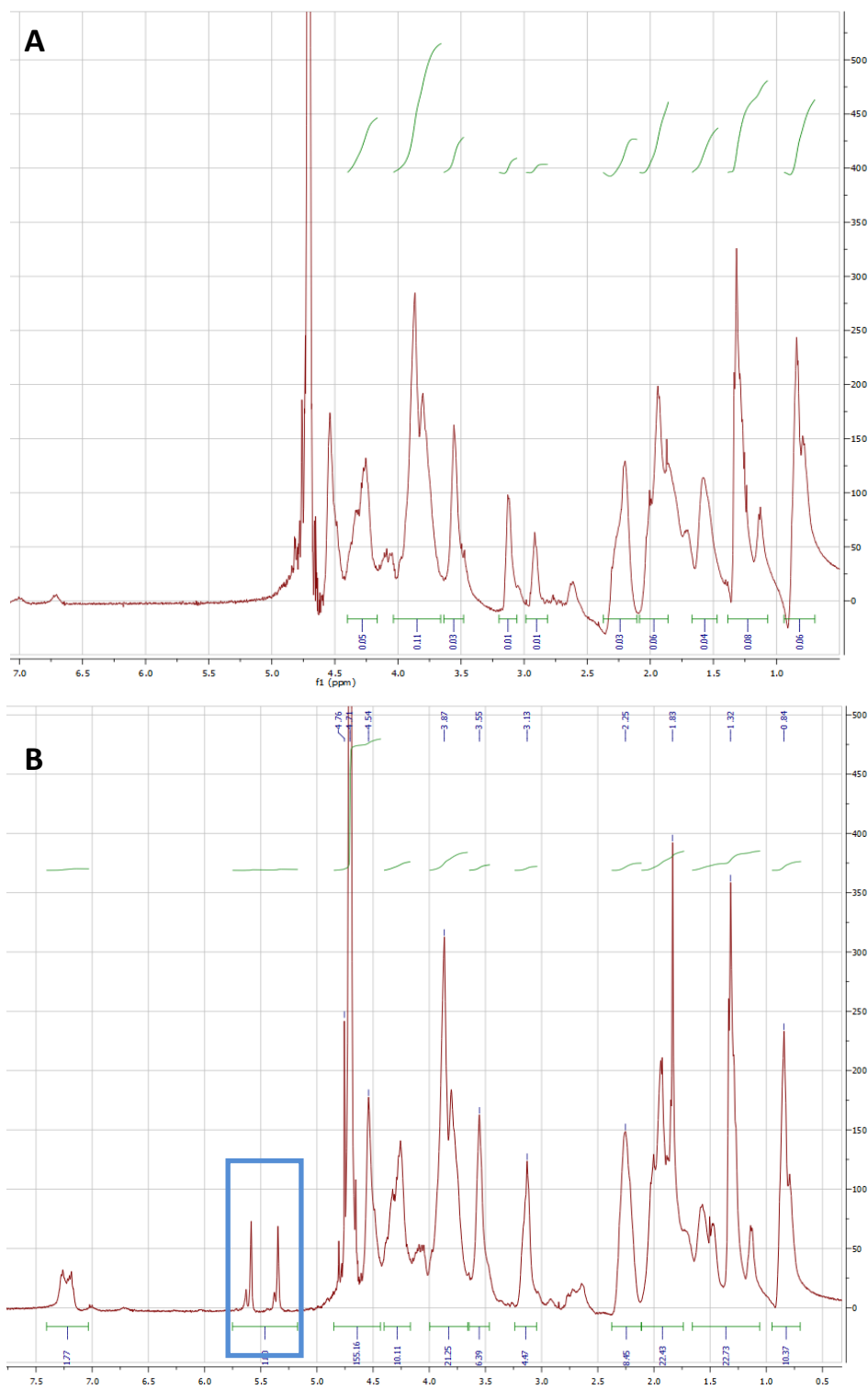
Figure 5.11: Analysis of synthesised gelatin methacrylate. Proton NMR spectra of gelatin (**A**) and synthesised gelatin methacrylate (**B**). Methacrylate vinyl peaks highlighted in blue rectangle.

corresponds to 0.3836 mol/ 100 g (sum of known composition of these amino acids in gelatin). The total amount of available amine groups in gelatin is equal to 0.0385 mol/ 100g. Therefore the percentage of methacrylation within the synthesised GelMa can be expressed using the following equation:

$$DM\%=\frac{5.6ppm\times0.3836}{0.84ppm\times0.0385}\times100$$

Using this equation the percentage of methacrylation was calculated to be 81.01%. The synthesised GelMa was electrospun using a 10% (*w/v*) solution (**Figure 5.12A**) SEM image analysis was used to determine the average fibre diameter (297.4 ± 101.1 nm (mean ± standard deviation)) and degree of fibre alignment (49.79% of fibres within 10° of the mean fibre angle) of the electrospun scaffolds. Distribution curves of the fibre diameter and angle are displayed in **Figure B** and **C** respectively.

GelMa scaffolds were cut and adhered to acetate frames before being crosslinked using UV light in the presence of a photoinitiator in solution (1% *w/v* solution of 2-Hydroxy-4'-(2-hydroxyethoxy)-2-methylpropiophenone). In order to prevent the GelMa scaffolds from dissolving during the crosslinking process, a number of solvent mixtures were investigated. These ranged from pure ethanol to a 9:1 ethanol: water mixture. Scaffolds would not crosslink in pure ethanol with the scaffolds dissolving when washed following the crosslinking process. Solutions with greater than 10% water content dissolved the scaffolds upon contact. Three different ethanol: water solutions were chosen to crosslink the GelMa scaffolds; these were 39:1 (2.5% H_2O), 19:1 (5.0% H_2O) and 9:1 (10% H_2O). Tensile tests of the different crosslinked GelMa scaffolds were run to calculate the Young's modulus of each. Young's modulus increased with the increasing water content in the crosslinking solutions: average Young's moduli were 142.2 ± 25.39, 158.7 ± 95.33 and 451.5 ± 111.3 kPa (mean ± standard deviation) for scaffolds crosslinked in 2.5%, 5.0% and 10% water in ethanol solutions respectively (**Figure 5.13A**). Scaffolds crosslinked in 10% H_2O were in ethanol significantly stiffer than those crosslinked in 5% and 2.5% H_2O in ethanol
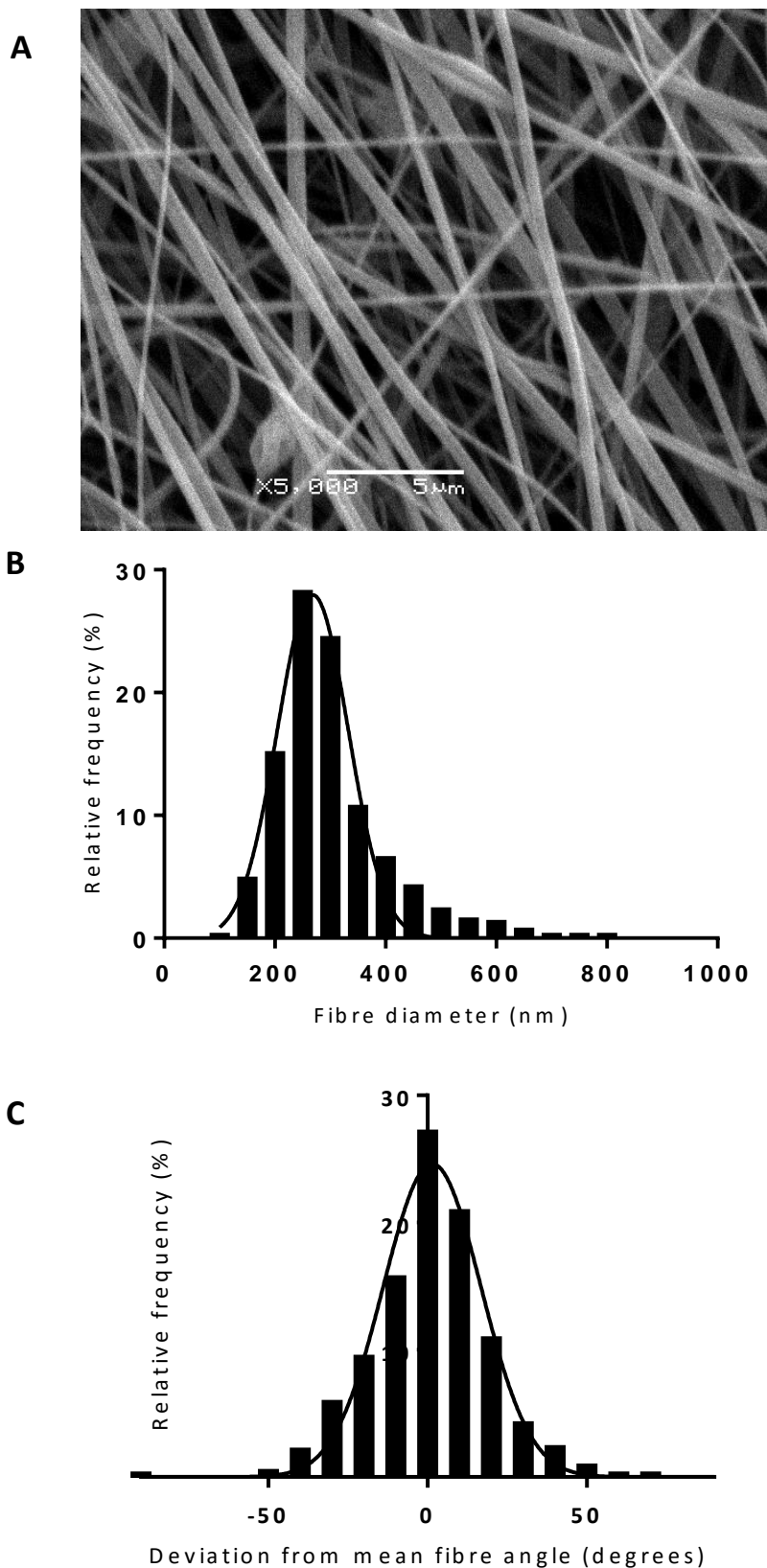
Figure 5.12: Properties of electrospun GelMa scaffolds. SEM image of aligned electrospun GelMa spun from a 10% *w/v* solution before cross-linking (**A**). Histograms and Gaussian distribution curves of fibre diameter (**B**) and fibre alignment (**C**) are presented.
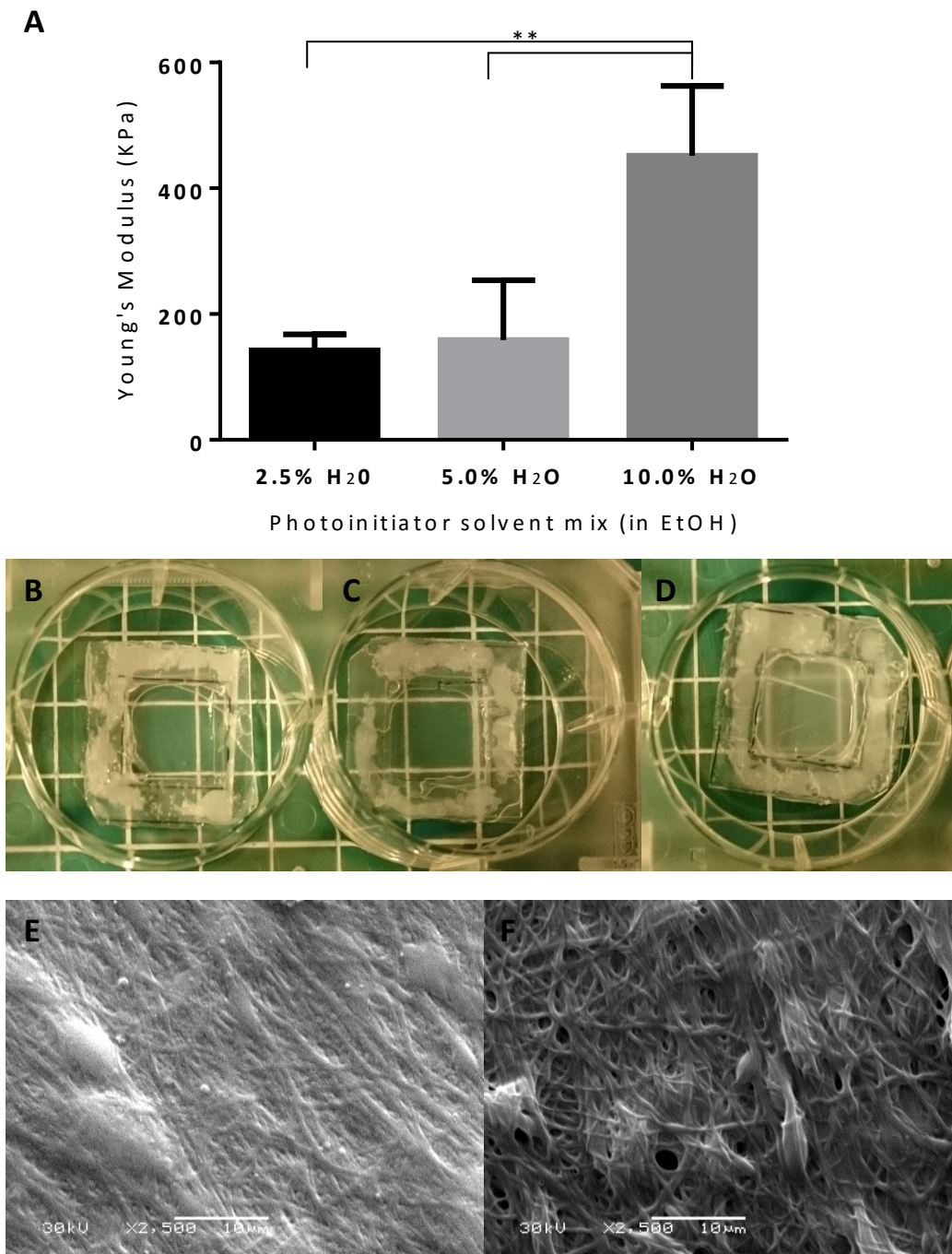
Figure 5.13: Crosslinking electrospun GelMa scaffolds. Average Young's moduli of GelMa scaffolds crosslinked in different H_2O:EtOH mixtures (**A**). Error bars represent standard deviation (n=4). One way ANOVA with Tukey's multiple comparisons test was carried out between the Young's modulus of all scaffolds (P<0.01) Photographs of scaffolds crosslinked in 2.5%, 5.0% and 10.0% (*v/v*) H_2O in ethanol show increasing scaffold opacity. SEM images of crosslinked GelMa scaffolds crosslinked in 5.0% (**E**) and 10.0% (**F**) H_2O.

solutions (P<0.01). Scaffold opacity increased with increasing crosslinking water content (**Figure 5.13B-D**), in addition when crosslinking in 2.5% H_2O in ethanol the failure rate of the scaffolds during post cross-linking washing was muchhigher. Scaffold fibre analysis post-crosslinking was not possible due to a lack of fibre resolution; fibres appeared to merge together during crosslinking although the aligned fibre morphology can still be seen when cross-linked in 5% and 10% H_2O in ethanol solutions (**Figure 5.13E**-**F** respectively). Due to the high failure rates of 2.5% H_2O in ethanol crosslinked scaffolds and the significantly higher Young's modulus of the 10% H_2O crosslinked scaffolds, the scaffolds crosslinked in 5% H_2O in ethanol were chosen to be used for cell culture investigations.

5.4.5 Culture of RASM cells on GelMa scaffolds

RASM cells were cultured on crosslinked aligned GelMa scaffolds for a period of 10 days. During that time cell metabolic activity was monitored using the PrestoBlue® assay. Cell metabolism increased steadily throughout the 10 day period (**Figure 5.14A**) indicating RASM proliferation over that time. Samples were fixed after the 10 day period and stained for the SM markers SM22α and calponin and stained for the gap junction protein connexin (**Figure 5.15A, B** and **C** respectively). Samples stained positive for all markers. In addition, the samples stained negatively for desmin. Unlike RASM cells cultured upon gelatin scaffolds, those cultured upon GelMa scaffolds did not stain positively for vinculin, with no clear focal adhesions present. RASM cell alignment on the GelMa scaffolds was similar to the degree of alignment achieved on 8% and 6% gelatin scaffolds with 23.42% of nuclei oriented within 10° of the mean (**Figure 5.14B**).

5.4.6 Contraction of RASM seeded GelMa scaffolds

Crosslinked GelMa scaffolds were seeded with RASM cells at a density of 2 x 10^5 cells cm^{-2} and incubated for 10 days before scaffolds were cut away from the supporting acetate frames. Scaffolds were stimulated with 100 µM UTP and imaged to assess the degree of scaffold contraction. **Figures 13A** and **B** display
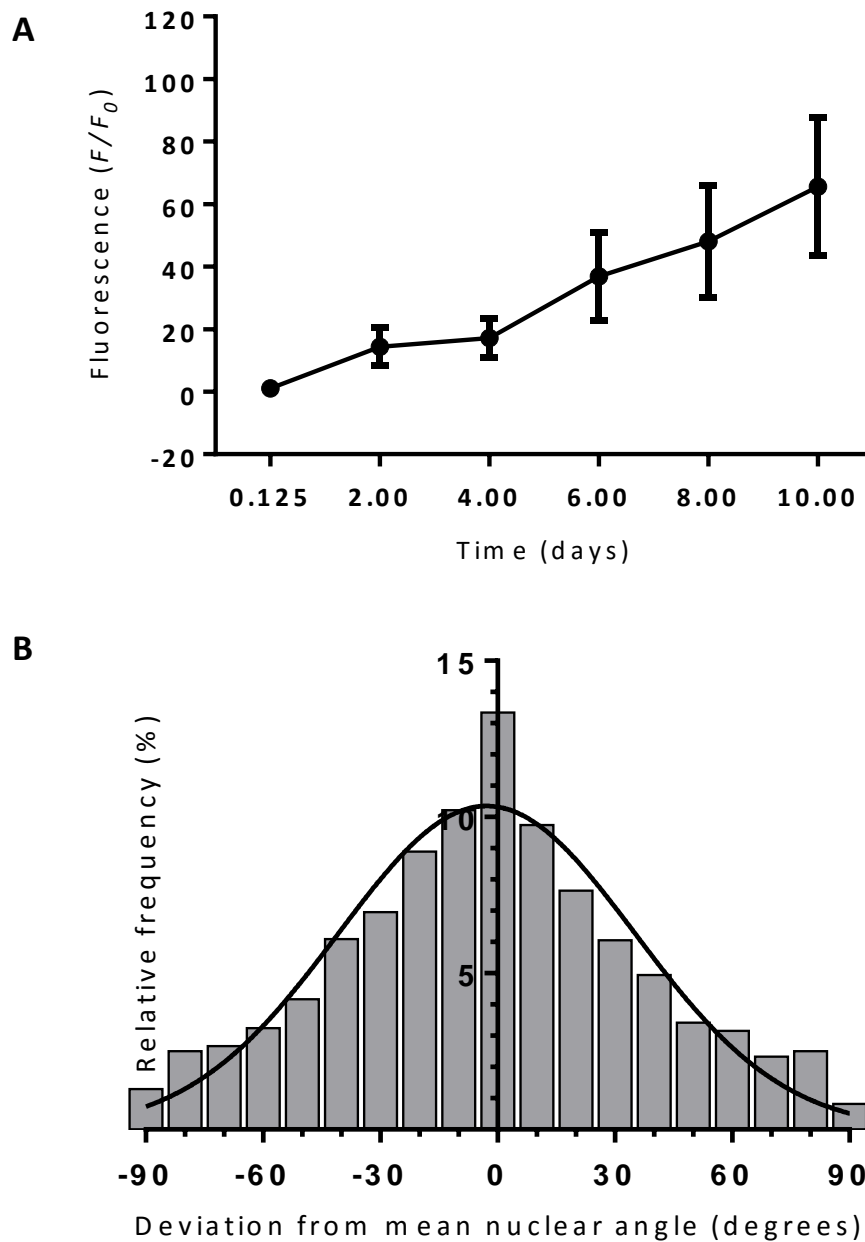
Figure 5.14: Culture of RASM cells on crosslinked GelMa scaffolds. RASM cells were cultured on crosslinked GelMa scaffold for 10 days, cell metabolism was monitored periodically using the PrestoBlue® assay (**A**); error bars represent the standard error of the mean (n=6). Samples were fixed after 10 days and cell nuclei stained. Image analysis of stained samples was carried out in order to determine the alignment of the cells (**B**).
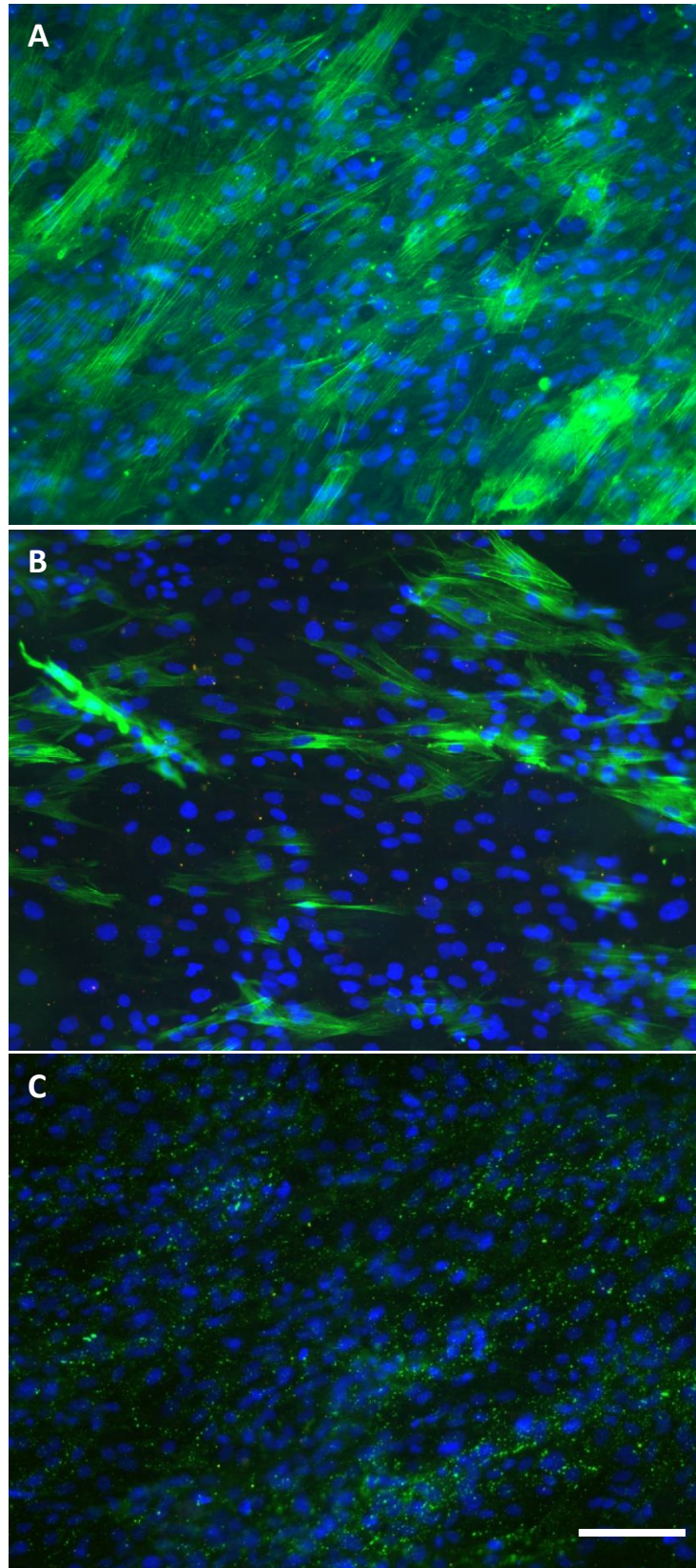
Figure 5.15: Immunostaining of RASM cells on electrospun GelMa scaffolds. RASM cells were fixed and stained with SM22α (**A**), calponin (**B**), and connexin (**C**) (all green). Cells were also stained for desmin (**C**) and vinculin (**B**) (both red). All samples were additionally stained with the nuclear stain Hoechst 33342 (blue). Scale bar = 100μm.
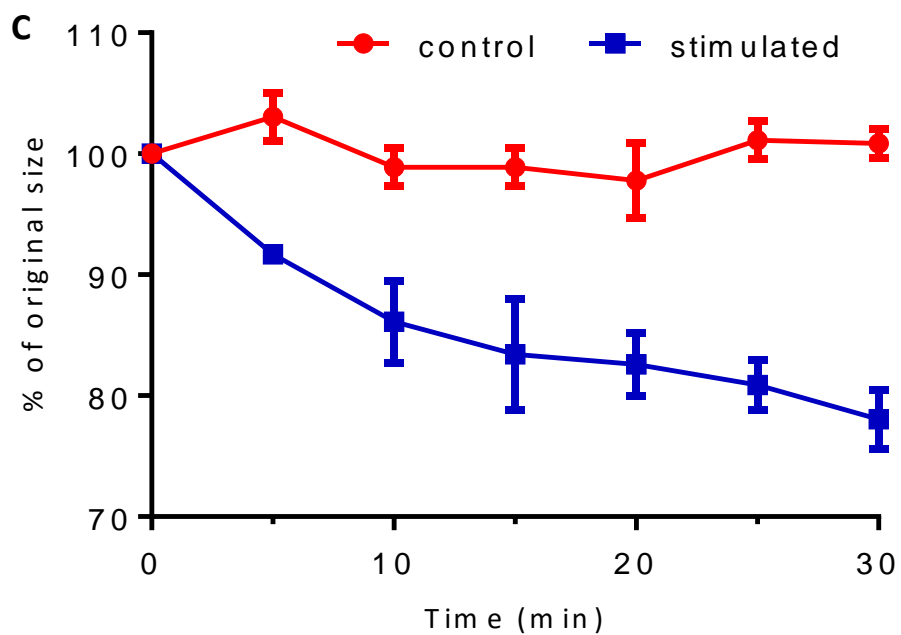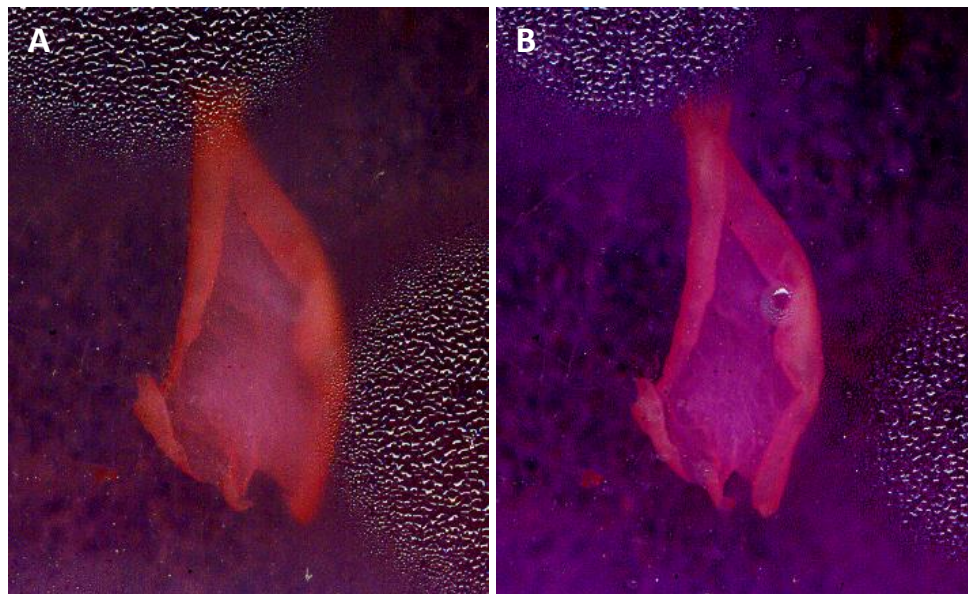
Figure 5.16: Contraction of RASM seeded GelMa scaffolds. Scanned images of a RASM seeded GelMa scaffold at T=0 (**A**) and T=30 minutes (**B**) following stimulation with UTP. Image analysis of the scaffolds at multiple time points was used to assess the level of scaffold contraction (**C**), error bars represent standard deviation (n=3).

images of a RASM seeded gelatin scaffold at times t=0 and t=30 minutes respectively, by comparing the surface area of the scaffold across this time period, RASM contraction can be measured (**Figure 5.16C**). Over the 30 minute period, scaffolds reduced to 78.0 ± 2.5% (mean ± standard deviation) of their original size (22% reduction in size), after 30 minutes no further contraction was observed. Unstimulated controls remained close to 100% their original size throughout the study. The level of scaffold contraction observed in this study was much closer to the level of contraction seen in collagen RASM constructs, the amount of contraction (reduction in size) was actually slightly higher than witnessed in the collagen hydrogels. Following these results, the direct force measurement of RASM seeded GelMa scaffold contraction was attempted using the same muscle physiology apparatus used to measure RASM collagen construct contraction described in chapter 3.

RASM cells were cultured upon rectangular crosslinked GelMa scaffolds for 10 days. Rectangular scaffolds were chosen to match the shape and dimensions of the previously developed collagen constructs. After the 10 day culture period, scaffolds were removed from their acetate frames and attached to the force transducer (**Figure 5.17A**); once attached the force was allowed to stabilise before recording started. The stable force reading was measured for 3 minutes before the constructs were stimulated with 100 µM UTP. Control studies were stimulated with serum free DMEM. An increase in force was detected within seconds of adding the agonist solution and continued to rise quickly for 20 minutes before slowing. Force continued to increase for a further 30 minutes before beginning to plateau (**Figure 5.17B**). The maximal force generated by the RASM constructs ranged from 755.22 µN to 1356.37 µN with the average max force being 1008.12 ± 251.59 µN (mean ± standard deviation). The majority of contraction occured within the first 5 minutes following stimulation with 42.46 ± 2.85% of the maximal force measured occurring within this time; 59.89 ± 3.65% measured 10 minutes following stimulation and 94.69 ± 1.55% after 40 minutes stimulation. As shown in **Figure 5.17C**, the contractile forces generated by the
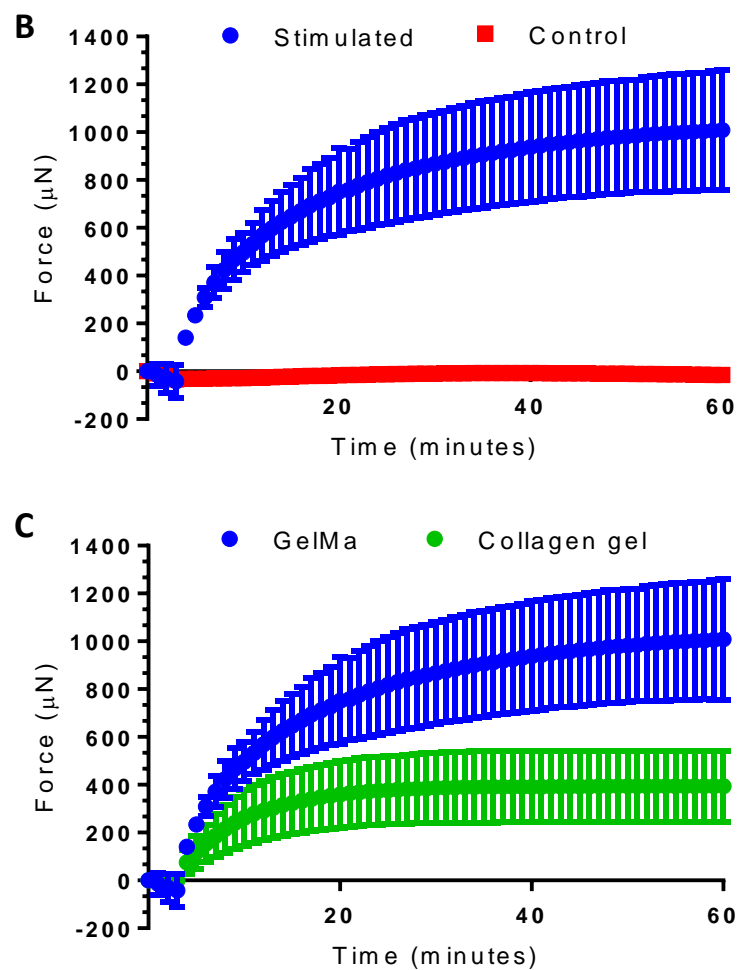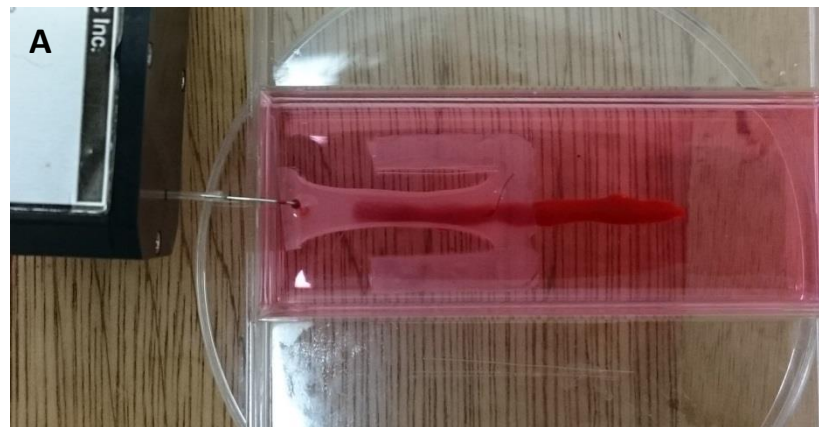
Figure 5.17: Direct force measurement of RASM contraction on electrospun GelMa scaffolds. Photograph of a RASM seeded GelMa scaffold contracting whilst attached to the force transducer. Force vs. time curves comparing the average contractile force of stimulated GelMa scaffolds against unstimulated controls (**B**) and RASM seeded collagen gels (**C**). Error bars represent standard deviation (n=4).

RASM cells on the GelMa scaffolds was over 2.5 times greater than those generated by RASM cells in the collagen constructs (1008 vs 394 µN at T= 60). Furthermore, the results generated when using the GelMa scaffolds were less variable than when using the collagen constructs. This is shown by representingthe standard deviation as a percentage of the mean max force (24.96% vs 37.47%; GelMa scaffolds vs collagen constructs).

5.5 Discussion

The mechanical properties of materials used to develop scaffolds for tissue engineering purposes have a great impact on the behaviour of the cells cultured upon/ within them. Given the wide range of polymers available when electrospinning, the potential fibrous scaffolds can possess Young's moduli ranging from a few hundred kPa (Kharaziha et al. 2013) to several hundred MPa (Hadjizadeh et al. 2011b). This wide range in stiffness will greatly impact on the attachment (Haugh et al. 2011), proliferation (Skotak et al. 2010), movement (Keogh et al. 2010) and even differentiation (Breuls et al. 2008; Park et al. 2012) of the cells. It is therefore important to choose a material with mechanical properties that match the mechanical properties that the cells experience *in vivo*. This will be a more effective way of producing tissue engineered constructs with functional outputs (such as contraction) that match the functionality of the *in vivo* tissue. Of course, other material properties such as surface chemistry, biodegradability and biocompatibility all need to be considered when choosing materials for tissue engineering applications. In this chapter of work, the contractile behaviour of RASM cells cultured upon electrospun scaffolds that greatly differ in their mechanical properties was explored. In addition, using the scaffold that best facilitated SM contraction, the physical force generated during agonist induced SM contraction was actively measured using muscle physiology apparatus.

In the previous chapter HASM cells were cultured upon electrospun PET scaffolds for up to 14 days and expressed markers of a contractile SM phenotype. When stimulated with bradykinin or histamine however no visible contraction was measured. Scaffolds did not change in size or shape indicating that either the cells were not contracting or that the scaffold fibres were too stiff for the SM cells to displace. Due to the presence of the same markers seen in the collagen gel model (which did contract), it was hypothesised that the scaffolds were restricting SM contraction given that the Young's modulus of *in vivo* SM is much

lower than the Young's moduli of the PET scaffolds (200-300 MPa). For example, the Young's moduli of human arteries and porcine bronchi range from 0.1 to 1.0 MPa and 0.35 to 1.35 MPa respectively (Riley et al. 1992; Wang, Patrick Mesquida, et al. 2011). These values are 100 to 1000 times smaller than the values obtained for the PET scaffolds. As a result, a much less stiff material was required to provide suitable mechanical properties that would facilitate SM contraction. The first material investigated was gelatin, which was chosen as it is possible to electrospin, is biocompatible, is chemically similar to collagen and inexpensive, in addition to its favourable mechanical properties.

5.5.1 Production of electrospun gelatin fibre scaffolds and their use as scaffolds for the culture of contractile SM cells

Gelatin fibre scaffolds were electrospun from gelatin solutions ranging from 6% to 10% *w/v* in concentration. Scaffold fibre diameter increased with gelatin concentration and ranged from 286 nm to 1.24 μm, a diameter range similar to previously published work when similar concentrations of gelatin in fluorinated alcohols were electrospun (Tsai et al. 2012; Skotak et al. 2010). When gelatin has been electrospun using aqueous solutions however, much greater concentrations (30-40% *w/v*) have been used to achieve similar sized fibres (Zhang et al. 2008; Panzavolta et al. 2011). This once again illustrates the effect that different electrospinning parameters (such as the solvent used) can have on the resultant fibres. Scaffold fibre alignment was high for all scaffolds.

Cross-linking of the gelatin scaffolds was attempted using both glutaraldehyde vapour and EDC and NHS although glutaraldehyde cross-linked scaffolds failed to produce reproducible results. This is possibly because the glutaraldehyde cross-links the scaffolds in the vapour phase. As the level of glutaraldehyde vapour in the chamber can be affected by environmental parameters such as temperature and humidity; that would mean that the level of cross-linking would not necessarily be the same for different batches. The EDC and NHS cross-linking method on the other hand, is carried out in a temperature controlled refrigerator in the liquid phase resulting in a more reliable method. Image analysis of the

scaffolds after cross-linking shows that the scaffolds appear slightly less uniform and that the degree of alignment had decreased slightly. This is due to several fibres merging together during cross-linking as cross-links formed between fibres, this also lead to a reduction in visible pores between fibres but the aligned fibrous topography of the scaffolds remained. Cross-linking also resulted in an increase in fibre diameter in all of the gelatin scaffolds; this has also been reported by Zhang *et al*. (Zhang et al. 2008) who crosslinked gelatin scaffolds with EDC and NHS at 25mM EDC. Fibre swelling has also been reported when cross-linking gelatin scaffolds with genipin (Panzavolta et al. 2011). The fibre swelling is thought to be due to the absorption of water. In this case, the cross-linked scaffolds appear to behave like a hydrogel, swelling in size with reduced stiffness, but retain their fibrous structure. Zhang *et al*. also found that when wet; the Young's modulus of crosslinked gelatin scaffolds dramatically decreases (Zhang et al. 2008). As the scaffolds produced in this study were to be used for cell culture, only the wet state Young's modulus was measured, this ranged from 3.80 to 1.54 MPa, values similar in magnitude to those measured by Zhang for similar sized fibre scaffolds.

RASM cells were seeded onto the 10% cross-linked gelatin scaffolds to assess cell attachment, proliferation and phenotype. Scaffolds spun from 10% *w/v* gelatin solutions were chosen for further experiments due to the high alignment that RASM cells displayed upon them. Cells achieved confluency quickest when seeded at a density of $2x10^5$ cells ml^{-1} and cultured for 9 days. Parallel PrestoBlue® tests showed a steady rise in metabolic activity over the same time period; indicating that cells were proliferating on the scaffolds. Immunostaining of fixed confluent scaffolds for SM markers SM22α and calponin showed that both proteins were present within the cells in addition to illustrating the aligned, spindle-shaped morphology of the cells. All of which are indicative of a contractile SM phenotype. In addition, the cells stained positive for the gap junction protein connexin, with gap junctions seen between cells. Focal adhesions were also seen on the scaffolds with cells staining positive for vinculin. Once again, cells stained negative for desmin.

RASM cells were grown to confluency on cross-linked 10% gelatin scaffold squares before contraction of the scaffolds was attempted. Scaffolds were stimulated with 100 µM UTP and imaged periodically to measure any visible scaffold contraction. Scaffolds reduced in size by an average of 9.5% over 20 minutes following stimulation in comparison to unstimulated controls. Although the level of contraction was only small compared to the previously established hydrogels, this showed an improvement on the level of contraction compared to PET scaffolds. By reducing the scaffold stiffness further, it may be possible to create RASM seeded electrospun aligned scaffold constructs that contract to a similar degree as the RASM seeded hydrogels.

5.5.2 Production of electrospun GelMa scaffolds and their use as scaffolds for the culture of contractile SM cells

Due to the multiple ways in which the mechanical properties of GelMa hydrogels can be manipulated, as discussed previously, GelMa was considered as an attractive material that could potentially produce electrospun scaffolds with Young's moduli lower than those seen in the electrospun gelatin scaffolds. GelMa was successfully synthesised following a previously published method (Van Den Bulcke et al. 2000; Nichol et al. 2010; Nikkhah et al. 2012). Following synthesis, the degree of methacrylation of the gelatin was calculated using the NMR spectra of the GelMa; methacrylation was calculated to be approximately 80%. This level of methacrylation matches previously published calculated values for the same gelatin: methacrylic anhydride ratio (Nichol et al. 2010; Hosseini et al. 2012; Nikkhah et al. 2012). Hence, 80% of the once free amino groups now possess the methacrylamide functional group and are available during UV cross-linking.

The synthesised GelMa was electrospun at a concentration of 10% *w/v* generating aligned fibres around 300 nm in diameter. When compared to gelatin fibres electrospun from the equivalent concentration (average diameter of 1.24 µm), the GelMa fibres were much thinner. This is most probably due to a change in the net charge during GelMa synthesis whereby consumption of the majority

of free amines by methacrylation (and no change to the number of free carboxylate groups) will lead to an increased negative charge at neutral pH due to deprotonated carboxylic acid groups (Zhou et al. 2014). This will affect the conductivity of the electrospinning solution, leading to the thinner fibres. As there is no published literature on electrospun GelMa scaffolds a cross-linking method had to be developed where the scaffolds retained their fibrous architecture whilst submerged in a photoinitiator solution. In order to work the photoinitiator needs to be in an aqueous solution. Previous studies have cross-linked GelMa hydrogels in PBS (Nichol et al. 2010; Nikkhah et al. 2012; Ovsianikov et al. 2011), but this was not possible with the electrospun scaffolds due to the high solubility of GelMa (the scaffolds dissolve instantly on contact with water). In order to overcome this issue, the EDC and NHS gelatin crosslinking method (Zhang et al. 2008) was adapted. This method uses a 9:1 ethanol: water mix, in this solution the scaffolds do not dissolve but are crosslinked. Therefore a selection of ethanol: water mixtures were investigated for use as the solvent for the photoinitiator solution. Any mixture with a water content higher than 10% (*v/v*) caused the scaffolds to dissolve and a water content less than 2.5% failed to sufficiently cross-link the scaffolds under UV light, leading to dissolution of the scaffolds upon washing with PBS. By changing the ethanol to water ratio it was possible to partially control the level of GelMa cross-linking and, as a result, the mechanical properties of the scaffolds. Young's moduli of the scaffolds ranged from 142 kPa (2.5% water) to 451 kPa (10% water); in addition the scaffolds became more opaque as the level of cross-linking increased. SEM images of cross-linked scaffolds suggested that during cross-linking, scaffolds appeared to lose their porous structure due to fibre swelling however, the aligned fibrous topography of the scaffolds was still visible.

RASM cells were cultured upon GelMa scaffolds cross-linked in a 5% water: ethanol solution. These scaffolds were chosen for further cell culture experiments due to their low Young's modulus and high cross-linking success rate when compared to the 10% and 2.5% (cross-linking solution water in ethanol ratio) respectively. As with the gelatin scaffolds, RASM cells attached to

and proliferated on the surface of the GelMa scaffolds over a 10 day period, cells aligned upon the scaffolds indicating that the surface topography of the scaffolds remained intact after cross-linking. However it is worth noting that the degree of nuclear alignment was lower on the GelMa scaffolds than on the PET scaffolds (23.42 vs 48.78% (10% *w/v* PET scaffolds, 7 days of culture) of cells within 10° of the mean), this correlates with the loss of alignment seen when cross-linking the electrospun gelatin scaffolds. RASM cells once again stained positive for SM22α, calponin and connexin. Unlike the gelatin scaffolds however, RASM cells on GelMa scaffolds showed no clear positive staining for vinculin, meaning no focal adhesion points could be identified. It has been previously documented that the level of vinculin bound to the cytoskeleton, and the amount of vinculin localizing at focal adhesions is larger on stiffer surfaces than on more elastic ones (Yamashita et al. 2014; Discher 2005). The difference in stiffness between the GelMa and gelatin scaffolds could be the reason why no vinculin localisation was seen on the GelMa scaffolds.

As previously attempted with the gelatin scaffolds, RASM cells were cultured upon square cross-linked electrospun GelMa scaffolds for 10 days prior to contraction studies. When stimulated to contract with 100 µM UTP, the RASM seeded GelMa scaffolds reduced in surface area by an average of 22% due to RASM contraction. This level of contraction is even greater than the gel length reduction of RASM collagen constructs seen in chapter 3. For this reason, and that this level of contraction was higher than that seen on gelatin and PET scaffolds, GelMa scaffolds were chosen to be used to measure the physical force exerted by SM cells during contraction.

5.5.3 Measuring the physical contractile force of SM cells cultured upon electrospun scaffolds

RASM cells were seeded upon cross-linked GelMa scaffolds and cultured for 10 days to achieve a confluent layer of cells. Scaffolds were rectangular in shape with dimensions matching the previously established collagen gel constructs. After the 10 days the scaffolds were attached to the muscle physiology

apparatus (isometric force transducer) that was used to measure the contractile force generated by the collagen constructs. Scaffolds were designed and attached to the transducer so that scaffold (and therefore cell) alignment was along the length of the rectangular scaffolds and parallel to the direction of force measurement. Scaffolds that were stimulated with 100 µM UTP contracted instantly and generated average maximal forces that were over 2.5 times greater than those achieved by collagen constructs. This could be due to several factors such as greater cell alignment and much more uniform distribution on the scaffolds than in the collagen gels. This will lead to more uniaxial force generated by the scaffolds. Also, collagen gels have been shown to restrict the proliferation of cells (Jones et al. 1997) compared to denatured collagen, arresting the cell cycle in G1 (Koyama et al. 1996). A study by Li *et al.* showed that vascular SM cells cultured in a 3D collagen matrix display an increased expression of p21 (Li et al. 2002), a cyclin-dependent kinase inhibitor known to inhibit SM proliferation (Chang et al. 1995; Tanner et al. 2000). Additionally, they also found that there were a significantly lower proportion of cells in the S phase and more in the G0/G1 phase in a 3D collagen matrix than a 2D one; suggestive of a lower proliferation rate in 2D. Therefore, whilst reaching confluency, the number of cells on the scaffolds could very well have increased to a number much greater than the number within the gels. This greater number of cells would logically produce a greater force. The actual change in cell number during the 10 day incubation will have to be assessed in future work. Although electrospun gelatin scaffolds have been used to produce contractile tissues such as cardiac (Kharaziha et al. 2013) and skeletal (Ostrovidov et al. 2014) muscle previously, this is the first time that SM contraction has been assessed using electrospun scaffolds. In addition, this is also the first time that the physical force of contraction from any cell type has been directly measured on electrospun scaffolds. With their greater cell alignment and distribution uniformity, force generation and reproducibility when compared to collagen gels, the electrospun GelMa scaffolds are a promising platform for direct measurement of contractile tissue engineered constructs.

5.5.4 Chapter Summary

Within this chapter of work, both gelatin and GelMa scaffolds were successfully electrospun and cross-linked using different cross-linking methods. The two materials produced scaffolds with different mechanical properties and including the PET scaffolds, Young's moduli of the scaffolds ranged from around 100 kPa to 300 MPa. The mechanical properties of the GelMa scaffolds can be manipulated by controlling the amount of water in the photoinitiator solution (which predominantly consisted of ethanol). SM cells readily attached to and proliferated upon both gelatin and GelMa scaffolds, expressing expected contractile SM markers in all cases. When cultured upon GelMa scaffolds however, no localised vinculin could be seen; a potential indicator of the scaffolds' low stiffness. SM cells were able to contract both gelatin and GelMa scaffolds with greater contraction seen on the less stiff GelMa scaffolds. The GelMa scaffolds were attached to force monitoring equipment and stimulated to contract with an agonist. Immediately following agonist stimulation scaffolds produced forces much greater than seen in collagen hydrogels. Limitations of the GelMa scaffolds are that they are fragile and require careful handling. Also, the method of attachment to the force transducer still requires the use of a minuten pin which adds variability into the setup, albeit less variability than when using collagen gels. This work represents the first time that GelMa has been electrospun and cross-linked using the methods described here. Additionally, the first time that the contractile forces generated by a confluent, aligned sheet of SM cells cultured upon an electrospun scaffold have been directly measured.

6. General Discussion

The experimental data collected and presented in this thesis illustrate the steps taken towards developing a tissue engineered *in vitro* model of contractile smooth muscle tissue using electrospun scaffolds. The role of the electrospun scaffolds is to provide a matrix with a surface topography that can support the growth of an aligned, confluent population of SM cells. In addition to this, the scaffolds provide a mechanical environment akin to what the cells experience *in vivo* (Wang, P Mesquida, et al. 2011). This allows the scaffolds to facilitate the functional output of the SM cells (contraction), producing a functional, contractile model of SM. By attaching the scaffolds to an appropriate force measurement apparatus, the physical force of this contraction can be measured. The ultimate goal of this work was to provide a tissue engineered alternative to traditional *ex vivo* models such as bronchial segments and TCLS during drug screening studies and when studying SM physiology and the pathophysiology of diseases such as asthma and atherosclerosis. The work described here has taken steps towards reaching that goal, resulting in a functional cell/ scaffold construct designed to be attached to traditional muscle physiology apparatus. With some refinement of the scaffold design and validation studies with primary human cells; further development of the model could easily take place.

SM plays a key role in the modulation of airway tone; in airway diseases such as asthma excessive contraction of the ASM tissue leads to increased airway resistance and shortness of breath. Models studying the role of ASM in these diseases generally involve the use of animals, be that *in vivo* (Zosky & Sly 2007) or *ex vivo* (Gunst & Mitzner 1981; Bergner & Sanderson 2002a). The use of animals in the study of human disease however raises several issues that a tissue engineered model would hope to solve. Firstly, although hypersensitivity (a key symptom of asthma) can be induced in many animal models (Johnson et al. 2004; Shinagawa & Kojima 2003), asthma is a disease that only affects humans.

Therefore, all animal models of asthma lack some elements of the disease (Holmes et al. 2011; Krug & Rabe 2008), raising questions over their accuracy. Similarly, due to genetic differences between species, drugs that produce positive effects in animal models may not necessarily be replicated in humans (Henig et al. 2000; Bryan et al. 2000). By using the approach developed in this thesis, human ASM cells could be cultured upon the electrospun scaffolds. Furthermore, by obtaining the cells from donors with asthma or COPD, the behaviour of the diseased ASM could be closely studied without the need for an induced disease phenotype. This would overcome the issue of different drug interactions between species and will also allow for studies into variation between human donors.

Another issue that a tissue engineered model would combat is the ethical concerns expressed towards animal models (Levy 2012). Although the majority of work done in this thesis used aortic SM cells from rats, the number of cells obtained from one donor (cultured through 3 passages) could provide enough cells for at least 20-30 individual scaffolds. This is working towards the 3R's guidelines (https://www.gov.uk/guidance/research-and-testing-using-animals) and EU regulation (REACH) (NC3Rs 2014), reducing the number of animals used in research. Furthermore, if the model is used with primary human cells as intended, the need for animal donors would be removed completely.

6.1   Key findings

Although there has been much work previously published where SM cells have been seeded onto/ into various materials for tissue engineering purposes (Baker et al. 2006; Nivison-Smith & Weiss 2012; De Filippo et al. 2003; Rayatpisheh et al. 2012; Schaner et al. 2004), few of these studies actually study the contractile force generated by the seeded SM cells (Grosberg et al. 2012; Nesmith et al. 2014; Alford et al. 2011; West et al. 2013). Very few have directly measured this force, and those that did were carried out in collagen hydrogels (Oishi et al. 2000) or required prior implantation *in vivo* (Lai et al. 2002; De Filippo et al. 2003). In this thesis, RASM cells were successfully isolated from sacrificed rats

and characterised *in vitro*, staining positive for expected contractile SM markers. When seeded into collagen hydrogels both RASM and human ASM cells were found to contract in response to chemical stimuli as previously reported (Matsumoto et al. 2007; Sakota et al. 2014). Using the design of an established C2C12 model (Sharples et al. 2012; Cheema et al. 2003), RASM constructs were developed and cultured for 3 days prior to contraction studies. During this time, the cells remodelled the collagen matrix and aligned parallel to the tension lines formed in the construct. Constructs were stimulated to contract whilst both free floating and attached to force measurement apparatus. During contraction studies using a force transducer, the forces generated by RASM construct contraction were measured and found to be agonist concentration dependant. Additionally, the contraction could be inhibited by L-type Ca^{2+} channel inhibition.

Electrospinning offers an attractive method to develop fibrous matrices for the culture of many different cell types (Nandakumar et al. 2013; Chew et al. 2008; Yan et al. 2012). By altering the many electrospinning parameters and the polymers used, the morphological and mechanical properties of these fibres can be tuned to match the properties of the desired tissue (Pham et al. 2006). Here, PET fibres were electrospun whilst varying the electrospinning parameters in order to produce multiple scaffolds varying in fibre diameter. PET was initially chosen due to its biocompatibility, its stability (not biodegradable; long shelf life) and its low cost. As previously reported, the key parameters controlling the fibre diameter were the polymer concentration and the flow rate (Hadjizadeh et al. 2011b; Veleirinho et al. 2007). Lowering the surface tension and increasing the conductivity of the PET solutions by adding an anionic surfactant reduced the amount of beading observed when spinning low concentrations of PET. Beading was also reduced by spinning through a narrower needle which increased solution velocity at the same flow rates. Altering the source of PET dramatically changed the morphology of the resultant fibres; this is highly likely due to differences in the purity and the polymer molecular weight (Kim et al. 2004; Gupta et al. 2005) in each source. By electrospinning nanofibres directly onto microfibre scaffolds it was possible to create a bi-phasic scaffold providing

different matrices for the co-culture of different cell types. Electrospinning onto a rapidly rotating mandrel made the production of highly aligned polymer fibres possible. Aligned PET scaffolds were used for the culture of HASM cells. Cells aligned along the direction of the fibres with greater alignment seen on thicker fibres. Cells proliferated on the surface of the scaffolds and formed a highly aligned, confluent layer of HASM after 14 days in culture.

When attempting to replicate the contraction studies carried out in collagen hydrogels on the PET scaffolds, no visual contraction was recorded. It was proposed that this was due to the stiffness' of the PET scaffolds which were much greater than SM would experience *in vivo*. As a result, gelatin and for the first time, GelMa, scaffolds were electrospun and cross-linked. The two materials produced scaffolds which were approximately 100 to 1000 times (respectively) less stiff than the PET scaffolds. The mechanical properties of the GelMa scaffolds were manipulated by controlling the water content of the photoinitiator solution. RASM cells attached to and proliferated upon gelatin and GelMa scaffolds, expressing characteristic contractile SM markers in all cases. Loss of localised vinculin, associated with less stiff extracellular environments (Yamashita et al. 2014; Discher 2005) was seen on GelMa scaffolds highlighting the difference in stiffness between the scaffolds. Contraction of RASM cells could be seen visually (change in scaffold shape/size) upon both of these scaffolds; more so on GelMa scaffolds than on gelatin scaffolds which were more stiff than the GelMa scaffolds..

Finally, the GelMa scaffolds were attached to force monitoring equipment and stimulated with a contractile agonist, representing the first time that SM contraction studies have been carried out with smooth muscle cells on electrospun scaffolds. Immediately following agonist stimulation, cell seeded scaffolds produced forces much greater than seen in collagen hydrogels demonstrating that electrospun GelMa scaffolds could be a more suitable scaffold to use for contraction studies than the previously developed hydrogel models due to their greater uniformity in alignment and their ability to proliferate upon the scaffolds (Jones et al. 1997; Koyama et al. 1996). This in

turn, provides a much more confluent, uniaxial population of cells than what is achieved in collagen gels, even with the addition of uniaxial tension.

6.2 Current limitations

Due to a limited supply of primary human cells, the development and optimisation of this model was carried out using SM cells from rats. Therefore, it is unknown how human cells will respond when cultured upon GelMa scaffolds and whether they would produce similar force readings in response to agonist stimulation. In chapters 3 and 5, collagen gels and GelMa scaffolds were attached to an isometric force transducer to measure the force of SM contraction. Although this proved to be successful and provided interesting results, all results were highly variable. This is thought to be due to the method of attachment which is quite rudimentary in nature, and a major source of variability. In order to increase the accuracy of experiments in future work, this experimental design will need to be addressed. It is worth mentioning though, that less variability was seen with cell seeded GelMa scaffolds; this was most probably due to the positioning of a thin strip of acetate at the end of each scaffold to prevent the pin tearing through the scaffold. As this strip was in a similar position each time, this meant that attachment of the scaffolds to the transducer was slightly more reproducible than when attaching gels. Also, the fragile nature of the GelMa scaffolds made them difficult to handle during cell culture and contraction studies; however, any attempt to strengthen the scaffolds would be of detriment to the scaffolds' mechanical properties.

Another important point is that this model uses only SM cells and is devoid of any diffusion barrier that would be present *in vivo*. Therefore, if this model is to be used to study the effects of drugs on airway or blood vessel physiology, it will need to be incorporated into a more complex model that (or need further development itself so that it) includes an epithelial/ endothelial layer to form this barrier. The presence of an epithelium can cause significantly different reactions to molecules and cross-communication between the tissues is of great importance when understanding disease mechanisms (Miyagi et al. 1996; White

et al. 1990; Gourgoulianis et al. 1998). This will therefore provide results that better represent drug response *in vivo*.

6.3 Future work

This model of SM can be used to assess the level of contractile forces generated in response to agonist stimulation. In order to validate the model further, there are several experiments that need to be carried out. Firstly, the sensitivity of the model should be tested by performing a dose-response experiment similar to those carried out on the collagen constructs. Ideally, these experiments could be carried out in a perfused chamber, removing the need for constant volume changes within the vessel. Also, it is unknown whether the scaffolds return to their original state following contraction as the cells relax; this could be investigated by adding cytochalasin D to the cells to disrupt the actin cytoskeleton, causing relaxation of the SM (Saito et al. 1996; Mortensen & Larsson 2003). This is an important question as it could enable long term or multiple contraction studies using the same scaffold.

An important step in developing the model further would be the transition from primary rat cells to those from human donors. By using SM cells from both diseased and normal human donors, the role of SM in different diseases could be investigated with comparisons made between donors. One example would be comparing the forces generated by asthmatic ASM cells with those from healthy donors, indicating whether excessive ASM contraction in asthma is due to ASM dysfunction or other facets of the disease such as airway remodelling. The complexity of the model could be increased by co-culture of SM cells with other cell types such as epithelial or fibroblast cells. This could be achieved using the biphasic scaffolds described in chapter 4, although potentially using gelatin or GelMa instead of PET. Another co-culture model to investigate would be SM cells co-cultured with immune cells such as mast cells, which are thought to embed themselves in the ASM bundle in asthma sufferers (Brightling et al. 2002; Woodman et al. 2008). By co-culturing ASM cells and mast cells from both

asthmatic and non-asthmatic donors, the interaction between ASM and mast cells could be investigated further.

6.4 Final conclusions

A key product of the work represented in this thesis is a contractile model of SM tissue that can be used to physically measure the forces generated by the SM cells during contraction. Using aligned electrospun scaffolds, an aligned population of cells is produced as the cells use the topographical cues provided by the fibrous scaffold. By using aligned electrospun scaffolds, cells are morphologically similar to their *in vivo* state and contract uniaxially. The presence of gap junctions between the cells also suggests they are behaving as a syncytium. Hopefully, this model can go some way to help shift the focus of pre-clinical studies from animals to tissue engineered alternatives and aid in the development of new drugs for diseases such as asthma and atherosclerosis. The benefits of this model over existing models are that; the contractile force can be directly measured, no extra load (other than the scaffold) is applied to the system, and it can be used for the study of single cell types and multiple cell types (with some modification such as the use of a biphasic scaffold). Finally, the successful use of GelMa as a material for electrospinning opens up avenues for the future study of other soft or contractile tissues such as cardiac and skeletal muscle in addition to further studies investigating SM biology.

7. Appendix 1: List of Publications

Bridge, J. C.; Morris, G. E.; Aylott, J. W.; et al. 2015, Developing an in vitro Model to Measure Smooth Muscle Contraction. 4th TERMIS World Congress, Boston, MA. SEP 08-11, 2015. *Tissue Engineering Part A,* 21(1), pp S253-S253

Morris, G. E.; Bridge, J. C.; Brace, L.; et al. 2015. Developing Electropsun Scaffolds to Influence Mammalian Cell Phenotype; Building an In Vitro Model of the Human Bronchial Airway. 4th TERMIS World Congress, Boston, MA. SEP 08-11, 2015. *Tissue Engineering Part A,* 21(1), pp S252-S252

Bridge, J. C., Aylott, J. W., Brightling, C. E., Ghaemmaghami, A. M., Knox, A. J., Lewis, M. P., et al. 2015. Adapting the Electrospinning Process to Provide Three Unique Environments for a Tri-layered In Vitro Model of the Airway Wall. *J. Vis. Exp.* (101), e52986, doi:10.3791/52986

Morris, G. et al., 2014. Human airway smooth muscle maintain in situ cell orientation and phenotype when cultured on aligned electrospun scaffolds. *American Journal of Physiology - Lung Cellular and Molecular Physiology*, 307(1), pp.L38–L47. http://ajplung.physiology.org/content/307/1/L38.abstract.

Morris, G.E. et al., 2014. A novel electrospun biphasic scaffold provides optimal three-dimensional topography for in vitro co-culture of airway epithelial and fibroblast cells. *Biofabrication*, 6(3), p.035014. Available at: http://www.ncbi.nlm.nih.gov/pubmed/24925127

8. References

Achilli, M. & Mantovani, D., 2010. Tailoring mechanical properties of collagen-based scaffolds for vascular tissue engineering: The effects of pH, temperature and ionic strength on gelation. *Polymers*, 2(4), pp.664–680.

Aguilar, H.N. & Mitchell, B.F., 2010. Physiological pathways and molecular mechanisms regulating uterine contractility. *Human reproduction update*, 16(6), pp.725–44. Available at: http://www.ncbi.nlm.nih.gov/pubmed/20551073.

Ahn, H.Y., Karaki, H. & Urakawa, N., 1988. Inhibitory effects of caffeine on contractions and calcium movement in vascular and intestinal smooth muscle. *British journal of pharmacology*, 93(2), pp.267–74. Available at: http://www.pubmedcentral.nih.gov/articlerender.fcgi?artid=1853798&tool=pmcentrez&rendertype=abstract.

Ahvaz, H.H. et al., 2012. Effective combination of hydrostatic pressure and aligned nanofibrous scaffolds on human bladder smooth muscle cells: implication for bladder tissue engineering. *Journal of materials science. Materials in medicine*, 23(9), pp.2281–90. Available at: http://www.ncbi.nlm.nih.gov/pubmed/22673873 [Accessed November 1, 2013].

Alberts, B., Johnson, A. & Lewis, J., 2002. Cell Junctions. In *Molecular Biology of the Cell. 4th edition.* New York: Garland Science.

Alford, P.W. et al., 2010. Biohybrid thin films for measuring contractility in engineered cardiovascular muscle. *Biomaterials*, 31(13), pp.3613–3621. Available at: http://www.ncbi.nlm.nih.gov/pubmed/20149449 [Accessed May 23, 2013].

Alford, P.W. et al., 2011. Vascular smooth muscle contractility depends on cell shape. *Integrative biology : quantitative biosciences from nano to macro*, 3(11), pp.1063–70. Available at: http://www.ncbi.nlm.nih.gov/pubmed/21993765 [Accessed February 24, 2014].

Antoine, E.E., Vlachos, P.P. & Rylander, M.N., 2014. Review of collagen I hydrogels for bioengineered tissue microenvironments: characterization of mechanics, structure, and transport. *Tissue engineering. Part B, Reviews*, 20(6), pp.683–696.

Arner, A. & Pfitzer, G., 2005. Regulation of cross-bridge cycling by Ca2+ in smooth muscle. In *Reviews of Physiology, Biochemistry and Pharmacology*. Springer, pp. 63–146.

Awad, H. a. et al., 2000. In vitro characterization of mesenchymal stem cell-seeded collagen scaffolds for tendon repair: Effects of initial seeding density on contraction kinetics. *Journal of Biomedical Materials Research*, 51(2), pp.233–240.

Babij, P. & Periasamy, M., 1989. Myosin heavy chain isoform diversity in smooth muscle is produced by differential {RNA} processing. *Journal of Molecular Biology*, 210(3), pp.673–679. Available at: http://www.sciencedirect.com/science/article/pii/0022283689901423.

Baker, S.C. et al., 2006. Characterisation of electrospun polystyrene scaffolds for three-dimensional in vitro biological studies. *Biomaterials*, 27(16), pp.3136–3146.

Bancroft, J. & Gamble, M., 2001. *Theory and Practice of Histological Techniques* 5th ed., Churchill Livingstone.

Bashur, C.A., Dahlgren, L.A. & Goldstein, A.S., 2006. Effect of fiber diameter and orientation on fibroblast morphology and proliferation on electrospun poly(D,L-lactic-co-glycolic acid) meshes. *BIOMATERIALS*, 27(33), pp.5681–5688.

Bates, J.H.T. & Irvin, C.G., 2003. Measuring lung function in mice: the phenotyping uncertainty principle. *Journal of applied physiology (Bethesda, Md. : 1985)*, 94(4), pp.1297–306. Available at: http://www.ncbi.nlm.nih.gov/pubmed/12626466 [Accessed July 18, 2013].

Baumgarten, P., 1971. Electrostatic spinning of acrylic microfibres. *Journal of Colloid and Interface science*, 36(1), p.71–&.

Berglund, J.D. et al., 2003. A biological hybrid model for collagen-based tissue engineered vascular constructs. *Biomaterials*, 24(7), pp.1241–1254.

Bergner, A. & Sanderson, M.J., 2002a. Acetylcholine-induced Calcium Signaling and Contraction of Airway Smooth Muscle Cells in Lung Slices. *J. Gen. Physiol. %R 10.1085/jgp.119.2.187*, 119(2), pp.187–198.

Bergner, A. & Sanderson, M.J., 2002b. ATP stimulates Ca2+ oscillations and contraction in airway smooth muscle cells of mouse lung slices. *American journal of physiology. Lung cellular and molecular physiology*, 283(6), pp.L1271–9. Available at: http://www.ncbi.nlm.nih.gov/pubmed/12388370.

Bertassoni, L.E. et al., 2014. Direct-write bioprinting of cell-laden methacrylated gelatin hydrogels. *Biofabrication*, 6(2), p.024105. Available at: http://www.ncbi.nlm.nih.gov/pubmed/24695367.

Bettinelli, D. et al., 2002. Effect of gravity and posture on lung mechanics. *Journal of applied physiology (Bethesda, Md. : 1985)*, 93(6), pp.2044–2052.

Bhat, R. & Karim, A.A., 2009. Ultraviolet irradiation improves gel strength of fish gelatin. *Food Chemistry*, 113(4), pp.1160–1164. Available at: http://www.sciencedirect.com/science/article/pii/S0308814608010042.

Bigi, A. et al., 2002. Stabilization of gelatin films by crosslinking with genipin. *Biomaterials*, 23(24), pp.4827–4832. Available at: http://www.sciencedirect.com/science/article/pii/S0142961202002351.

Bion, A. et al., 2002. Biphasic culture of rat lung slices for pharmacotoxicological evaluation of complex atmospheres. *Cell biology and toxicology*, 18(5), pp.301–314.

Bock, N. et al., 2011. Electrospraying, a reproducible method for production of polymeric microspheres for biomedical applications. *Polymers*, 3(1), pp.131–149.

Borkowski, J. a. et al., 1995. Targeted Disruption of a B2 Bradykinin Receptor Gene in Mice Eliminates Bradykinin Action in Smooth Muscle and Neurons. *Journal of Biological Chemistry*, 270(23), pp.13706–13710. Available at: http://www.jbc.org/content/270/23/13706.abstract?ijkey=222d59ab2b506 05a233c532519954e3d6aa08008&keytype2=tf_ipsecsha.

Bosnakovski, D. et al., 2005. Chondrogenic Differentiation of Bovine Bone Marrow Mesenchymal Stem Cells (MSCs) in Different Hydrogels: Influence of Collagen Type II Extracellular Matrix on MSC Chondrogenesis. *Biotechnology and bioengineering*, 93(6), pp.1152–1163.

Boudou, T. et al., 2012. A Microfabricated Platform to Measure and Manipulate the Mechanics of Engineered Cardiac Microtissues. *Tissue Engineering Part A*, 18(9-10), pp.910–919.

Brady, M.A., Lewis, M.P. & Mudera, V., 2008. Synergy between myogenic and non-myogenic cells in a 3D tissue-engineered craniofacial skeletal muscle construct. *Journal of tissue engineering and regenerative medicine*, 2, pp.408–417.

Breuls, R.G.M., Jiya, T.U. & Smit, T.H., 2008. Scaffold Stiffness Influences Cell Behavior: Opportunities for Skeletal Tissue Engineering. *The open orthopaedics journal*, 2(21), pp.103–109. Available at: http://www.pubmedcentral.nih.gov/articlerender.fcgi?artid=2687114&tool =pmcentrez&rendertype=abstract.

Brightling, C.E. et al., 2002. Mast-cell infiltration of airway smooth muscle in asthma. *The New England journal of medicine*, 346(22), pp.1699–1705.

Brinkman, W.T. et al., 2003. Photo-cross-linking of type I collagen gels in the presence of smooth muscle cells: mechanical properties, cell viability, and function. *Biomacromolecules*, 4(4), pp.890–895.

Brown, T.D., Dalton, P.D. & Hutmacher, D.W., 2011. Direct writing by way of melt electrospinning. *Advanced materials Deerfield Beach Fla*, 23(47), pp.5651–7. Available at: http://www.ncbi.nlm.nih.gov/pubmed/22095922 [Accessed May 28, 2013].

Bryan, S.A. et al., 2000. Effects of recombinant human interleukin-12 on eosinophils, airway hyper-responsiveness, and the late asthmatic response. *The Lancet*, 356(9248), pp.2149–2153. Available at: http://www.sciencedirect.com/science/article/pii/S0140673600034978.

Buchko, C.J. et al., 1999. Processing and microstructural characterization of porous biocompatible protein polymer thin films. *POLYMER*, 40(26), pp.7397–7407.

Van Den Bulcke, A.I. et al., 2000. Structural and Rheological Properties of Methacrylamide Modified Gelatin Hydrogels. *Biomacromolecules*, 1(1), pp.31–38. Available at: http://pubs.acs.org/doi/abs/10.1021/bm990017d.

Bye, F.J. et al., 2013. Development of bilayer and trilayer nanofibrous/microfibrous scaffolds for regenerative medicine. *Biomaterials Science*, 1(9), p.942. Available at: http://xlink.rsc.org/?DOI=c3bm60074b [Accessed October 17, 2014].

Casper, C.L. et al., 2004. Controlling surface morphology of electrospun polystyrene fibers: Effect of humidity and molecular weight in the electrospinning process. *Macromolecules*, 37(2), pp.573–578.

Castellano, J., Nasarre, L. & Badimon, L., 2015. Differential Effect of Hypoxia in Human and Mouse Vascular Smooth Muscle Cell Migration through LRP1-pPyk2-MMP-9 Axis. , 2015, pp.1–10.

Ceresa, C.C., Knox, A.J. & Johnson, S.R., 2009. Use of a three-dimensional cell culture model to study airway smooth muscle- mast cell interactions in airway remodeling. , (6), pp.1059–1066.

Chang, M.W. et al., 1995. Adenovirus-mediated over-expression of the cyclin/cyclin-dependent kinase inhibitor, p21 inhibits vascular smooth muscle cell proliferation and neointima formation in the rat carotid artery model of balloon angioplasty. *The Journal of clinical investigation*, 96(5), pp.2260–8. Available at:

http://www.pubmedcentral.nih.gov/articlerender.fcgi?artid=185876&tool=
pmcentrez&rendertype=abstract.

Chaurey, V. et al., 2012. Nanofiber size-dependent sensitivity of fibroblast
directionality to the methodology for scaffold alignment. *Acta biomaterialia*,
8(11), pp.3982–90. Available at:
http://www.ncbi.nlm.nih.gov/pubmed/22789616 [Accessed May 30, 2013].

Cheema, U. et al., 2003. 3-D in vitro model of early skeletal muscle development.
Cell motility and the cytoskeleton, 54(3), pp.226–236.

Chew, S.Y. et al., 2008. The effect of the alignment of electrospun fibrous
scaffolds on Schwann cell maturation. *Biomaterials*, 29(6), pp.653–661.

Chiu, L.L.Y., Janic, K. & Radisic, M., 2012. Engineering of oriented myocardium on
threedimensional micropatterned collagen-chitosan hydrogel. *International
Journal of Artificial Organs*, 35(4), pp.237–250.

Choe, M.M., Sporn, P.H.S. & Swartz, M. a, 2006. Extracellular matrix remodeling
by dynamic strain in a three-dimensional tissue-engineered human airway
wall model. *American journal of respiratory cell and molecular biology*,
35(3), pp.306–13. Available at:
http://www.pubmedcentral.nih.gov/articlerender.fcgi?artid=2643283&tool
=pmcentrez&rendertype=abstract [Accessed July 21, 2013].

Churg, A. et al., 2009. The role of interleukin-1beta in murine cigarette smoke-
induced emphysema and small airway remodeling. *American journal of
respiratory cell and molecular biology*, 40(4), pp.482–490.

Cirillo, M. et al., 1993. Regulation of Ca2+ transport by platelet-derived growth
factor-BB in rat vascular smooth-muscle cells. *Circulation Research*, 72(4),
pp.847–856.

Clark, R. a et al., 1977. Transbronchial lung biopsy: A review of 85 cases. *Thorax*,
32(5), pp.546–549.

Cooke, P.H. & Chase, R.H., 1971. Potassium chloride-insoluble myofilaments in
vertebrate smooth muscle cells. *Experimental cell research*, 66(2), pp.417–
425.

Dalton, P.D. et al., 2008. Patterned melt electrospun substrates for tissue
engineering. *Biomedical Materials*, 3(3), p.34109. Available at:
http://stacks.iop.org/1748-605X/3/i=3/a=034109.

Dandurand, R.J. et al., 1993. Responsiveness of individual airways to
methacholine in adult rat lung explants. *Journal of Applied Physiology*, 75(1),
pp.364–372. Available at:
http://jap.physiology.org/content/75/1/364.abstract.

Davis, M.J., Donovitz, J.A. & Hood, J.D., 1992. Stretch-activated single-channel and whole cell currents in vascular smooth muscle cells. *American Journal of Physiology - Cell Physiology*, 262(4), pp.C1083–C1088. Available at: http://ajpcell.physiology.org/content/262/4/C1083.abstract.

Deitzel, J.. et al., 2001. The effect of processing variables on the morphology of electrospun nanofibers and textiles. *Polymer*, 42(1), pp.261–272. Available at: http://linkinghub.elsevier.com/retrieve/pii/S0032386100002500.

Delmotte, P. & Sanderson, M.J., 2008. Effects of albuterol isomers on the contraction and Ca2+ signaling of small airways in mouse lung slices. *American journal of respiratory cell and molecular biology*, 38(5), pp.524–31. Available at: http://www.pubmedcentral.nih.gov/articlerender.fcgi?artid=2335335&tool=pmcentrez&rendertype=abstract.

DeLustro, F. et al., 1986. A comparative study of the biologic and immunologic response to medical devices derived from dermal collagen. *Journal of biomedical materials research*, 20(1), pp.109–120.

Dennis, R.G. & Kosnik, P.E., 2000. Excitability and isometric contractile properties of mammalian skeletal muscle constructs engineered in vitro. *In vitro cellular & developmental biology. Animal*, 36(5), pp.327–335.

Discher, D.E., 2005. Tissue Cells Feel and Respond to the Stiffness of Their Substrate. *Science*, 310(5751), pp.1139–1143. Available at: http://www.sciencemag.org/cgi/doi/10.1126/science.1116995.

Draeger, A. et al., 1990. The cytoskeletal and contractile apparatus of smooth muscle: contraction bands and segmentation of the contractile elements. *The Journal of cell biology*, 111(6 Pt 1), pp.2463–2473.

Drenckhahn, D. et al., 1988. Identification and subcellular location of talin in various cell types and tissues by means of [125I]vinculin overlay, immunoblotting and immunocytochemistry. *European journal of cell biology*, 46(3), p.513—522. Available at: http://europepmc.org/abstract/MED/3141185.

Duan, B. et al., 2004. Electrospinning of chitosan solutions in acetic acid with poly(ethylene oxide). *Journal of Biomaterials Science, Polymer Edition*, 15(6), pp.797–811.

Duan, Y. et al., 2011. Hybrid gel composed of native heart matrix and collagen induces cardiac differentiation of human embryonic stem cells without supplemental growth factors. *Journal of Cardiovascular Translational Research*, 4(5), pp.605–615.

Eastwood, M. et al., 1998. Effect of precise mechanical loading on fibroblast populated collagen lattices: Morphological changes. *Cell Motility and the Cytoskeleton*, 40(1), pp.13–21.

Eastwood, M. et al., 1996. Quantitative analysis of collagen gel contractile forces generated by dermal fibroblasts and the relationship to cell morphology. *Journal of cellular physiology*, 166(1), pp.33–42.

Eastwood, M., McGrouther, D. & Brown, R., 1994. A culture force monitor for measurement of contraction forces generated in human dermal fibroblast cultures: evidence for cell-matrix mechanical signalling. *Biochimica et Biophysica Acta (BBA) - General Subjects*, 1201(2), pp.186–192. Available at: http://www.sciencedirect.com/science/article/pii/030441659490040X [Accessed June 29, 2014].

Egelman, E.H., Francis, N. & DeRosier, D.J., 1982. F-actin is a helix with a random variable twist. *Nature*, 298(5870), pp.131–135.

Eidelman, D.H., Bellofiore, S. & Martin, J.G., 1988. Late Airway Responses to Antigen Challenge in Sensitized Inbred Rats. *American Review of Respiratory Disease*, 137(5), pp.1033–1037. Available at: http://dx.doi.org/10.1164/ajrccm/137.5.1033.

Elias, J., Lee, C. & Zheng, T., 2003. New insights into the pathogenesis of asthma. *Journal of Clinical …*, 111(3), pp.291–297. Available at: http://www.jci.org/cgi/content/full/111/3/291.

Elsayed, Y. et al., 2015. Smooth muscle tissue engineering in crosslinked electrospun gelatin scaffolds. *Journal of biomedical materials research. Part A*.

Fall, M. et al., 2008. Toxicological study of emissions resulting from a diesel and a gazoline engine using an organotypic culture of lung slice. *Dakar medical*, 53(1), pp.52–60.

Fattouh, R. et al., 2005. House dust mite facilitates ovalbumin-specific allergic sensitization and airway inflammation. *American journal of respiratory and critical care medicine*, 172(3), pp.314–21. Available at: http://www.ncbi.nlm.nih.gov/pubmed/15879422.

Fay, F.S. et al., 1983. Distribution of alpha-actinin in single isolated smooth muscle cells. *The Journal of cell biology*, 96(7), pp.783–795.

De Filippo, R.E., Yoo, J.J. & Atala, A., 2003. Engineering of vaginal tissue in vivo. *Tissue Engineering*, 9(2), pp.301–306. Available at: http://www.ncbi.nlm.nih.gov/pubmed/12740092.

Fish, S.C. et al., 2005. IgE Generation and Mast Cell Effector Function in Mice Deficient in IL-4 and IL-13. *The Journal of Immunology*, 174(12), pp.7716–7724. Available at: http://www.jimmunol.org/cgi/content/abstract/174/12/7716.

Fitzpatrick, M., Donovan, C. & Bourke, J.E., 2013. Prostaglandin E2 elicits greater bronchodilation than salbutamol in mouse intrapulmonary airways in lung slices. *Pulmonary Pharmacology and Therapeutics*, 28(1), pp.1–9. Available at: http://www.ncbi.nlm.nih.gov/pubmed/24291048.

Formhals, A., 1939. Method and apparatus for spinning; US Patent 2160962.

Formhals, A., 1934. Process and apparatus for preparing artificial threads; US Patent 1975504.

Foster, P.S. et al., 1996. Interleukin 5 deficiency abolishes eosinophilia, airways hyperreactivity, and lung damage in a mouse asthma model. *The Journal of experimental medicine*, 183(1), pp.195–201.

Fujimoto, T., 1991. Calcium pump of the plasma membrane is localized in Caleolae. *The Journal of Cell Biology*, 120(5), pp.129–153.

Gabbiani, G. et al., 1981. Vascular smooth muscle cells differ from other smooth muscle cells: predominance of vimentin filaments and a specific alpha-type actin. *Proceedings of the National Academy of Sciences of the United States of America*, 78(1), pp.298–302.

Gabella, G., 1981. Structure of Smooth Muscle. In *Smooth Muscle: An Assessment of Current Knowledge*. London: Arnold, pp. 1–46.

Garg, K. & Bowlin, G.L., 2011. Electrospinning jets and nanofibrous structures. *Biomicrofluidics*, 5(1), pp.1–19.

Gauvin, R. et al., 2012. Microfabrication of complex porous tissue engineering scaffolds using 3D projection stereolithography. *Biomaterials*, 33(15), pp.3824–3834.

Geisler, N. & Weber, K., 1983. Amino acid sequence data on glial fibrillary acidic protein (GFA); implications for the subdivision of intermediate filaments into epithelial and non-epithelial members. *The EMBO journal*, 2(11), pp.2059–63. Available at: http://www.pubmedcentral.nih.gov/articlerender.fcgi?artid=555409&tool=pmcentrez&rendertype=abstract.

Gerthoffer, W.T., Elorza, M. & Singer, C., 2007. Contraction of Immortalized human airway smooth muscle cells in 3D collagen rings. In *Biomedical Engineering Society conference*. Los Angeles, CA.

Giembycz, M.A. & Raeburn, D., 1992. Current concepts on mechanisms of force generation and maintenance in airways smooth muscle. *Pulmonary pharmacology*, 5(4), pp.279–297.

Gilmont, R.R. et al., 2013. Bioengineering of physiologically functional intrinsically innervated human Internal Anal Sphincter constructs. *Tissue engineering. Part A*, 20, pp.1–28. Available at: http://www.ncbi.nlm.nih.gov/pubmed/24328537.

GINA, 2006. Global Strategy for Asthma Management and Prevention. Global Initiative for Asthma (GOLD). Available at: www.ginasthma.org.

Ginis, I. et al., 2004. Differences between human and mouse embryonic stem cells. *Developmental Biology*, 269(2), pp.360–380.

Gnavi, S. et al., 2015. The Effect of Electrospun Gelatin Fibers Alignment on Schwann Cell and Axon Behavior and Organization in the Perspective of Artificial Nerve Design. *International Journal of Molecular Sciences*, 16(6), pp.12925–12942. Available at: http://www.mdpi.com/1422-0067/16/6/12925/.

Gnavi, S. et al., 2014. The influence of electrospun fibre diameter on Schwann cell behavior and axonal outgrowth. *Journal of tissue engineering and regenerative medicine*, 8(1, SI), p.327.

Gollasch, M. et al., 1998. L-type calcium channel expression depends on the differentiated state of vascular smooth muscle cells. *The FASEB journal : official publication of the Federation of American Societies for Experimental Biology*, 12(7), pp.593–601.

Górecka, A., Aksoy, M.O. & Hartshorne, D.J., 1976. The effect of phosphorylation of gizzard myosin on actin activation. *Biochemical and Biophysical Research Communications*, 71(1), pp.325–331. Available at: http://www.sciencedirect.com/science/article/pii/0006291X76902862.

Gorgieva, S. & Kokol, V., 2011. Collagen- vs Gelatine-Based Biomaterials and Their Biocompatibility : Review and Perspectives. In R. Pignatello, ed. *Biomaterials Applications for Nanomedicine*. InTech.

Gourgoulianis, K. et al., 1998. Epithelium-dependent regulation of airways smooth muscle function. A histamine-nitric oxide pathway. *Mediators of inflammation*, 7(6), pp.409–11. Available at: http://www.pubmedcentral.nih.gov/articlerender.fcgi?artid=1781871&tool=pmcentrez&rendertype=abstract.

Grosberg, A. et al., 2012. Muscle on a chip: In vitro contractility assays for smooth and striated muscle. *Journal of Pharmacological and Toxicological*

Methods, 65(3), pp.1–10. Available at:
http://www.ncbi.nlm.nih.gov/pubmed/22521339 [Accessed May 30, 2013].

Gunst, S.J. & Mitzner, W., 1981. Mechanical properties of contracted canine bronchial segments in vitro. *Journal of applied physiology: respiratory, environmental and exercise physiology*, 50(6), p.1236—1247. Available at: http://europepmc.org/abstract/MED/7263384.

Gunst, S.J. & Zhang, W., 2008. Actin cytoskeletal dynamics in smooth muscle: a new paradigm for the regulation of smooth muscle contraction. *American journal of physiology. Cell physiology*, 295(3), pp.C576–87.

Guo, S.S. et al., 2011. Manufacture of Composite Nanofiber Mats with Fiber Diameters Grads by Electrospinning for Filtration Use. *Advanced Materials Research*, 331, pp.206–209. Available at: http://www.scientific.net/AMR.331.206 [Accessed May 30, 2013].

Gupta, P. et al., 2005. Electrospinning of linear homopolymers of poly(methyl methacrylate): exploring relationships between fiber formation, viscosity, molecular weight and concentration in a good solvent. *Polymer*, 46(13), pp.4799–4810. Available at: http://www.sciencedirect.com/science/article/pii/S0032386105004167.

Hadač, J., Slobodian, P. & Sáha, P., 2007. Volume relaxation in amorphous and semicrystalline PET. *Journal of Materials Science*, 42(11), pp.3724–3731. Available at: http://dx.doi.org/10.1007/s10853-006-0378-z.

Hadjizadeh, A., Ajji, A. & Bureau, M.N., 2011a. Nano/micro electro-spun polyethylene terephthalate fibrous mat preparation and characterization. *Journal of the mechanical behavior of biomedical materials*, 4(3), pp.340–51. Available at: http://www.ncbi.nlm.nih.gov/pubmed/21316622 [Accessed November 1, 2013].

Hadjizadeh, A., Ajji, A. & Bureau, M.N., 2011b. Nano/micro electro-spun polyethylene terephthalate fibrous mat preparation and characterization. *Journal of the mechanical behavior of biomedical materials*, 4(3), pp.340–51. Available at: http://www.ncbi.nlm.nih.gov/pubmed/21316622 [Accessed May 30, 2013].

Hakkinen, K.M. et al., 2011. Direct comparisons of the morphology, migration, cell adhesions, and actin cytoskeleton of fibroblasts in four different three-dimensional extracellular matrices. *Tissue engineering. Part A*, 17(5-6), pp.713–724.

Hamelmann, E. et al., 1997. Noninvasive measurement of airway responsiveness in allergic mice using barometric plethysmography. *American Journal of Respiratory and Critical Care Medicine*, 156(3 I), pp.766–775.

Harper, S. et al., 1998. Evidence that P2Y4 nucleotide receptors are involved in the regulation of rat aortic smooth muscle cells by UTP and ATP. *British journal of pharmacology*, 124(4), pp.703–710.

Haugh, M.G. et al., 2011. Crosslinking and mechanical properties significantly influence cell attachment, proliferation, and migration within collagen glycosaminoglycan scaffolds. *Tissue engineering. Part A*, 17(9-10), pp.1201–1208.

Hayashi, K. et al., 2010. T-type Ca channel blockade as a determinant of kidney protection. *Keio Journal of Medicine*, 59(3), pp.84–95.

Hayashi, K., Kumagai, H. & Saruta, T., 2003. Inhibitors on Proteinuria in Human. *Science*, pp.116 –122.

Hayati, I., Bailey, A.I. & Tadros, T.F., 1987. Investigations into the mechanisms of electrohydrodynamic spraying of liquids. 1. Effect of electric-field and the environment on pendant drops and factors affecting the formation of stable jets and atomization. *Journal of Colloid and Interface science*, 117(1), pp.205–221.

Heard, B.E. & Hossain, S., 1973. Hyperplasia of bronchial muscle in asthma. *The Journal of Pathology*, 110(4), pp.319–331. Available at: http://dx.doi.org/10.1002/path.1711100406.

Henig, N.R. et al., 2000. Effect of recombinant human platelet-activating factor-acetylhydrolase on allergen-induced asthmatic responses. *American journal of respiratory and critical care medicine*, 162(2 Pt 1), pp.523–7. Available at: http://www.ncbi.nlm.nih.gov/pubmed/10934081.

Herszberg, B. et al., 2006. Heaves, an asthma-like equine disease, involves airway smooth muscle remodeling. *The Journal of allergy and clinical immunology*, 118(2), pp.382–388.

Hinds, S. et al., 2011. The role of extracellular matrix composition in structure and function of bioengineered skeletal muscle. *Biomaterials*, 32(14), pp.3575–3583. Available at: http://dx.doi.org/10.1016/j.biomaterials.2011.01.062.

Hirokawa, N. & Heuser, J.E., 1981. Quick-freeze, deep-etch visualization of the cytoskeleton beneath surface differentiations of intestinal epithelial cells. *The Journal of cell biology*, 91(2 Pt 1), pp.399–409.

Hirst, S.J., 1996. Airway smooth muscle cell culture: application to studies of airway wall remodelling and phenotype plasticity in asthma. *European Respiratory Journal*, 9(4), pp.808–820. Available at: http://erj.ersjournals.com/content/9/4/808 [Accessed August 7, 2013].

Hodgkinson, T., Yuan, X.-F. & Bayat, a., 2014. Electrospun silk fibroin fiber diameter influences in vitro dermal fibroblast behavior and promotes healing of ex vivo wound models. *Journal of Tissue Engineering*, 5(0). Available at: http://tej.sagepub.com/lookup/doi/10.1177/2041731414551661.

Holmes, A.M., Solari, R. & Holgate, S.T., 2011. Animal models of asthma: value, limitations and opportunities for alternative approaches. *Drug discovery today*, 16(15-16), pp.659–670.

Hongliang Jiang, † et al., 2004. Optimization and Characterization of Dextran Membranes Prepared by Electrospinning. *Biomacromolecules*, 5(2), pp.326–333. Available at: http://dx.doi.org/10.1021/bm034345w.

Horiuti, K. et al., 1989. Kinetics of contraction initiated by flash photolysis of caged adenosine triphosphate in tonic and phasic smooth muscles. *The Journal of general physiology*, 94(4), pp.769–781. Available at: papers://4c48fe13-7c69-4b65-a0fa-467dccdedc3f/Paper/p217.

Hossain, S., 1973. Quantitative measurement of bronchial muscle in men with asthma. *The American review of respiratory disease*, 107(1), pp.99–109.

Hosseini, V. et al., 2012. Engineered contractile skeletal muscle tissue on a microgrooved methacrylated gelatin substrate. *Tissue engineering Part A*, 18(23-24), pp.2453–65. Available at: http://www.ncbi.nlm.nih.gov/pubmed/22963391 [Accessed May 30, 2013].

https://www.gov.uk/guidance/research-and-testing-using-animals, Research and testing using animals.

Huang, L. et al., 2001. Engineered collagen – PEO nanofibers and fabrics. *J Biomater Sci Polymer Edn*, 12(9), pp.979–993.

Huang, Y. et al., 2005. Rapid formation of functional muscle in vitro using fibrin gels. *Journal of Applied Physiology*, 98, pp.706–713.

Huiatt, T.W. et al., 1980. Desmin from avian smooth muscle. Purification and partial characterization. *The Journal of biological chemistry*, 255(14), pp.6981–6989.

Hutmacher, D.W. & Dalton, P.D., 2011. Melt Electrospinning. *Chemistry- An Asian Journal*, 6(1), pp.44–56.

Hylkema, M.N. et al., 2002. The strength of the OVA-induced airway inflammation in rats is strain dependent. *Clinical and Experimental Immunology*, 129, pp.390–396.

Ilagan, R.M. et al., 2010. Linear measurement of cell contraction in a capillary collagen gel system. *BioTechniques*, 48(2), pp.153–155.

Ip, W. et al., 1985. Subunit structure of desmin and vimentin protofilaments and how they assemble into intermediate filaments. *Annals of the New York Academy of Sciences*, 455, pp.185–199.

Jahoda, C. a et al., 1991. Smooth muscle alpha-actin is a marker for hair follicle dermis in vivo and in vitro. *Journal of cell science*, 99 (Pt 3), pp.627–36. Available at: http://www.ncbi.nlm.nih.gov/pubmed/1939373.

Jarusuwannapoom, T. et al., 2005. Effect of solvents on electro-spinnability of polystyrene solutions and morphological appearance of resulting electrospun polystyrene fibers. *European Polymer Journal*, 41(3), pp.409–421.

Jensen, A.M., 2005. Potential roles for BMP and Pax genes in the development of iris smooth muscle. *Developmental dynamics : an official publication of the American Association of Anatomists*, 232(2), pp.385–392.

Jia, J. et al., 2007. Preparation and Characterization of Antibacterial Silver-containing Nanofibers for Wound Dressing Applications. *Journal of US-China Medical Science*, 4(2), pp.52–54.

Johnson, J.D. et al., 1996. Effects of myosin light chain kinase and peptides on Ca2+ exchange with the N- and C-terminal Ca2+ binding sites of calmodulin. *The Journal of biological chemistry*, 271(2), pp.761–767.

Johnson, J.R. et al., 2004. Continuous Exposure to House Dust Mite Elicits Chronic Airway Inflammation and Structural Remodeling. *American Journal of Respiratory and Critical Care Medicine*, 169(3), pp.378–385. Available at: http://www.atsjournals.org/doi/abs/10.1164/rccm.200308-1094OC.

Jones, P.L., Crack, J. & Rabinovitch, M., 1997. Regulation of Tenascin-C, a Vascular Smooth Muscle Cell Survival Factor that Interacts with the alphaV-beta3 Integrin to Promote Epidermal Growth Factor Receptor Phosphorylation and Growth. *The Journal of cell biology*, 139(1), pp.279–293.

Jorge-Herrero, E. et al., 1999. Influence of different chemical cross-linking treatments on the properties of bovine pericardium and collagen. *Biomaterials*, 20(6), pp.539–545.

Jun, Z. et al., 2003. Poly-L-lactide nanofibers by electrospinning - Influence of solution viscosity and electrical conductivity on fiber diameter and fiber morphology. *E-POLYMERS*.

Kamm, K.E. & Stull, J.T., 1986. Activation of smooth muscle contraction: relation between myosin phosphorylation and stiffness. *Science* , 232 (4746), pp.80–82. Available at: http://www.sciencemag.org/content/232/4746/80.abstract.

Karol, M.H.M., 1994. Animal models of occupational asthma. *European Respiratory Journal*, 7(3), pp.555–568. Available at: http://erj.ersjournals.com/cgi/content/abstract/7/3/555\nhttp://www.ingentaselect.com/rpsv/cgi-bin/cgi?ini=xref&body=linker&reqdoi=10.1183/09031936.94.07030555.

Kaur, D. et al., 2006. Airway smooth muscle and mast cell-derived CC chemokine ligand 19 mediate airway smooth muscle migration in asthma. *American journal of respiratory and critical care medicine*, 174(11), pp.1179–88. Available at: http://www.ncbi.nlm.nih.gov/pubmed/16959919 [Accessed June 30, 2014].

Keogh, M.B., O'Brien, F.J. & Daly, J.S., 2010. Substrate stiffness and contractile behaviour modulate the functional maturation of osteoblasts on a collagen-GAG scaffold. *Acta biomaterialia*, 6(11), pp.4305–4313.

Khan, M.A. et al., 2010. Influence of airway wall stiffness and parenchymal tethering on the dynamics of bronchoconstriction. *American journal of physiology. Lung cellular and molecular physiology*, 299(1), pp.L98–L108.

Kharaziha, M. et al., 2013. PGS:Gelatin nanofibrous scaffolds with tunable mechanical and structural properties for engineering cardiac tissues. *Biomaterials*, 34(27), pp.6355–66. Available at: http://www.ncbi.nlm.nih.gov/pubmed/23747008 [Accessed May 23, 2014].

Khodabukus, A. & Baar, K., 2009. Regulating fibrinolysis to engineer skeletal muscle from the C2C12 cell line. *Tissue engineering. Part C, Methods*, 15(3), pp.501–511.

Khor, E., 1997. Methods for the treatment of collagenous tissues for bioprostheses. *Biomaterials*, 18(2), pp.95–105.

Khromov, a et al., 1995. The role of MgADP in force maintenance by dephosphorylated cross-bridges in smooth muscle: a flash photolysis study. *Biophysical journal*, 69(6), pp.2611–2622. Available at: http://dx.doi.org/10.1016/S0006-3495(95)80132-3.

Ki, C.S. et al., 2005. Characterization of gelatin nanofiber prepared from gelatin-formic acid solution. *Polymer*, 46(14), pp.5094–5102.

Kim, B. et al., 2005. Poly(acrylic acid) nanofibers by electrospinning. *Materials Letters*, 59(7), pp.829–832.

Kim, H.S. et al., 2005. Morphological characterization of electrospun nano-fibrous membranes of biodegradable poly(L-lactide) and poly(lactide-co-glycolide). *Macromolecular Symposia*, 224, pp.145–154.

Kim, K.W. et al., 2004. The effect of molecular weight and the linear velocity of drum surface on the properties of electrospun poly(ethylene terephthalate) nonwovens. *Fibers and Polymers*, 5(2), pp.122–127. Available at: http://link.springer.com/10.1007/BF02902925.

Kirber, M., Walsh Jr., J. & Singer, J., 1988. Stretch-activated ion channels in smooth muscle: a mechanism for the initiation of stretch-induced contraction. *Pflügers Archiv*, 412(4), pp.339–345. Available at: http://dx.doi.org/10.1007/BF01907549.

Kobayashi, R., Kubota, T. & Hidaka, H., 1994. Purification, characterization, and partial sequence analysis of a new 25-kDa actin-binding protein from bovine aorta: a SM22 homolog. *Biochemical and biophysical research communications*, 198(3), pp.1275–1280.

Koski, A., Yim, K. & Shivkumar, S., 2004. Effect of molecular weight on fibrous PVA produced by electrospinning. *Materials Letters*, 58(3-4), pp.493–497.

Koumoundouros, E. et al., 2006. Chronic airway disease: deteriorating pulmonary function in sheep associated with repeated challenges of house dust mite. *Experimental Lung Research*, 32(7), pp.321–330. Available at: http://dx.doi.org/10.1080/01902140600916960.

Koyama, H. et al., 1996. Fibrillar collagen inhibits arterial smooth muscle proliferation through regulation of Cdk2 inhibitors. *Cell*, 87(6), pp.1069–78. Available at: http://www.ncbi.nlm.nih.gov/pubmed/8978611.

Kriel, H., Sanderson, R.D. & Smit, E., 2012. Coaxial electrospinning of miscible PLLA-core and PDLLA-shell solutions and indirect visualisation of the core-shell fibres obtained. *Fibres and Textiles in Eastern Europe*, 91(2), pp.28–33.

Krug, N. & Rabe, K.F., 2008. Animal models for human asthma: the perspective of a clinician. *Current Drug Targets*, 9(6), pp.438–442.

Kucharewicz, I., Bodzenta-łukaszyk, A. & Bucko, W., 2008. Experimental asthma in rats. *Pharmacological Reports*, 60(6), pp.783–788.

Kudo, M. et al., 2012. IL-17A produced by αβ T cells drives airway hyper-responsiveness in mice and enhances mouse and human airway smooth muscle contraction. *Nature Medicine*, 18(4), pp.547–554. Available at: http://www.ncbi.nlm.nih.gov/pubmed/22388091 [Accessed May 30, 2013].

Kuijpers, A.J. et al., 2000. Cross-linking and characterisation of gelatin matrices for biomedical applications. *Journal of Biomaterials Science, Polymer*

Edition, 11(3), pp.225–243. Available at:
http://www.tandfonline.com/doi/abs/10.1163/156856200743670
[Accessed February 4, 2014].

Kumari, R. et al., 2003. ATP and UTP responses of cultured rat aortic smooth
muscle cells revisited: dominance of P2Y2 receptors. *British journal of
pharmacology*, 140(7), pp.1169–76. Available at:
http://www.pubmedcentral.nih.gov/articlerender.fcgi?artid=1574131&tool
=pmcentrez&rendertype=abstract [Accessed September 1, 2014].

Kumbar, S.G. et al., 2007. A preliminary report on a novel electrospray technique
for nanoparticle based biomedical implants coating: Precision
electrospraying. *Journal of biomedical materials research Part B-Applied
Biomaterials*, 81B(1), pp.91–103.

Kuppan, P., Sethuraman, S. & Krishnan, U.M., 2015. Interaction of human smooth
muscle cells with nanofibrous scaffolds: Effect of fiber orientation on cell
adhesion, proliferation, and functional gene expression. *Journal of
Biomedical Materials Research Part A*, 103(7), pp.2236–2250. Available at:
http://dx.doi.org/10.1002/jbm.a.35360.

Kuzuya, M. et al., 2004. Pitavastatin, a 3-hydroxy-3-methylglutaryl-coenzyme A
reductase inhibitor, blocks vascular smooth muscle cell populated-collagen
lattice contraction. *Journal of cardiovascular pharmacology*, 43(6), pp.808–
814.

Lai, J.-Y. et al., 2002. Phenotypic and functional characterization of in vivo tissue
engineered smooth muscle from normal and pathological bladders.
International braz j urol official journal of the Brazilian Society of Urology,
28(5), pp.1853–1857; discussion 1858. Available at:
http://www.ncbi.nlm.nih.gov/pubmed/12352375 [Accessed May 30, 2013].

Larrondo, L. & Manley, R.S.J., 1981a. Electrostatic fiber spinning from polymer
melts .1. Experimental-observations on fiber formationand properties.
Journal of Polymer science Part B: Physics, 19(6), pp.909–920.

Larrondo, L. & Manley, R.S.J., 1981b. Electrostatic fiber spinning from polymer
melts .2. Examination of the flow field in an electrically driven jet. *Journal of
Polymer science Part B: Physics*, 19(6), pp.921–932.

Larrondo, L. & Manley, R.S.J., 1981c. Electrostatic fiber spinning from polymer
melts .3. Elecetostatic deformation of a pendant drop of polymer melt.
Journal of Polymer science Part B: Physics, 19(6), pp.933–940.

Lee, C.H. et al., 2005. Nanofiber alignment and direction of mechanical strain
affect the ECM production of human ACL fibroblast. *Biomaterials*, 26(11),
pp.1261–1270.

Lee, J.S. et al., 2004. Role of molecular weight of atactic poly(vinyl alcohol) (PVA) in the structure and properties of PVA nanofabric prepared by electrospinning. *Journal of Applied Polymer Science*, 93(4), pp.1638–1646.

Lee, T.L. et al., 1999. The effect of propofol on human gastric and colonic muscle contractions. *Anesthesia and analgesia*, 89(5), pp.1246–1249.

Lee, W. et al., 2009. Multi-layered culture of human skin fibroblasts and keratinocytes through three-dimensional freeform fabrication. *Biomaterials*, 30(8), pp.1587–1595. Available at: http://dx.doi.org/10.1016/j.biomaterials.2008.12.009.

Lees-Miller, J.P. et al., 1987. Isolation and characterization of an abundant and novel 22-kDa protein (SM22) from chicken gizzard smooth muscle. *Journal of Biological Chemistry*, 262(7), pp.2988–2993.

Lees-Miller, J.P., Heeley, D.H. & Smillie, L.B., 1987. An abundant and novel protein of 22 kDa (SM22) is widely distributed in smooth muscles. Purification from bovine aorta. *The Biochemical journal*, 244(3), pp.705–709.

Legant, W.R. et al., 2009. Microfabricated tissue gauges to measure and manipulate forces from 3D microtissues. *Proceedings of the National Academy of Sciences of the United States of America*, 106(25), pp.10097–10102.

Levy, N., 2012. The use of animal as models: ethical considerations. *International journal of stroke : official journal of the International Stroke Society*, 7(5), pp.440–442.

Li, D., Wang, Y. & Xia, Y., 2003. Electrospinning of polymeric and ceramic nanofibers as uniaxially aligned arrays. *Nano Letters*, 3(8), pp.1167–1171.

Li, D. & Xia, Y.N., 2004. Direct fabrication of composite and ceramic hollow nanofibers by electrospinning. *NANO LETTERS*, 4(5), pp.933–938.

Li, M. et al., 2005. Electrospun protein fibers as matrices for tissue engineering. *Biomaterials*, 26(30), pp.5999–6008. Available at: http://www.ncbi.nlm.nih.gov/pubmed/15894371 [Accessed February 7, 2014].

Li, S. et al., 2002. Genomic analysis of smooth muscle cells in 3-dimensional collagen matrix. *FASEB*, 17, pp.97–99.

Li, W.-J., Jiang, Y.J. & Tuan, R.S., 2006. Chondrocyte phenotype in engineered fibrous matrix is regulated by fiber size. *TISSUE ENGINEERING*, 12(7), pp.1775–1785.

Lin, J.C.-J. et al., 2012. An ex vivo approach to the differential parenchymal responses induced by cigarette whole smoke and its vapor phase. *Toxicology*, 293(1-3), pp.125–131.

Lin, T. et al., 2004. The charge effect of cationic surfactants on the elimination of fibre beads in the electrospinning of polystyrene. *Nanotechnology*, 15(9), pp.1375–1381. Available at: http://stacks.iop.org/0957-4484/15/i=9/a=044?key=crossref.5b515c7aa2b25c7a8c11a41ff90a7fcf [Accessed May 30, 2013].

Liu, J.Q., Yang, D. & Folz, R.J., 2006. A novel bronchial ring bioassay for the evaluation of small airway smooth muscle function in mice. *American journal of physiology. Lung cellular and molecular physiology*, 291(2), pp.L281–8. Available at: http://www.ncbi.nlm.nih.gov/pubmed/16648239 [Accessed July 30, 2013].

Liu, S., Chihara, K. & Maeyama, K., 2005. The contribution of mast cells to the late-phase of allergic asthma in rats. *Inflammation Research*, 54(5), pp.221–228. Available at: http://dx.doi.org/10.1007/s00011-005-1346-9.

Liu, T. et al., 2010. Photochemical crosslinked electrospun collagen nanofibers: synthesis, characterization and neural stem cell interactions. *Journal of biomedical materials research. Part A*, 95(1), pp.276–282.

Lloyd, C.M., 2012. Building Better Mouse Models of Asthma. , 7(3), pp.231–236.

Lou, X. & Chirila, T. V, 1999. Swelling behavior and mechanical properties of chemically cross-linked gelatin gels for biomedical use. *Journal of biomaterials applications*, 14(2), pp.184–191.

Loufrani, L. et al., 2002. Selective microvascular dysfunction in mice lacking the gene encoding for desmin. *FASEB journal : official publication of the Federation of American Societies for Experimental Biology*, 16(1), pp.117–119.

Di Lullo, G. a. et al., 2002. Mapping the ligand-binding sites and disease-associated mutations on the most abundant protein in the human, type I collagen. *Journal of Biological Chemistry*, 277(6), pp.4223–4231.

Lundblad, L.K. a. et al., 2007. Airway Hyperresponsiveness in Allergically Inflamed Mice. *American Journal of Respiratory and Critical Care Medicine*, 175(8), pp.768–774. Available at: http://www.atsjournals.org/doi/abs/10.1164/rccm.200610-1410OC.

Lynn, A.K., Yannas, I. V & Bonfield, W., 2004. Antigenicity and immunogenicity of collagen. *Journal of biomedical materials research. Part B, Applied biomaterials*, 71(2), pp.343–354.

Ma, Z. et al., 2005. Surface engineering of electrospun polyethylene terephthalate (PET) nanofibers towards development of a new material for blood vessel engineering. *Biomaterials*, 26(15), pp.2527–2536. Available at: http://www.ncbi.nlm.nih.gov/pubmed/15585255 [Accessed May 21, 2013].

Macchiarini, P. et al., 2008. Clinical transplantation of a tissue-engineered airway. *Lancet*, 372(9655), pp.2023–30. Available at: http://www.ncbi.nlm.nih.gov/pubmed/19022496 [Accessed July 17, 2014].

Margulis, A. et al., 2009. Mast cell-dependent contraction of human airway smooth muscle cell-containing collagen gels: influence of cytokines, matrix metalloproteases, and serine proteases. *Journal of immunology (Baltimore, Md. : 1950)*, 183(3), pp.1739–1750.

Martens, W. et al., 2014. Human dental pulp stem cells can differentiate into Schwann cells and promote and guide neurite outgrowth in an aligned tissue-engineered collagen construct in vitro. *FASEB Journal*, 28(4), pp.1634–1643.

Martin, C. et al., 1989. Caffeine-induced inhibition of calcium channel current in cultured smooth muscle cells from pregnant rat myometrium. *British Journal of Pharmacology*, 98(2), pp.493–498. Available at: http://doi.wiley.com/10.1111/j.1476-5381.1989.tb12622.x.

Martin, C., Uhlig, S. & Ullrich, V., 1996. Videomicroscopy of methacholine-induced contraction of individual airways in precision-cut lung slices. *European Respiratory Journal*, 9(12), pp.2479–2487.

Martin, N.R.W. et al., 2015. Neuromuscular junction formation in tissue engineered skeletal muscle augments contractile function and improves cytoskeletal organisation. *Tissue Engineering Part A*, (July), p.150713044049008. Available at: http://online.liebertpub.com/doi/10.1089/ten.TEA.2015.0146.

Matsuda, S. et al., 1999. Bioadhesion of gelatin films crosslinked with glutaraldehyde. *Journal of biomedical materials research*, 45(1), pp.20–7. Available at: http://www.ncbi.nlm.nih.gov/pubmed/11246944.

Matsui, M. et al., 2002. Mice lacking M2 and M3 muscarinic acetylcholine receptors are devoid of cholinergic smooth muscle contractions but still viable. *The Journal of neuroscience : the official journal of the Society for Neuroscience*, 22(24), pp.10627–32. Available at: http://www.ncbi.nlm.nih.gov/pubmed/12486155.

Matsumoto, H. et al., 2007. Comparison of gel contraction mediated by airway smooth muscle cells from patients with and without asthma. *Thorax*, 62(10), pp.848–54. Available at:

http://www.pubmedcentral.nih.gov/articlerender.fcgi?artid=2094259&tool
=pmcentrez&rendertype=abstract [Accessed September 4, 2013].

Matthews, J. a et al., 2003. Electrospinning of Collagen Type II: A Feasibility
Study. *Journal of Bioactive and Compatible Polymers*, 18(March 2003),
pp.125–134.

Matthews, J.A. et al., 2002. Electrospinning of Collagen Nanofibers. , 1(Iii),
pp.232–238.

McKee, M.G. et al., 2004. Correlations of Solution Rheology with Electrospun
Fiber Formation of Linear and Branched Polyesters. *Macromolecules*, 37(5),
pp.1760–1767. Available at:
http://pubs.acs.org/doi/abs/10.1021/ma035689h.

McManus, M. et al., 2007. Electrospun nanofibre fibrinogen for urinary tract
tissue reconstruction. *Biomedical Materials*, 2(4), p.257. Available at:
http://stacks.iop.org/1748-605X/2/i=4/a=008.

McManus, M.C. et al., 2007. Electrospun fibrinogen: feasibility as a tissue
engineering scaffold in a rat cell culture model. *Journal of Biomedical
Materials Research Part A*, 81(2), pp.299–309. Available at:
http://onlinelibrary.wiley.com/doi/10.1002/jbm.a.30989/full.

Meng, Z.X. et al., 2010. Electrospinning of PLGA/gelatin randomly-oriented and
aligned nanofibers as potential scaffold in tissue engineering. *Materials
Science and Engineering: C*, 30(8), pp.1204–1210. Available at:
http://linkinghub.elsevier.com/retrieve/pii/S0928493110001530 [Accessed
November 1, 2013].

Meurs, H. et al., 2006. A guinea pig model of acute and chronic asthma using
permanently instrumented and unrestrained animals. *Nature protocols*,
1(2), pp.840–847.

Miller, C., George, S. & Niklason, L., 2010. Developing a tissue-engineered model
of the human bronchiole. , (July), pp.619–627.

Mitchell, H.W. & Sparrow, M.P., 1994. Video-imaging of lumen narrowing;
muscle shortening and flow responsiveness in isolated bronchial segments
of the pig. *European Respiratory Journal*, 7(7), pp.1317–1325. Available at:
http://erj.ersjournals.com/content/7/7/1317.

Mithieux, S.M. et al., 2005. A model two-component system for studying the
architecture of elastin assembly in vitro. *Journal of structural biology*,
149(3), pp.282–289.

Mit-uppatham, C., Nithitanakul, M. & Supaphol, P., 2004. Ultratine electrospun
polyamide-6 fibers: Effect of solution conditions on morphology and

average fiber diameter RID C-4353-2008. *Macromolecular Chemistry and Physics*, 205(17), pp.2327–2338.

Miyagi, Y. et al., 1996. Dual regulation of cerebrovascular tone by UTP : P2u receptor- mediated contraction and endothelium-dependent relaxation. , pp.847–856.

Miyaguchi, K., 2000. Ultrastructure of the zonula adherens revealed by rapid-freeze deep-etching. *Journal of structural biology*, 132(3), pp.169–178.

Morin, J.-P. et al., 2008. Prevalidation of in vitro continuous flow exposure systems as alternatives to in vivo inhalation safety evaluation experimentations: Outcome from MAAPHRI-PCRD5 research program. *Experimental and Toxicologic Pathology*, 60(2–3), pp.195–205. Available at: http://www.sciencedirect.com/science/article/pii/S0940299308000304.

Mortensen, K. & Larsson, L.-I., 2003. Effects of cytochalasin D on the actin cytoskeleton: association of neoformed actin aggregates with proteins involved in signaling and endocytosis. *Cellular and molecular life sciences : CMLS*, 60(5), pp.1007–1012.

Mudera, V. et al., 2010. The effect of cell density on the maturation and contractile ability of muscle derived cells in a 3D tissue-engineered skeletal muscle model and determination of the cellular and mechanical stimuli required for the synthesis of a postural phenotype. *Journal of cellular physiology*, 225(3), pp.646–53. Available at: http://www.ncbi.nlm.nih.gov/pubmed/20533296 [Accessed June 6, 2014].

Muiznieks, L.D., Jensen, S.A. & Weiss, A.S., 2003. Structural changes and facilitated association of tropoelastin. *Archives of Biochemistry and Biophysics*, 410(2), pp.317–323. Available at: http://www.sciencedirect.com/science/article/pii/S0003986102007191.

Murphy, R.A., 1994. What is special about smooth muscle? The significance of covalent crossbridge regulation. *FASEB journal : official publication of the Federation of American Societies for Experimental Biology*, 8(3), pp.311–318.

Murphy, R.A., Driska, S.P. & Cohen, D.M., 1977. Variations in actin to myosin ratios and cellular force generation in vertebrae smooth muscles. In *Excitation contraction coupling in smooth muscle*. Elsevier, pp. 417–424.

Murray, B.Y.R.K. & Kotlikoff, M.I., 1991. Receptor-activated calcium influx in human airway smooth muscle cells. *Journal of Physiology*, (435), pp.123–144.

Nabeshima, Y. et al., 1987. Nonmuscle and Smooth Muscle Myosin Light Chain mRNAs Are Generated from a Single Gene by the Tissue-specific Alternative

RNA Splicing *. *The Journal of Biological Chemistry*, 262(22), pp.10608–10612.

Nagai, R. et al., 1989. Identification of two types of smooth muscle myosin heavy chain isoforms by cDNA cloning and immunoblot analysis. *The Journal of biological chemistry*, 264(17), pp.9734–9737. Available at: http://www.jbc.org/content/264/17/9734.long\npapers://4c48fe13-7c69-4b65-a0fa-467dccdedc3f/Paper/p11610.

Nandakumar, A. et al., 2013. Surface modification of electrospun fibre meshes by oxygen plasma for bone regeneration. *Biofabrication*, 5(1), p.015006. Available at: http://www.ncbi.nlm.nih.gov/pubmed/23229020 [Accessed November 25, 2014].

NC3Rs, 2014. REACH - Minimisation of Animal Testing REACH - Minimisation of Animal Testing. *Regulation*, 2(18).

Nesmith, A.P. et al., 2014. Human airway musculature on a chip: an in vitro model of allergic asthmatic bronchoconstriction and bronchodilation. *Lab on a chip*. Available at: http://www.ncbi.nlm.nih.gov/pubmed/25093641 [Accessed September 5, 2014].

Nichol, J.W. et al., 2010. Cell-laden microengineered gelatin methacrylate hydrogels. *Biomaterials*, 31(21), pp.5536–44. Available at: http://www.pubmedcentral.nih.gov/articlerender.fcgi?artid=2878615&tool=pmcentrez&rendertype=abstract [Accessed July 11, 2014].

Nikkhah, M. et al., 2012. Directed endothelial cell morphogenesis in micropatterned gelatin methacrylate hydrogels. *Biomaterials*, 33(35), pp.9009–9018.

Nirmalanandhan, V.S. et al., 2006. Effects of cell seeding density and collagen concentration on contraction kinetics of mesenchymal stem cell-seeded collagen constructs. *Tissue engineering*, 12(7), pp.1865–1872.

Nivison-Smith, L. & Weiss, A.S., 2012. Alignment of human vascular smooth muscle cells on parallel electrospun synthetic elastin fibers. *Journal of biomedical materials research. Part A*, 100(1), pp.155–61. Available at: http://www.ncbi.nlm.nih.gov/pubmed/21997972 [Accessed November 1, 2013].

Noble, P.B. et al., 2013. Airway narrowing and bronchodilation to deep inspiration in bronchial segments from subjects with and without reported asthma. *Journal of applied physiology (Bethesda, Md. : 1985)*, 114(10), pp.1460–1471.

Noble, P.B., McFawn, P.K. & Mitchell, H.W., 2004. Intraluminal pressure oscillation enhances subsequent airway contraction in isolated bronchial

segments. *J Appl Physiol*, 96(3), pp.1161–5. Available at: http://www.ncbi.nlm.nih.gov/pubmed/14634031.

Noble, P.B., Turner, D.J. & Mitchell, H.W., 2002. Relationship of airway narrowing, compliance, and cartilage in isolated bronchial segments. *Journal of applied physiology*, 92(3), pp.1119–24. Available at: http://www.ncbi.nlm.nih.gov/pubmed/11842048.

North, a J. et al., 1994. Calponin is localised in both the contractile apparatus and the cytoskeleton of smooth muscle cells. *Journal of cell science*, 107 (Pt 3, pp.437–444.

O'Brien, J. et al., 2000. Investigation of the Alamar Blue (resazurin) fluorescent dye for the assessment of mammalian cell cytotoxicity. *European Journal of Biochemistry*, 267(17), pp.5421–5426.

Oishi, K. et al., 2000. Agonist-induced isometric contraction of smooth muscle cell-populated collagen gel fiber. *American journal of physiology. Cell physiology*, 279(5), pp.C1432–C1442.

Oishi, K. et al., 2002. Contractile responses of smooth muscle cells differentiated from rat neural stem cells. *The Journal of physiology*, 540(Pt 1), pp.139–152.

Ostrom, R.S. & Insel, P. a, 2004. The evolving role of lipid rafts and caveolae in G protein-coupled receptor signaling: implications for molecular pharmacology. *British Journal of Pharmacology*, 143(2), pp.235–245. Available at: http://doi.wiley.com/10.1038/sj.bjp.0705930.

Ostrovidov, S. et al., 2014. Myotube formation on gelatin nanofibers - multi-walled carbon nanotubes hybrid scaffolds. *Biomaterials*, 35(24), pp.6268–77. Available at: http://www.ncbi.nlm.nih.gov/pubmed/24831971 [Accessed August 8, 2014].

Ouedraogo, N. & Roux, E., 2014. Physiology of Airway Smooth Muscle Contraction: An Overview. *Pulmonary & Respiratory Medicine*, 4(6).

Ovsianikov, A. et al., 2011. Laser fabrication of three-dimensional CAD scaffolds from photosensitive gelatin for applications in tissue engineering. *Biomacromolecules*, 12(4), pp.851–858.

Panzavolta, S. et al., 2011. Electrospun gelatin nanofibers: optimization of genipin cross-linking to preserve fiber morphology after exposure to water. *Acta biomaterialia*, 7(4), pp.1702–9. Available at: http://www.ncbi.nlm.nih.gov/pubmed/21095244 [Accessed March 21, 2014].

Park, J.S. et al., 2012. The Effect of Matrix Stiffness on the Differentiation of Mesenchymal Stem Cells in Response to TGF-β. , 32(16), pp.3921–3930.

Parker, K.H. & Winlove, C.P., 1988. The macromolecular and ultrastructural basis of the permeability properties of the vascular wall. *Engineering in medicine*, 17(4), pp.175–180.

Pasterkamp, G. et al., 1996. Atherosclerotic Arterial Remodeling in the Superficial Femoral Artery: Individual Variation in Local Compensatory Enlargement Response . *Circulation* , 93 (10), pp.1818–1825. Available at: http://circ.ahajournals.org/content/93/10/1818.abstract.

Pasterkamp, G. et al., 1997. The Impact of Atherosclerotic Arterial Remodeling on Percentage of Luminal Stenosis Varies Widely Within the Arterial System: A Postmortem Study . *Arteriosclerosis, Thrombosis, and Vascular Biology* , 17 (11), pp.3057–3063. Available at: http://atvb.ahajournals.org/content/17/11/3057.abstract.

Pauwels, R. a, Brusselle, G.J. & Kips, J.C., 1997. Cytokine manipulation in animal models of asthma. *American journal of respiratory and critical care medicine*, 156(4 Pt 2), pp.S78–81. Available at: http://www.ncbi.nlm.nih.gov/pubmed/9351584.

Pelipenko, J. et al., 2013. The impact of relative humidity during electrospinning on the morphology and mechanical properties of nanofibers. *International Journal of Pharmaceutics*, 456, pp.125–134.

Perez-reyes, E., Deusen, A.L. Van & Vitko, I., 2009. Molecular Pharmacology of Human Ca v 3 . 2 T-Type Ca 2 ɛ Channels : Block by Antihypertensives , Antiarrhythmics , and Their Analogs. , 328(2), pp.621–627.

Pham, Q.P., Sharma, U. & Mikos, A.G., 2006. Electrospinning of polymeric nanofibers for tissue engineering applications: a review. *Tissue engineering*, 12(5), pp.1197–211. Available at: http://www.ncbi.nlm.nih.gov/pubmed/16771634.

Plopper, C.G., Mariassy, A.T. & Lollini, L.O., 1983. Structure as revealed by airway dissection. A comparison of mammalian lungs. *The American review of respiratory disease*, 128(2 Pt 2), pp.S4–7.

Pohl, J. et al., 1997. Phosphorylation of calponin in airway smooth muscle. *The American journal of physiology*, 272(1 Pt 1), pp.L115–L123.

Popescu, L. & Diculescu, I., 1975. Calcium in Smooth Muscle Sarcoplasmic Reticulum in Situ. *THE JOURNAL OF CELL BIOLOGY*, 67(15), pp.911–918.

Powell, C. a et al., 2002. Mechanical stimulation improves tissue-engineered human skeletal muscle. *American journal of physiology. Cell physiology*, 283(5), pp.C1557–C1565.

Prasertsung, I., Damrongsakkul, S. & Saito, N., 2013. Crosslinking of a Gelatin Solutions Induced by Pulsed Electrical Discharges in Solutions. *Plasma Processes and Polymers*, 10(9), pp.792–797. Available at: http://dx.doi.org/10.1002/ppap.201200148.

Prendergast, C.E. et al., 2006. Species-dependent smooth muscle contraction to Neuromedin U and determination of the receptor subtypes mediating contraction using NMU1 receptor knockout mice. *British journal of pharmacology*, 147(8), pp.886–896.

Putney, J.W.J., 1993. Excitement about calcium signaling in inexcitable cells. *Science (New York, N.Y.)*, 262(5134), pp.676–678.

Ramón-Azcón, J. et al., 2012. Gelatin methacrylate as a promising hydrogel for 3D microscale organization and proliferation of dielectrophoretically patterned cells. *Lab on a Chip*, 12(16), p.2959.

Ramshaw, J.A., Shah, N.K. & Brodsky, B., 1998. Gly-X-Y tripeptide frequencies in collagen: a context for host-guest triple-helical peptides. *Journal of structural biology*, 122(1-2), pp.86–91.

Ratanavaraporn, J. et al., 2010. Influences of physical and chemical crosslinking techniques on electrospun type A and B gelatin fiber mats. *International journal of biological macromolecules*, 47(4), pp.431–438.

Rattan, S. & Ali, M., 2015. Role of SM22 in the differential regulation of phasic vs. tonic smooth muscle. *American Journal of Physiology - Gastrointestinal and Liver Physiology*, 308(7), pp.G605–G612. Available at: http://ajpgi.physiology.org/lookup/doi/10.1152/ajpgi.00360.2014.

Raub, C. et al., 2010. Predicting bulk mechanical properties of cellularized collagen gels using multiphoton microscopy. *Acta biomaterialia*, 6(12), pp.4657–4665.

Rayatpisheh, S., Li, P. & Chan-Park, M.B., 2012. Argon-plasma-induced ultrathin thermal grafting of thermoresponsive pNIPAm coating for contractile patterned human SMC sheet engineering. *Macromolecular bioscience*, 12(7), pp.937–45. Available at: http://www.ncbi.nlm.nih.gov/pubmed/22535772 [Accessed March 12, 2014].

Razani, B., Woodman, S.E. & Lisanti, M.P., 2002. Caveolae: from cell biology to animal physiology. *Pharmacological reviews*, 54(3), pp.431–467.

Redden, R. a & Doolin, E.J., 2003. Collagen crosslinking and cell density have distinct effects on fibroblast-mediated contraction of collagen gels. *Skin research and technology : official journal of International Society for Bioengineering and the Skin (ISBS) [and] International Society for Digital*

Imaging of Skin (ISDIS) [and] International Society for Skin Imaging (ISSI), 9(3), pp.290–293.

Reimer, L., 1998. *Scanning Electron Microscopy: Physics of Image Formation and Microanalysis*, Springer.

Reneker, D.H. & Chun, I., 1996. Nanometre diameter fibres of polymer, produced by electrospinning. *Nanotechnology*, 7(3), pp.216–223. Available at: http://stacks.iop.org/0957-4484/7/i=3/a=009?key=crossref.b62a3c509c723c5a2561f1e345fc1706.

Ressmeyer, a. R. et al., 2006. Characterisation of guinea pig precision-cut lung slices: comparison with human tissues. *European Respiratory Journal*, 28(3), pp.603–611. Available at: http://erj.ersjournals.com/cgi/doi/10.1183/09031936.06.00004206.

Riley, W. a et al., 1992. Ultrasonic measurement of the elastic modulus of the common carotid artery. The Atherosclerosis Risk in Communities (ARIC) Study. *Stroke; a journal of cerebral circulation*, 23(7), pp.952–956.

Roscioni, S.S. et al., 2011. Protein kinase A and the exchange protein directly activated by cAMP (Epac) modulate phenotype plasticity in human airway smooth muscle. *British journal of pharmacology*, 164(3), pp.958–969. Available at: http://www.ncbi.nlm.nih.gov/entrez/query.fcgi?cmd=Retrieve&db=PubMed&dopt=Citation&list_uids=21426315 [Accessed May 30, 2013].

Rosenfeldt, H.M. et al., 2003. Sphingosine-1-phosphate stimulates contraction of human airway smooth muscle cells. *The FASEB journal : official publication of the Federation of American Societies for Experimental Biology*, 17(13), pp.1789–1799.

Rovner, A.S., Thompson, M.M. & Murphy, R.A., 1986. Two different heavy chains are found in smooth muscle myosin. *The American journal of physiology*, 250(6 Pt 1), pp.C861–70.

Rueder, C. et al., 2013. Influence of fibre diameter and orientation of electrospun copolyetheresterurethanes on smooth muscle and endothelial cell behaviour. *CLINICAL HEMORHEOLOGY AND MICROCIRCULATION*, 55(4), pp.513–522.

Saito, S.Y. et al., 1996. Cytochalasin D inhibits smooth muscle contraction by directly inhibiting contractile apparatus. *Journal of smooth muscle research = Nihon Heikatsukin Gakkai kikanshi*, 32(2), pp.51–60.

Sakota, Y. et al., 2014. Collagen gel contraction assay using human bronchial smooth muscle cells and its application for evaluation of inhibitory effect of

formoterol. *Biological & Pharmaceutical Bulletin*, 37(6), pp.1014–20. Available at: http://www.ncbi.nlm.nih.gov/pubmed/24882412.

Sandberg, L.B., Soskel, N.T. & Leslie, J.G., 1981. Elastin structure, biosynthesis, and relation to disease states. *The New England journal of medicine*, 304(10), pp.566–579.

Schaner, P.J. et al., 2004. Decellularized vein as a potential scaffold for vascular tissue engineering. *Journal of Vascular Surgery*, 40(1), pp.146–153.

Scheideler, W.J. & Chen, C.H., 2014. The minimum flow rate scaling of Taylor cone-jets issued from a nozzle. *Applied Physics Letters*, 104(2), pp.1–4.

Schiffers, P.M. et al., 2000. Altered flow-induced arterial remodeling in vimentin-deficient mice. *Arteriosclerosis, thrombosis, and vascular biology*, 20(3), pp.611–616.

Schlepütz, M., Uhlig, S. & Martin, C., 2011. Electric field stimulation of precision-cut lung slices. *Journal of applied physiology (Bethesda, Md. : 1985)*, 110(2), pp.545–554. Available at: http://www.ncbi.nlm.nih.gov/pubmed/21109600\nfile:////Users/mw1608/DesktopMendeley Desktop/Schlep?tz, Uhlig, Martin - 2011 - Electric field stimulation of precision-cut lung slices.pdf\nfile:///C:/Users/mbirrhl/Dropbox/Mendeley Desktop/Schlep?tz, Uhlig, M.

Schlesinger, R.B. & McFadden, L.A., 1981. Comparative morphometry of the upper bronchial tree in six mammalian species. *The Anatomical record*, 199(1), pp.99–108.

Schmid, E. et al., 1982. Distribution of vimentin and desmin filaments in smooth muscle tissue of mammalian and avian aorta. *Experimental Cell Research*, 137(2), pp.329–340. Available at: http://www.sciencedirect.com/science/article/pii/0014482782900349.

Selig, W.M. & Chapman, R.W., 1999. Asthma. In D. W. Morgan & L. A. Marshall, eds. *In vivo models of inflammation*. Basel: Birkhauser Verlag, pp. 111–135.

Sell, S. a. et al., 2009. Electrospinning of collagen/biopolymers for regenerative medicine and cardiovascular tissue engineering. *Advanced Drug Delivery Reviews*, 61(12), pp.1007–1019. Available at: http://dx.doi.org/10.1016/j.addr.2009.07.012.

Serra, T. et al., 2013. 3D printed PLA-based scaffolds. *Organogenesis*, 9(4), pp.239–244.

Shang, S. et al., 2010. The effect of electrospun fibre alignment on the behaviour of rat periodontal ligament cells. *European Cells and Materials*, 19, pp.180–192.

Sharples, A.P. et al., 2012. Modelling in vivo skeletal muscle ageing in vitro using three-dimensional bioengineered constructs. *Aging cell*, 11(6), pp.986–95. Available at: http://www.ncbi.nlm.nih.gov/pubmed/22882433 [Accessed June 23, 2014].

Shin, Y.M. et al., 2001. Electrospinning: A whipping fluid jet generates submicron polymer fibers. *Applied Physics Letters*, 78(8).

Shin, Y.S., Takeda, K. & Gelfand, E.W., 2009. Understanding asthma using animal models. *Allergy, asthma & immunology research*, 1(1), pp.10–8. Available at: http://www.pubmedcentral.nih.gov/articlerender.fcgi?artid=2831565&tool=pmcentrez&rendertype=abstract [Accessed May 26, 2014].

Shinagawa, K. & Kojima, M., 2003. Mouse Model of Airway Remodeling. *American Journal of Respiratory and Critical Care Medicine*, 168(8), pp.959–967. Available at: http://www.atsjournals.org/doi/abs/10.1164/rccm.200210-1188OC.

Shore, S.A., 2003. Modeling airway remodeling: the winner by a nose? *American journal of respiratory and critical care medicine*, 168(8), pp.910–911.

Siminski, J.T. et al., 1992. Long-term maintenance of mature pulmonary parenchyma cultured in serum-free conditions. *The American journal of physiology*, 262(1 Pt 1), pp.L105–10.

Sisson, K. et al., 2009. Evaluation of Cross-Linking Methods for Electrospun Gelatin on Cell Growth and Viability. *Biomacromolecules*, 10(7), pp.1675–1680. Available at: http://dx.doi.org/10.1021/bm900036s.

Skotak, M. et al., 2010. Electrospun cross-linked gelatin fibers with controlled diameter: the effect of matrix stiffness on proliferative and biosynthetic activity of chondrocytes cultured in vitro. *Journal of biomedical materials research. Part A*, 95(3), pp.828–36. Available at: http://www.ncbi.nlm.nih.gov/pubmed/20824648 [Accessed June 29, 2014].

Small, J. V & Gimona, M., 1998. The cytoskeleton of the vertebrate smooth muscle cell. *Acta physiologica Scandinavica*, 164(4), p.341—348. Available at: http://dx.doi.org/10.1046/j.1365-201X.1998.00441.x.

Smith, a. S.T. et al., 2012. Characterization and optimization of a simple, repeatable system for the long term in vitro culture of aligned myotubes in 3D. *Journal of Cellular Biochemistry*, 113(3), pp.1044–1053.

Snider, M.E., Nuzum, D.S. & Veverka, A., 2008. Long-acting nifedipine in the management of the hypertensive patient. *Vascular Health and Risk Management*, 4(6), pp.1249–1257.

Solway, J. et al., 1995. Structure and Expression of a Smooth Muscle Cell-specific. *Biochemistry*, 270, pp.13460–13469.

Son, W.K. et al., 2004. The effects of solution properties and polyelectrolyte on electrospinning of ultrafine poly(ethylene oxide) fibers. *POLYMER*, 45(9), pp.2959–2966.

Speer, D.P. et al., 1980. Biological effects of residual glutaraldehyde in glutaraldehyde-tanned collagen biomaterials. *Journal of biomedical materials research*, 14(6), pp.753–764.

Stephens, N.L. et al., 1986. Changes in cross-bridge properties of sensitized airway smooth muscle. *Journal of applied physiology (Bethesda, Md. : 1985)*, 61(4), pp.1492–1498.

Streck, E. et al., 2010. Effects of cigarette smoke extract and nicotine on bronchial tone and acetylcholine-induced airway contraction in mouse lung slices. *Journal of investigational allergology & clinical immunology : official organ of the International Association of Asthmology (INTERASMA) and Sociedad Latinoamericana de Alergia e Inmunología*, 20(4), pp.324–30. Available at: http://www.ncbi.nlm.nih.gov/pubmed/20815310.

Takahashi, K., Hiwada, K. & Kokubu, T., 1986. Isolation and characterization of a 34,000-dalton calmodulin- and F-actin-binding protein from chicken gizzard smooth muscle. *Biochemical and biophysical research communications*, 141(1), pp.20–26.

Talebian, a, Kordestani, S. & Rashidi, a, 2007. The Effect of Glutaraldehyde on the Properties of Gelatin Films. *Kemija u …*, 56(11), pp.537–541. Available at: http://hrcak.srce.hr/index.php?show=clanak&id_clanak_jezik=26968.

Tanner, F. et al., 2000. Differential effects of the cyclin-dependent kinase inhibitors p27(Kip1), p21(Cip1), and p16(Ink4) on vascular smooth muscle cell proliferation. *Circulation*, 101, pp.2022–2025. Available at: http://circ.ahajournals.org/cgi/doi/10.1161/01.CIR.0000015465.73933.3B.

Taube, C., Dakhama, A. & Gelfand, E.W., 2004. Insights into the Pathogenesis of Asthma Utilizing Murine Models. *International Archives of Allergy and Immunology*, 135(2), pp.173–186. Available at: http://www.karger.com/DOI/10.1159/000080899.

Taylor, G., 1969. Electrically Driven Jets. *Proceedings of the Royal Society A: Mathematical, Physical and Engineering Sciences*, 313(1515), pp.453–475. Available at:

http://rspa.royalsocietypublishing.org.ezproxy.uct.ac.za/content/313/1515/453.abstract.

Thomas-Young, R.J., Smith, T.C. & Levinson, C., 1993. REGULATORY VOLUME DECREASE IN EHRLICH ASCITES TUMOR-CELLS IS NOT MEDIATED BY A RISE IN INTRACELLULAR CALCIUM. *BIOCHIMICA ET BIOPHYSICA ACTA*, 1146(1), pp.81–86.

Thornbury, K.D., 1999. Tonic and phasic activity in smooth muscle. *Irish journal of medical science*, 168(3), pp.201–207.

Tonsomboon, K. & Oyen, M.L., 2013. Composite electrospun gelatin fiber-alginate gel scaffolds for mechanically robust tissue engineered cornea. *Journal of the mechanical behavior of biomedical materials*, 21, pp.185–94. Available at: http://www.ncbi.nlm.nih.gov/pubmed/23566770 [Accessed November 1, 2013].

Tsai, C.C. et al., 2000. In vitro evaluation of the genotoxicity of a naturally occurring crosslinking agent (genipin) for biologic tissue fixation. *Journal of biomedical materials research*, 52(1), pp.58–65.

Tsai, S.-W. et al., 2012. MG63 osteoblast-like cells exhibit different behavior when grown on electrospun collagen matrix versus electrospun gelatin matrix. *PloS one*, 7(2), p.e31200. Available at: http://www.pubmedcentral.nih.gov/articlerender.fcgi?artid=3271086&tool=pmcentrez&rendertype=abstract [Accessed March 12, 2014].

Tsukita, S., Tsukita, S. & Ishikawa, H., 1983. Association of actin and 10 nm filaments with the dense body in smooth muscle cells of the chicken gizzard. *Cell and tissue research*, 229(2), pp.233–242.

Turner, D.J. et al., 2002. Decreased airway narrowing and smooth muscle contraction in hyperresponsive pigs. *Journal of applied physiology (Bethesda, Md. : 1985)*, 93(4), pp.1296–300. Available at: http://www.ncbi.nlm.nih.gov/pubmed/12235028.

Urquilla, P.R., 1978. Prolonged contraction of isolated human and canine cerebral arteries induced by uridine 5'-triphosphate. *Stroke*, 9(2), pp.133–136. Available at: http://stroke.ahajournals.org/cgi/doi/10.1161/01.STR.9.2.133 [Accessed September 1, 2014].

Usta, M. et al., 2003. Behavior and properties of neat and filled gelatins. *BIOMATERIALS*, 24(1), pp.165–172.

Vandenburgh, H. et al., 2008. Drug-screening platform based on the contractility of tissue-engineered muscle. *Muscle and Nerve*, 37(4), pp.438–447.

Vasiev, I. et al., 2013. Self-folding nano- and micropatterned hydrogel tissue engineering scaffolds by single step photolithographic process. *Microelectronic Engineering*, 108, pp.76–81. Available at: http://dx.doi.org/10.1016/j.mee.2013.04.003.

Veleirinho, B., Rei, M.F. & Lopes da Silva, J.A., 2007. Solvent and Concentration Effects on the Properties of Electrospun Poly (ethylene terephthalate) Nanofiber Mats. *Journal of Polymer Science: Part B: Polymer Physics*, pp.460–471. Available at: http://onlinelibrary.wiley.com/doi/10.1002/polb.21380/full [Accessed November 26, 2014].

Vrhovski, B., Jensen, S. & Weiss, A.S., 1997. Coacervation characteristics of recombinant human tropoelastin. *European journal of biochemistry / FEBS*, 250(1), pp.92–98.

Vyavahare, N.R. et al., 1997. Current progress in anticalcification for bioprosthetic and polymeric heart valves. *CARDIOVASCULAR PATHOLOGY*, 6(4), pp.219–229.

Wang, J.-Y., Mesquida, P., et al., 2011. Dynamic Elastic Properties of Human Bronchial Airway Tissues. , pp.1–8.

Wang, J.-Y., Mesquida, P. & Lee, T., 2011. Young's modulus measurement on pig trachea and bronchial airways. *Conference proceedings : ... Annual International Conference of the IEEE Engineering in Medicine and Biology Society. IEEE Engineering in Medicine and Biology Society. Conference*, 2011, pp.2089–92. Available at: http://www.ncbi.nlm.nih.gov/pubmed/22254749.

Wang, Y. et al., 2014. Electrospun tubular scaffold with circumferentially aligned nanofibers for regulating smooth muscle cell growth. *ACS applied materials & interfaces*, 6(4), pp.2958–2962.

Waugh Young, A., 1914. ON THE MOVEMENTS OF THE ISOLATED SMALL INTESTINE AND THE ACTION OF VARIOUS DRUGS AND EXTRACTS UPON THEM. *Quarterly Journal of Experimental Physiology*, 8(4), pp.347 – 375.

West, A.R. et al., 2013. Development and characterization of a 3D multicell microtissue culture model of airway smooth muscle. *American journal of physiology. Lung cellular and molecular physiology*, 304(1), pp.L4–16. Available at: http://www.ncbi.nlm.nih.gov/pubmed/23125251 [Accessed May 28, 2013].

White, S.R. et al., 1990. Epithelium-dependent contraction of airway smooth muscle caused by eosinophil MBP. *The American journal of physiology*, 259(4 Pt 1), pp.L294–303.

Winder, S.J. & Walsh, M.P., 1990. Smooth muscle calponin. Inhibition of actomysosin MgATPase and regulation by phosphorylation. *Journal of Biological Chemistry*, 265(17), pp.10148–10155.

Wnek, G.E. et al., 2003. Electrospinning of nanofiber fibrinogen structures. *Nano Letters*, 3(2), pp.213–216.

Wójciak-Stothard, B. et al., 1995. Activation of macrophage-like cells by multiple grooved substrata. Topographical control of cell behaviour. *Cell biology international*, 19(6), pp.485–490.

Woodman, L. et al., 2008. Mast cells promote airway smooth muscle cell differentiation via autocrine up-regulation of TGF-beta 1. *Journal of immunology (Baltimore, Md. : 1950)*, 181(7), pp.5001–7. Available at: http://www.ncbi.nlm.nih.gov/pubmed/18802103.

Word, R.A. & Kamm, K.E., 1997. Regulation of smooth muscle contraction by myosin phosphorylation. In C. Y. Kao & M. E. Carsten, eds. *Cellular aspects of smooth muscle function*. Cambridge, pp. 209–252.

Wright, D.B. et al., 2013. Phenotype modulation of airway smooth muscle in asthma. *Pulmonary pharmacology & therapeutics*, 26(1), pp.42–9. Available at: http://www.ncbi.nlm.nih.gov/pubmed/22939888 [Accessed November 1, 2013].

Wynne, B.M., Chiao, C.-W. & Webb, R.C., 2009. Vascular Smooth Muscle Cell Signaling Mechanisms for Contraction to Angiotensin II and Endothelin-1. *J Am Soc Hypertens*, 3(2), pp.84–95.

Xu, C.Y. et al., 2004. Aligned biodegradable nanofibrous structure: A potential scaffold for blood vessel engineering. *Biomaterials*, 25(5), pp.877–886. Available at: http://linkinghub.elsevier.com/retrieve/pii/S0142961203005933 [Accessed November 1, 2013].

YAFFE, D. & SAXEL, O.R.A., 1977. Serial passaging and differentiation of myogenic cells isolated from dystrophic mouse muscle. *Nature*, 270(5639), pp.725–727. Available at: http://dx.doi.org/10.1038/270725a0.

Yamamoto, S. et al., 2013. Feasibility of using gelatin-microbial transglutaminase complex to repair experimental retinal detachment in rabbit eyes. *Graefe's archive for clinical and experimental ophthalmology = Albrecht von Graefes Archiv fur klinische und experimentelle Ophthalmologie*, 251(4), pp.1109–1114.

Yamashita, H. et al., 2014. The role of the interaction of the vinculin proline-rich linker region with vinexin alpha in sensing the stiffness of the extracellular matrix. *Journal of cell science*, 127(Pt 9), pp.1875–1886.

Yan, H., Liu, L. & Zhang, Z., 2009. Alignment of electrospun nanofibers using dielectric materials. *APPLIED PHYSICS LETTERS*, 95(14).

Yan, J. et al., 2012. Effect of fiber alignment in electrospun scaffolds on keratocytes and corneal epithelial cells behavior. *Journal of Biomedical Materials Research - Part A*, 100 A(2), pp.527–535.

Yang, D. et al., 2009. Control of the morphology of micro/nanostructures of polycarbonate via electrospinning. *Chinese Science Bulletin*, 54(17), pp.2911–2917. Available at: http://link.springer.com/10.1007/s11434-009-0241-0 [Accessed May 30, 2013].

Yang, L. et al., 2008. Mechanical properties of single electrospun collagen type I fibers. *Biomaterials*, 29(8), pp.955–962.

Yao, L. et al., 2003. Electrospinning and stabilization of fully hydrolyzed poly(vinyl alcohol) fibers. *CHEMISTRY OF MATERIALS*, 15(9), pp.1860–1864.

Yost, M.J. et al., 2005. Tissue Engineered Heart Tube Using Embryonic Tissues. *Microscopy and Microanalysis*, 11(S02), pp.1252–1253.

Yu, D.G. et al., 2011. Solid dispersions in the form of electrospun core-sheath nanofibers. *International journal of nanomedicine*, 6, pp.3271–3280.

Yu, W. et al., 2014. One-pot coaxial electrospinning fabrication and properties of magnetic-luminescent bifunctional flexible hollow nanofibers. *MATERIALS LETTERS*, 120, pp.126–129.

Yuan, X.Y. et al., 2004. Morphology of ultrafine polysulfone fibers prepared by electrospinning. *POLYMER INTERNATIONAL*, 53(11), pp.1704–1710.

Zeng, J. et al., 2003. Biodegradable electrospun fibers for drug delivery. *Journal of Controlled Release*, 92(3), pp.227–231. Available at: http://www.sciencedirect.com/science/article/pii/S0168365903003729.

Zeugolis, D.I. et al., 2008. Electro-spinning of pure collagen nano-fibres - just an expensive way to make gelatin? *Biomaterials*, 29(15), pp.2293–2305.

Zhang, C. et al., 2005. Study on morphology of electrospun poly(vinyl alcohol) mats. *European Polymer Journal*, 41(3), pp.423–432. Available at: http://linkinghub.elsevier.com/retrieve/pii/S0014305704003945 [Accessed July 30, 2013].

Zhang, S. et al., 2008. Gelatin nanofibrous membrane fabricated by electrospinning of aqueous gelatin solution for guided tissue regeneration. *Journal of biomedical materials research. Part A*, 90(3), pp.671–9. Available at: http://www.ncbi.nlm.nih.gov/pubmed/18563816 [Accessed May 12, 2014].

Zhang, Y. et al., 1997. Influence of the route of allergen administration and genetic background on the murine allergic pulmonary response. *American journal of respiratory and critical care medicine*, 155(2), pp.661–669.

Zhang, Y.Z. et al., 2006. Crosslinking of the electrospun gelatin nanofibers. *Polymer*, 47(8), pp.2911–2917. Available at: http://www.sciencedirect.com/science/article/pii/S0032386106001789.

Zhao, X. et al., 2015. Photocrosslinkable Gelatin Hydrogel for Epidermal Tissue Engineering. *Advanced Healthcare Materials*, p.n/a–n/a. Available at: http://doi.wiley.com/10.1002/adhm.201500005.

Zhong, J. et al., 2015. Effect of nanofiber orientation of electrospun nanofibrous scaffolds on cell growth and elastin expression of muscle cells. *Colloids and Surfaces B: Biointerfaces*, 136, pp.772–778. Available at: http://www.sciencedirect.com/science/article/pii/S0927776515302484.

Zhou, L. et al., 2014. Biomimetic mineralization of anionic gelatin hydrogels: effect of degree of methacrylation. *RSC Advances*, 4(42), p.21997. Available at: http://pubs.rsc.org/en/Content/ArticleHTML/2014/RA/C4RA02271H.

Zhu, Y. et al., 2010. Macro-alignment of electrospun fibers for vascular tissue engineering. *Journal of biomedical materials research. Part B, Applied biomaterials*, 92(2), pp.508–516.

Zhuo, H.T., Hu, J.L. & Chen, S.J., 2011. Coaxial electrospun polyurethane core-shell nanofibers for shape memory and antibacterial nanomaterials. *Express Polymer Letters*, 5(2), pp.182–187.

Zong, X. et al., 2002. Structure and process relationship of electrospun bioabsorbable nanofiber membranes. *Polymer*, 43(16), pp.4403–4412. Available at: http://linkinghub.elsevier.com/retrieve/pii/S0032386102002756.

Zosky, G.R. et al., 2004. The pattern of methacholine responsiveness in mice is dependent on antigen challenge dose. *Respiratory research*, 5, p.15.

Zosky, G.R. & Sly, P.D., 2007. Animal models of asthma. *Clinical and experimental allergy : journal of the British Society for Allergy and Clinical Immunology*, 37(7), pp.973–88. Available at: http://www.ncbi.nlm.nih.gov/pubmed/17581191 [Accessed October 22, 2014].

Zou, Y. & Zhang, Y., 2009. An experimental and theoretical study on the anisotropy of elastin network. *Annals of biomedical engineering*, 37(8), pp.1572–1583.